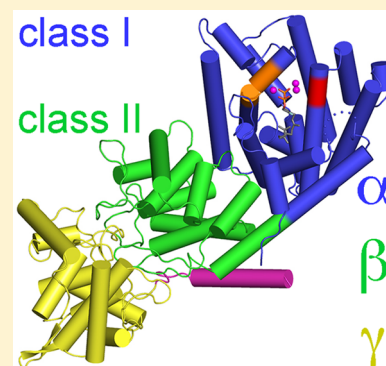


Structural and Chemical Biology of Terpenoid Cyclases

David W. Christianson*¹

Roy and Diana Vagelos Laboratories, Department of Chemistry, University of Pennsylvania, 231 South 34th Street, Philadelphia, Pennsylvania 19104-6323, United States

ABSTRACT: The year 2017 marks the twentieth anniversary of terpenoid cyclase structural biology: a trio of terpenoid cyclase structures reported together in 1997 were the first to set the foundation for understanding the enzymes largely responsible for the exquisite chemodiversity of more than 80000 terpenoid natural products. Terpenoid cyclases catalyze the most complex chemical reactions in biology, in that more than half of the substrate carbon atoms undergo changes in bonding and hybridization during a single enzyme-catalyzed cyclization reaction. The past two decades have witnessed structural, functional, and computational studies illuminating the modes of substrate activation that initiate the cyclization cascade, the management and manipulation of high-energy carbocation intermediates that propagate the cyclization cascade, and the chemical strategies that terminate the cyclization cascade. The role of the terpenoid cyclase as a template for catalysis is paramount to its function, and protein engineering can be used to reprogram the cyclization cascade to generate alternative and commercially important products. Here, I review key advances in terpenoid cyclase structural and chemical biology, focusing mainly on terpenoid cyclases and related prenyltransferases for which X-ray crystal structures have informed and advanced our understanding of enzyme structure and function.



CONTENTS

1. Introduction	11571	5.3.1. Cyclooctatenol Synthase (CotB2)	11613
2. Prenyltransferases	11574	5.3.2. <i>ent</i> -Kaurene Synthase	11614
2.1. Regular Isoprenoid Coupling Enzymes	11574	5.3.3. Taxadiene Synthase	11615
2.2. Irregular Isoprenoid Coupling Enzymes	11580	5.3.4. Labdane-Related Diterpene Cyclase (LrdC)	11617
3. Aromatic Prenyltransferases	11582	5.4. Sesterterpene Cyclases	11617
3.1. Soluble ABBA Prenyltransferases	11582	6. Class II Terpenoid Cyclases	11617
3.2. Membrane-Embedded UbiA Prenyltransferases	11583	6.1. Diterpene Cyclases	11617
4. Isoprenoid Diphosphate Lyases	11584	6.1.1. <i>ent</i> -Copalyl Diphosphate Synthase from <i>Arabidopsis thaliana</i>	11617
5. Class I Terpenoid Cyclases	11587	6.1.2. <i>ent</i> -Copalyl Diphosphate Synthase from <i>Streptomyces platensis</i> CB00739	11619
5.1. Monoterpene Cyclases	11587	6.2. Triterpene Cyclases	11619
5.1.1. (+)-Bornyl Diphosphate Synthase	11588	6.2.1. Squalene-Hopene Cyclase	11619
5.1.2. (–)-Limonene Synthase	11591	6.2.2. Oxidosqualene Cyclase	11621
5.1.3. (+)-Limonene Synthase	11593	6.3. Sesquiterpene Cyclases	11622
5.1.4. γ -Terpinene Synthase	11594	7. Bifunctional Terpenoid Cyclases	11623
5.1.5. Cineole Synthase	11594	7.1. Geosmin Synthase	11623
5.1.6. Methylisoborneol Synthase	11594	7.2. Abietadiene Synthase	11624
5.2. Sesquiterpene Cyclases	11597	7.3. Fusicoccadiene Synthase	11626
5.2.1. α -Bisabolol Synthase	11597	8. Oxidoreductase Terpenoid Cyclases	11628
5.2.2. α -Bisabolene Synthase	11598	8.1. Δ^1 -Tetrahydrocannabinolic Acid Synthase	11628
5.2.3. Epi-Isozizaene Synthase	11599	8.2. Iridoid Synthase	11630
5.2.4. Trichodiene Synthase	11600	9. Concluding Remarks	11630
5.2.5. Selinadiene Synthase	11604	Author Information	11633
5.2.6. Germacradien-4-ol Synthase	11604	Corresponding Author	11633
5.2.7. Aristolochene Synthase	11607	ORCID	11633
5.2.8. Epi-Aristolochene Synthase	11608	Notes	11633
5.2.9. Hedycaryol Synthase	11609		
5.2.10. (+)- δ -Cadinene Synthase	11610		
5.2.11. Pentalenene Synthase	11611		
5.3. Diterpene Cyclases	11613		

Received: May 20, 2017

Published: August 25, 2017

Biography	11633
Acknowledgments	11634
References	11634

1. INTRODUCTION

Terpenes, also known as terpenoids or isoprenoids, comprise the most chemically and structurally diverse family of natural products. Currently numbering more than 80000 members in a greater family that also includes steroids and carotenoids, the terpenome accounts for nearly one-third of all compounds currently characterized in the Dictionary of Natural Products (<http://dnp.chemnetbase.com>).^{1,2} The structural complexity of this vast chemical library belies relatively simple biosynthetic roots: head-to-tail coupling reactions of 5-carbon precursors yield linear, achiral C_{5n} isoprenoid diphosphates ($n = 1, 2, 3$, etc.) (Figure 1),^{3,4} which in turn undergo cyclization reactions to yield a myriad of products typically containing multiple fused rings and stereocenters (some examples are shown in Figure 2).^{5–19} These reactions are catalyzed by enzymes known as terpenoid synthases; terpenoid synthases that catalyze cyclization reactions are also known as terpenoid cyclases. Terpenoid cyclization reactions are the most complex reactions found in nature, in that on average more than half of the substrate carbon atoms undergo changes in bonding, hybridization, and stereochemistry during the course of a multistep cyclization cascade. Moreover, since cyclic terpenoids typically cannot be generated from linear precursors in the absence of an enzyme, the catalytic rate enhancement of a terpenoid cyclase over the uncatalyzed rate is immeasurably large.

Additional structural diversity in terpenoid natural products arises from the coupling chemistry employed to link C_5 isoprenoid precursors. For example, C_5 dimethylallyl diphosphate (DMAPP) and C_5 isopentenyl diphosphate (IPP) can be linked in regular (i.e., head-to-tail) fashion to yield C_{10} geranyl diphosphate, which in turn can undergo condensation with additional IPP molecules to yield C_{15} farnesyl diphosphate (FPP), C_{20} geranylgeranyl diphosphate (GGPP), C_{25} geranyl-farnesyl diphosphate (GFPP), and so on (terpenoid nomencla-

ture and commonly used acronyms are summarized in Figure 1). Alternatively, two isoprenoid allylic groups can undergo irregular coupling reactions,²⁰ such as cyclobutanation, branching, or cyclopropanation reactions, to yield alternative carbon skeletons that further diversify the terpenome (Figure 2).^{21,22}

A hallmark of most reactions catalyzed by a terpenoid synthase is the cascade of multiple carbocation intermediates that define the reaction coordinate of catalysis. Such highly reactive intermediates could potentially alkylate and inactivate the enzyme, so the terpenoid synthase typically contains a nonpolar active site pocket that enables effective management and manipulation of these intermediates. However, this does not preclude the presence of occasional polar groups or solvent molecules in the terpenoid synthase active site (e.g., as observed in bornyl diphosphate synthase from *Salvia officinalis* and aristolochene synthase from *Aspergillus terreus*).^{23–25} Although such potential nucleophiles could rapidly quench a carbocation intermediate, they will not do so as long as they are fixed in positions where they are not properly oriented to react. Since some terpenoid cyclases generate hydroxylated products, reflecting quenching of the final carbocation intermediate by a water molecule, it is logical that these cyclases have evolved with suitable water management strategies to prevent premature quenching of carbocation intermediates.

Quantum mechanical studies of terpenoid cyclase reaction mechanisms indicate that tertiary carbocation intermediates are much more common than secondary carbocation intermediates.^{26–28} Additionally, these studies show that many carbocation intermediates in terpenoid cyclization cascades are subject to electron delocalization (e.g., through hyperconjugation and other through-bond coupling) that influences and directs the cyclization trajectory. Carbocation intermediates can be stabilized in the active site of a terpenoid cyclase by weakly polar interactions involving charge–charge, charge–dipole, and charge–quadrupole interactions with suitably oriented amino acid side chains. In particular, carbocation intermediates can be stabilized by the substantial partial negative charge generated by the ring π electrons of the aromatic side chains of phenylalanine, tyrosine, and tryptophan through cation– π interactions (Figures

Carbon Atoms	Terpene Prefix	Linear Isoprenoid Precursor	Synthase Class	Domain Architecture
5	hemi-	 dimethylallyl diphosphate (DMAPP) ↔ isopentenyl diphosphate (IPP)	I	$\alpha\beta$
10	mono-	 geranyl diphosphate (GPP)	I	$\alpha\beta$
15	sesqui-	 farnesyl diphosphate (FPP)	I	$\alpha, \alpha\alpha, \alpha\beta, \alpha\beta\gamma$
20	di-	 geranylgeranyl diphosphate (GGPP)	I, II	$\alpha, \alpha\alpha, \alpha\beta\gamma$
25	sester-	 geranyl-farnesyl diphosphate (GFPP)	I, II	$\alpha, \alpha\alpha$
30	tri-	 squalene	II	$\beta\gamma, \alpha\beta\gamma$

Figure 1. General scheme of terpene nomenclature, linear precursors (OPP = diphosphate), synthase classification, and commonly observed domain architectures.

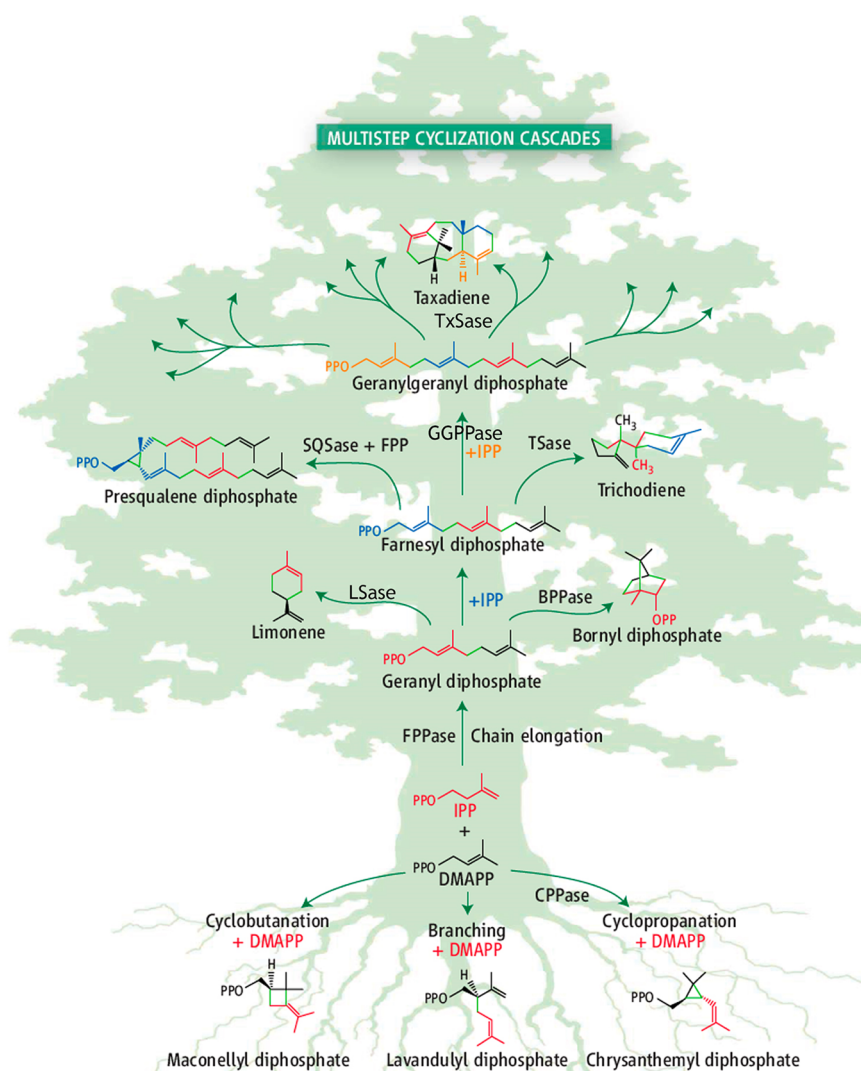


Figure 2. Chemodiversity is a hallmark of the branches of the terpenome family tree. Individual 5-carbon isoprenoid groups are color-coded to highlight their biosynthetic fates. Enzyme abbreviations: BPPase, bornyl diphosphate synthase; CPPase, chrysanthemyl diphosphate synthase; FPPase, farnesyl diphosphate synthase; GGPPase, geranylgeranyl diphosphate synthase; LSase, limonene synthase; SQSase, squalene synthase; TSase, trichodiene synthase; TxSase, taxadiene synthase. Reprinted with permission from ref 22. Copyright 2007 AAAS.

3 and 4).^{29–31} Such carbocation stabilization can generally be achieved without risk of alkylation and accordingly comprises a

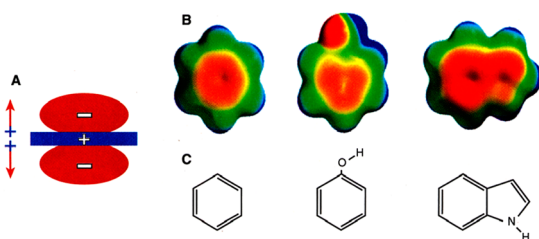


Figure 3. (A) An aromatic ring is an electronic quadrupole, with no net charge and no net dipole. (B and C) Electrostatic surface potentials for the side chain aromatic groups of phenylalanine, tyrosine, and tryptophan reveal that the faces of these aromatic residues bear significant partial negative charge. Aromatic residues can accordingly stabilize carbocation intermediates in terpenoid cyclase mechanisms through quadrupole–charge or cation– π interactions. Reprinted with permission from ref 29. Copyright 1996 AAAS.

strategy for electrostatic stabilization of multiple transition states in the terpenoid cyclization cascade.

Although there are interesting exceptions,³² including antibodies that catalyze isoprenoid-like cyclization reactions,^{33–35} terpenoid cyclases generally fall into two main classes depending on the chemical strategy for initial carbocation formation:⁸ a class I terpenoid cyclase utilizes a trinuclear metal cluster to trigger the ionization of an isoprenoid diphosphate substrate to yield an allylic cation and inorganic pyrophosphate, whereas a class II terpenoid cyclase relies on a general acid (an aspartic acid side chain) to protonate the terminal carbon–carbon double bond of an isoprenoid substrate to yield a tertiary carbocation. The first X-ray crystal structures of terpenoid cyclases revealed evolutionarily distinct α -helical folds for class I and class II enzymes.^{36–38} As classified by Oldfield and colleagues,^{39,40} the active site of a class I cyclase such as bacterial pentalenene synthase³⁶ or plant epi-aristolochene synthase³⁷ is located in the middle of an α -helical bundle designated the “ α fold”, and the active site of a class II cyclase such as squalene-hopene cyclase³⁸ is located at the interface of two α -helical domains designated “ β ” and “ γ ” (Figure

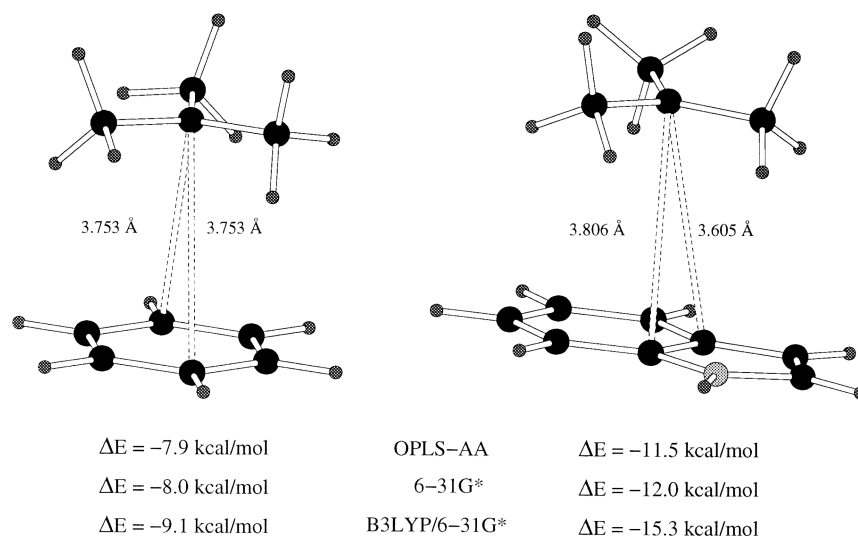


Figure 4. Optimized geometries and stabilization energies calculated for carbocation- π interactions with benzene and indole indicate that the π systems of the side chains of phenylalanine, tyrosine, and tryptophan are capable of stabilizing carbocation intermediates in the active site of a terpenoid cyclase. Reproduced from ref 31. Copyright 1997 American Chemical Society.

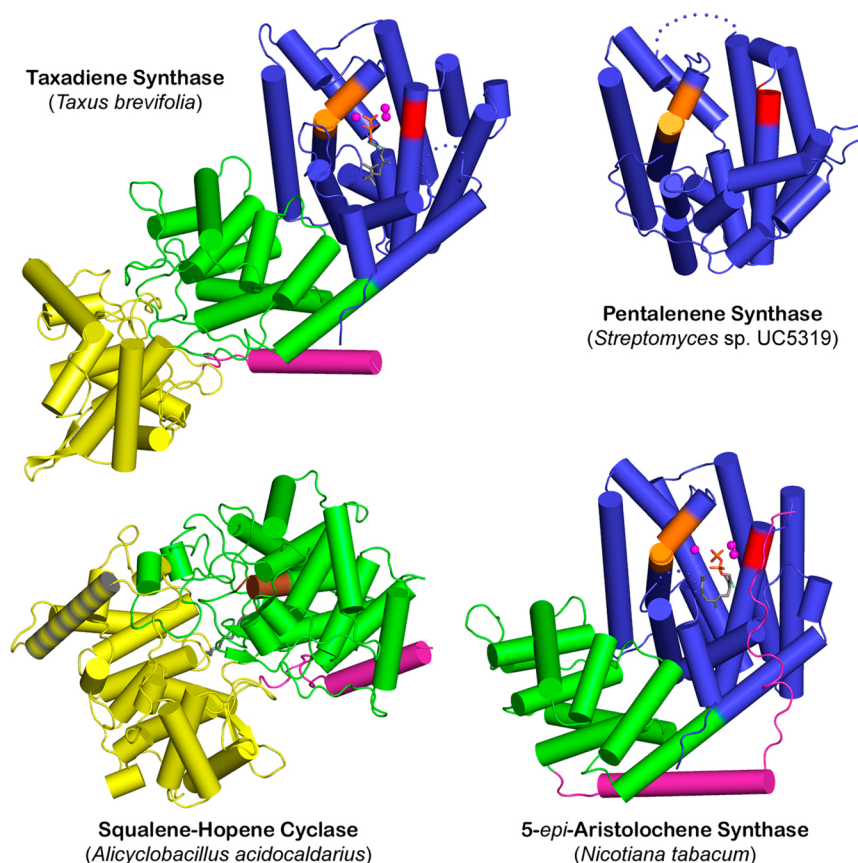


Figure 5. Domain diversity: terpenoid synthase structures generally consist of α , β , and γ domains (blue, green, and yellow, respectively) in various combinations. The γ domain is an insertion domain between the first and second helices of the β domain; the N-terminal helix of the β domain is magenta. The α domain represents the class I terpenoid synthase fold and is found as a single domain in bacterial pentalene synthase,³⁶ an $\alpha\beta$ domain assembly in tobacco epi-aristolochene synthase,³⁷ and an $\alpha\beta\gamma$ domain assembly in taxadiene synthase from the Pacific yew.⁴² Metal-binding motifs in each α domain (red and orange) coordinate to a trinuclear metal cluster that activates an isoprenoid diphosphate substrate for catalysis. The $\beta\gamma$ domain assembly represents the class II terpenoid synthase fold as first observed in bacterial squalene-hopene cyclase.³⁸ An aspartic acid motif (brown) contains a general acid that initiates the class II cyclization reaction. The γ domain of squalene-hopene cyclase contains a membrane-anchoring helix (stippled yellow-gray) which is absent from the γ domain of taxadiene synthase. Reprinted with permission from ref 42. Macmillan Publishers Ltd. 2011 Copyright.

5). Structural homology and 23% amino acid sequence identity between the β and γ domains of squalene-hopene cyclase⁸ suggest a primordial gene duplication and fusion event with evolution of catalytic activity at the domain–domain interface, so the γ domain of a class II terpenoid cyclase can also be considered as a β' domain. Similarly, gene duplication and fusion of an ancient 4-helix bundle protein yielded the α fold of a class I terpenoid cyclase (see section 2.1).⁴¹

The crystal structure of taxadiene synthase, a diterpene cyclase from the Pacific yew, was the first to reveal that a class I terpenoid cyclase could exist as a fusion of $\alpha\beta\gamma$ domains (the α domain is catalytically active and the $\beta\gamma$ domain is an inactive vestige) (Figure 5),⁴² in accord with predictions based on bioinformatics and experimental studies.^{39,43} Since epi-aristolochene synthase adopts $\alpha\beta$ domain architecture (Figure 5),³⁷ domain architecture for a class I terpenoid synthase is thus found as α , $\alpha\beta$, or $\alpha\beta\gamma$. Interestingly, the crystal structure of the class II terpenoid cyclase *ent*-copalyl diphosphate synthase reveals $\alpha\beta\gamma$ domain architecture with a functional active site at the $\beta\gamma$ domain interface and an inactive, vestigial α domain.⁴⁴ Thus, domain architecture for a class II terpenoid cyclase can be $\beta\gamma$ or $\alpha\beta\gamma$. The evolution of catalytic activity in the class I or class II active site is accordingly a function of the biosynthetic needs of the cell and the particular organic reaction mechanism required for catalysis. The crystal structure of abietadiene synthase from the grand fir was the first to reveal the structure of a bifunctional $\alpha\beta\gamma$ terpenoid synthase with catalytically active class I and class II active sites that catalyze tandem diterpene cyclization reactions,⁴⁵ and the crystal structure of α -bisabolene synthase from the grand fir revealed that a class I sesquiterpene cyclase could also adopt $\alpha\beta\gamma$ domain architecture.⁴⁶

The domain architectures summarized in Figure 5 thus represent the context for the vast majority of terpenoid cyclization reactions in biology. Each terpenoid cyclase is found with tertiary structure consisting of a core domain architecture of α , $\alpha\beta$, $\beta\gamma$, or $\alpha\beta\gamma$, as summarized in Figure 1. Notably, $\alpha\alpha$ domain architecture is also observed in certain bifunctional terpenoid synthases (see section 7). In terms of quaternary structure, dimers, tetramers, and hexamers are observed, examples of which are discussed throughout this Review.

The terpenoid cyclization reactions discussed in this Review focus on those that utilize linear isoprenoid diphosphate substrates with all-*(E)* (i.e., all *trans*) isoprenoid double bonds, as illustrated in Figure 1. Indeed, terpenoid cyclization products of *trans*-isoprenoid substrates account for the great majority of terpenoid natural products. However, it should be noted that some terpenoid synthases utilize or generate linear isoprenoid diphosphates containing (*Z*) (i.e., *cis*) double bonds.^{47–51} Perhaps the most prominent example is undecaprenyl diphosphate synthase, which generates a C_{55} isoprenoid that functions in bacterial cell wall biosynthesis.⁵² These *cis*-prenyltransferases adopt a completely different fold⁵³ in comparison with *trans*-prenyltransferases and therefore evolved independently of the enzymes discussed in this Review. It is interesting, however, that the *trans*-prenyltransferase FPP synthase also generates minor amounts of *cis* isomers (i.e., products GPP or FPP containing a C2–C3 *cis*-double bond),⁵⁴ and that a *cis*-FPP synthase has been identified in *Mycobacterium tuberculosis*.⁵⁵ Moreover, the sesquiterpene cyclase epi-aristolochene synthase from tobacco can utilize (*cis,trans*)-FPP as a cyclization substrate to generate an alternative array of cyclization products,⁵⁶ and certain class II diterpene cyclases

can utilize neryleryl diphosphate as a substrate.⁵⁷ Such catalytic versatility enhances the chemodiversity of the terpenome.

The remainder of this Review includes much of the classic work underlying modern studies and applications of terpenoid biosynthesis yet also emphasizes studies that have emerged since my last Review on this topic.¹³ As prominent terpenoid synthase archetypes are discussed, common mechanistic themes emerge regarding the chemical strategy for initial carbocation formation, carbon–carbon bond-forming reactions in multistep cyclization cascades, the fidelity or promiscuity of the protein catalyst in chaperoning these cascades, and the chemical strategy for terminating the cyclization cascade by proton elimination or capture by solvent. To set the stage for understanding the structural and chemical biology of terpene cyclases, it is instructive to first review the coupling enzymes that generate the linear substrates for terpene cyclization reactions. These chain elongation reactions are catalyzed by prenyltransferases.

2. PRENYLTRANSFERASES

The era of terpenoid synthase structural biology began with the X-ray crystal structure of avian FPP synthase, which catalyzes the 1'-4 (i.e., head-to-tail) coupling of C_5 isoprenoid units (as represented by the "trunk" of the tree of terpenoid diversity shown in Figure 2).⁵⁸ Also referred to as a regular coupling reaction and more generally as a prenyltransferase reaction, the 1'-4 chain elongation reaction is the most important of all nine possible isoprenoid couplings found in nature (Figure 6) because

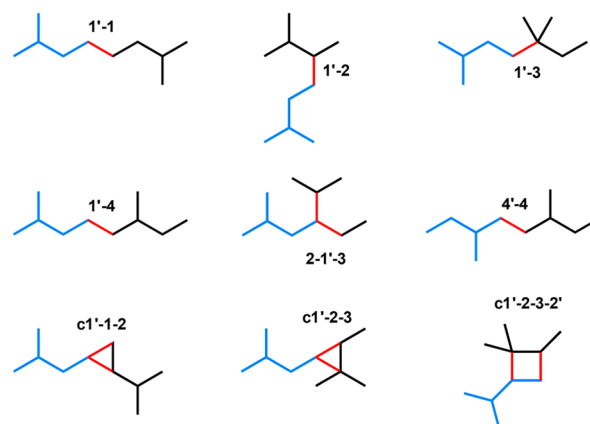


Figure 6. Naturally occurring isoprenoid coupling patterns. Individual C_5 isoprenoid units are black and blue, and bonds between them are shown in red. Terpenoid synthases catalyze coupling reactions that yield these connections. The 1'-4 (head-to-tail) connection is referred to as a regular coupling; all other connections are referred to as irregular couplings.

it provides the linear achiral substrates for cyclization by terpenoid cyclases. All other couplings illustrated in Figure 6 are referred to as irregular coupling reactions. As summarized in this section, both regular and irregular coupling reactions are catalyzed by metal-dependent enzymes that exhibit the α fold of a class I terpenoid synthase. As such, the FPP synthase structure⁵⁸ foreshadowed the first terpenoid cyclase structures that would follow three years later.^{36–38}

2.1. Regular Isoprenoid Coupling Enzymes

Farnesyl diphosphate synthase is the archetype of a regular coupling enzyme. This class I terpenoid synthase catalyzes the condensation of DMAPP and two molecules of IPP to yield FPP.

The enzyme adopts a unique α -helical fold characterized by bundles of α -helices,⁵⁸ later designated the class I terpenoid synthase fold,^{8,36} and more recently designated the α fold.^{39,40,59} FPP synthase is a homodimer in which the active sites are oriented in parallel fashion (Figure 7), with aspartate-rich metal

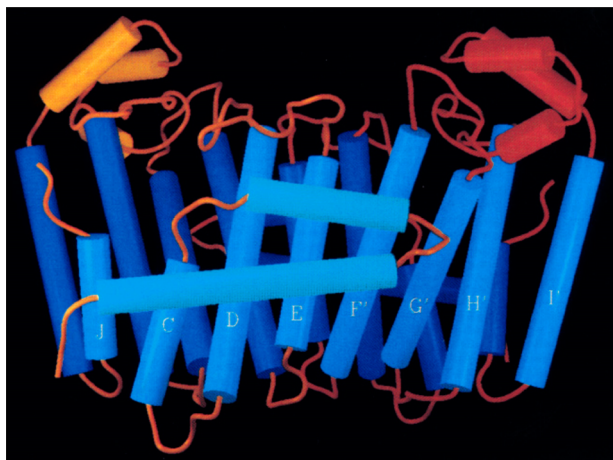


Figure 7. Crystal structure of avian FPP synthase, an isologous dimer of 44-kD subunits, was the first to reveal the α fold of a class I terpenoid synthase. The active site of each monomer opens toward the top and is partially capped by loops and additional helices (yellow and red cylinders). Helices in one subunit are labeled by capital letters, and helices in the other subunit are labeled by primed capital letters. Active sites are oriented in parallel fashion (i.e., the active sites of the left and right subunits open to the top of the figure). Reproduced from ref 58. Copyright 1994 American Chemical Society.

ion binding motifs DDXXD located on the upper wall of the active site on helices D and H in each subunit. Earlier studies of the related coupling enzyme hexaprenyl diphosphate synthase and other prenyltransferases,^{60,61} as well as FPP synthase from

different species,^{62,63} implicated these aspartate-rich motifs for a metal binding function in catalysis. This metal binding function was confirmed in the initial X-ray crystal structure determination, in which these motifs were observed to coordinate to samarium (Sm^{3+}) ions used as heavy atom derivatives to phase the initial electron density map.⁵⁸ Later, the crystal structure of F112A/F113S avian FPP synthase complexed with GPP (the product of the first coupling reaction with DMAPP and IPP) revealed the binding of 2 Mg^{2+} ions, each coordinated by the first and last aspartate in the first aspartate-rich motif D¹¹⁷DDXXD (Figure 8).⁶⁴ The second aspartate-rich motif does not coordinate to metal ions in this complex, which represents an incomplete enzyme–substrate complex for the second coupling reaction of GPP and IPP to generate FPP.

In FPP synthase from *Escherichia coli*, the first aspartate-rich segment has a two-residue insertion so that it appears as DDXXXXD; thus, there can be subtle variations in this sequence that nonetheless sustain metal-binding function. The X-ray crystal structure of this enzyme complexed with IPP and the unreactive analogue of DMAPP, dimethylallyl-S-thiodiphosphate (DMSPP), shows that both aspartate-rich motifs and the thiodiphosphate group of DMSPP coordinate to 3 Mg^{2+} ions; octahedral metal coordination polyhedra are completed by solvent molecules (Figure 9).⁶⁵ It is now clear that 3 metal ions are required to provide the electrophilic driving force that triggers isoprenoid diphosphate ionization and initial carbocation formation in most if not all terpenoid synthases that adopt the α fold.⁶⁶ Ligand binding causes conformational changes that serve to cap the active site, thereby protecting reactive carbocation intermediates from bulk solvent.

These structures provide a framework for understanding earlier enzymological and mechanistic studies of FPP synthase indicating an ionization-condensation-elimination sequence for catalysis.⁵ Coordination to 3 metal ions and hydrogen bond interactions with 3 basic residues (arginine and/or lysine residues)⁶⁶ triggers the ionization of the allylic diphosphate moiety of DMAPP to yield a tightly bound allylic carbocation-

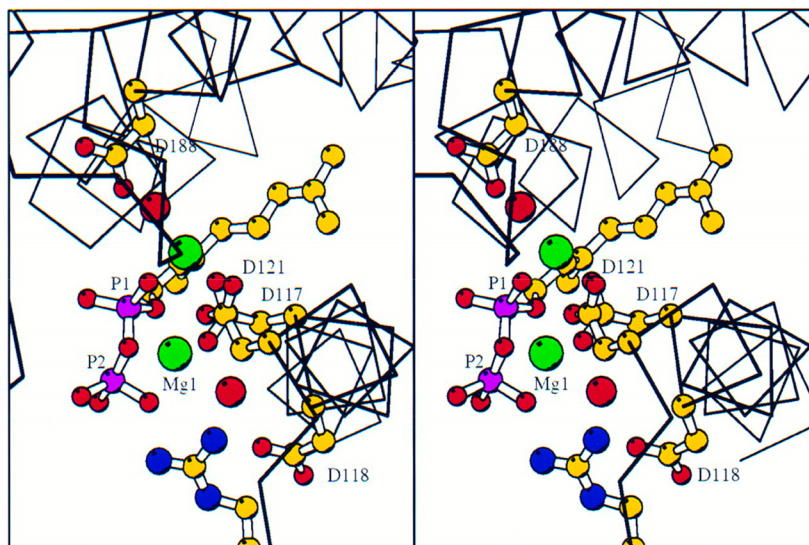


Figure 8. Stereoview of avian F112A/F113S FPP synthase complexed with GPP. The side chains of D117 and D121 in the first aspartate-rich motif coordinate to two Mg^{2+} ions (green spheres), which in turn are coordinated by the diphosphate group of the substrate (C = yellow, P = purple, and O = red). The side chain of R126 (unlabeled, N = blue) also forms a hydrogen bond with the terminal phosphate group, thereby ensuring specificity for the allylic diphosphate substrate. Metal-bound solvent molecules are shown as red spheres. Reprinted with permission from ref 64. Copyright 1996 National Academy of Sciences.

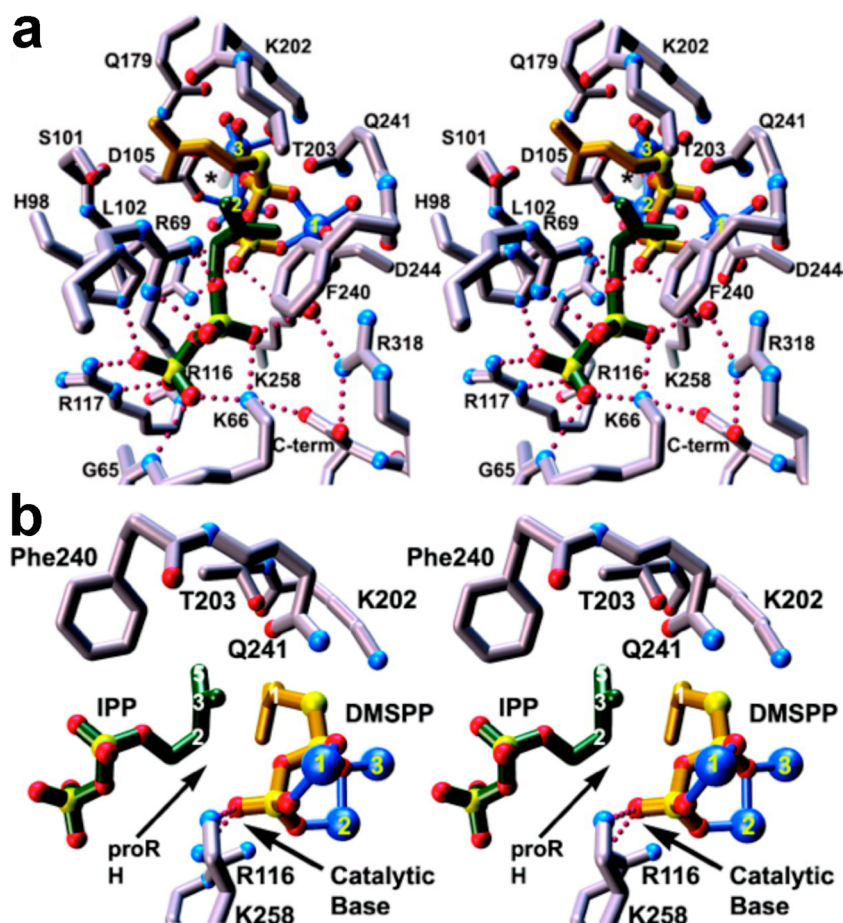


Figure 9. (a) Stereoview of the active site of FPP synthase from *E. coli* complexed with IPP (C = green, O = red, and P = yellow) and the unreactive substrate analogue DMSPP (C = brown and S = yellow) reveals the binding of a full complement of 3 Mg^{2+} ions (blue spheres 1, 2, and 3). Metal coordination and hydrogen bond interactions are indicated by solid blue and dotted red lines, respectively. (b) Alternative orientation of the complex shown in (a) reveals that the diphasphate group of DMSPP, which ultimately becomes coproduct inorganic pyrophosphate, is suitably oriented to serve as the catalytic general base that mediates stereospecific deprotonation of the pro-*R* proton at C2 of IPP. Originally published in ref 65. Copyright 2004 American Society for Biochemistry & Molecular Biology.

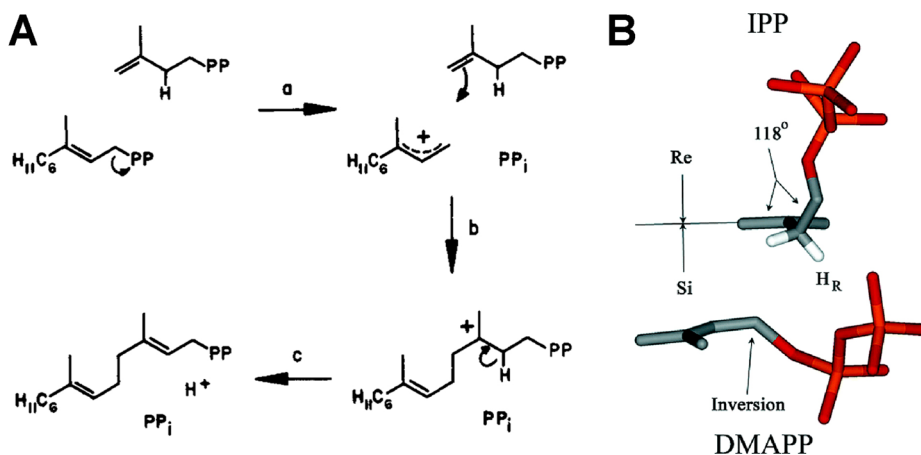


Figure 10. (A) FPP synthase is a processive enzyme that catalyzes the coupling of IPP molecules to a growing isoprenoid chain. Condensation of DMAPP and IPP yields GPP. In the second round of the chain elongation reaction, (a) ionization of GPP yields an allylic cation that (b) undergoes condensation with a second molecule of IPP. The chain elongation product, bearing a tertiary carbocation at C3, undergoes stereospecific proton elimination (c) to yield FPP. Abbreviations: PP = diphosphate, PP_i = inorganic pyrophosphate. Reproduced from ref 67. Copyright 1981 American Chemical Society. (B) Model of the precatalytic enzyme-substrate complex showing the intermolecular orientations of DMAPP and IPP required in the reaction catalyzed by FPP synthase. Reproduced from ref 54. Copyright 2006 American Chemical Society.

inorganic pyrophosphate ion pair (Figure 10).^{67–69} Interestingly, the possibility of such an ion pair to initiate an ionization-

condensation-elimination sequence, as opposed to a concerted condensation-elimination sequence, had first been proposed in

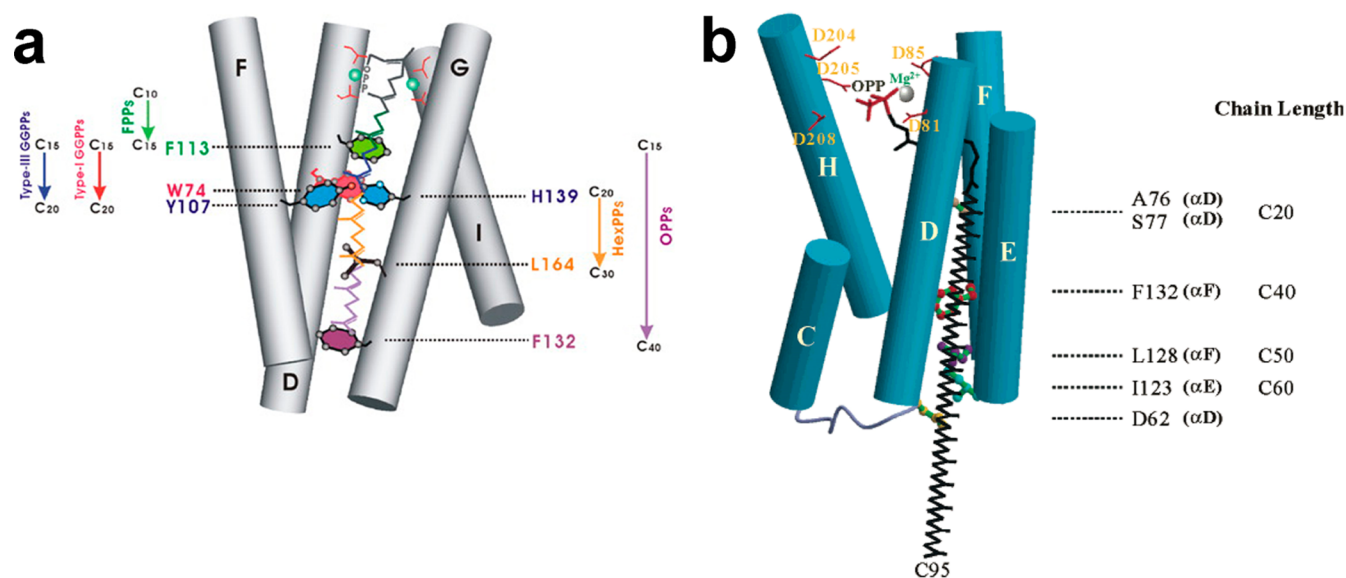


Figure 11. (a) A “molecular ruler” governs product chain length in short-, medium-, and long-chain prenyltransferases: bulky hydrophobic residues define the base of the pocket that serves as a template to direct product chain length. In general, active site pockets are increasingly deeper and wider for increasingly longer chain elongation products. Originally published in ref 87. Copyright 2006 American Society for Biochemistry & Molecular Biology. (b) The base of the product-determining pocket in octaprenyl pyrophosphate synthase can be engineered to yield an unprecedented C₉₅ *trans*-isoprenoid diphosphate product. Reproduced from ref 84. Copyright 2004 American Chemical Society.

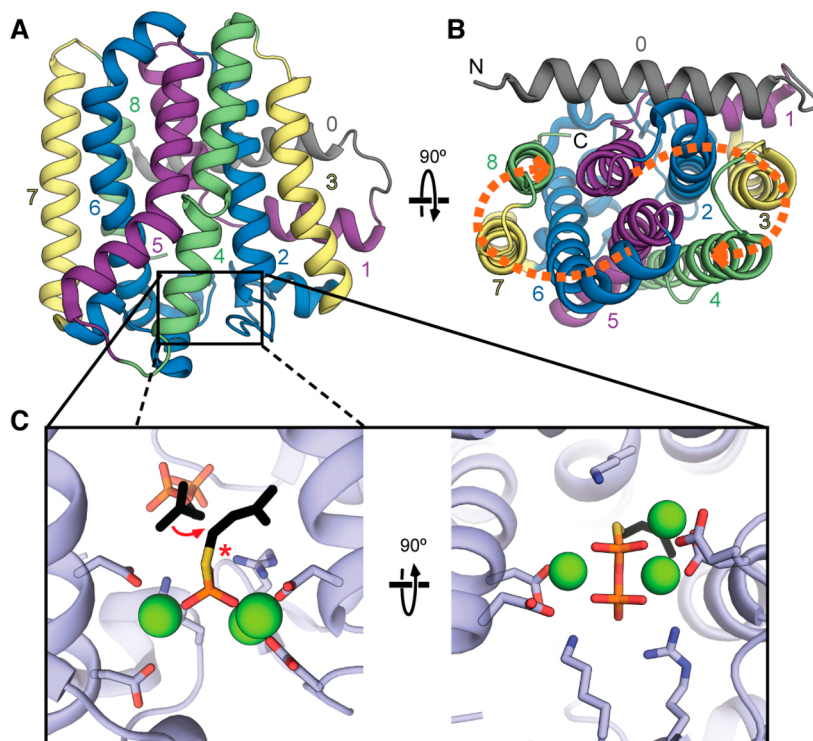


Figure 12. (A and B) The crystal structure⁶⁵ of FPP synthase from *E. coli* reveals quasi-2-fold symmetry in the α fold resulting from the assembly of two 4-helix bundles, in which helices 1–4 of one bundle correspond to helices 5–8 of the second bundle.⁴¹ Topologically identical helices have identical colors. This architecture suggests that a primordial gene duplication and fusion event involving a 4-helix bundle protein yielded the modern day class I terpenoid synthase fold. (C) Aspartate-rich metal-binding motifs are conserved on topologically equivalent helices 2 and 6. The view shows the complex with DMSPP, IPP, and 3 Mg²⁺ ions. In the left panel, a red asterisk indicates what would be the scissile C–O bond of DMAPP, and the red arrow indicates the trajectory of C–C bond formation between IPP and DMAPP. This is an alternate view of the complex shown in Figure 9. Reprinted from ref 41. Creative Commons Attribution 4.0 International Public License, <http://creativecommons.org/licenses/by/4.0/legalcode>.

mechanistic studies of squalene biosynthesis.^{70–72} Alkylation of the *si* face of the C3–C4 double bond of IPP with inversion of configuration at the C1 atom of DMAPP yields a tertiary carbocation intermediate,⁷³ which then undergoes elimination of

the pro-R proton at C2 to yield the chain elongation product GPP.⁷⁴ The crystal structure of the *E. coli* FPP synthase–DMSPP–IPP complex reveals that the diphosphate group of DMSPP is suitably oriented to mediate the stereospecific proton elimi-

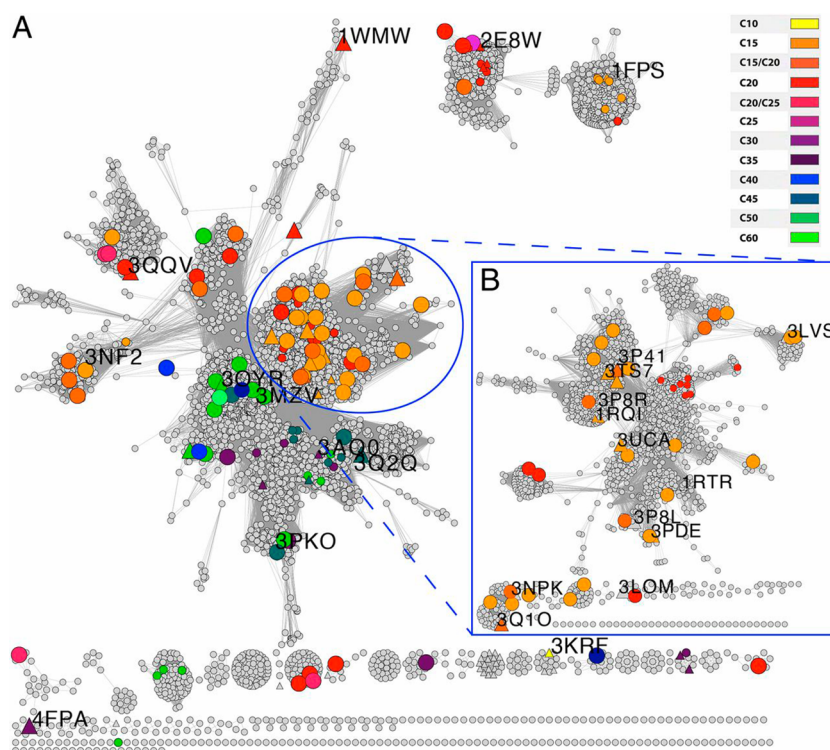


Figure 13. (A) Sequence similarity network of prenyltransferases with BLAST e-value cutoff = $1e^{-50}$. (B) Sequence similarity network of prenyltransferases with BLAST e-value cutoff = $1e^{-70}$. Nodes are color-coded according to the product generated by the indicated prenyltransferase. PDB accession codes are indicated for prenyltransferases with experimentally determined crystal structures. Reprinted from ref 92. Copyright 2013 National Academy of Sciences.

nation that terminates the coupling reaction.⁶⁵ General base catalysis by coproduct inorganic pyrophosphate had previously been suggested for FPP synthase;^{3,75–78} multistep general base-general acid functions for inorganic pyrophosphate may also prevail for terpenoid cyclases, as initially considered⁷⁹ based on structural analysis of aristolochene synthase from *Penicillium roqueforti* as well as other cyclases.⁸⁰ In accord with the processive function of FPP synthase, GPP then shifts to allow the binding of another molecule of IPP and a second ionization-condensation-elimination sequence, which generate the final product FPP as shown in Figure 10.

Being a processive enzyme, FPP synthase requires a stop signal to ensure that the reaction sequence is terminated upon generation of the correct final product. The active site of FPP synthase provides a template for catalysis that serves as a “molecular ruler”. Mutagenesis and structural studies of avian FPP synthase⁶⁴ reveal that the side chain of F113 buttressed by the side chain of F112 forms the base of the pocket that dictates product isoprenoid chain length. The F112A and F113S mutations deepen the pocket by 5.8 Å. When incubated with DMAPP and IPP, this double mutant generates an array of C₂₀–C₇₀ isoprenoid products. Thus, the newly formed base of the pocket in F112A/F113S FPP synthase can undergo slight structural changes so as to open up to bulk solvent, thereby enabling the formation of longer products. Conversely, the active site pocket can be made more shallow by introducing the A116W or N114W constrictions, which introduces significant selectivity for GPP synthesis.⁸¹ Random chemical mutagenesis of FPP synthase from *Bacillus stearothermophilus* similarly identify active site residues that, when mutated, lead to the generation of mixtures of GPP, GGPP, and FPP.⁸²

Since the initial structure determination of avian FPP synthase nearly 25 years ago,⁵⁸ crystal structures of coupling enzymes that generate GPP, GGPP, hexaprenyl diphosphate, and octaprenyl diphosphate have also appeared.^{83–95} These enzymes similarly adopt the α fold of a class I terpenoid synthase, and their active site pockets are shallower or deeper to direct the chain elongation reaction to form short-chain, medium-chain, or long-chain isoprenoid products. Analysis of these structures illuminates details regarding the molecular ruler governing product chain length, which provides a foundation for protein engineering experiments in which alternative isoprenoid products can be generated.⁸⁷ In one particularly striking example, octaprenyl pyrophosphate synthase from *Thermotoga maritima* can be engineered to make a linear C₉₅ isoprenoid, which is the longest product generated by any *trans*-prenyltransferase (Figure 11).⁸⁴

Notably, a recent structural analysis indicates that the core α fold of FPP synthase likely resulted from a gene duplication and fusion event involving a primordial 4-helix bundle protein (Figure 12).⁴¹ In this analysis, which utilized the structure of FPP synthase from *E. coli*, the aspartate-rich metal-binding motifs on helices D and H are topologically equivalent. Given the utility of 4-helix bundles in the modular design of de novo functional proteins,^{96–102} their appearance in terpenoid synthases suggests that new avenues in terpenoid biosynthesis might be explored through the de novo design and assembly of 4-helix bundles.

Recently, Poulter, Jacobson, and colleagues have reported the development of a new computational bioinformatics-directed approach for the study of more than 5000 terpenoid synthases putatively assigned as *trans*-prenyltransferases.⁹² In this study, genomic and crystal structure data are used to predictively guide the discovery and functional evaluation of short-, medium-, or long-chain *trans*-prenyltransferases. Impressively, the prediction

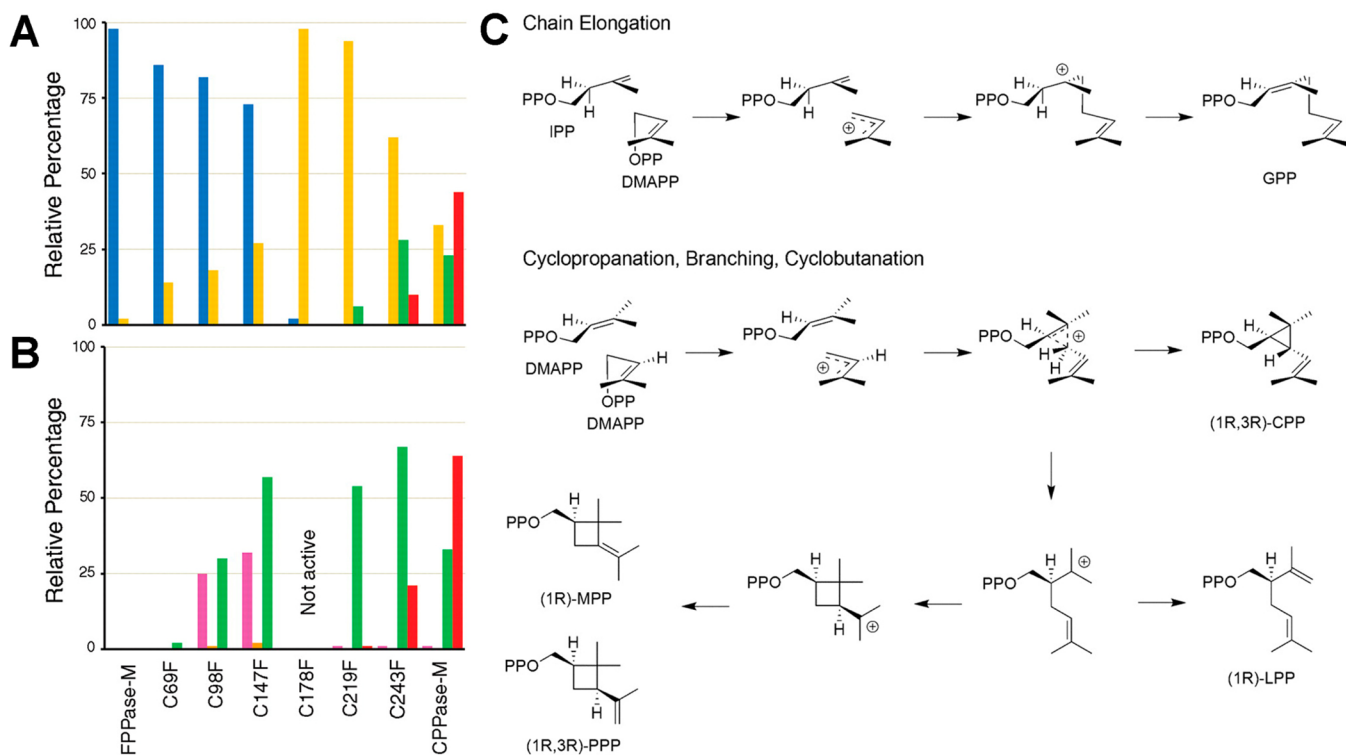


Figure 14. Chimeric terpenoid synthases generated from FPP synthase (FPPase-M) and chrysanthemyl diphosphate synthase (CPPase-M) generate all four fundamental isoprenoid coupling products when incubated with (A) DMAPP and IPP or just (B) DMAPP. Products are color-coded as follows: FPP, blue; GPP, gold; lavender diphosphate (LPP), green; chrysanthemyl diphosphate (CPP), red; maconellyl diphosphate (MPP), magenta; planococyl diphosphate (PPP), orange. Mechanisms of product formation are illustrated in (C). Reprinted with permission from ref 105. Copyright 2007 AAAS.

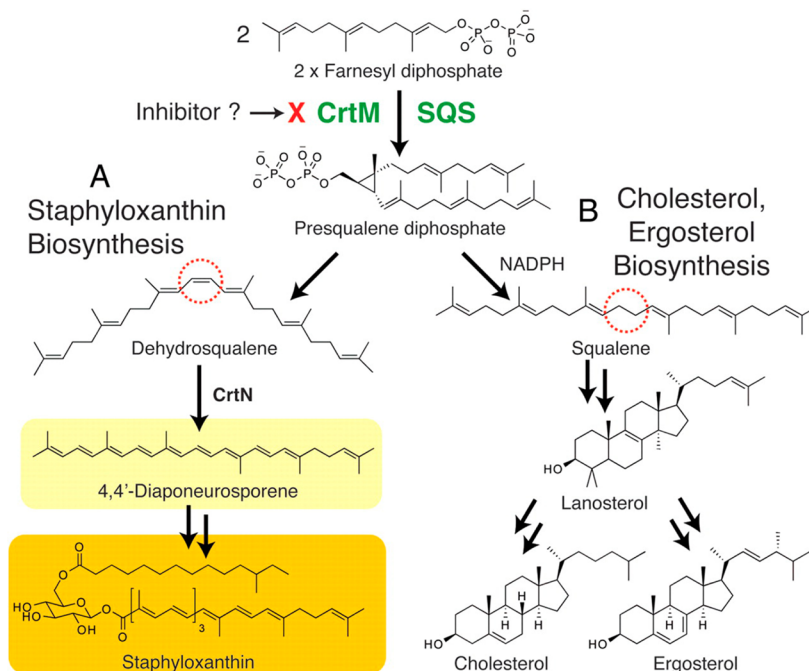


Figure 15. Human squalene synthase (SQS) catalyzes the coupling of two FPP molecules to yield presqualene diphosphate, a critical intermediate in steroid biosynthesis. Dehydrosqualene synthase (CrtM) catalyzes the same reaction in the biosynthesis of the golden pigment staphyloxanthin in *S. aureus*. Reprinted with permission from ref 109. Copyright 2008 AAAS.

of function in new enzymes is 62% correctly predicted and 94% correctly predicted within plus or minus a single 5-carbon

isoprene unit. Sequence similarity networks^{103,104} illustrate evolutionary relationships in Figure 13.

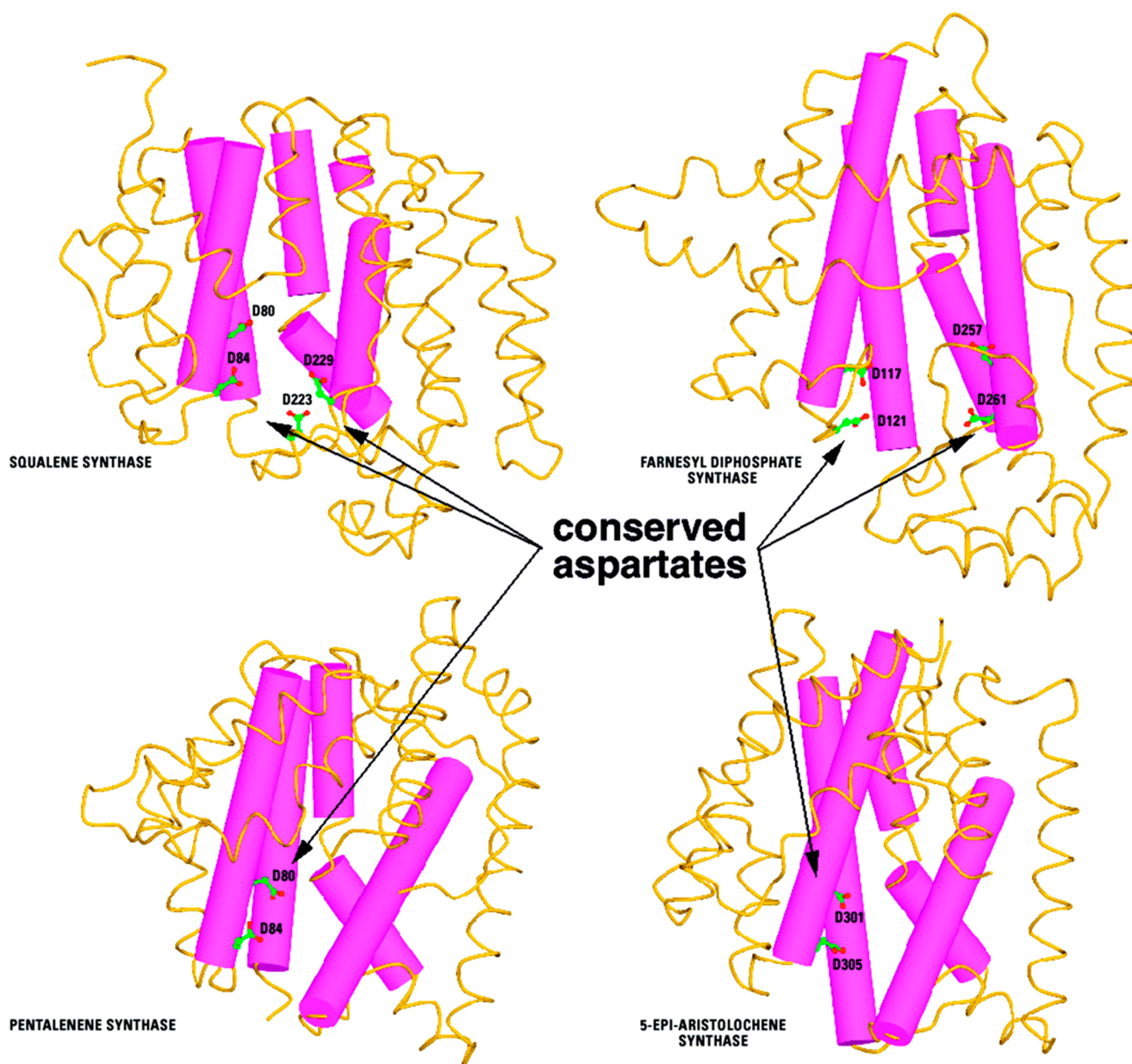


Figure 16. Human squalene synthase, avian FPP synthase, bacterial pentalenene synthase, and plant 5-epi-aristolochene synthase share insignificant overall amino acid sequence identity, yet these enzymes share the class I terpenoid synthase fold with conservation of aspartate-rich metal-binding motifs as well as a kink in helix G (the purple helix bent into two parts connected by a short loop). This kink orients main chain carbonyl groups of helix G1 into the active site, where the negative electrostatic potential of the helix dipole may stabilize carbocation intermediates in isoprenoid coupling or cyclization reactions. Originally published in ref 107. Copyright 2000 The American Society for Biochemistry & Molecular Biology.

2.2. Irregular Isoprenoid Coupling Enzymes

Irregular coupling reactions, also known as nonhead-to-tail coupling reactions, yield the general coupling patterns shown in Figure 6. Strikingly different carbon skeletons result from alternative isoprenoid coupling reactions, and this bond-making variability contributes to the vast chemodiversity of the terpenome. The major irregular isoprenoid coupling reactions include $c1'-1-2$ and $c1'-2-3$ cyclopropanation reactions, $c1'-2-3-2'$ cyclobutanation reactions, and $1'-2$ branching reactions. Both regular and irregular isoprenoid coupling reactions comprise the roots of terpenoid diversity as represented in Figure 2.

In an elegant set of experiments involving the design, preparation, and analysis of chimeric terpenoid synthases,

Poulter and colleagues demonstrated that cyclobutanation, cyclopropanation, and branching reactions can be catalyzed by a metal-dependent class I terpenoid synthase.¹⁰⁵ To construct these chimeras, the amino acid sequence of sagebrush FPP synthase was progressively substituted with the amino acid sequence of sagebrush chrysanthemyl diphosphate synthase (75%/96% amino acid sequence identity/similarity). Strikingly, while FPP synthase generates FPP almost exclusively and chrysanthemyl diphosphate synthase generates monoterpene cyclopropanation and branching products, FPP synthase-chrysanthemyl diphosphate synthase chimeras generate varying arrays of regular and irregular monoterpene coupling products, including cyclobutanation products, through dissociative electrophilic alkylation mechanisms (Figure 14). Although the recent crystal structure of lavandulyl diphosphate synthase reveals a

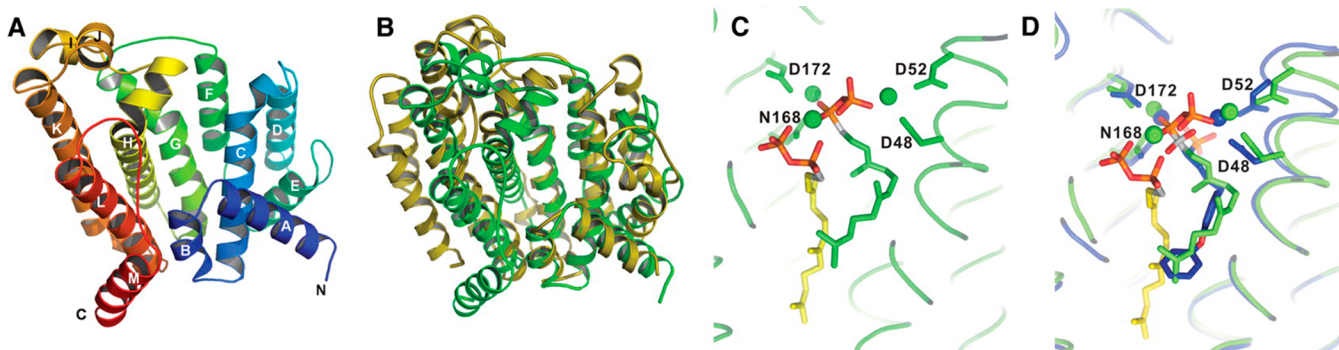


Figure 17. (A) Dehydroqualene synthase (CrtM) from *S. aureus* adopts the α fold of a class I terpenoid synthase. (B) Superposition of bacterial dehydroqualene synthase (green) and human squalene synthase (yellow) reveals homologous structures. (C) Two molecules of the unreactive substrate analogue FSPP bind in the active site of dehydroqualene synthase; one FSPP molecule is poised for ionization and allylic cation formation by coordination to 3 Mg^{2+} ions. (D) Crystal structure of dehydroqualene synthase complexed with the inhibitor BPH-652 superimposed on the complex with two FSPP molecules reveals that the inhibitor binding site partially overlaps with both FSPP binding sites. Reprinted with permission from ref 109. Copyright 2008 AAAS.

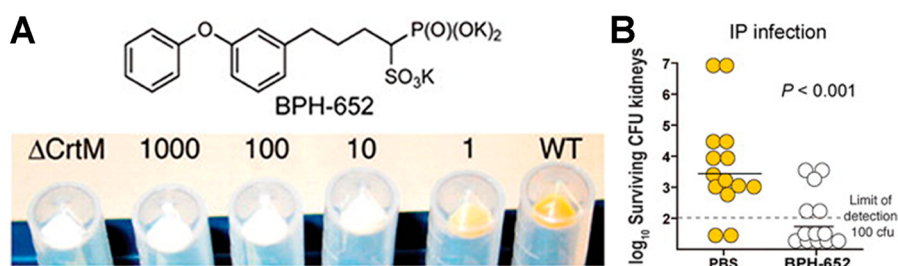


Figure 18. (A) Inhibition of dehydroqualene synthase with 0–1000 mM BPH-652 blocks staphyloxanthin pigment biosynthesis in *S. aureus* (IC_{50} = 110 nM). (B) Administration of BPH-652 exhibits substantial bactericidal activity against *S. aureus* following intraperitoneal injection in live mice. Reprinted with permission from ref 109. Copyright 2008 AAAS.

protein fold unrelated to the characteristic α fold of a class I terpenoid synthase, it is notable that this coupling chemistry can be catalyzed in two distinct protein scaffolds.¹⁰⁶

Irregular isoprenoid coupling reactions in biological systems are not limited to monoterpene biosynthesis. Consider the condensation of two FPP molecules to yield presqualene diphosphate (Figure 15). This reaction is catalyzed by human squalene synthase in the cholesterol biosynthesis pathway; the second step of the reaction is reduction by NADPH to yield products squalene and inorganic pyrophosphate. The crystal structure of human squalene synthase reveals the core α fold of a class I terpenoid synthase.¹⁰⁷ Despite relatively low amino acid sequence identity with other class I terpenoid synthases, conservation of the overall α fold and signature aspartate-rich metal binding motifs (appearing in slightly varied form as D⁸⁰TLED and D²¹⁹YLED) similarly indicates evolutionary divergence from a common ancestral class I terpenoid synthase (Figure 16). Interestingly, Pandit and colleagues note that the kink in helix G of squalene synthase is conserved in other terpenoid synthases; this kink exposes the main chain carbonyl groups of V175 and A176 to the active site cavity, such that the negative electrostatic potential of the helix dipole may stabilize carbocation intermediates in catalysis.¹⁰⁷ More recent structural studies of hedycaryol synthase complexed with nerolidol also suggest a role for the helix G kink in carbocation stabilization.¹⁰⁸

Related to the eukaryotic squalene synthase reaction is the prokaryotic presqualene diphosphate synthase reaction catalyzed by the coupling enzyme dehydroqualene synthase in *Staphylococcus aureus* (Figure 15).¹⁰⁹ In this bacterial pathogen, the FPP coupling reaction is the first committed step in the

biosynthesis of the golden pigment staphyloxanthin, which is responsible for the eponymous coloration of *S. aureus* (“aureus” is the Latin term for a gold coin used in the Roman Empire).^{110,111} The extended conjugated π system of staphyloxanthin confers protective antioxidant properties, capable of trapping reactive oxygen species that might otherwise kill the bacterium. Staphyloxanthin is thus a potent virulence factor, and inhibition of its biosynthesis would render *S. aureus* more susceptible to the oxidative countermeasures of the human immune response in the event of infection.

The crystal structure of bacterial dehydroqualene synthase reveals a class I terpenoid synthase fold similar to that of human squalene synthase; the ternary complex of dehydroqualene synthase with two molecules of farnesyl thiolodiphosphate (FSPP, an unreactive FPP analogue) reveals how the two coupling substrates bind in the active site: the diphosphate group of one FSPP molecule coordinates to a full complement of 3 Mg^{2+} ions that are also coordinated by three aspartate residues and one asparagine residue in the aspartate-rich metal-binding motifs (Figure 17).¹⁰⁹ This is the first view of precatalytic substrate binding for a cyclopropanation reaction in the active site of a terpenoid synthase.

Noting the structural and functional similarities between dehydroqualene synthase and squalene synthase, Oldfield and colleagues suggest that inhibitors developed against squalene synthase in the development of cholesterol-lowering drugs might also inhibit dehydroqualene synthase and render *S. aureus* defenseless against oxidative reagents, or more importantly, to the oxidative burst of the mammalian immune system.¹⁰⁹ Incubation of *S. aureus* with various squalene synthase inhibitors

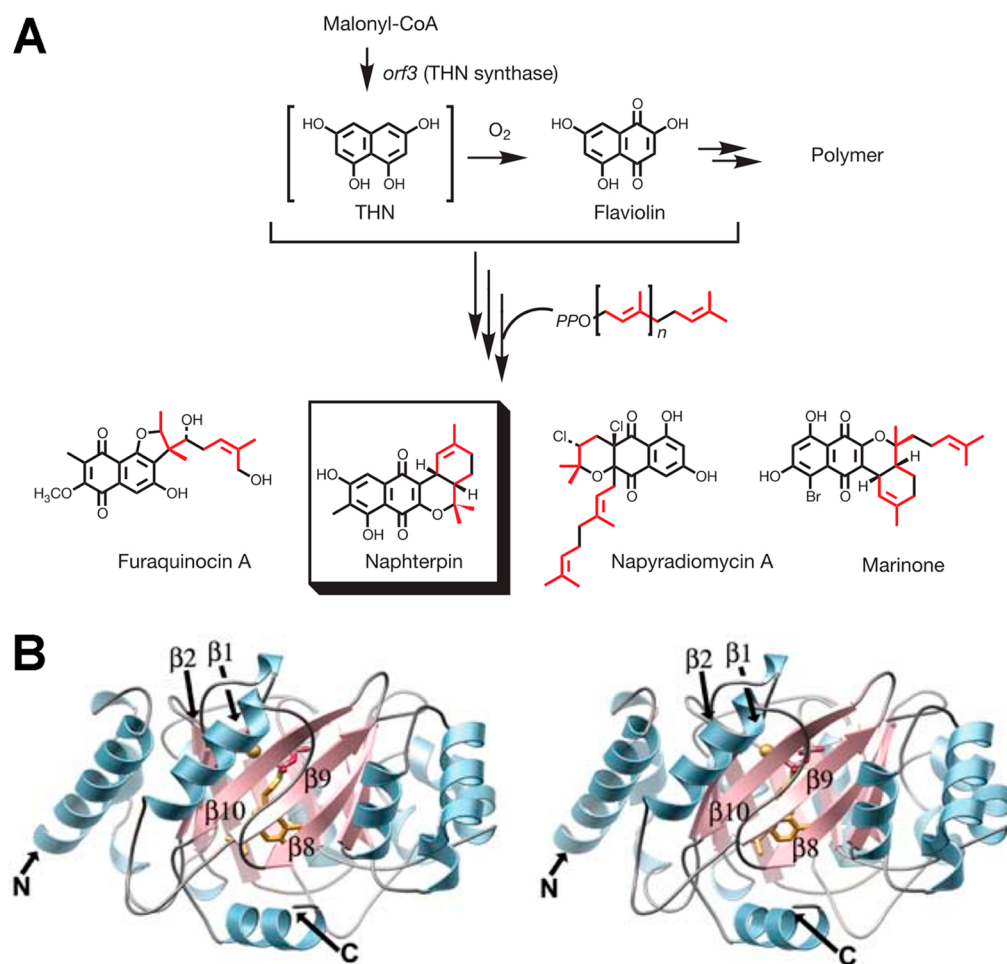


Figure 19. (A) Prenylation of 1,3,6,8-tetrahydroxynaphthalene (THN) or flaviolin by GPP is a critical step early in the biosynthesis of the antioxidant naphterpin. Other hybrid isoprenoid-polyketides are generated in similar fashion using isoprenoid substrates DMAPP, GPP, or FPP. (B) Stereoview of the ABBA prenyltransferase NphB (formerly named Orf2) reveals the 10-stranded antiparallel β -barrel consisting of 5 repeated $\alpha\beta\beta\alpha$ motifs. The active site is in the middle of the barrel, indicated by bound substrates (yellow and red stick figures). Reprinted with permission from ref 119. Copyright 2005 Macmillan Publishers Ltd.

does indeed inhibit generation of the golden staphyloxanthin pigment; treatment with the cholesterol-lowering agent BPH-652 (Figure 18) makes the resulting unpigmented bacteria ~15-fold more susceptible to killing by 1.5% hydrogen peroxide. In an animal model of *S. aureus* infection, mice treated with BPH-652 by intraperitoneal injection contain 98% fewer surviving bacteria (Figure 18). Thus, inhibition of the class I terpenoid synthase dehydrosqualene synthase comprises a new therapeutic strategy for the treatment of methicillin-resistant *S. aureus* infection.^{109,112–117}

Finally, it is interesting to note that the coupling of two FPP molecules to generate squalene requires a sequence of three separate steps catalyzed by three distinct enzymes in bacteria. Poulter and colleagues¹¹⁸ demonstrate that the first enzyme catalyzes the coupling of two FPP molecules to generate presqualene diphosphate, which is converted to hydroxysqualene by the second enzyme in the biosynthetic sequence. Bacterial squalene synthase then utilizes FADH_2 to reduce hydroxysqualene to squalene. Thus, prokaryotic squalene biosynthesis contrasts with eukaryotic squalene biosynthesis in terms of the number of enzymes involved in the biosynthetic sequence as well as the cofactor utilized for redox chemistry [human squalene synthase¹⁰⁷ requires NADPH (Figure 15)].

3. AROMATIC PRENYLTRANSFERASES

3.1. Soluble ABBA Prenyltransferases

Cytosolic aromatic prenyltransferases are enzymes that catalyze the transfer of isoprenoid chains to aromatic rings (e.g., phenyl, naphthyl, or indole rings) in biosynthetic reactions leading to hybrid natural products that serve critical functions in biological systems. For example, the biosynthetic origins of the antioxidant naphterpin, an isoprenoid-polyketide natural product, are rooted in 1,3,6,8-tetrahydroxynaphthalene and GPP (Figure 19A). These substrates are coupled through an alkylation reaction reminiscent of a classic Friedel–Crafts reaction. The X-ray crystal structure of an aromatic prenyltransferase reveals a novel 10-stranded antiparallel β -barrel fold, termed a PT-barrel fold,¹¹⁹ with an overall topology consisting of five repeated $\alpha\beta\beta\alpha$ motifs (Figure 19B). Accordingly, these enzymes are designated as ABBA prenyltransferases.¹²⁰

Many ABBA prenyltransferases require Mg^{2+} to trigger the ionization of the isoprenoid diphosphate group, forming inorganic pyrophosphate and the allylic cation that alkylates the aromatic ring of the cosubstrate. Some, such as dimethylallyl tryptophan synthase, do not require Mg^{2+} but instead utilize a broad array of hydrogen bond interactions to trigger substrate ionization.¹²¹ Regardless, ABBA prenyltransferases do not adopt

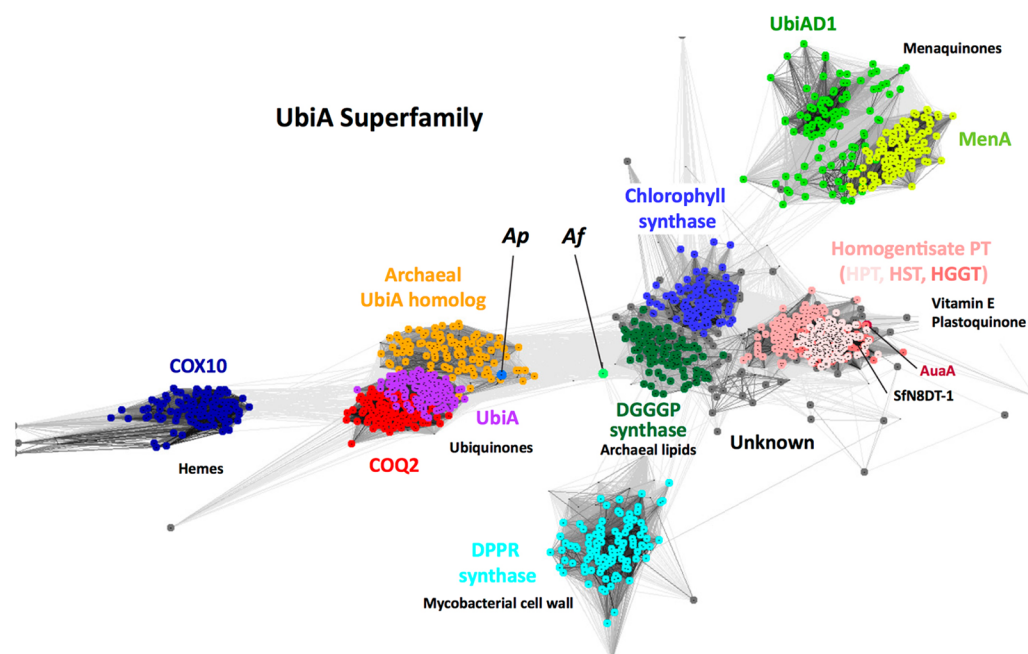


Figure 20. Sequence similarity network of the UbiA prenyltransferase superfamily. Key members include ApUbiA and AfUbiA, which function in ubiquinone biosynthesis. As described by Li,¹²² homologues of significant similarity form clusters; increasingly darker gray lines indicate increasingly similar amino acid sequences. The UbiA superfamily includes: bacterial UbiA (magenta), archaeal UbiA (orange), and their eukaryotic COQ2 homologues (red); bacterial MenA (yellow) and eukaryotic UbiAD1 (green); homogentisate prenyltransferases from plants (shades of pink: HPT, homogentisate phytyl transferase; HST, homogentisate solanesyl transferase; HGGT, homogentisate geranylgeranyl transferase); plant chlorophyll synthase (blue); eukaryotic protoheme farnesyltransferase COX10 (dark blue); archaeal digeranylgeranyl glyceryl phosphate synthase (DGGGP, dark green); and mycobacterial decaprenylphosphate-5-phosphoribose synthase (DPPR, cyan). Reprinted with permission from ref 122. Copyright 2016 Elsevier.

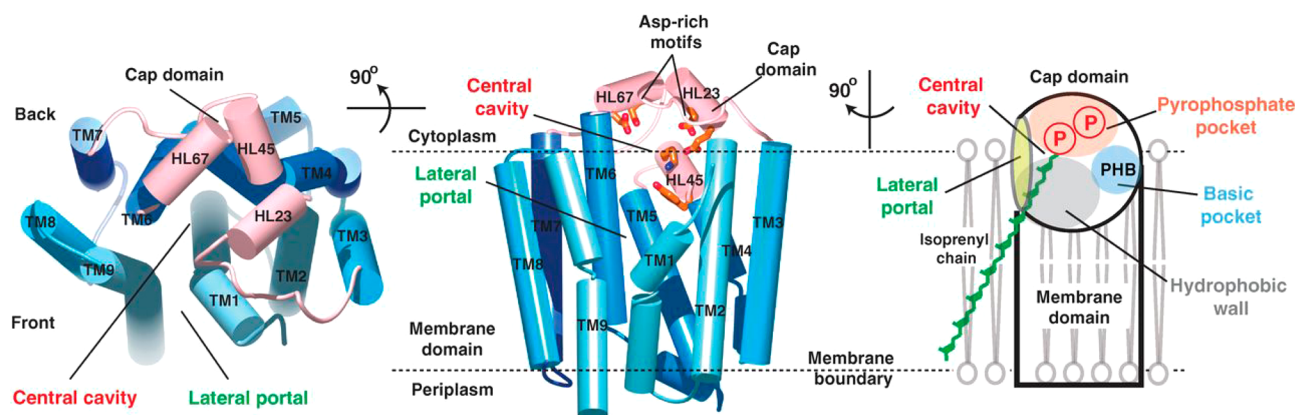


Figure 21. Crystal structure of ApUbiA reveals the characteristic α fold of a soluble class I terpenoid synthase adapted for function as an integral membrane protein. The cap domain (pink) encloses the hydrophobic central cavity formed by transmembrane helices (blue); aspartate-rich motifs implicated in Mg^{2+} binding are indicated. The isoprenoid substrate is also embedded in the membrane and is proposed to access the active site through a lateral portal. Reprinted with permission from ref 128. Copyright 2014 AAAS.

the protein fold of a class I or class II terpenoid synthase, nor do they contain the signature aspartate-rich motifs that characterize a class I terpenoid synthase. The crystal structure of the bacterial prenyltransferase functioning in naphthepin biosynthesis complexed with the unreactive substrate analogue geranyl thiolodiphosphate (GSPP) reveals that a Mg^{2+} ion is coordinated by the thiolodiphosphate group of GSPP and only a single protein residue, D62.¹¹⁹

3.2. Membrane-Embedded UbiA Prenyltransferases

In contrast with cytosolic ABBA prenyltransferases, prenyltransferases belonging to the UbiA superfamily are polytopic membrane proteins that catalyze the first committed steps in the

biosynthesis of ubiquinone, menaquinone (vitamin K), and other prenylated aromatic compounds. Archetypical members of this enzyme family include microbial UbiA and MenA, and their eukaryotic homologues COQ2 and UBIAD1, respectively; the entire superfamily has been recently reviewed (Figure 20).¹²² UbiA was first discovered by Young and colleagues¹²³ and catalyzes the coupling of polyprenyl diphosphates of varying lengths¹²⁴ to the ortho position (i.e., C3) of 4-hydroxybenzoic acid. Members of the UbiA superfamily are characterized by two aspartate-rich metal-binding motifs, NDXXDXXXD and DXXXX,^{61,125–127} which are reminiscent of the signature metal-binding motifs of class I terpenoid cyclases.

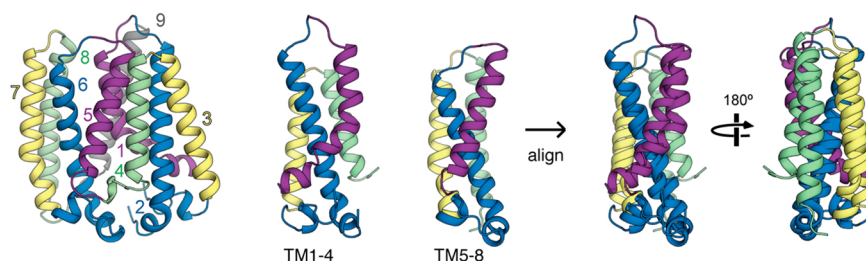


Figure 22. Crystal structure of AfUbiA reveals the characteristic α fold of a class I terpenoid synthase, which exhibits pseudo-2-fold symmetry between transmembrane helices TM1–4 and TM5–8. Superposition of TM1–4 and TM5–8 clearly reveals their structural homology, suggesting gene duplication and fusion of a primordial 4-helix bundle precursor. Reprinted from ref 41. Creative Commons Attribution 4.0 International Public License, <http://creativecommons.org/licenses/by/4.0/legalcode>.

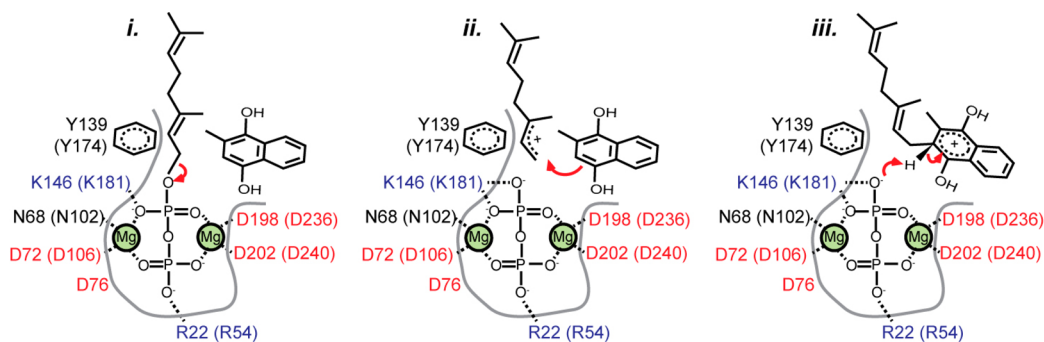


Figure 23. Proposed mechanism of AfUbiA, a member of the UbiA superfamily that adopts the α fold of a class I terpenoid synthase. Reprinted from ref 41. Creative Commons Attribution 4.0 International Public License, <http://creativecommons.org/licenses/by/4.0/legalcode>.

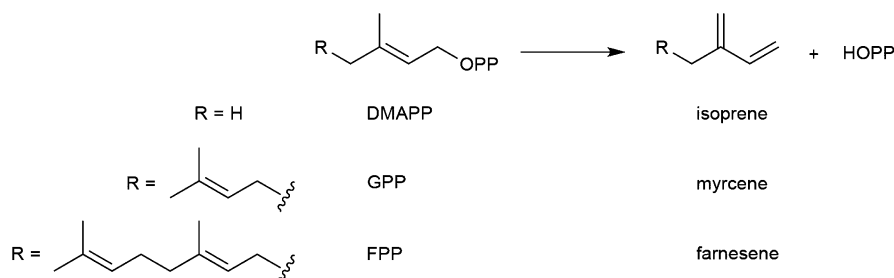


Figure 24. 1,4-conjugate elimination reaction of DMAPP yields isoprene as catalyzed by isoprene synthase. Similar reactions are catalyzed by myrcene synthase and farnesene synthase using substrates GPP and FPP, respectively. OPP = diphosphate, HOPP = inorganic pyrophosphate.

Recent crystal structure determinations of archaeal UbiA homologues from *Aeropyrum pernix* (ApUbiA) and *Achaeglobus fulgidus* (AfUbiA) reveal an overall α fold identical to that of the α domain of a class I terpenoid synthase.^{41,128} These structures reveal that the helical segments containing the aspartate-rich motifs form a cap domain that encloses the active site, thereby protecting reactive carbocation intermediates from premature quenching by bulk solvent (Figure 21). Huang and colleagues⁴¹ show that this fold exhibits pseudo 2-fold symmetry, identical to that of farnesyl diphosphate synthase, suggesting gene duplication and fusion of a primordial 4-helix bundle protein with the evolution of catalytic function at the interface of the two bundle domains (Figure 22).

Crystal structures of ApUbiA and AfUbiA reveal the binding of 2 Mg^{2+} ions in complexes with GPP or GSPP; while there are differences in metal coordination polyhedra between structures, some of these differences may be attributable to the lower resolution (3.6 Å) of the ApUbiA structure¹²⁸ in comparison with the higher resolution of the AfUbiA structure (2.4 Å).⁴¹ Two basic residues, an arginine and a lysine residue, also interact with the diphosphate group of GPP and presumably assist the

Mg^{2+} ions in triggering substrate ionization.⁴¹ The reaction mechanism proposed on the basis of the higher resolution AfUbiA structure is shown in Figure 23. This mechanism involves the characteristic ionization-condensation-elimination sequence of a class I terpenoid synthase, notable aspects of which include stabilization of the allylic carbocation intermediate through cation- π interactions with a highly conserved tyrosine residue and stereospecific proton elimination mediated by the inorganic pyrophosphate coproduct.⁴¹

4. ISOPRENOID DIPHOSPHATE LYASES

Perhaps the simplest reaction catalyzed by a terpenoid synthase is the conjugate 1,4-elimination reaction with DMAPP, yielding inorganic pyrophosphate and the volatile C_5 hydrocarbon isoprene (Figure 24). This reaction has tremendous ecological importance. Isoprene emission by plant life was first discovered more than 60 years ago by Sanadze,¹²⁹ and worldwide atmospheric isoprene emissions are approximately 100 billion kg/year.¹³⁰ The magnitude of hydrocarbon production by plant life is sometimes not fully appreciated, especially as it exceeds that generated by human activity.^{131–133} Rayleigh or Tyndall

scattering of sunlight from atmospheric isoprene gives rise to the eponymous blue haze observed in the Blue Ridge Mountains even on otherwise clear days; such blue hazes were also described in the notebooks of Leonardo Da Vinci,¹³⁴ who incorporated this feature into artwork such as the *Mona Lisa* (Figure 25) and the *Madonna of the Yarnwinder* (*Lansdowne Madonna*).

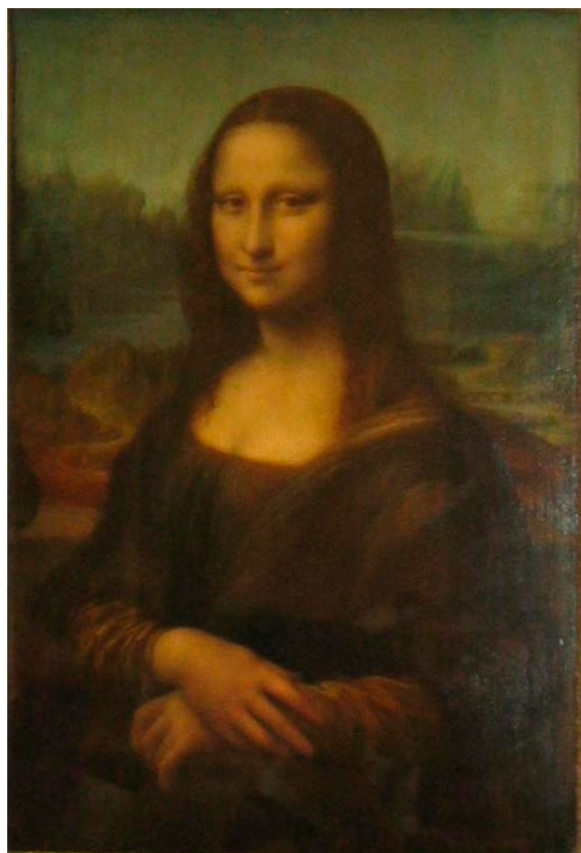


Figure 25. *Mona Lisa*. Leonardo da Vinci, ca. 1503. Oil on wood panel. Although somewhat yellowed, the faint blue haze in the background was inspired by the isoprene-derived blue haze in the hills of the Tuscan countryside, as recorded in Leonardo's notebooks. For comparison, a higher-resolution version of this painting is available from ref 547.

Isoprene is also generated by certain bacteria and is generated at particularly high levels by *Bacillus subtilis*.¹³⁵ Additionally, isoprene is the principal hydrocarbon identified in human breath,¹³⁶ exhaled isoprene concentrations in a crowded football stadium are sufficiently high that they are measured to spike when goals are scored or when other exciting events occur on the field of play that inspire the roar of the crowd.¹³⁷ Isoprene in human breath is also being studied as a biomarker for high cholesterol levels,^{138–140} muscular dystrophy,¹⁴¹ fibrotic liver disease,¹⁴² diabetes,¹⁴³ and lung cancer.¹⁴⁴ In bacteria and plants, isoprene is generated by isoprene synthase, a hemiterpene synthase.^{145–147} No human isoprene synthase enzyme is known, but nonenzymatic solvolysis of DMAPP may account for some,¹³⁸ but not all,¹⁴⁵ isoprene generation. It is conceivable that the 1,4-conjugate elimination reaction of DMAPP is catalyzed to some degree by another terpenoid biosynthetic enzyme *in vivo*, particularly given the correlation between isoprene and cholesterol levels.^{138–140}

Plant isoprene synthase is a Mg^{2+} -dependent class I terpenoid synthase.^{148–150} The enzyme from the gray poplar hybrid *Populus × canescens* has been cloned and expressed in *E. coli*.¹⁵¹ The crystal structure of this enzyme reveals a dimer of 64-kD subunits, each of which exhibits $\alpha\beta$ domain architecture (Figure 26).¹⁵² Dimeric quaternary structure enables cooperativity in catalysis, since native isoprene synthase exhibits a sigmoidal kinetic profile with a Hill coefficient of 1.9.¹⁵² The crystal structure of the complex with the unreactive DMAPP analogue dimethylallyl-S-thiolodiphosphate reveals that three Mg^{2+} ions are coordinated by metal-binding motifs on helices D and H and the substrate diphosphate group.¹⁵² The first metal-binding motif on helix D, D³⁴⁵DXXD, coordinates to Mg^{2+}_A and Mg^{2+}_C and is similar to the aspartate-rich motif first identified in prenyltransferases; the second metal-binding motif on helix H has a divergent amino acid sequence, N⁴⁸⁹DXXSXXE, which chelates Mg^{2+}_B (metal ligands are in boldface) and is referred to as the NSE motif. While two aspartate-rich DDXXD metal-binding motifs almost always signal a prenyltransferase, the combination of one DDXXD motif and one NSE motif generally signals a lyase or cyclase enzyme. The substrate binding cleft of isoprene synthase is hydrophobic and relatively shallow to confer specificity for the C_5 substrate, and the base of the cleft is largely defined by the aromatic side chains of F338 and F485 (Figure 27).

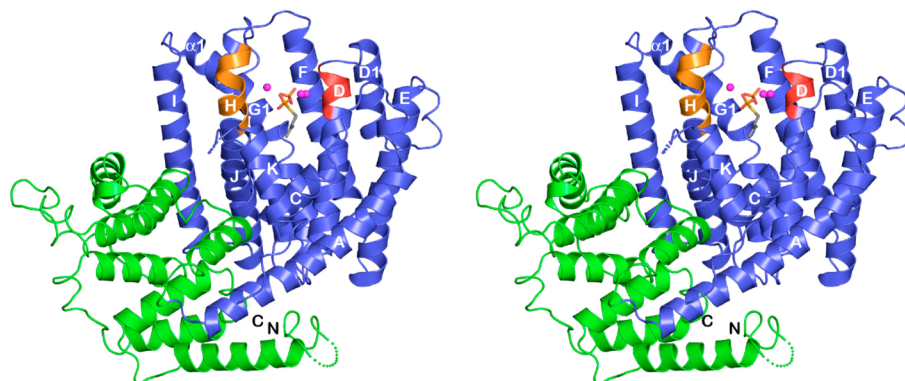


Figure 26. Stereoview showing that each isoprene synthase monomer adopts $\alpha\beta$ domain architecture, in which the α domain (blue) contains the characteristic aspartate-rich (red) and NSE (orange) metal-binding motifs. The substrate analogue dimethylallyl-S-thiolodiphosphate (stick figure) and 3 Mg^{2+} ions (magenta spheres) are bound in the active site. The β domain has no known catalytic function. Reprinted with permission from ref 152. Copyright 2010 Elsevier.

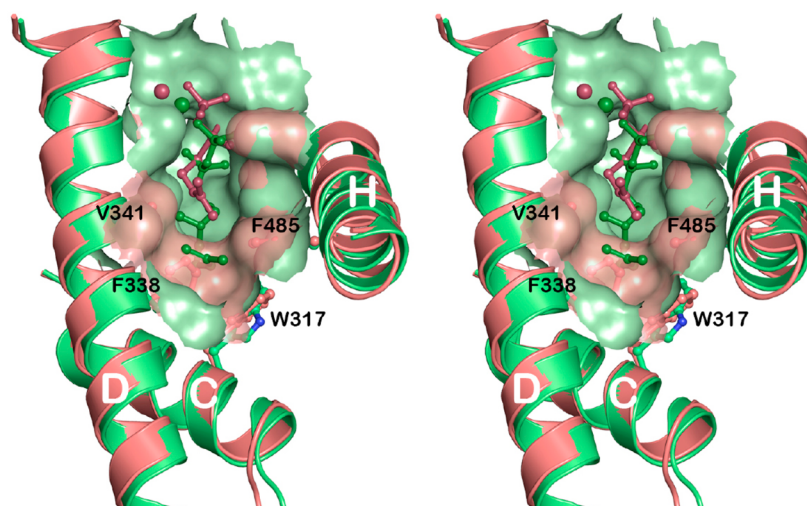


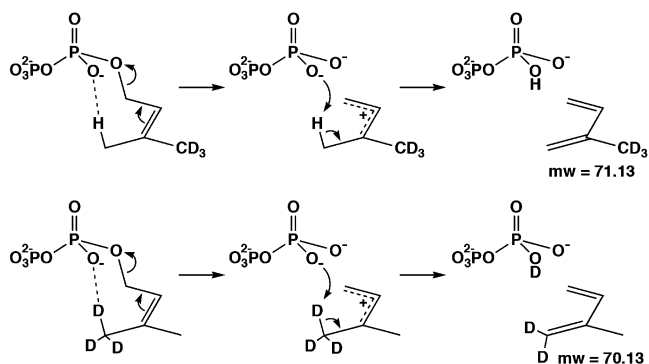
Figure 27. Stereoview showing a cut-away view of the active site surface of isoprene synthase complexed with the unreactive substrate analogue dimethylallyl-*S*-thiolodiphosphate (salmon) superimposed on the crystal structure of the monoterpene cyclase bornyl diphosphate synthase complexed with an unreactive analogue of GPP. The active site cleft of isoprene synthase is much more shallow than that of bornyl diphosphate synthase, which reflects the specificity of these terpene synthases for C_5 and C_{10} substrates, respectively. Selected residues at the base of the active site cleft of isoprene synthase are indicated. Reprinted with permission from ref 152. Copyright 2010 Elsevier.

The conformation of the bound substrate analogue in the active site of isoprene synthase suggests that the diphosphate group of DMAPP is ideally located to serve as the general base to deprotonate the allylic cation resulting from metal-triggered DMAPP ionization.¹⁵² While the α -phosphate group of the diphosphate group is closest to the (*Z*)-methyl group of the allylic cation, potentially indicating regioselective proton elimination to generate isoprene, recent studies using isotopically labeled DMAPP¹⁵³ indicate that this elimination reaction is not regioselective (Figure 28).¹⁵⁴

Isoprene synthase has become very important in recent years in biotechnology, since isoprene is a critical starting material for the generation of synthetic rubber for tire manufacturing. As the demand for synthetic rubber has increased in recent years, so too has the demand for isoprene increased. Since commercial feedstocks of isoprene derive mainly from petrochemical refinement, alternative sources of isoprene are being explored through metabolic engineering in bacteria and yeast to develop robust and renewable sources of isoprene.^{155–159} Such “bioisoprene” was used to manufacture the world’s first “green” rubber tire through a business collaboration between Goodyear and Genencor,¹⁶⁰ presented at the 2009 United Nations Climate Change Conference in Copenhagen, Denmark.

The 1,4-conjugate elimination reaction also occurs with substrates GPP and FPP (Figure 24; other regiomer elimination isomers can be formed as well), and these reactions are catalyzed in biological systems by myrcene synthase and (*E*)- β -farnesene synthase, respectively.^{161–165} Although crystal structures of these class I terpenoid synthases have not yet been reported, a separate farnesene synthase active site is found “moonlighting” in the structure of albaflavone synthase (but this bifunctional enzyme does not adopt the canonical α fold of a class I terpenoid synthase).¹⁶⁶ These enzymes are believed to operate through a mechanism similar to that of isoprene synthase, each proceeding through an allylic carbocation intermediate resulting from metal-triggered ionization of the diphosphate moiety. In the (*E*)- β -farnesene synthase reaction, Allemann and colleagues demonstrate that inorganic pyrophosphate can recombine with the initially formed allylic cation to

Regiospecific Elimination



Non-Regiospecific Elimination

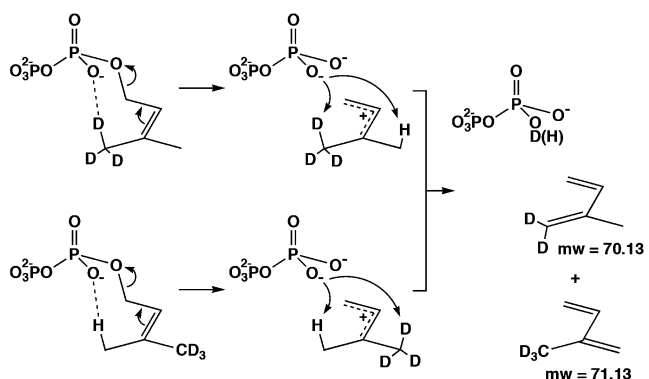


Figure 28. If the proton elimination step of isoprene synthase were regioselective then (*E*)-[4,4,4- 2H_3]DMAPP would exclusively yield [4,4,4- 2H_3]isoprene and (*Z*)-[4,4,4- 2H_3]DMAPP would exclusively yield [1,1- 2H_2]isoprene. However, each isotopically labeled substrate yields an equal mixture of both isotopically labeled products, indicating that proton elimination is nonregioselective. Reproduced from ref 154. Copyright 2012 American Chemical Society.

form a *trans*-nerolidyl diphosphate intermediate, which then reionizes to complete the elimination reaction.¹⁵⁴ Notably,

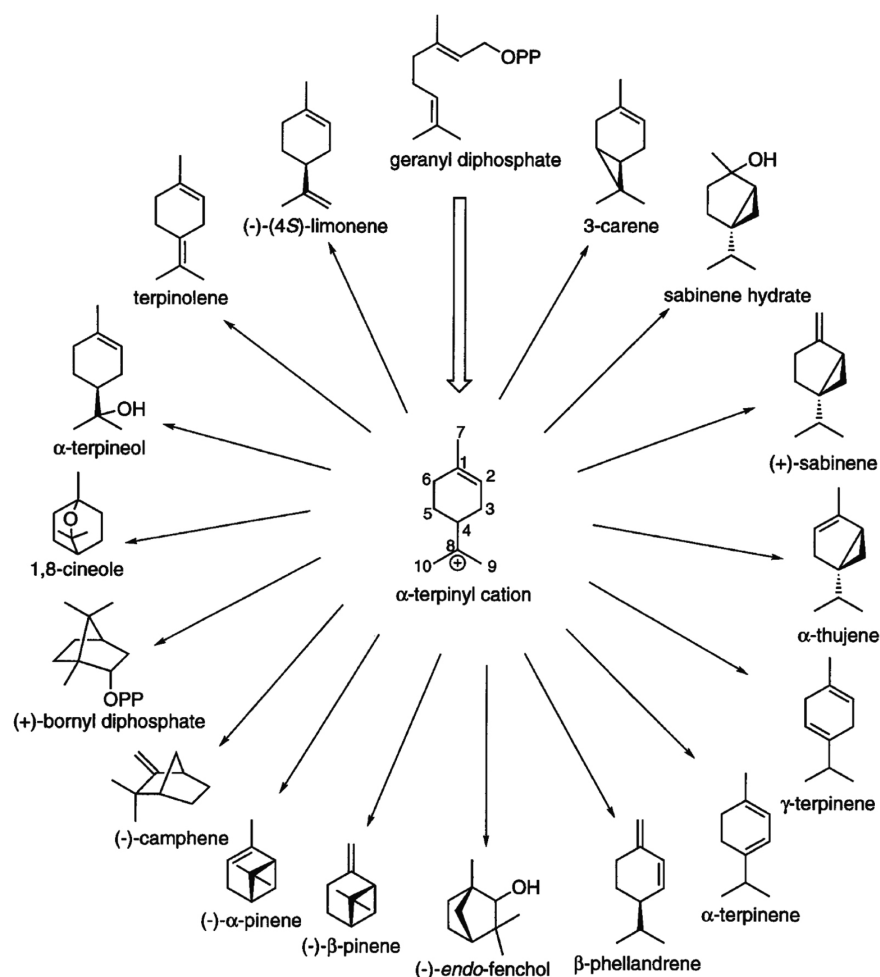


Figure 29. Cyclization of GPP through C1–C6 bond formation yields the α -terpinyl cation, which undergoes further reaction to yield a diverse array of cyclization products. Reprinted with permission from ref 9. Copyright 2000 Springer-Verlag.

farnesene synthase is currently utilized in a large-scale metabolic engineering process to generate farnesene-based jet fuel.^{167–169}

5. CLASS I TERPENOID CYCLASES

Class I terpenoid cyclases are metal-dependent enzymes that catalyze the cyclization of isoprenoid diphosphate substrates to form hydrocarbon products containing one or more fused rings and stereocenters. Class I terpenoid cyclases adopt the same α fold as that first observed in the crystal structure of avian FPP synthase.⁵⁸ These enzymes are found with α , $\alpha\beta$, and $\alpha\beta\gamma$ domain architectures, and bifunctional enzymes are found with $\alpha\alpha$ (class I-class I) and $\alpha\beta\gamma$ (class I-class II) domain architectures. Like FPP synthase, these cyclases contain metal-binding motifs on helices D and H on the upper walls of their active sites. However, while the first metal-binding motif on helix D is typically an aspartate-rich DDXXD motif, the second metal-binding motif on helix H is almost always (N,D)D(L,I,V)X(S,T)XXXE in a cyclase (boldface residues indicate metal ligands).¹⁷⁰ The second metal-binding motif is accordingly designated the NSE or DTE motif. As noted in section 4, isoprene synthase has DDXXD and NSE metal-binding motifs, so the presence of an NSE/DTE motif usually distinguishes isoprenoid diphosphate lyases and terpenoid cyclases from prenyltransferases containing two DDXXD metal-binding motifs such as FPP synthase (section 2). The remainder of this section outlines structure-mechanism relationships for class I terpenoid cyclases, focusing mainly on

cyclases with known crystal structures that utilize GPP, FPP, and GGPP substrates.

5.1. Monoterpene Cyclases

The C_{10} isoprenoid GPP (Figure 1) is the minimum-length cyclization substrate in terpenoid biosynthesis, and the monoterpene cyclization cascade typically proceeds through the α -terpinyl carbocation resulting from C1–C6 bond formation (Figure 29). A structurally and stereochemically diverse array of carbon skeletons result from subsequent reactions of this important intermediate as governed by its conformation, which in turn is enforced by the three-dimensional contour of the enzyme active site. The active site contour serves as a template for catalysis, ensuring that the substrate and intermediates adopt only those conformations leading to the formation of the correct product(s). Accordingly, active site contours are productlike, especially for high-fidelity cyclases, to ensure the generation of a specific product. Additionally notable is the role of water in the chemistry of GPP cyclization: the final carbocation intermediate in some monoterpene cyclization cascades is quenched by the addition of a solvent molecule, so this solvent molecule must be strictly controlled so that it does not prematurely quench carbocation intermediates in the cyclization cascade. Various aspects of these features are evident in structural and functional studies of monoterpene cyclases that have yielded crystal structures to date.

5.1.1. (+)-Bornyl Diphosphate Synthase. Isolated from *Salvia officinalis* (culinary sage), (+)-bornyl diphosphate synthase is a homodimer of 64-kD subunits that catalyzes an unusual reaction sequence, in that the substrate diphosphate group dissociates and rebinds to carbocation intermediates twice during the GPP cyclization cascade (Figure 30).¹⁷¹ Molecular details of

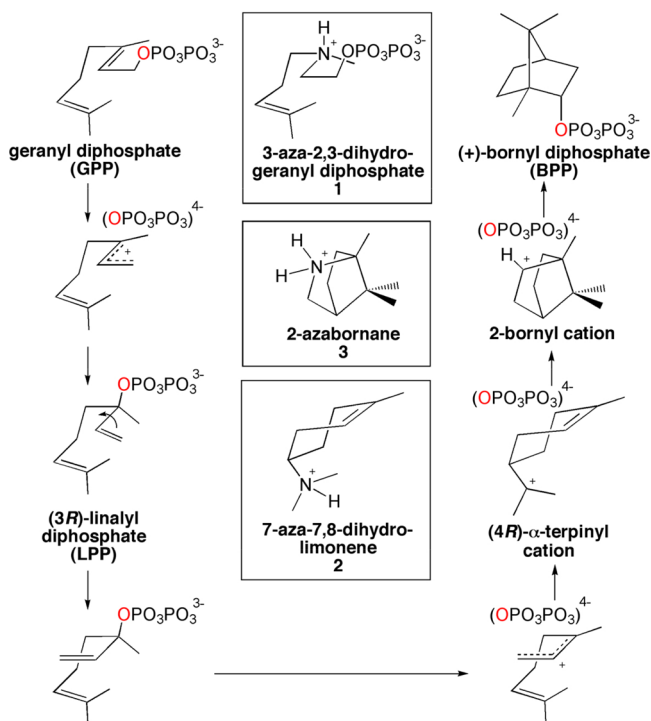


Figure 30. GPP cyclization cascade catalyzed by (+)-bornyl diphosphate synthase. Positional isotope exchange experiments show that the prenyl diphosphate ester oxygen atom of the substrate (red) is the same as that of the product. Aza analogues of carbocation intermediates are shown in boxes. Reprinted from ref 23. Copyright 2002 National Academy of Sciences.

the catalytic mechanism have been delineated in a variety of enzymological studies,^{172–175} including positional isotope exchange experiments conclusively demonstrating that the same diphosphate ester oxygen atom makes the prenyl linkage of substrate GPP and product (+)-bornyl diphosphate.^{176,177} Formation of the 6-membered ring of the α -terpinyl cation intermediate first requires isomerization of the C2–C3 double bond from a *trans* configuration to a *cis* configuration. This isomerization cannot occur directly, of course, due to the ~ 60 kcal/mol rotational barrier of the double bond. As summarized in Figure 30, this isomerization is achieved by metal-triggered ionization of GPP to form a *trans*-allylic cation intermediate, followed by readdition of inorganic pyrophosphate at C3 to yield linalyl diphosphate. Only when the C2–C3 single bond is fully formed can rotation occur from a *transoid* to a *cisoid* conformation which, following reionization to yield a *cis*-allylic cation intermediate, enables C1–C6 bond formation to generate the α -terpinyl cation. The conformation of this cation is held in such a way that a second carbon–carbon bond is formed to yield the 2-bornyl cation, which is ultimately quenched by readdition of inorganic pyrophosphate to yield (+)-bornyl diphosphate.

The crystal structures of (+)-bornyl diphosphate synthase and its complexes determined at resolutions of 2.0–2.4 Å were the first of a monoterpene cyclase and revealed $\alpha\beta$ domain

architecture²³ similar to that first observed in epi-aristolochene synthase.³⁷ Such $\alpha\beta$ domain architecture is characteristic for plant terpenoid cyclases. Two monomers of (+)-bornyl diphosphate synthase assemble in antiparallel fashion with an extensive dimer interface mediated by their α domains (Figure 31). Although this monoterpene cyclase is not an allosteric

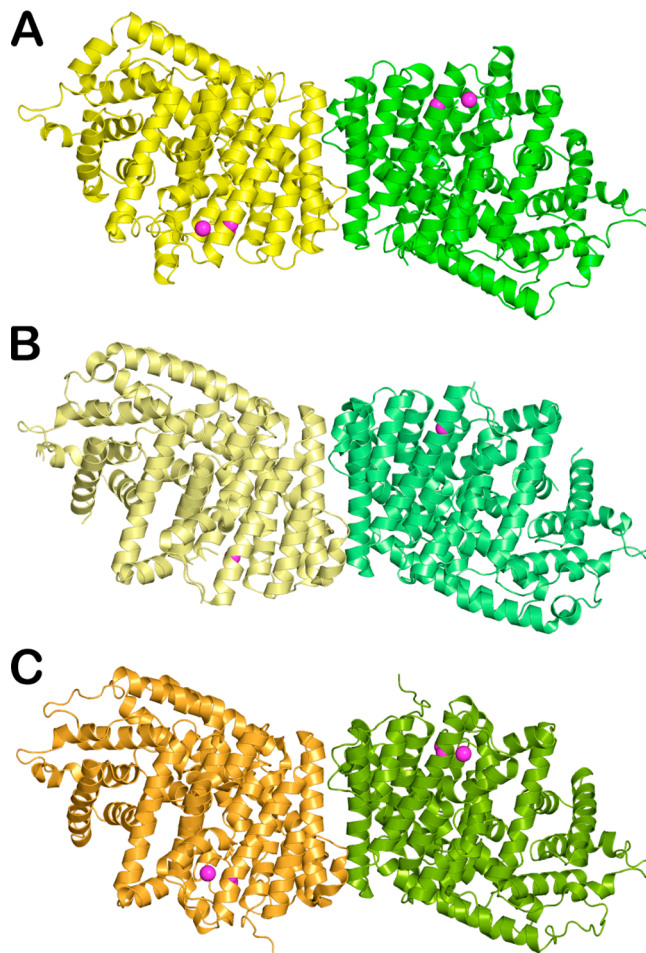


Figure 31. Isoprene synthase (A), (+)-bornyl diphosphate synthase (B), and (-)-limonene synthase adopt similar $\beta\alpha$ dimeric quaternary structures with more than 1000 Å² buried surface area at the dimer interface. Active sites in each dimer are oriented in antiparallel fashion (i.e., the active site of the subunit on the left opens toward the bottom and the active site of the subunit on the right opens toward the top), as indicated by bound metal ions (magenta) at the mouth of each active site. Reprinted with permission from ref 152. Copyright 2010 Elsevier.

enzyme, it is interesting that its quaternary structure is identical to that of isoprene synthase, which exhibits cooperativity in the 1,4-conjugate elimination reaction with DMAPP (section 4). It is further interesting to note that this quaternary structure is also shared with other dimeric plant monoterpene cyclases such as (-)-limonene synthase (section 5.1.2) (Figure 31). More recently, identical quaternary structures have been observed for the $\alpha\beta$ monoterpene cyclases (+)-limonene synthase (section 5.1.3) and γ -terpinene synthase (section 5.1.4), so the common quaternary structures illustrated in Figure 31 may represent a universal dimerization mode for plant terpenoid cyclases with $\alpha\beta$ domain architecture.

Crystal structures of several complexes of (+)-bornyl diphosphate synthase complexed with inorganic pyrophosphate,

aza analogues of carbocation intermediates (illustrated in Figure 30), and the product (+)-bornyl diphosphate show that 3 Mg^{2+} ions liganded by DDXXD and DTE motifs hold a diphosphate group rigidly in place, effectively capping the mouth of the active site cavity (Figure 32).²³ Assisting the metal ions in diphosphate

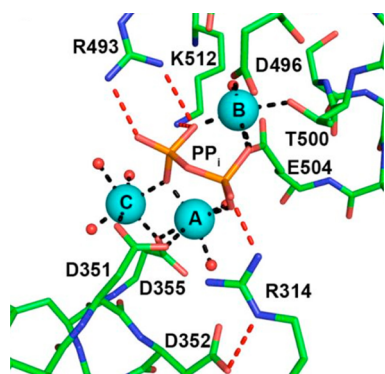


Figure 32. Three metal ions and three basic residues (R314, R493, and K512) are critical for the molecular recognition of the diphosphate group in the active site of (+)-bornyl diphosphate synthase. This is a common theme for diphosphate recognition in the active sites of other terpenoid synthases as well. Reprinted with permission from ref 66. Copyright 2010 International Union of Pure and Applied Chemistry.

complexation are three basic residues, R314, R493, and K512. Thus, 3 metal ions and 3 basic residues comprise a diphosphate recognition motif in the active site of this and other terpenoid cyclases.⁶⁶ Comparison of the unliganded and liganded enzyme

structures reveals that the binding of 3 metal ions and the diphosphate group triggers a conformational change from an open to a closed active site conformation (Figure 33). The second aspartate in the DDXXD motif, D352, hydrogen bonds with R314 to stabilize the closed active site conformation; since R314 also donates a hydrogen bond to the diphosphate group, this interaction directly links the binding of the substrate diphosphate group with active site closure. The conformational change from an open active site conformation to a closed active site conformation ensures that highly reactive carbocation intermediates in catalysis are protected from bulk solvent, and such a conformational change is common to all class I terpenoid synthases. Similar conformational changes are observed in FPP synthase upon ligand binding in the active site (section 2.1).

The active site of (+)-bornyl diphosphate synthase serves as a template that strictly enforces the left-handed helical conformation of GPP required for the generation of (+)-bornyl diphosphate via the (4*R*)- α -terpinyl cation. However, the template is not completely perfect, and minor quantities of alternative cyclic monoterpenes such as pinenes, camphene, and limonene are also generated.¹⁷¹ Interestingly, F578 and W323 form part of the active site contour, and they may also stabilize carbocation intermediates through cation- π interactions. Two or three aromatic residues are typically found in most terpenoid cyclase active sites where they may serve this function, stabilizing high-energy carbocation intermediates as well as the transition states flanking these intermediates.

Surprisingly, a water molecule (no. 110) is trapped in the active site of (+)-bornyl diphosphate synthase in the crystal structures of all enzyme-ligand complexes, including the complex

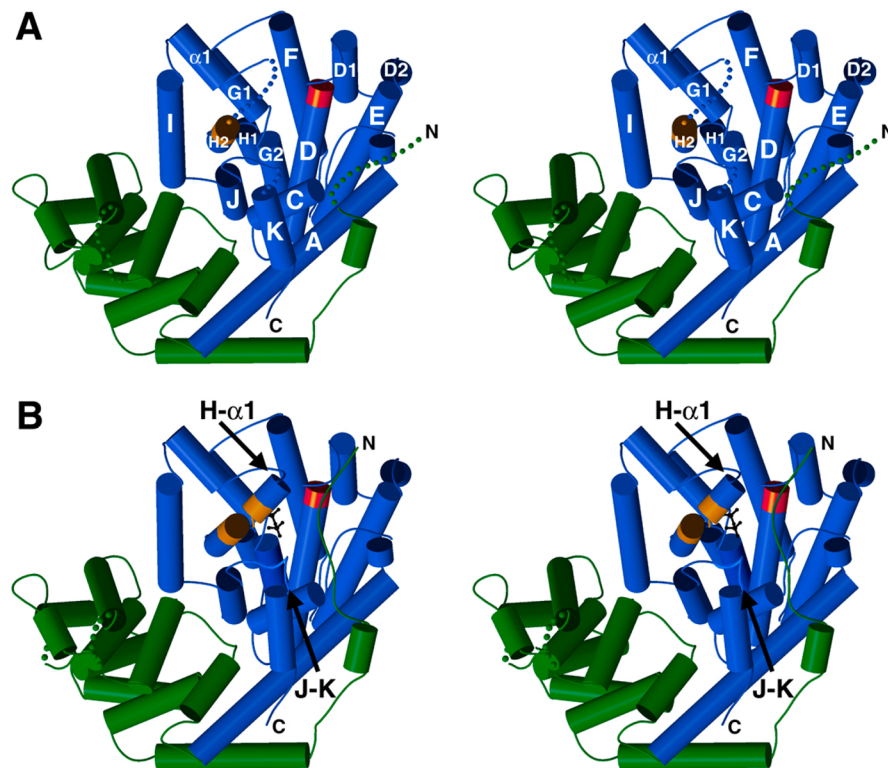


Figure 33. (A) Stereoview of unliganded (+)-bornyl diphosphate synthase, looking into the active site in the α domain (blue). Disordered polypeptide segments are indicated by dotted lines and include the N-terminal segment of the β domain (green). Aspartate-rich and DTE metal-binding motifs are red and orange, respectively. (B) Stereoview of the (+)-bornyl diphosphate synthase- Mg^{2+} -inorganic pyrophosphate complex. Comparison with the unliganded structure in (A) reveals conformational changes that completely enclose the active site. These conformational changes include the ordering of the N-terminal segment, which helps cap the active site. Reprinted from ref 23. Copyright 2002 National Academy of Sciences.

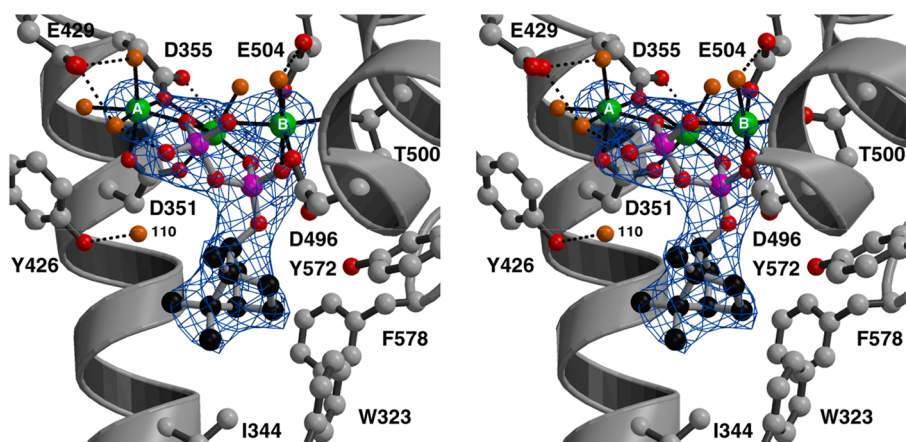


Figure 34. Stereoview of the simulated annealing electron density map of the (+)-bornyl diphosphate synthase- Mg^{2+}_3 -(+)-bornyl diphosphate complex. Metal coordination and hydrogen bond interactions are indicated by solid and dashed black lines, respectively. Water molecule no. 110 remains trapped in the active site in all enzyme-ligand complexes, including this complex with the monoterpene product. Reprinted from ref 23. Copyright 2002 National Academy of Sciences.

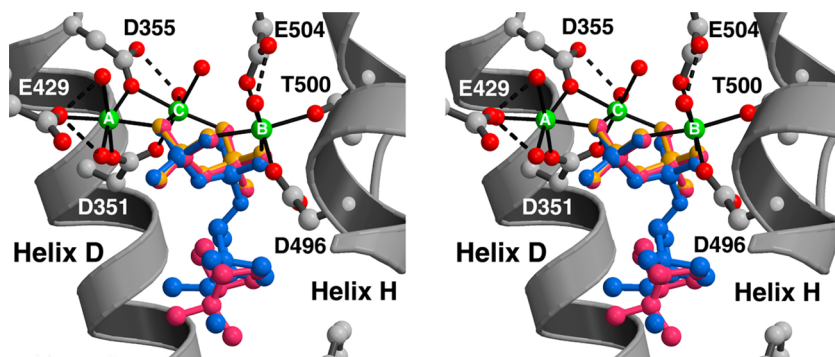
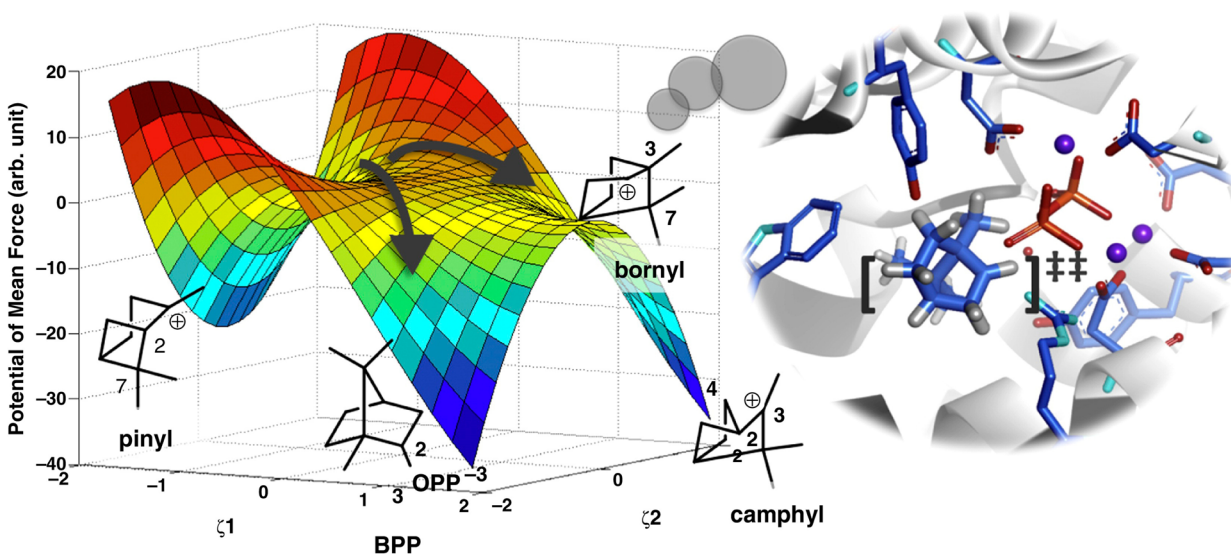


Figure 35. Stereoview of the superposition of the (+)-bornyl diphosphate synthase complexes with Mg^{2+}_3 and inorganic pyrophosphate (yellow), inorganic pyrophosphate and 2-azabornane (magenta), and (+)-bornyl diphosphate (blue). The molecular recognition of the diphosphate moiety is essentially identical in all complexes. Comparison of the latter two structures provides a “before and after” picture of the C–O bond-forming reaction that generates (+)-bornyl diphosphate. Reprinted from ref 23. Copyright 2002 National Academy of Sciences.



Current Opinion in Chemical Biology

Figure 36. Theoretical and computational chemistry studies indicate that the 2-bornyl cation is actually a transition state at a bifurcation point on the reaction coordinate leading to either (+)-bornyl diphosphate or the camphyl cation, which can undergo proton elimination to yield camphene. Reprinted with permission from ref 182. Copyright 2014 Elsevier.

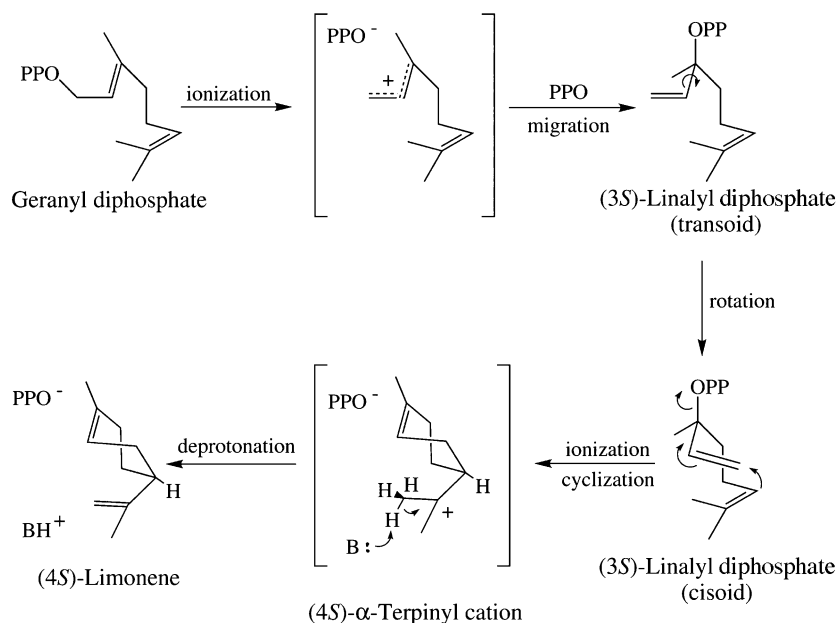


Figure 37. Proposed mechanism of GPP cyclization catalyzed by (–)-(4S)-limonene synthase. Reprinted from ref 190. Copyright 2007 National Academy of Sciences.

with product (+)-bornyl diphosphate itself.²³ This water molecule forms hydrogen bonds with the diphosphate group of the ligand, Y426, and the backbone carbonyl of S451. This water molecule, located near the geminal-dimethyl group of (+)-bornyl diphosphate (Figure 34), likely remains bound in the active site upon binding of the actual substrate GPP and is presumably restrained in place so that it cannot prematurely quench carbocation intermediates in the cyclization cascade. Thus, a trapped water molecule can serve as part of the active site contour in a terpenoid cyclase, contributing to the conformational control of substrate binding. In terpenoid cyclases that generate hydroxylated products, the precise control of a trapped water molecule is critically important for the fidelity of the cyclization cascade in generating the desired product.

Curiously, some aza analogues of carbocation intermediates illustrated in Figure 30 do not bind in catalytically productive conformations. For example, 3-aza-2,3-dihydrogeranyl diphosphate does not bind with the left-handed helical conformation that would be required for GPP to generate the (4R)- α -terpinyl cation intermediate. This phenomenon is not uncommon for the binding of flexible unreactive substrate analogues in terpenoid cyclase active sites and may result from the imperfect mimicry between the analogue and the substrate or intermediate after which it is designed. Moreover, the thermodynamically stable structure corresponding to a crystalline enzyme-analogue complex at equilibrium does not necessarily correspond to the structure of the enzyme-carbocation intermediate complex with the lowest accessible transition state. In other words, achieving productive conformations along a reaction pathway during catalysis is under kinetic control and not thermodynamic control. This distinction may account for anomalous binding modes observed for certain unreactive analogues of natural carbocation intermediates.¹⁷⁸

Notably, however, other analogues bind in a productive fashion. For example, the (+)-bornyl diphosphate synthase-Mg²⁺₃-2-azabornane complex aligns nearly perfectly with that of the complex with 3 Mg²⁺ ions and the actual product, (+)-bornyl diphosphate, comparison of these two structures serves as a

“before and after” picture of the C–O bond-forming reaction with the 2-bornyl cation (Figure 35).

The reaction mechanism of (+)-bornyl diphosphate synthase has been studied extensively using theoretical and computational methods.^{179–182} Notably, these studies indicate that the 2-bornyl cation represents a transition state, rather than an actual intermediate, that follows the formation of an intermediate pinyl cation; moreover, Major and Weitman show that the 2-bornyl cation is a bifurcation point on the free energy surface that can lead to formation of product (+)-bornyl diphosphate or side product camphene via the camphyl cation (Figure 36).¹⁸¹ This sort of bifurcation was first observed in theoretical and computational studies of terpenoid biosynthesis in studies of diterpene synthase mechanisms by Hong and Tantillo.¹⁸³ In (+)-bornyl diphosphate synthase, a bifurcated free energy surface is one factor that can compromise cyclization fidelity by enabling the formation of alternate side products, as long as the conformations required to generate them can be accommodated by the active site template. If the 2-bornyl cation represents a transition state rather than an intermediate in the catalytic mechanism, then 2-azabornane is a productlike transition state analogue.

5.1.2. (–)-Limonene Synthase. The generation of (–)-limonene is perhaps the simplest cyclization reaction catalyzed by a class I terpenoid cyclase, since the α -terpinyl carbocation intermediate merely undergoes an E1 elimination reaction (Figure 37). Notably, the terpinyl carbocation in this reaction is the enantiomer of that formed in the (+)-bornyl diphosphate synthase reaction (Figure 30), indicating that the active site template of (–)-limonene synthase enforces a right-handed binding conformation for substrate GPP. (–)-Limonene synthase from *Mentha spicata*^{184–188} is a high-fidelity enzyme and generates 94% (–)-limonene; approximately 4% pinene isomers and 2% myrcene side products are also generated, the latter of which reflects unsuccessful C1–C6 bond formation.¹⁸⁹

The crystal structure of (–)-limonene synthase determined at 2.7 Å resolution reveals a tertiary structure with $\alpha\beta$ domain architecture and dimeric $\beta\alpha:\alpha\beta$ quaternary structure identical to

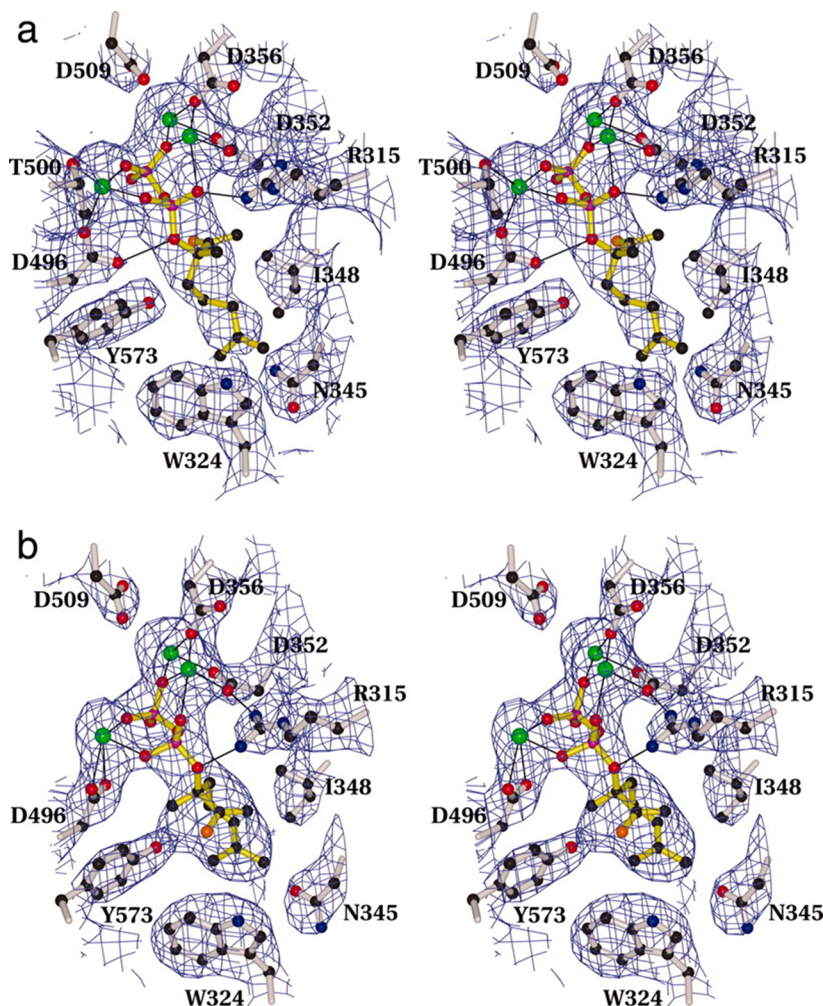


Figure 38. (a) Stereoview of an electron density map calculated with Fourier coefficients $2|F_o| - |F_c|$ and phases calculated from the final model showing (–)-limonene synthase complexed with substrate analogue 2-fluorolinalyl diphosphate generated enzymatically from 2-fluorogeranyl diphosphate. The analogue binds in an extended conformation that is not productive with regard to the cyclization reaction. (b) Stereoview of an electron density map calculated with Fourier coefficients $2|F_o| - |F_c|$ and phases calculated from the final model showing (–)-limonene synthase complexed with substrate analogue 2-fluorolinalyl diphosphate prepared by direct cocrystallization. The analogue binds in a helical conformation that is productive for the cyclization reaction. Reprinted from ref 190. Copyright 2007 National Academy of Sciences.

that observed for isoprene synthase and (+)-bornyl diphosphate synthase (Figure 31).¹⁹⁰ The β domain has no known catalytic function, so it is probably an evolutionary vestige; however, the N-terminal polypeptide segment can assist in stabilizing the closed active site conformation, as observed in the crystal structure of (+)-bornyl diphosphate synthase.²³ Intron conservation patterns in plant terpenoid cyclases suggest that $\alpha\beta$ cyclases evolved from ancestral $\alpha\beta\gamma$ cyclases in which both domains were catalytically active.¹⁹¹ A modern-day example of such a bifunctional $\alpha\beta\gamma$ cyclase is abietadiene synthase, which catalyzes an overall reaction sequence involving an initial class II cyclization reaction followed by a class I cyclization reaction (section 7.2).^{45,192}

Surprisingly, cocrystallization of (–)-limonene synthase with the substrate analogue 2-fluorogeranyl diphosphate yields the structure of the complex with 2-fluoro-(3*S*)-linalyl diphosphate.¹⁹⁰ While fluorination of the substrate at C2 is intended to destabilize and thwart formation of the allylic cation that would be formed upon substrate ionization, Croteau and colleagues demonstrate that this substrate analogue is slowly reactive in solution and in the crystal.¹⁹⁰ The direct cocrystallization of

(–)-limonene synthase with racemic 2-fluorolinalyl diphosphate yields an electron density map that can be fit with either enantiomer in helical conformations required for cyclization to products of respective stereochemistry. Interestingly, cocrystallization of (–)-limonene synthase with 2-fluorogeranyl diphosphate yields the crystal structure of bound 2-fluorolinalyl diphosphate with a catalytically nonproductive conformation. The relatively low 2.7 Å resolution of these crystal structure determinations limits the interpretation of electron density maps (Figure 38), but these maps nonetheless show how the binding conformations of 2-fluorolinalyl diphosphate differ depending on how the complexes were prepared. This observation may suggest that the substrate need not be in the productive helical conformation required for cyclization in the first step of the reaction, the isomerization of geranyl diphosphate to linalyl diphosphate. Indeed, an extended conformation may be required for this isomerization step, since a helical conformation could conceivably hinder the allylic diphosphate isomerization and transoid-cisoid conformational change preceding the cyclization step (two different substrate conformations are similarly implicated in the isomerization and cyclization steps of

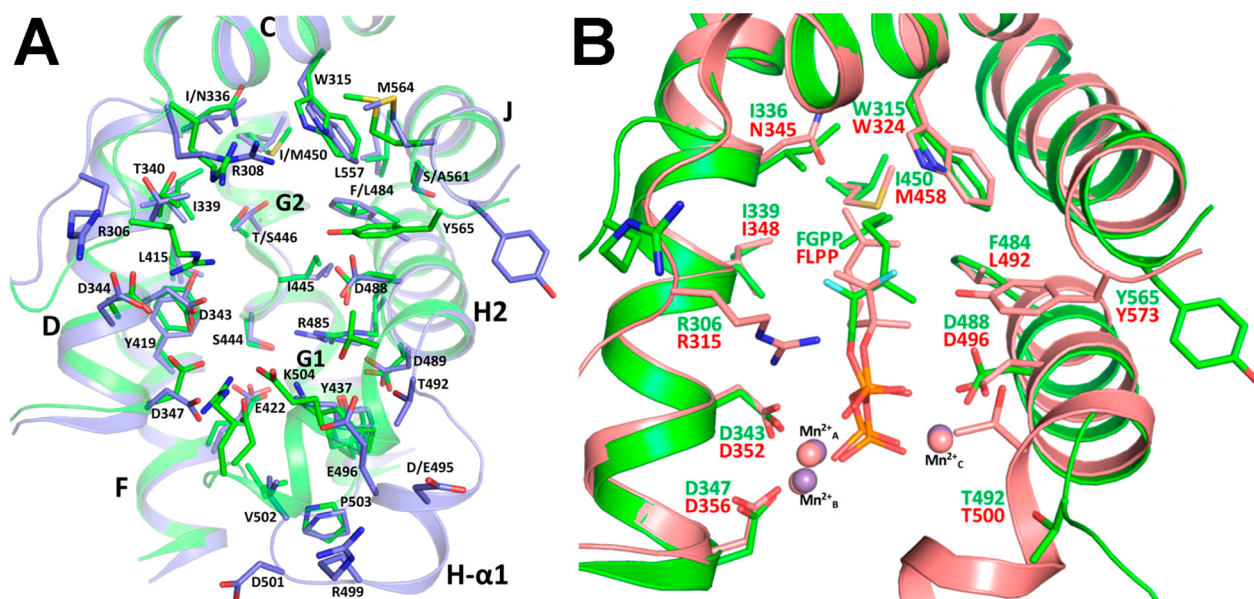


Figure 39. (A) Comparison of (+)-limonene synthase (blue) and (-)-limonene synthase (green) showing that most active site residues are conserved. Reproduced from ref 194. Copyright 2017 American Chemical Society. (B) Superposition of the (+)-limonene synthase-2-fluorogeranyl diphosphate complex (green) and the (-)-limonene synthase-2-fluorolinalyl diphosphate complex (salmon). Active site residues M458/I450 and N345/I336 of (-)-limonene synthase/(+)-limonene synthase appear to be the principal determinants of right-handed/left-handed helical conformations of the substrate leading to formation of the proper limonene stereoisomer. Reproduced from ref 195. Copyright 2017 American Chemical Society.

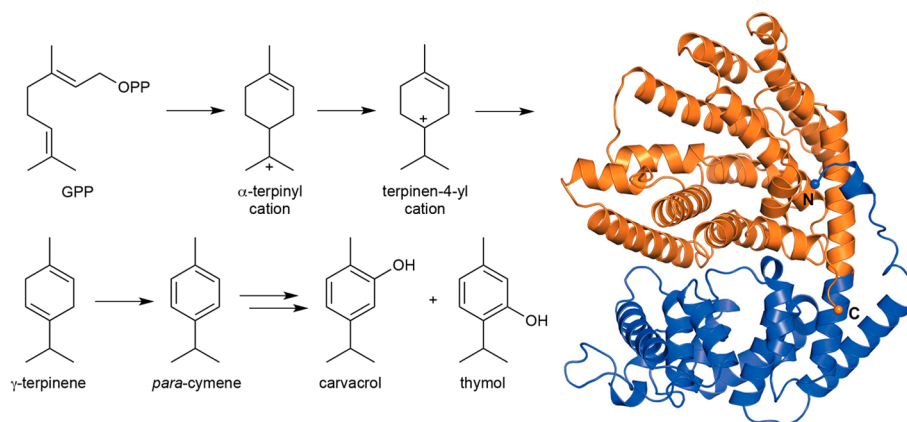


Figure 40. Cyclization reaction catalyzed by γ -terpinene synthase is the first committed step in the biosynthesis of carvacrol and thymol. This monoterpene cyclase adopts the characteristic $\alpha\beta$ domain architecture of a plant monoterpene cyclase. Reprinted from ref 199. Copyright 2016 International Union of Crystallography.

amorphadiene synthase¹⁹³). The catalytically productive helical conformation can then be achieved after the isomerization step to complete the cyclization sequence.¹⁹⁰

5.1.3. (+)-Limonene Synthase. Recently, the crystal structures of unliganded (+)-limonene synthase from navel orange (*Citrus sinensis*) and its complexes with fluorinated substrate analogues have been reported at resolutions of 2.2–2.4 Å.^{194,195} These structures reveal the characteristic $\alpha\beta$ fold of a plant terpenoid cyclase with dimeric quaternary structure. However, even though 3 Mn²⁺ ions are bound in the complexes with fluorinated substrate analogues, the enzyme active site remains in the open conformation, apparently blocked from forming a fully closed conformation by crystal lattice contacts. Even so, comparison with the crystal structure of (-)-limonene synthase complexed with 2-fluorolinalyl diphosphate (45% amino acid sequence identity) provides an excellent opportunity for studying the active site closure mechanism. Structural

changes triggered by the binding of substrate analogue and 3 metal ions are generally similar to those observed in (+)-bornyl diphosphate synthase (Figure 33).²³ Interestingly, however, the side chain of highly conserved residue Y565 on helix J of (-)-limonene synthase undergoes a conformational transition from an “out” conformation in the unliganded enzyme to an “in” conformation in the analogue-bound enzyme. The Y565F mutant exhibits a 50-fold loss of catalytic activity, but the molecular basis of Y565 function is not yet fully established. Oprian and colleagues suggest that it might help block water from entering the active site, stabilize reaction intermediates, and/or stabilize metal ion binding through hydrogen bonding to an aspartate metal ligand.¹⁹⁴

The crystal structures of (+)-limonene synthase and (-)-limonene synthase are the first to be solved of terpenoid cyclases that generate product enantiomers. The generation of (+)-limonene requires a left-handed binding conformation for

substrate GPP and intermediate linalyl diphosphate, whereas the generation of (–)-limonene requires a right-handed binding conformation for substrate GPP and intermediate linalyl diphosphate (Figure 37). Despite the dramatically different substrate binding conformations required for catalysis, it is striking that the amino acid residues lining the active sites of (+)-limonene synthase and (–)-limonene synthase are highly conserved (Figure 39).¹⁹⁴ What, then, provides the stereochemical imperative for substrate binding and catalysis?

On the basis of analysis of enzyme complexes with fluorinated analogues, Oprian and colleagues suggest that active site residues M458/I450 and N345/I336 of (–)-limonene synthase/(+)-limonene synthase govern stereospecificity of the respective GPP cyclization cascades.¹⁹⁵ The δ atom of the M458 side chain would sterically clash with the terminal methyl groups of 2-fluorolinalyl diphosphate if it adopted an incorrect left-handed conformation in the active site of (–)-limonene synthase, and the γ 2 group of I336 would similarly clash with the terminal methyl groups of 2-fluorogeranyl diphosphate if it adopted an incorrect right-handed conformation in the active site of (+)-limonene synthase (Figure 39). This is an elegant demonstration showing how the active site contour of a terpenoid cyclase is a template that directs structure and stereochemistry in a cyclization cascade.

5.1.4. γ -Terpinene Synthase. The generation of γ -terpinene from GPP proceeds through the universal α -terpinyl cation (Figure 29), which then undergoes a 1,2-hydride shift to yield the terpinen-4-yl cation, which after endocyclic proton elimination yields γ -terpinene (Figure 40). This reaction is important in the biosynthetic pathways of carvacrol and thymol, antimicrobial monoterpene phenols responsible for the distinctive odors and flavors of oregano and thyme, respectively.^{196,197} To date, γ -terpinene synthase enzymes have been identified in several plant species.¹⁹⁸

Recently, γ -terpinene synthase from *Thymus vulgaris* (common thyme) has been cloned and expressed, and its crystal structure has been determined in the unliganded state at 1.65 Å resolution.¹⁹⁹ The crystal structure reveals the characteristic $\alpha\beta$ domain architecture (Figure 40) and $\beta\alpha:\alpha\beta$ dimeric quaternary structure of plant monoterpene and hemiterpene synthases. Although crystal structures of γ -terpinene synthase complexed with substrate analogues are not yet available, the structure of the unliganded enzyme will serve as a valuable reference point for understanding structure–activity relationships in site-specific mutants.

5.1.5. Cineole Synthase. Cineole, also known as 1,8-cineole or more popularly as eucalyptol, is the primary component of eucalyptus oil and has a pleasant spicy aroma and taste. Eucalyptol is also being explored as a potential therapeutic agent due to its anti-inflammatory and antioxidant properties.^{200,201} Although cineole derives from the universal cyclic monoterpene intermediate α -terpinyl cation (Figure 29), this cyclic monoterpene is unique in that the final product of the overall cyclization cascade is an ether. Strictly speaking, two cyclization sequences are catalyzed in the active site of cineole synthase: (1) a canonical metal-triggered class I GPP cyclization reaction leading to formation of the α -terpinyl cation, quenched by a water molecule trapped in the active site to form α -terpineol and (2) a protonation-induced cyclization reaction, in which the carbon–carbon double bond of α -terpineol is protonated to generate a tertiary carbocation intermediate which subsequently undergoes intramolecular attack by the hydroxyl group to yield cineol (Figure 41).

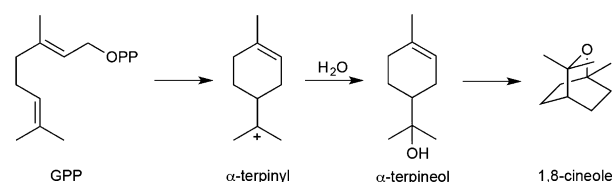


Figure 41. Reaction sequence catalyzed by the monoterpene cyclase cineole synthase. The ionization-dependent class I cyclization reaction of GPP forming α -terpineol is followed by a second protonation-induced cyclization reaction to yield 1,8-cineole.

The crystal structure of cineole synthase from *Salvia fruticosa* (Greek oregano) determined at 1.95 Å resolution in the unliganded state reveals characteristic $\alpha\beta$ domain architecture (Figure 42) and $\beta\alpha:\alpha\beta$ dimeric quaternary structure of plant monoterpene and hemiterpene synthases.²⁰² Although the crystal structure of cineole synthase provides limited mechanistic inferences in the absence of bound substrate analogues, superposition with (+)-bornyl diphosphate synthase complexed with the analogue 3-aza-2,3-dihydrogeranyl diphosphate²³ confirms the location of the active site (Figure 42). The authors suggest that a water molecule hydrogen bonded to N338 in cineole synthase is trapped in the enzyme active site along with GPP to facilitate hydroxylation of the α -terpinyl cation and formation of the α -terpineol intermediate.²⁰² However, the trapped water molecule hydrogen bonded to Y426 and inorganic pyrophosphate in (+)-bornyl diphosphate synthase (Figure 34) could similarly be trapped and hydrogen bonded to conserved residue Y420 and inorganic pyrophosphate in the active site of cineole synthase. Since this water molecule is located near the geminal dimethyl group of 2-azabornane and (+)-bornyl diphosphate, which accordingly would be in the vicinity of the geminal dimethyl group of the α -terpinyl cation intermediate, it is possible that this water molecule hydroxylates the α -terpinyl cation in the cineole synthase mechanism. Given the likely role of coproduct inorganic pyrophosphate as a potential general base-general acid catalyst,⁸⁰ inorganic pyrophosphate may deprotonate this water molecule upon hydroxylation of the α -terpinyl cation and then protonate the carbon–carbon double bond of α -terpineol to enable cineole formation as shown in Figure 41.

Kampranis and colleagues use the cineole synthase structure to guide intriguing protein engineering experiments.²⁰² The N338I substitution results in the generation of 48% sabinene and 37% limonene as major products, with no generation of hydroxylated products. The N338A substitution enlarges the active site and converts cineole synthase into a sesquiterpene synthase capable of utilizing FPP as a substrate, generating 49% *trans*- α -bergamotene as its major cyclic product. Thus, N338 appears to be a “hot spot” for the evolution of cyclization specificity and fidelity in this terpenoid cyclase.

5.1.6. Methylisoborneol Synthase. While the great majority of terpenoid cyclases utilize canonical C_{5n} isoprenoid diphosphate substrates such as GPP, there are occasional examples of cyclases capable of utilizing modified substrates in the laboratory or in nature. A rare example found in nature is methylisoborneol synthase from *Streptomyces coelicolor* A3(2), a monoterpene synthase that catalyzes the cyclization of a noncanonical C_{11} substrate to form 2-methylisoborneol (Figure 43). This unusual terpenoid is a potent odorant and is responsible for the musty smell of contaminated water,^{203–205} but it is also responsible for the pleasing, earthy aroma of Brie and Camembert cheeses.²⁰⁶ The novel cyclization substrate, 2-

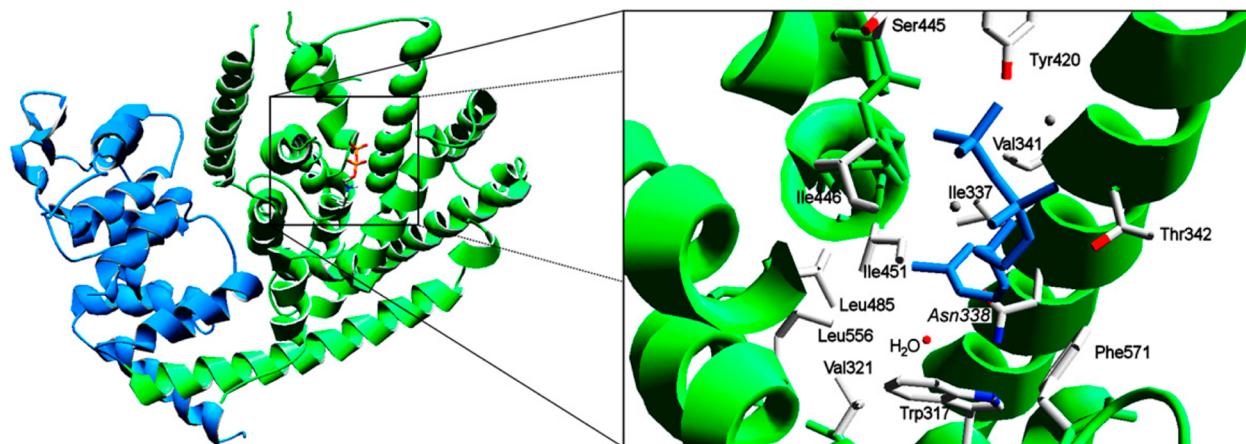


Figure 42. Structure of cineole synthase; the α domain is green and the β domain is blue. The inset shows a close-up view of the active site, with the bound conformation of 3-aza-2,3-dihydrogeranyl diphosphate modeled in based on the corresponding structure of its complex with (+)-bornyl diphosphate synthase. The water molecule hydrogen bonded to N338 (red) is proposed to be involved in catalysis. Reprinted with permission from ref 202. Copyright 2007 American Society of Plant Biologists.

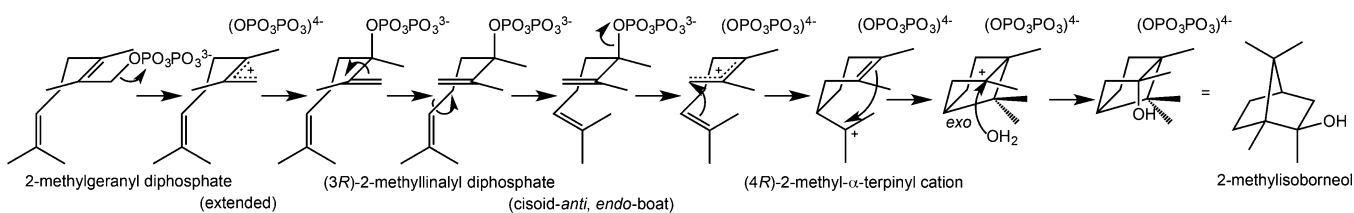


Figure 43. Reaction sequence catalyzed by monoterpene synthase methylisoborneol synthase, which utilizes the novel C_{11} substrate 2-methylgeranyl diphosphate. Isomerization to (3R)-2-methylallanyl diphosphate does not require the substrate to be in a cyclization-competent conformation. Reproduced from ref 213. Copyright 2013 American Chemical Society.

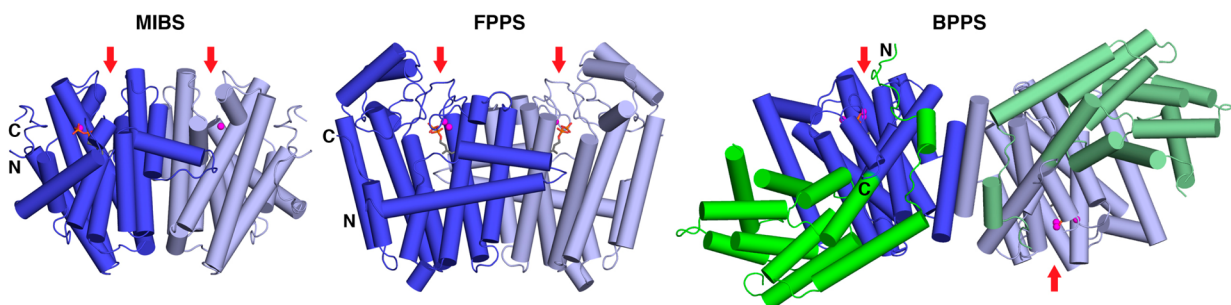


Figure 44. Dimeric quaternary structure of bacterial methylisoborneol synthase (MIBS), avian farnesyl diphosphate synthase (FPPS), and (+)-bornyl diphosphate synthase (BPPS). Catalytic α domains are blue, and the β domains of (+)-bornyl diphosphate synthase are green. Active sites cavities are indicated by red arrows and are oriented in parallel fashion (MIBS, FPPS) or antiparallel fashion (BPPS). Reproduced from ref 212. Copyright 2012 American Chemical Society.

methyl-GPP, derives from the *S*-adenosylmethionine-dependent methylation of GPP in a reaction catalyzed by geranyl diphosphate methyltransferase.^{207–211}

Methylisoborneol synthase is the first example of a naturally occurring terpenoid cyclase that utilizes a noncanonical acyclic substrate,^{209,210} and several orthologues are found in other bacterial and cyanobacterial species. The crystal structures of the unliganded enzyme and its complexes with the substrate analogues geranyl-*S*-thiolodiphosphate, 2-fluorogeranyl diphosphate, and 2-fluoroneryl diphosphate determined at resolutions of 1.8–2.0 Å reveal several unusual features.^{212,213} First, although most bacterial cyclases consist of a single α domain, methylisoborneol synthase contains an additional 13-kD N-terminal domain with more than 25% proline content; surprisingly, this domain is completely disordered in the crystal.

SDS–PAGE analysis confirms that this domain is present in the protein construct used for crystallization. The function of this proline-rich domain is unknown, but it is conserved in most methylisoborneol synthase orthologues; it is not found in any other enzyme.

Methylisoborneol synthase forms a dimer in which enzyme active sites are oriented in parallel fashion, similar to the parallel quaternary structure of FPP synthase but contrasting with the antiparallel quaternary structure of plant monoterpene cyclases such as (+)-bornyl diphosphate synthase (Figure 44). Even so, the same face of the α domain is utilized for dimerization in bacterial and plant terpenoid synthases, although different helices on this face of the protein can be involved. The crystal structures of complexes between methylisoborneol synthase and different substrate analogues reflect incomplete binding of metal ions by

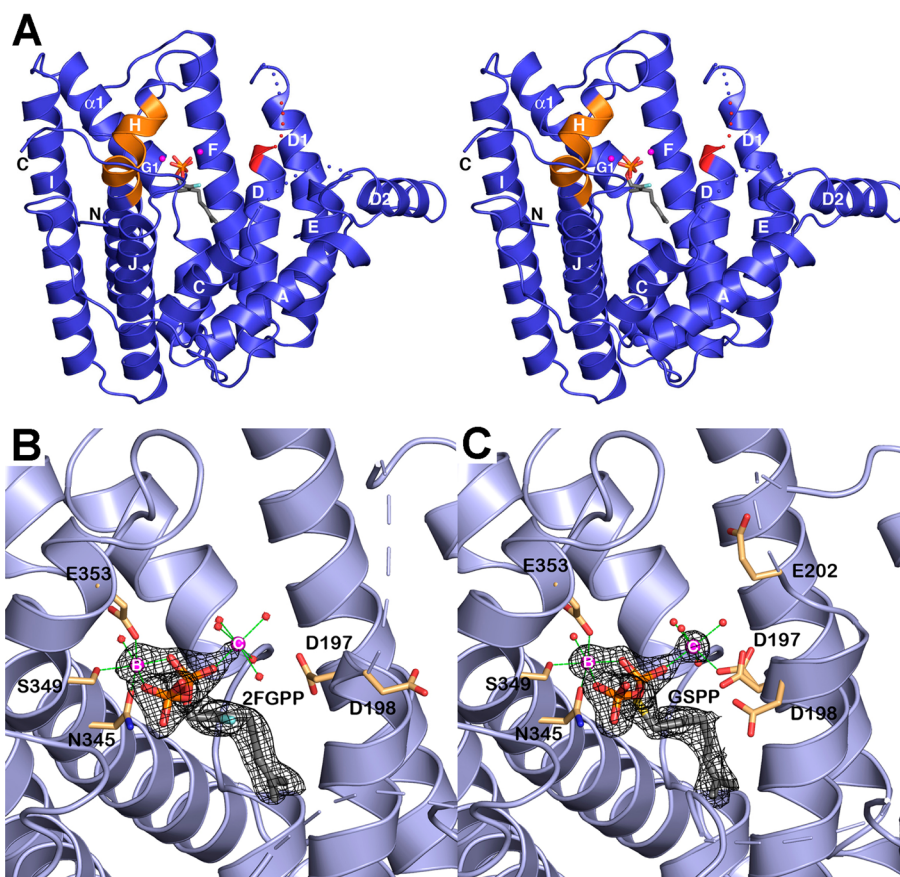


Figure 45. (A) Stereoview of the complex between methylisoborneol synthase and 2-fluorogeranyl diphosphate. The aspartate-rich and NSE metal-binding motifs are red and orange, respectively. (B) Simulated annealing omit map showing the binding of 2-fluorogeranyl diphosphate in the active site of methylisoborneol synthase. Only two metal ions bind in this complex; metal coordination interactions are indicated by thin green lines. (C) Simulated annealing omit map showing the binding of geranyl-*S*-thiolodiphosphate in the active site of methylisoborneol synthase. Here, too, only two metal ions bind; metal coordination interactions are indicated by thin green lines. Reproduced from ref 212. Copyright 2012 American Chemical Society.

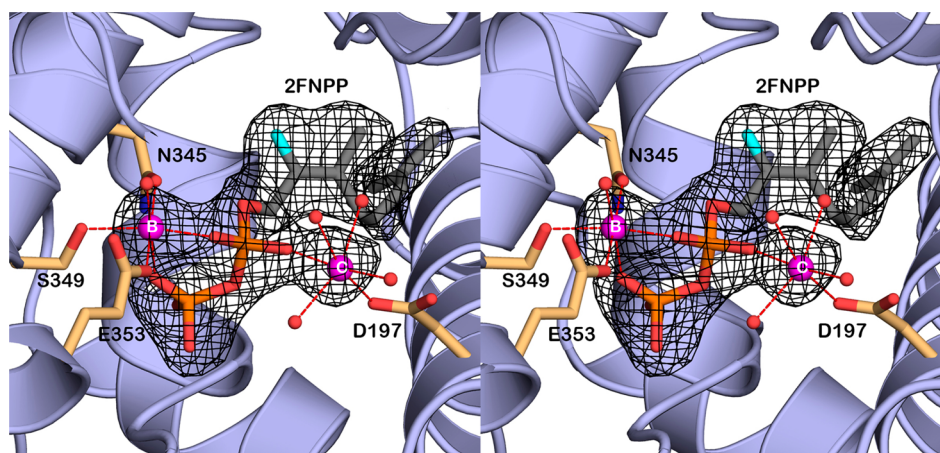


Figure 46. Stereoview of the simulated annealing omit map of 2-fluoroneryl diphosphate (2FNPP) bound in the active site of methylisoborneol synthase. Only two metal ions bind in this complex; metal coordination interactions are indicated by red dashed lines. This complex was obtained by cocrystallizing the enzyme with racemic 2-fluorolinalyl diphosphate, indicating that fluorination does not completely hinder ionization and formation of this catalytic intermediate. Reproduced from ref 213. Copyright 2013 American Chemical Society.

the aspartate-rich and NSE motifs on helices D and H, respectively; only Mg^{2+}_B and Mg^{2+}_C accommodate the diphosphate group of the substrate analogue, suggesting incomplete active site closure. Additionally, the enzyme must sequester a water molecule in the active site for use in quenching

the final carbocation intermediate, but no clues are evident in the active site structure as to where such a water molecule might reside during catalysis so as to not prematurely quench the cyclization cascade. A stereoview of the enzyme complex with 2-fluorogeranyl diphosphate is shown in Figure 45A, and electron

density maps showing the binding of this analogue as well as geranyl-S-thiolodiphosphate are found in Figure 45 (panels B and C, respectively).

Surprisingly, cocrystallization of methylisoborneol synthase with the fluorinated analogue of the tertiary allylic diphosphate intermediate, 2-fluorolinalyl diphosphate, yields the crystal structure of the complex with the primary *cis*-allylic diphosphate, 2-fluoroneryl diphosphate (Figure 46).²¹³ This unexpected reactivity indicates that fluorination does not completely block ionization of the diphosphate group or reaction of the resultant formed allylic cation. 2-Fluorolinalool is the major product isolated after incubation of methylisoborneol synthase with 2-fluorolinalyl diphosphate for 12 h; however, minor amounts of camphor are also detected, indicating that ionization and cyclization of the fluorinated substrate analogue can slowly proceed to yield 2-fluoroisoborneol, which rapidly eliminates HF to yield camphor.

5.2. Sesquiterpene Cyclases

In contrast with GPP cyclization reactions, which typically proceed through an ionization-recombination-reionization sequence to enable C1–C6 bond formation and generation of the α -terpinyl cation intermediate (Figure 29), FPP cyclization reactions can proceed through C1–C6, C1–C7, C1–C10, and C1–C11 bond forming reactions depending on which carbon–carbon double bond reacts with the initially formed allylic carbocation (Figure 47).²¹⁴ In turn, the resulting carbocation

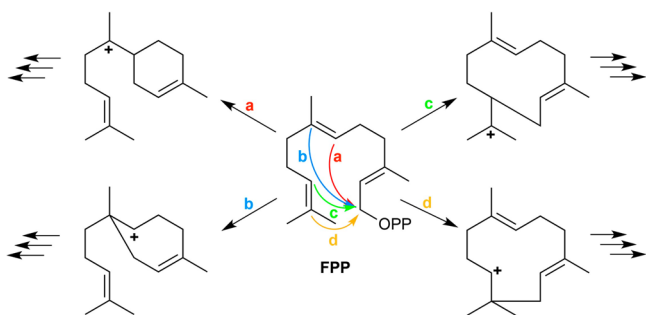


Figure 47. Possible trajectories of initial carbon–carbon bond formation in sesquiterpene cyclization reactions (OPP = diphosphate).

intermediate can undergo further cyclization reactions, hydride transfers, methyl migrations, etc., before termination of the reaction sequence. Thus, in comparison with monoterpene cyclization reactions, increasingly diverse arrays of carbon skeletons result from sesquiterpene cyclization reactions owing to the additional carbon–carbon bond-forming trajectories available to the larger substrate.

The active site contour in the α domain of an enzyme with overall α or $\alpha\beta$ domain architecture serves as a template for catalysis by a sesquiterpene cyclase, ensuring that substrate FPP and subsequently formed intermediates adopt only those conformations leading to formation of the correct product(s). Accordingly, active site contours are productlike, especially for high-fidelity cyclases, to ensure the generation of a specific product. Numerous sesquiterpene cyclases have yielded crystal structures in the past two decades, and each structure has advanced our understanding of the general features underlying the chemistry of terpenoid cyclization reactions in biology. Below, cyclases are discussed in order of complexity of their initial cyclization reactions, and then in order of increasing complexity of their overall cyclization cascades: C1–C6 cyclases

(α -bisabolol synthase, α -bisabolene synthase, epi-isozizaene synthase, trichodiene synthase); C1–C10 cyclases (selinadiene synthase, germacradien-4-ol synthase, aristolochene synthase, epi-aristolochene synthase, hedyeryol synthase, (+)- δ -cadinene synthase); and a C1–C11 cyclase (pentalenene synthase).

5.2.1. α -Bisabolol Synthase. The sesquiterpene alcohol α -bisabolol is responsible for many of the beneficial effects of chamomile (*Matricaria recutita*), a common herbal remedy.^{215,216} α -Bisabolol is reported to exhibit antibacterial and anti-inflammatory properties,^{217–219} and its derivatives are also potential cancer chemotherapeutic agents through their activity in blocking the expression of the serine/threonine kinase AKT.^{220–222} Interestingly, α -bisabolol is also a biosynthetic precursor of hernandulcin, a natural sweetener generated in the leaves of *Lippia dulcis*. Also known as *Phyla dulcis*, this plant is a perennial herb indigenous to Central America where it is also known as Aztec sweet herb or honey herb.²²³

The generation of α -bisabolol from FPP is catalyzed by α -bisabolol synthase. This reaction requires an ionization-recombination-reionization sequence²²⁴ identical to that described in the previous section leading to formation of the α -terpinyl cation, so as to ensure C1–C6 bond formation and generation of the 6-membered ring (Figure 48).²²⁵ The resulting bisabolyl cation is then quenched by a solvent molecule that is trapped in the active site along with the substrate. This solvent molecule must be suitably restrained so as not to prematurely quench the reaction sequence prior to formation of the bisabolyl carbocation intermediate.

α -Bisabolol synthase from *Artemisia annua* was recently cloned and expressed in *E. coli*, and the crystal structure of the unliganded wild-type enzyme has been determined at 2.0 Å resolution.²²⁵ The enzyme exhibits the characteristic $\alpha\beta$ domain architecture of a plant terpenoid cyclase, with the nonpolar active site located exclusively in the α domain (Figure 49). Interestingly, although the aspartate-rich metal-binding motif DDXXD is located on helix D as expected based on structural homology with other terpenoid cyclases, the NSE/DTE metal-binding motif on helix H appears as NGE; moreover, this segment is partially disordered, probably due to the lack of bound metal ions and ligand. The substitution of metal ligand serine with nonliganding residue glycine in this motif is occasionally observed in plant terpenoid cyclases, so the central serine or threonine residue in the NSE/DTE metal binding motif is occasionally dispensable for Mg^{2+} binding.²²⁶

α -Bisabolol synthase is a relatively high-fidelity enzyme, in that the wild-type enzyme generates 92.8% α -bisabolol [minor side products include *trans*- α -bisabolene (1.1%), *cis*- α -bisabolene (1.2%), *cis*- γ -bisabolene (2.4%), β -bisabolene (1.9%), and β -sesquiphellandrene (0.51%)].²²⁵ Analysis of the active site structure led to the design and preparation of a penta-substituted mutant (V373N, L381A, I395V, N398I, and L399T) designated M2- α -bisabolol synthase. The major cyclization product generated by this mutant is γ -humulene (68.8%), indicating that the array of mutations enables anti-Markovnikov C1–C11 bond formation after the ionization-recombination-reionization sequence (Figure 48). The 2.0 Å-resolution crystal structure of M2- α -bisabolol synthase²²⁵ reveals that the 5 amino acid substitutions cause minor changes in the conformations of helices G1 and F, but significant structural changes result in the three-dimensional shape of the active site pocket. These changes must influence the binding conformation of FPP and cause it to reorient so as to favor C1–C11 bond formation. These structural and functional studies illuminate structure-mechanism relation-

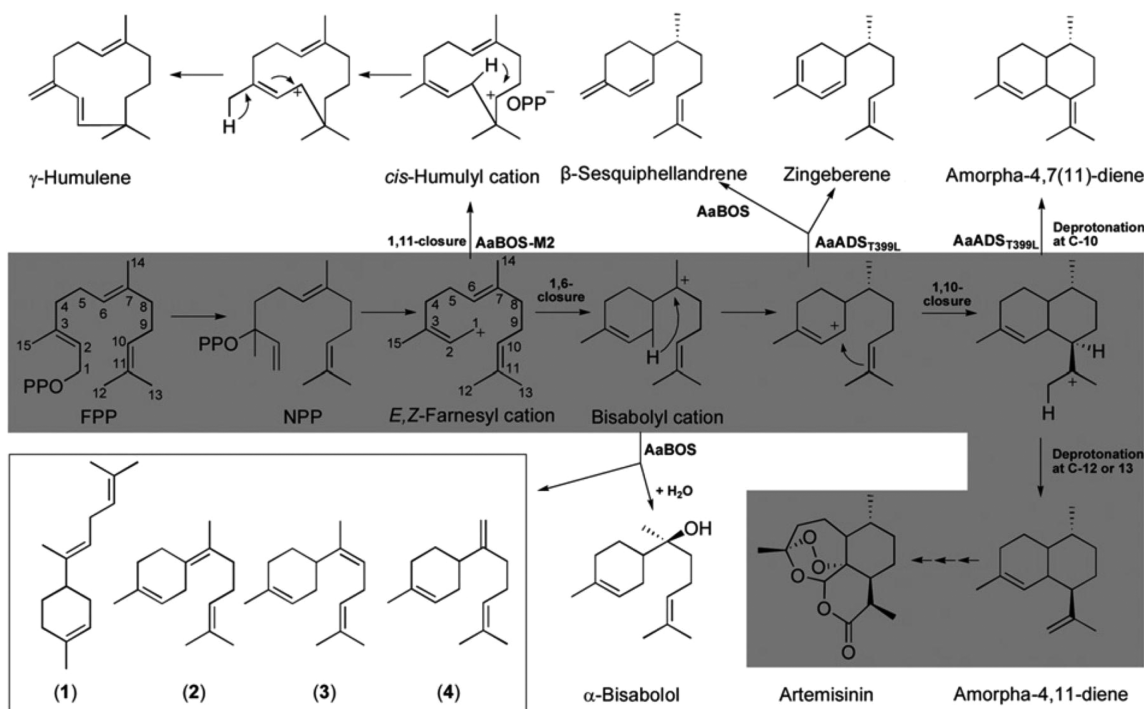


Figure 48. Mechanisms of FPP cyclization catalyzed by α -bisabolol synthase (AaBOS) and the penta-substituted mutant AaBOS-M2. These reaction sequences are compared with the reactions catalyzed by the related sesquiterpene cyclase amorphadiene synthase (AaADS). Artemisinin is a well-known antimalarial drug, and its biosynthetic pathway is highlighted in gray. Numbered products are *trans*- α -bisabolene (1), *cis*- γ -bisabolene (2), *cis*- α -bisabolene (3), and β -bisabolene (4). Reprinted with permission from ref 225. Copyright 2013 Biochemical Society.

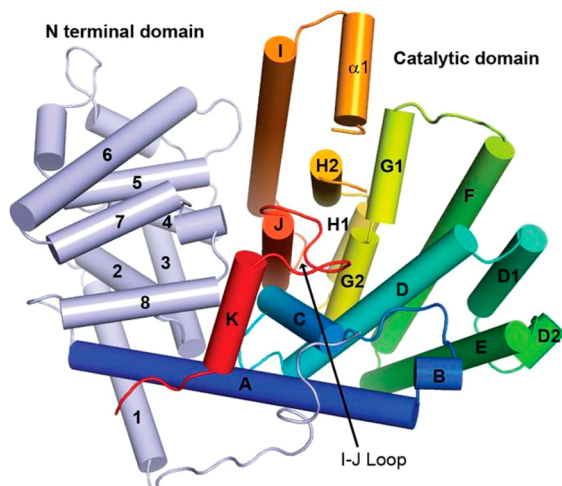


Figure 49. Crystal structure of α -bisabolol synthase reveals $\alpha\beta$ domain architecture. The active site resides in the α domain (catalytic domain) and the β domain has no known catalytic function. Reprinted with permission from ref 225. Copyright 2013 Biochemical Society.

ships in the related sesquiterpene cyclase amorphadiene synthase, which catalyzes the first committed step of artemisinin biosynthesis (Figure 48).²²⁵

5.2.2. α -Bisabolene Synthase. In response to insect attack, various conifer species generate complex terpenoid mixtures to ward off the attacking species.^{227–229} This chemical defense system consists of numerous volatile monoterpenes and sesquiterpenes, a mixture known informally as turpentine, as well as nonvolatile diterpene resin acids (rosin). The volatile terpenoids generated are typically toxic for the invading insect; these lower molecular weight species also solubilize the higher

molecular weight diterpene resin acids, which plug the lesion caused by the insect bite after evaporation of the volatile components.²³⁰

The sesquiterpene mixture generated by conifer species in response to insect attack is particularly notable with regard to both short-term and long-term chemical defense strategies. Not only are these compounds immediately toxic when encountered by the invading insect, but they can also disrupt the insect life cycle, thereby comprising a second line of defense for long-term protection.^{231–234} For example, todomatuic acid and its methyl ester juvabionine inhibit the ability of insects to molt into adults, presumably due to mimicry of insect juvenile hormones.²³⁵ Todomatuic acid is believed to derive from α -bisabolene (Figure 50A), and α -bisabolene synthase is accordingly upregulated in response to stem wounding in *Abies grandis* (grand fir).²³⁶

α -Bisabolene synthase from *Abies grandis* has been cloned and expressed in *E. coli*, and its functional properties have been described.²³⁶ Using FPP as a substrate, α -bisabolene synthase generates >99% α -bisabolene, so it is a high-fidelity cyclase. Interestingly, the enzyme also converts GPP into (+)-limonene, but this activity is not believed to be biologically significant due to the localization of α -bisabolene synthase in the cell cytosol (in plants, GPP and monoterpene cyclization reactions are compartmentalized in the plastid). The reaction sequence for α -bisabolene synthase (Figure 50A) is analogous to that required for the generation of limonene (Figure 37), in that both require the ionization-recombination-reionization sequence through a tertiary diphosphate intermediate to enable C1–C6 bond formation.

The 2.14 Å resolution crystal structure of unliganded α -bisabolene synthase⁴⁶ reveals $\alpha\beta\gamma$ domain architecture (Figure 50B), in which the class I active site resides in the α domain; the $\beta\gamma$ domains have no known catalytic function, other than perhaps

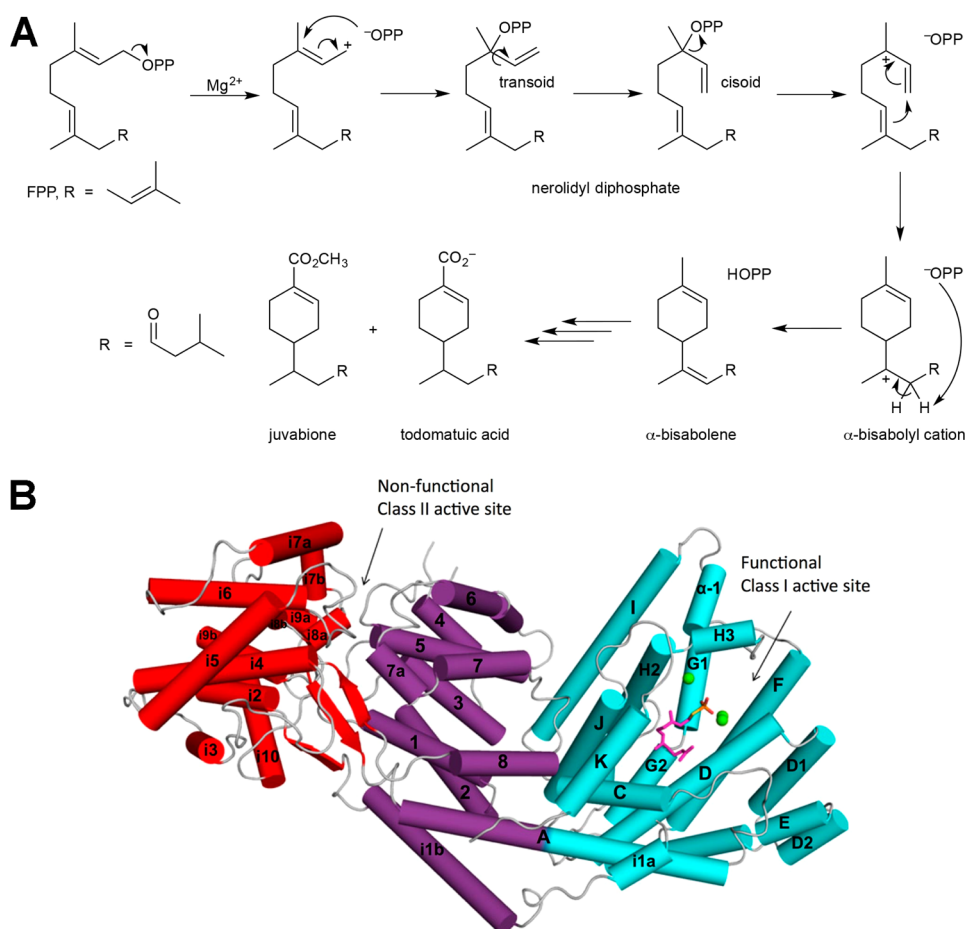


Figure 50. (A) The catalytic mechanism of α -bisabolene synthase proceeds through a characteristic ionization-recombination-reionization sequence in order to facilitate C1–C6 bond formation. The cyclization product, α -bisabolene, is a biosynthetic precursor of juvabione and todomatuic acid, which mimic insect juvenile hormones. (B) The crystal structure of α -bisabolene synthase reveals $\alpha\beta\gamma$ domain architecture. The α domain (cyan) contains the functional class I terpenoid cyclase active site; the $\beta\gamma$ domains (purple and red, respectively) are vestigial and have no known catalytic function. Reprinted with permission from ref 46. Copyright 2011 Elsevier.

for the N-terminal polypeptide segment to help cap the active site upon substrate binding. Crystal structures of complexes with substrate analogues as well as bisphosphonate inhibitors such as alendronate, pamidronate, and etidronate reveal characteristic molecular recognition of the diphosphate moiety by 3 Mg^{2+} ions complexed by the aspartate-rich and DTE metal-binding motifs in the active site. The catalytic efficiency of the enzyme is relatively modest,⁴⁶ with $k_{cat}/K_M = 38 M^{-1} s^{-1}$.

Notably, α -bisabolene synthase has been utilized in metabolic engineering experiments in the development of new approaches for the generation of advanced biofuels in yeast and cyanobacteria.^{237,238} The chemical hydrogenation of α -bisabolene yields the saturated hydrocarbon bisabolane, which has physical and chemical properties quite similar to those of D2 diesel fuel.²³⁷ Engineering and economic calculations by Keasling and colleagues indicate that the commercial production of α -bisabolene through metabolic engineering would yield a product for approximately \$6/gallon, which is currently more expensive than petrochemically derived D2 diesel fuel. Furthermore, large-scale hydrogenation of bioderived α -bisabolene would add to this cost. However, Keasling and colleagues anticipate terpene reduction reactions engineered in synthetic biology host systems using designer reductases, which could reduce the cost-per-gallon for a consumer-grade liquid fuel.²³⁷

5.2.3. Epi-Isozizaene Synthase. Alabaflavone is an antibiotic generated in the Gram-positive soil bacterium *Streptomyces coelicolor* A3(2) that derives from the cytochrome P450 170A1-mediated oxidation of the tricyclic sesquiterpene epi-isozizaene (Figure 51).^{239,240} Epi-isozizaene synthase²⁴¹

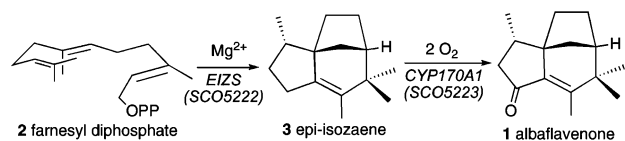


Figure 51. Cyclization of FPP (2) to yield epi-isozizaene (3) is catalyzed by the sesquiterpene cyclase epi-isozizaene synthase. Subsequent oxidation of epi-isozizaene yields the antibiotic alabaflavone (1). Reproduced from ref 242. Copyright 2009 American Chemical Society.

catalyzes the first step of alabaflavone biosynthesis through the initial C1–C6 cyclization of FPP through an ionization-recombination-reionization sequence forming the bisabolyl cation. In contrast with the sesquiterpene cyclase reactions discussed in sections 5.2.1 and 5.2.2, which terminate upon formation of the bisabolyl cation, the reaction catalyzed by epi-isozizaene synthase proceeds through a 1,2-hydride shift, which generates the homobisabolyl cation. In turn, this cation undergoes additional carbon–carbon bond-forming reactions

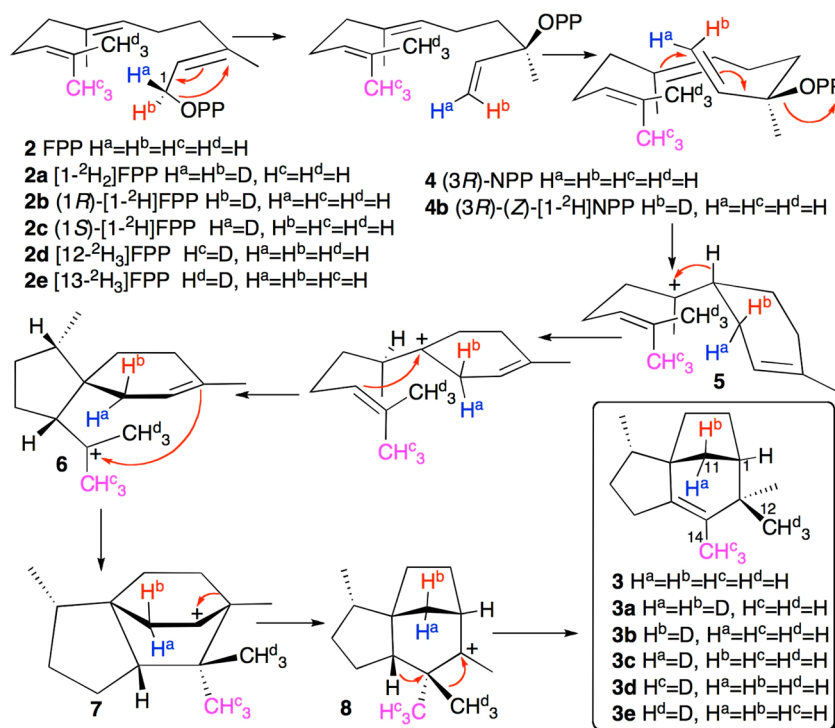


Figure 52. Mechanism of epi-isozizaene synthase as determined through the use of stereospecifically deuterium-labeled substrates. Reproduced from ref 242. Copyright 2009 American Chemical Society.

leading to epi-isozizaene formation as elegantly delineated through the study of isotopically labeled substrates by Cane and Lin (Figure 52).²⁴²

The 1.6 Å resolution crystal structure of epi-isozizaene synthase complexed with 3 Mg^{2+} ions, inorganic pyrophosphate, and the benzyltriethylammonium cation reveals a single α domain enzyme characteristic of bacterial cyclases (Figure 53A).²⁴³ Several features evident in this structure advance our understanding of the molecular basis of catalysis. First, 3 Mg^{2+} ions, 3 basic groups (R194, K247, and R338), and the phenolic hydroxyl group of Y339 comprise the molecular recognition motif for the diphosphate moiety (Figure 53B) and provide the electrophilic impetus to trigger substrate ionization and catalysis. Second, the benzyltriethylammonium cation binds in the hydrophobic active site, which is encapsulated by the enzyme with a fully closed active site conformation. The quaternary ammonium cation engages F95, F96, and F198 through cation- π interactions, with the positively charged ammonium nitrogen atom approximately 5 Å away from the ring centroid of each aromatic residue (Figure 53C). The structure of this complex provides a direct visualization of cation- π interactions in a terpenoid cyclase active site, demonstrating the feasibility of such interactions in stabilizing actual carbocation intermediates in catalysis. Such interactions will additionally stabilize the transition states flanking these intermediates, so cation- π interactions comprise an important strategy for transition state stabilization in a terpenoid cyclase active site.

Comparison with the 1.90 Å resolution structure of unliganded D99N epi-isozizaene synthase reveals the molecular details of active site closure (Figure 53A).²⁴³ Conformational changes in helix H, the H- α -1 loop, and the J-K loop are triggered by metal-binding and diphosphate complexation, and these conformational changes fully enclose the active site and protect it from bulk solvent. The enclosed active site contour does not

unambiguously fit the three-dimensional shape of epi-isozizaene, and this may reflect the fact that the enzyme is not a high-fidelity cyclase: it generates 79% epi-isozizaene and a handful of other sesquiterpene products. Remarkably, the generation of a library of 26 single-point mutants designed to remold the active site contour triples the overall number of major and minor products generated by epi-isozizaene synthase, including the conversion of the enzyme into six different sesquiterpene synthases generating alternative major products: the F96A mutant predominantly generates (*E*)- β -farnesene, the F96W mutant predominantly generates zizaene, the F95H mutant predominantly generates β -curcumene, the F95M mutant predominantly generates β -acoradiene, the F198L mutant predominantly generates β -cedrene, and the F96V and W203F mutants predominantly generate (*Z*)- γ -bisabolene (Figure 54A).²⁴⁴

The ability to reprogram the cyclization cascade catalyzed by a terpenoid cyclase has profound implications for biotechnology. For example, consider F95H epi-isozizaene synthase, which generates β -curcumene as its major sesquiterpene product.²⁴⁴ With $k_{cat}/K_M = 2600 M^{-1} s^{-1}$, the catalytic efficiency of this mutant enzyme is nearly 70-fold greater than that of α -bisabolene synthase (section 5.2.2).⁴⁶ Since, like α -bisabolene, β -curcumene can be chemically hydrogenated to form the hydrocarbon D2 diesel fuel substitute bisabolane (Figure 54B), protein engineering of a single α domain bacterial cyclase can yield a smaller and more robust catalyst than the $\alpha\beta\gamma$ domain plant cyclase initially utilized in this process.

5.2.4. Trichodiene Synthase. Trichothecene mycotoxins such as T-2 toxin, nivalenol, and vomitoxin are occasional contaminants of grains such as wheat, oats, and corn, and fungal outbreaks in the food chain can accordingly present serious challenges to public health.^{245–247} For example, in 1944 moldy grain and bread contaminated with T-2 toxin caused the death of more than 10% of the population of Orenburg, Russia, leading to

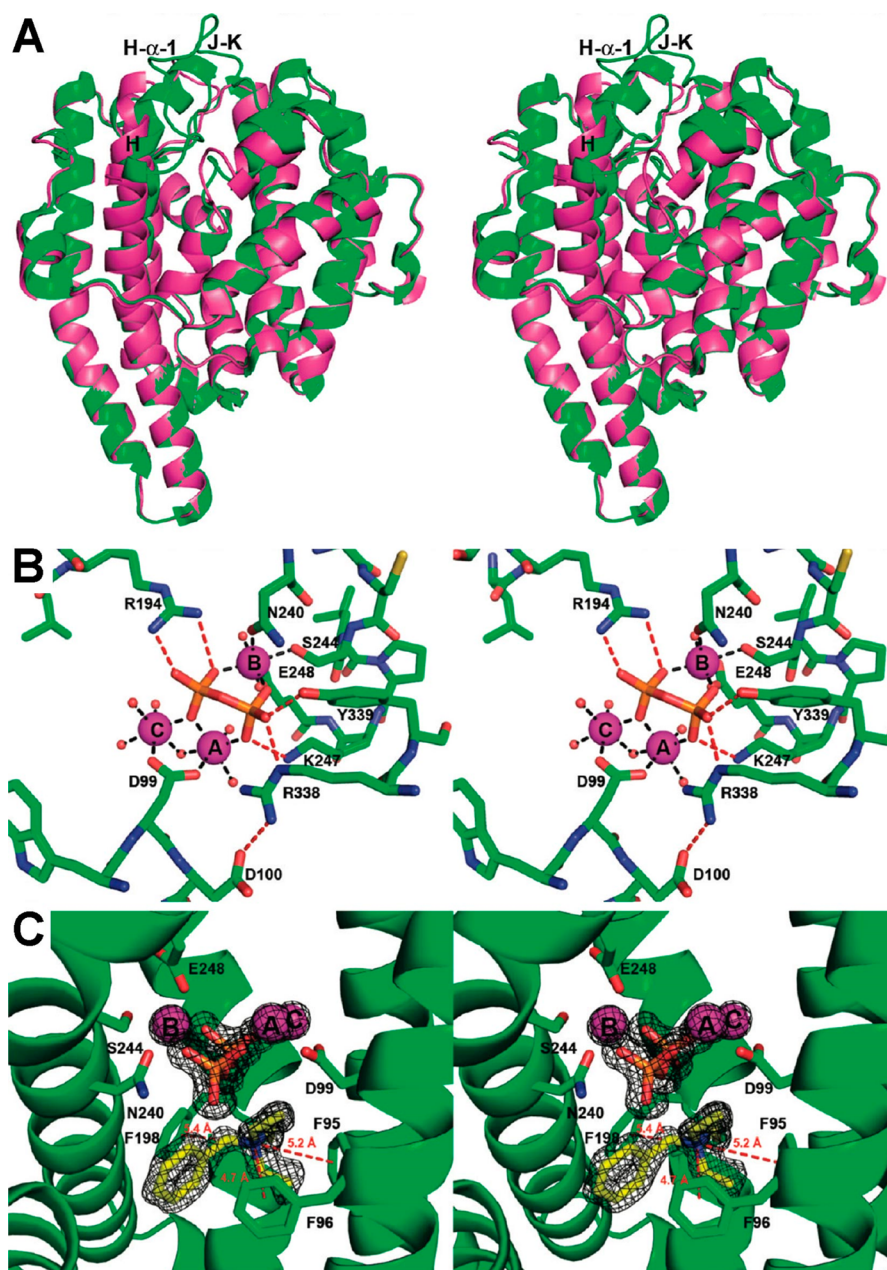


Figure 53. (A) Stereoview of unliganded D99N epi-isozizaene synthase (purple) superimposed on the wild-type epi-isozizaene synthase complex with inorganic pyrophosphate (green; ligands omitted for clarity). Structural changes in helix H and the H- α -1 and J-K loops accompany active site closure. (B) Stereoview showing metal coordination and hydrogen bond interactions (black and red dashed lines, respectively) in the epi-isozizaene synthase complex with inorganic pyrophosphate. (C) Stereoview showing simulated annealing omit maps of inorganic pyrophosphate, Mg²⁺ ions, and the benzyltriethylammonium cation (contoured at 5 σ). Cation- π interactions are evident between the quaternary ammonium cation and F95, F96, and F198 (red dashed lines). Reproduced from ref 243. Copyright 2010 American Chemical Society.

the exploration and weaponization of T-2 toxin and related mycotoxins for use in biological warfare.^{248,249} The first committed step in the biosynthesis of these mycotoxins is the cyclization of FPP to form the sesquiterpene hydrocarbon trichodiene, which is catalyzed by trichodiene synthase (Figure 55).^{250,251}

Trichodiene synthase from the fungus *Fusarium sporotrichioides* is a 90-kD dimer,²⁵² and the enzyme was cloned²⁵⁰ and overexpressed in *E. coli*.^{253,254} The 2.5 Å resolution crystal structures of the unliganded enzyme and its complex with 3 Mg²⁺ ions and inorganic pyrophosphate reveal that each monomer adopts the α domain fold of a class I terpenoid cyclase, with active

sites oriented in antiparallel fashion (Figure 56, panels A and B).¹⁷⁰ The binding of 3 Mg²⁺ ions and inorganic pyrophosphate triggers conformational changes that fully enclose the active site; the diphosphate group is firmly bound by metal coordination interactions and hydrogen bond interactions with 3 basic residues (R182, K232, and R304) and Y305 (Figure 56, panels C and D).

Enzymological studies using isotopically labeled FPP and nerolidyl diphosphate confirm that 3(*R*)-nerolidyl diphosphate²¹⁴ is a catalytic intermediate, as expected for the ionization-recombination-reionization sequence that enables initial C1–C6 bond formation.^{255,256} Single-turnover experi-

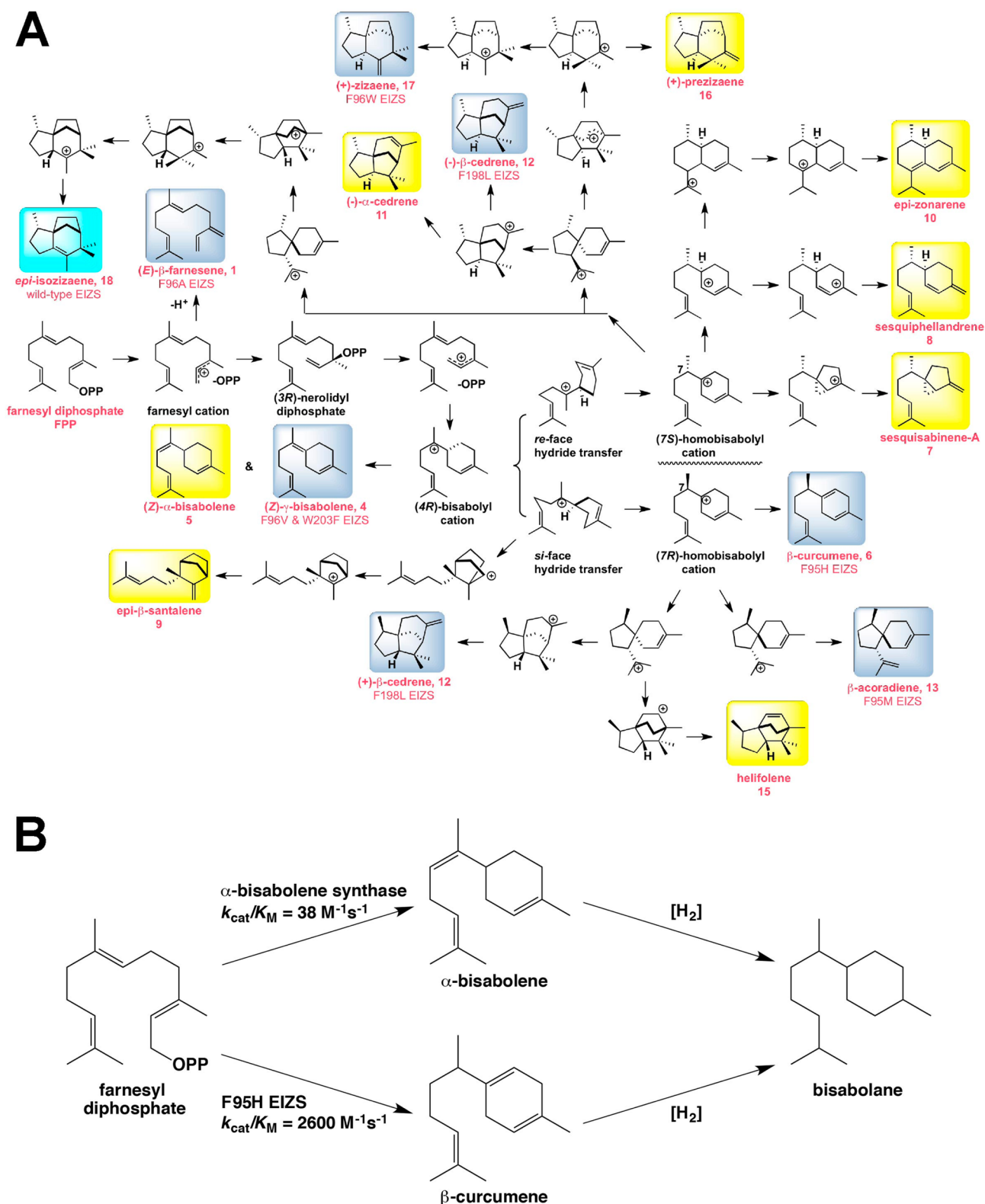


Figure 54. (A) Biosynthetic manifold of wild-type and mutant epi-isozizaene synthase enzymes. The predominant cyclization product of the wild-type enzyme, epi-isozizaene, is highlighted in a cyan box, and the predominant cyclization products of mutant enzymes are highlighted in blue boxes. Side products are highlighted in yellow boxes. Reproduced from ref 244. Copyright 2014 American Chemical Society. (B) F95H epi-isozizaene synthase (EIZS) generates β -curcumene with 68-fold enhanced catalytic efficiency compared with the generation of α -bisabolene by wild-type α -bisabolene synthase, thereby providing a more efficient route for the generation of the D2 diesel fuel substitute bisabolane.

ments indicate that FPP ionization is the rate-determining chemical step of catalysis, with product release being the overall rate-determining step of catalysis.²⁵⁷ Notably, incubation of

trichodiene synthase with the reduced substrate analogue 7(*S*)-*trans*-6,7-dihydrofarnesyl diphosphate or its enantiomer yields product arrays that reflect formation of the corresponding 6,7-

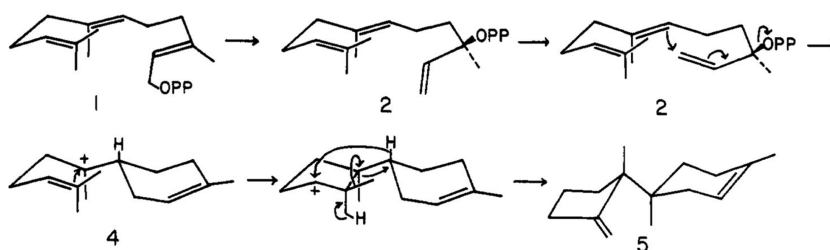


Figure 55. Ionization of FPP (1) and recombination of inorganic pyrophosphate yields 3(*R*)-nerolidyl diphosphate (2), which enables C1–C6 bond formation after reionization to yield the 4(*R*)-bisabolyl carbocation intermediate (4). Subsequent 1,4-hydride transfer, tandem 1,2-methyl migrations, and deprotonation yield trichodiene (5). Reproduced from ref 251. Copyright 1981 American Chemical Society.

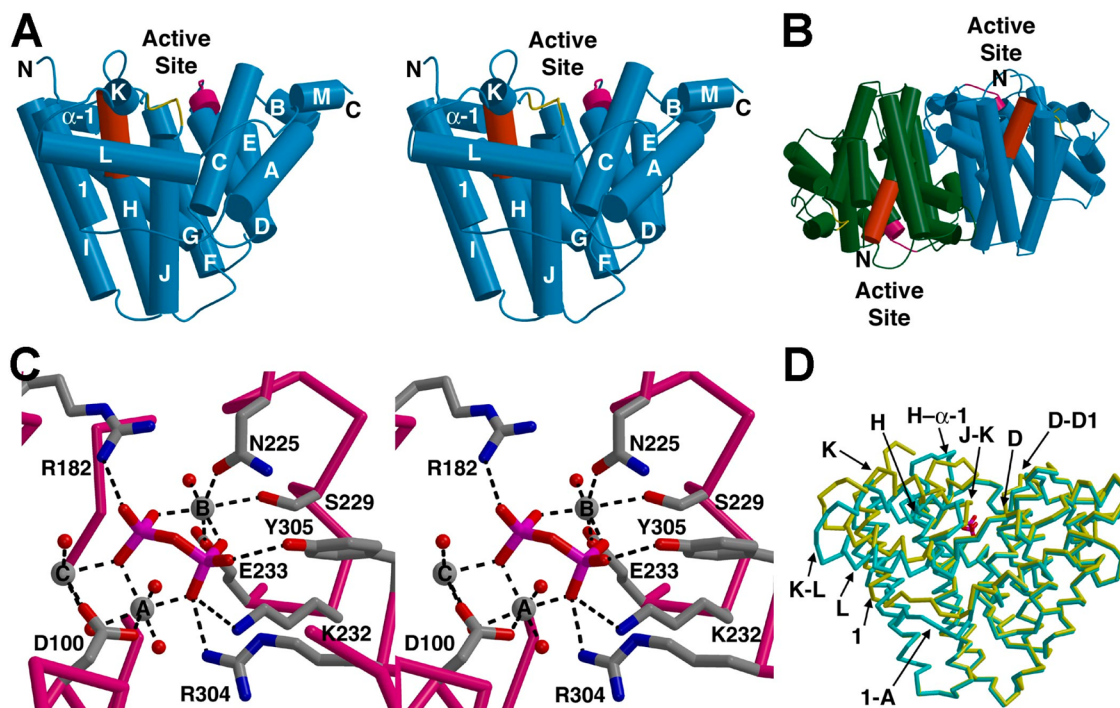


Figure 56. (A) Stereoview of trichodiene synthase. The aspartate-rich motif on helix D (magenta) and the NSE motif on helix H (red) are indicated. (B) Two monomers assemble in antiparallel fashion to form the trichodiene synthase dimer. (C) Stereoview of the trichodiene synthase complex with inorganic pyrophosphate and 3 Mg^{2+} ions, showing metal coordination and hydrogen bond interactions (dashed lines). (D) Structure of unliganded trichodiene synthase (cyan) superimposed on that of the pyrophosphate complex (yellow, with magenta pyrophosphate) reveals structural changes in the indicated helices and loops that accompany active site closure. Reprinted from ref 170. Copyright 2001 National Academy of Sciences.

dihydroneerolidyl diphosphate intermediate, thereby providing further support for 3(*R*)-nerolidyl diphosphate as an intermediate in the cyclization cascade.²⁵⁸

The tertiary 4(*R*)-bisabolyl cation results from C1–C6 bond formation (Figure 55), and this carbocation is analogous to the 4(*R*)- α -terpinyl cation intermediate of monoterpene cyclization reactions (Figure 29). Interestingly, just as a nonproductive binding conformation is observed for the aza analogue of the α -terpinyl cation bound in the active site of (+)-bornyl diphosphate synthase,²³ so too is a nonproductive binding conformation observed for the binding of the aza analogue of the 4(*R*)-bisabolyl cation;¹⁷⁸ indeed, the aza analogue of the 4(*S*)-bisabolyl cation binds with essentially equal affinity.²⁵⁹ Nonproductive binding conformations appear to be driven in part by favorable electrostatic interactions between the cationic aza moiety and the inorganic pyrophosphate anion,^{178,260} so here, too, the most thermodynamically stable structure corresponding to a crystalline enzyme–analogue complex at equilibrium may not necessarily correspond to the most easily accessible structure during catalysis. The trichodiene synthase reaction proceeds

through a 1,4-hydride transfer, tandem 1,2-methyl migrations, and deprotonation to yield trichodiene (Figure 55). Inorganic pyrophosphate is the most likely general base that mediates the final deprotonation.^{170,261}

Interestingly, mutation of residues that coordinate to Mg^{2+} ions or residues that hydrogen bond with inorganic pyrophosphate results in the generation of aberrant cyclization products, more so than generated by the wild-type enzyme.^{262–266} Structural analysis of certain mutants reveals incomplete active site closure and an enclosed active site volume 12% larger than that of the wild-type enzyme.²⁶¹ This compromises the template function of the active site and results in additional conformational flexibility for the substrate and intermediate carbocations, thereby allowing alternative carbon–carbon bond-forming trajectories that form alternative products. The proportion of alternative cyclization products increases when Mn^{2+} is substituted for Mg^{2+} in assays of mutants with substitutions in the aspartate-rich metal-binding motif,²⁶³ so metal coordination interactions must play a critical role in governing the substrate binding conformation prior to initiation of the cyclization

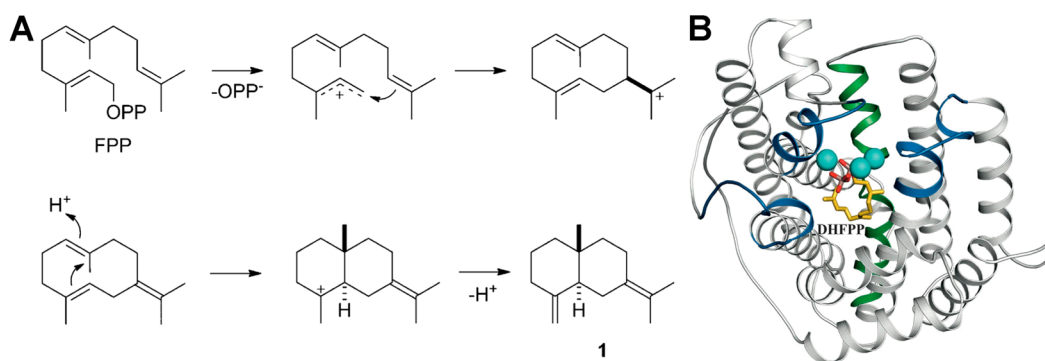


Figure 57. (A) Cyclization mechanism of selinadiene synthase. (B) Crystal structure of selinadiene synthase complexed with a substrate analogue (yellow stick figure) showing active site helices and loops that undergo structural changes to accommodate the bound analogue (blue). The break in helix G (green) is oriented so as to stabilize carbocation intermediates through interactions with the helix dipole. Reprinted with permission from ref 271. Copyright 2014 Wiley-VCH.

cascade. Analysis of the trichodiene synthase mechanism using theoretical and computational chemistry provides a framework for understanding cyclization specificity and highlights the importance of the bisabolyl cation intermediate as a critical branch point in the generation of alternative sesquiterpenes.²⁶⁷

5.2.5. Selinadiene Synthase. Selinenes contribute to the flavor and aroma of citrus fruits and German hops,^{268–270} and these compounds generally derive from an initial C1–C10 cyclization reaction that ultimately yields a bicyclic product (Figure 57A). The C2–C3 double bond remains in the *trans* configuration for the cyclization reaction, so this C1–C10 cyclization reaction does not require the ionization-recombination-reionization sequence described above for C1–C6 cyclization sequences. The 2.1 Å resolution crystal structure of unliganded selina-4(15),7(11)-diene synthase from *Streptomyces pristinaespiralis*, also known as γ -selinene synthase or simply selinadiene synthase, reveals the characteristic single α domain fold of a bacterial terpenoid cyclase with an open active site conformation; the 2.1 Å resolution crystal structure of the complex with a substrate analogue reveals a closed active site conformation in which the diphosphate group of the analogue coordinates to 3 Mg²⁺ ions (Figure 57B).²⁷¹ Theoretical and computational chemistry studies are consistent with the proposed role of the inorganic pyrophosphate coproduct as the general base–general acid that mediates the deprotonation–reprotonation sequence shown in Figure 57A, since no intramolecular proton transfers are energetically feasible in the cyclization cascade.²⁷²

Dickschat and colleagues report the preparation and functional evaluation of 28 site-specific mutants of selinadiene synthase designed to probe residues that define the active site contour, residues involved in the molecular recognition of the substrate diphosphate group, and residues involved in the conformational transition required for active site closure.²⁷¹ Substitution of aromatic residues indicates that these residues play important roles in stabilizing carbocation intermediates through cation– π interactions, especially F55 and F79. Conservative amino acid substitutions in the aspartate-rich metal-binding motif, D83N and D83E, do not disable the initial C1–C10 bond-forming reaction but instead compromise the second cyclization reaction mediated by the deprotonation–reprotonation sequence shown in Figure 57A. Possibly, conservative mutations of metal-binding residues slightly perturb the position of metal-bound inorganic pyrophosphate, which in

turn would compromise its proposed role as a general base–general acid in the cyclization sequence.

5.2.6. Germacradien-4-ol Synthase. Larvae of the North American sawfly, also known as the pine sawfly, feed on the needles of infested pine trees and are responsible for occasional large-scale forest defoliation events.²⁷³ Sawfly larvae abstract the resin from pine needles and utilize it for defense against insect and animal predators such as ants, wasps, lizards, and frogs. The principal component of this defensive resin is the sesquiterpene alcohol germacradien-4-ol.^{274–276} Two different numbering systems for this natural product are found in the literature, so it is also known as germacradien-5-ol, as explained in the report of its total synthesis.²⁷⁷

Germacradien-4-ol is also generated in certain bacteria, and recent genome mining studies led to the discovery of a germacradien-4-ol synthase in *Streptomyces citricolor*.²⁷⁸ Although the wild-type enzyme did not yield crystals suitable for X-ray structure determination, the E248A mutant in its unliganded form yielded crystals that diffracted to 1.50 Å resolution.²⁷⁹ The side chain of E248 is a surface residue more than 14 Å away from the active site, and it was identified as a candidate for substitution to facilitate crystallization using the Surface Entropy Reduction Server.²⁸⁰ The structure of germacradien-4-ol synthase reveals the association of two α domains that assemble with antiparallel quaternary structure (Figure 58).

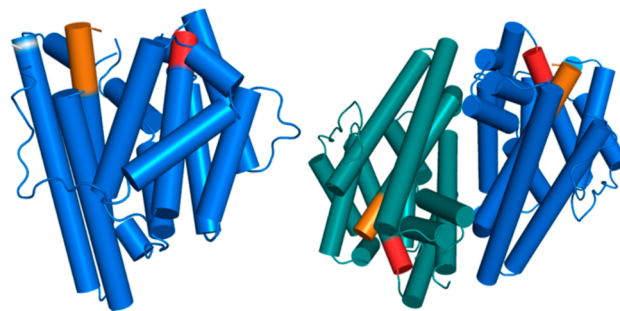


Figure 58. Structure of the monomer (left) and dimer (right) of germacradien-4-ol synthase; aspartate-rich and NSE metal-binding motifs are red and orange, respectively. The location of the E248A mutation required to facilitate crystallization is indicated by a white band. Reproduced from ref 279. Copyright 2016 American Chemical Society.

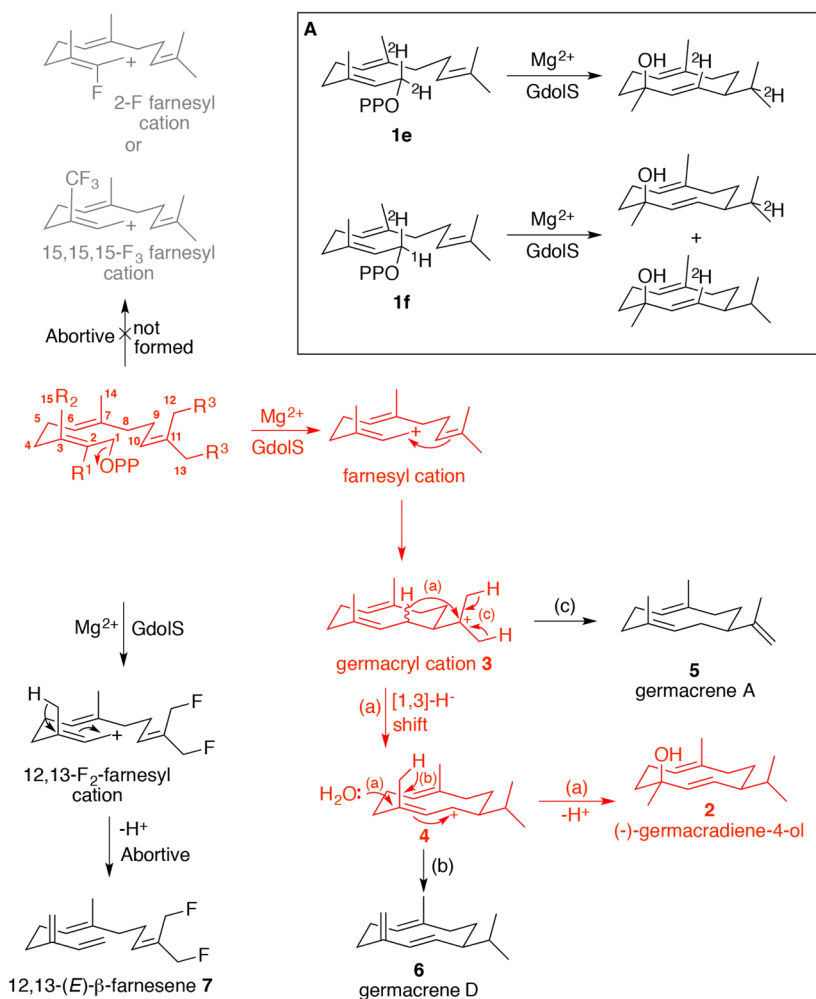


Figure 59. Cyclization of FPP by germacradien-4-ol synthase yields major and minor products, as probed using fluorinated substrate analogues. Reproduced from ref 279. Copyright 2016 American Chemical Society.

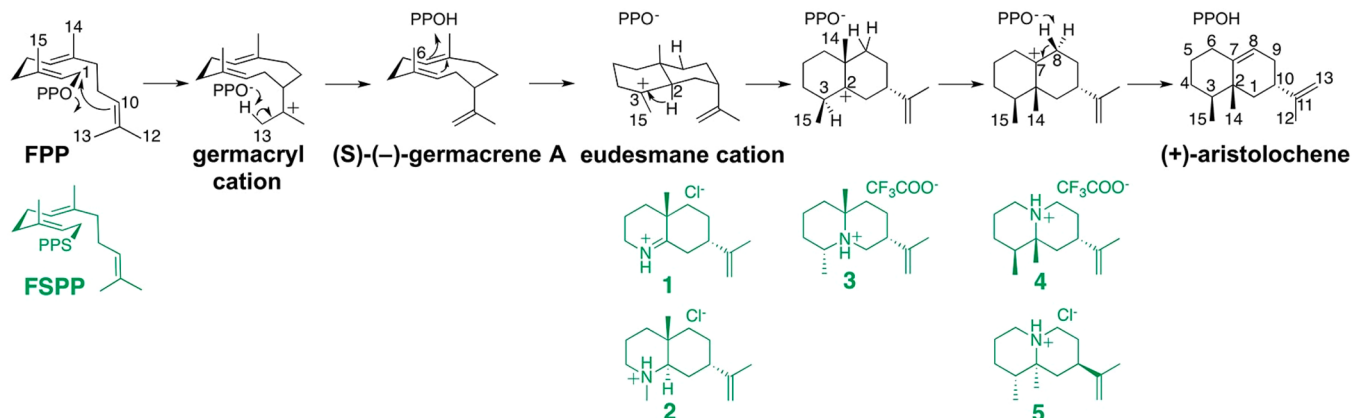


Figure 60. Mechanism of aristolochene synthase (PPO, diphosphate; PPO⁻, inorganic pyrophosphate). Some steps might proceed in concerted rather than stepwise fashion, in which case only partial positive charge would develop in place of full carbocations. The unreactive substrate analogue farnesyl-S-thiolodiphosphate (FSPF) and aza analogues of carbocation intermediates 1–5 studied in crystalline complexes with the *A. terreus* enzyme are illustrated. Reproduced from ref 24. Copyright 2013 American Chemical Society.

Recent enzymological studies of the wild-type enzyme and its site-specific mutants, including the use of fluorinated and isotopically labeled substrate analogues, illuminate key features of the FPP cyclization mechanism (Figure 59).²⁷⁹ Metal-triggered FPP ionization is followed by C1–C10 ring closure

to form the germacryl cation (the C2–C3 bond of FPP remains in the *trans* configuration). Next, a 1,3-hydride transfer occurs with undefined stereochemistry (the deuterium in the final product is scrambled when chiral FPP deuterated at C1 is utilized as a substrate). The resulting allylic cation undergoes addition of

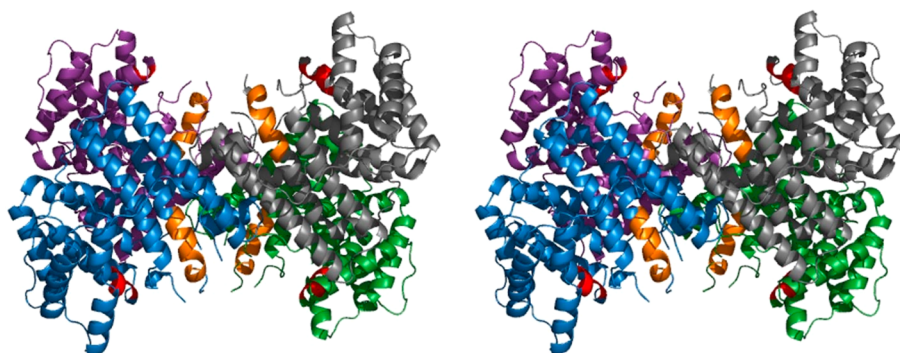


Figure 61. Aristolochene synthase from *A. terreus* crystallizes as a tetramer (i.e., a dimer of dimers). Aspartate-rich and NSE metal-binding motifs are red and orange, respectively. Reproduced from ref 286. Copyright 2007 American Chemical Society.

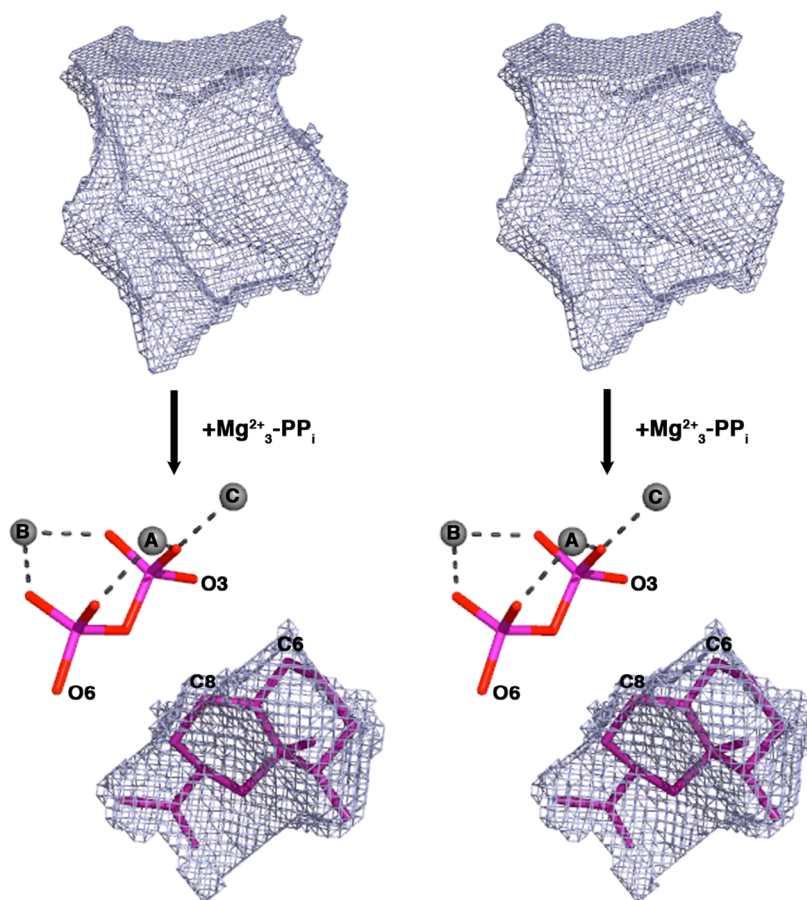


Figure 62. Stereoview of the three-dimensional active site contours of aristolochene synthase in the unliganded conformation (top) and in the complex with 3 Mg^{2+} ions and inorganic pyrophosphate (bottom). Ligand binding triggers conformational changes that fully enclose the active site. The enclosed active site contour is very productlike, as indicated by the modeling of aristolochene in this contour. The modeled position of aristolochene places the O3 atom of inorganic pyrophosphate close to the C6 and C8 atoms of aristolochene, consistent with the proposed role of inorganic pyrophosphate as the general base-general acid that functions in the cyclization mechanism outlined in Figure 60. Reproduced from ref 286. Copyright 2007 American Chemical Society.

water at the tertiary carbon to yield germacradien-4-ol; alternative minor products are generated by some mutants, as summarized in Figure 59.

Definitive structure-mechanism relationships regarding the enzymatic control of the biosynthetic water molecule cannot be made in the absence of crystal structures of enzyme–ligand complexes. Although some ordered water molecules are observed in the active site of the unliganded enzyme, it is unknown as to whether any of these water molecules remain

upon substrate binding to participate in catalysis. There are no obvious active site residues to serve as a general base to activate a nucleophilic water molecule, so the inorganic pyrophosphate coproduct may serve this role. Allemann and colleagues suggest that instead of reacting with a trapped water molecule, the final allylic carbocation may simply be quenched by a water molecule from bulk solvent, which may gain access to the active site through the movement of the flexible H-1 α and E-F loops flanking the active site.

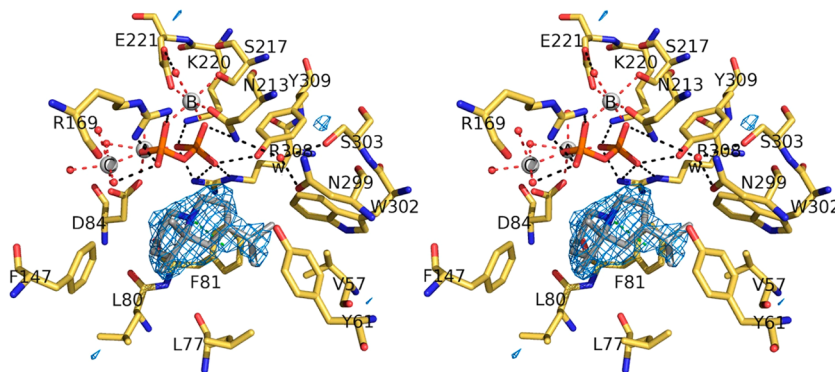


Figure 63. Stereoview of the simulated annealing omit map showing the binding of an aza analogue of the final carbocation intermediate (compound 4 in Figure 60) in the active site of aristolochene synthase. Metal coordination and hydrogen bond interactions are indicated by red and black dashed lines, respectively. The orientation of the analogue is close to that modeled in Figure 62 based on the three-dimensional productlike contour of the enclosed active site (the view here is rotated ca. 180° relative to that in Figure 62). Water molecule “w” (red sphere hydrogen bonded to N213, N299, and S303) remains trapped in the active site in all structures of enzyme–ligand complexes. Reproduced from ref 24. Copyright 2013 American Chemical Society.

5.2.7. Aristolochene Synthase. Generation of the bicyclic sesquiterpene aristolochene is the first committed step in the biosynthesis of several fungal toxins, including gigantene, sporogen-AO1, bipolaroxin, and PR-toxin.^{281,282} Aristolochene synthase from the blue cheese mold, *Penicillium roqueforti*, is a 37-kD enzyme²⁸³ that has been cloned²⁸² and overexpressed²⁸⁴ in *E. coli*, and the crystal structure of the unliganded enzyme has been determined at 2.5 Å resolution.⁷⁹ Aristolochene synthase from another fungus, *Aspergillus terreus*, has also been cloned and overexpressed in *E. coli*,²⁸⁵ and the crystal structure of the unliganded enzyme has been determined at 2.2 Å resolution.²⁸⁶ The *A. terreus* enzyme has proven to be much more amenable than the *P. roqueforti* enzyme for the study of complexes with analogues of the substrate and carbocation intermediates, and a total of 10 structures of enzyme–ligand complexes have been reported at 1.86–2.40 Å resolution.^{24,286,287}

Structural studies of *A. terreus* aristolochene synthase provide a useful framework for interpreting the results of early enzymological studies with stereospecifically labeled substrates,^{281,288,289} a mechanism-based inhibitor,²⁹⁰ and the modified substrate 7(*R*)-6,7-dihydrofarnesyl diphosphate.²⁹¹ These studies are consistent with the mechanism shown in Figure 60, which proceeds through initial C1–C10 bond formation to yield (*S*)-(-)-germacrene A (the C2–C3 bond of FPP remains in the *trans* configuration), which is then protonated at C6 to facilitate C2–C7 bond formation to yield the (+)-eudesmane carbocation. Stereospecific deprotonation of C8–H β , methyl migration, and hydride transfer yields (+)-aristolochene.

Additional experiments demonstrate that germacrene A is a minor product of the reaction catalyzed by *P. roqueforti* aristolochene synthase, consistent with the intermediacy of germacrene A in the cyclization cascade.²⁹² Site-directed mutagenesis studies also illuminate the role of active site aromatic residues in governing reactive conformations of the substrate and carbocation intermediates, as well as stabilizing carbocation intermediates through cation– π interactions.^{293–298} Cation– π interactions with active site aromatic residues presumably contribute to the potency of aza analogues of carbocation intermediates as inhibitors of aristolochene synthase.^{299,300} Interestingly, aristolochene synthase can accommodate modified substrates with varying degrees of reactivity. For example, 2-fluorofarnesyl diphosphate, 6-fluorofarnesyl diphosphate, and 14-fluorofarnesyl diphosphate are converted

to the corresponding fluorinated isomers of germacrene A,^{301,302} whereas 12,13-fluorofarnesyl diphosphate is an inhibitor of the enzyme.³⁰³ Such studies with modified substrates further inform our understanding of the catalytic mechanism.

Aristolochene synthase from *A. terreus* crystallizes as a tetramer of α domain subunits (Figure 61), although native gel analysis indicates dimeric quaternary structure in solution.²⁸⁶ Felicetti and Cane report that enzyme activity becomes attenuated at higher protein concentrations,³⁰⁴ so it is possible that tetramerization is inhibitory for the cyclization reaction. The dimer is likely to be the biologically relevant species, in which the active sites are oriented in antiparallel fashion.

Analysis of the three-dimensional structure of the active site in its fully closed conformation, complexed with 3 Mg²⁺ ions and inorganic pyrophosphate, reveals a productlike contour; when fit with a molecule of aristolochene, both C6 and C8 atoms are perfectly oriented for stereospecific proton transfers with inorganic pyrophosphate.²⁸⁶ Thus, inorganic pyrophosphate is likely to be the general base–general acid that mediates the proton transfer steps, including the final deprotonation of C8–H β (Figure 62). The subsequent crystal structure determination of the complex with an aristolochene-like analogue²⁴ verifies the previously modeled²⁸⁶ binding conformation of aristolochene (Figure 63). That the active site contour is very productlike reflects the template function of the active site. Consider that the isoprenoid substrate, FPP, is quite flexible: there are three carbon–carbon single bonds about which free rotation is possible between each 5-carbon isoprenoid unit, so the linear isoprenoid substrate is even more flexible than, for example, a polypeptide in which there are only two bond rotations per residue. Thus, the active site template must be strict as it enforces the initial binding conformation of the flexible substrate so as to ensure the correct trajectory of carbon–carbon bond formation.

All the information required to specify the final cyclization product (or products) is thus encoded in the three-dimensional contour of the active site. If this code can be deciphered then the product generated by a terpenoid cyclase can be predicted *de novo*. Importantly, successful attempts at predicting the product of a newly discovered sesquiterpene cyclase through computational approaches culminated in the recent discovery of cucumene synthase.³⁰⁵

Although a trapped water molecule comprises part of the active site contour of aristolochene synthase in the closed

conformation,²⁴ no hydroxylated products are generated by the enzyme. Moreover, mutagenesis of residues that hydrogen bond to this water molecule does not lead to the generation of hydroxylated products, so this water molecule appears to be located in a position where it simply cannot react with carbocation intermediates.²⁵ Thus, as long as a water molecule is held in a location where it cannot react with the empty *p* orbital on a carbocation intermediate, then there is no risk of prematurely quenching the cyclization cascade. How terpenoid cyclases control water for organic synthesis remains a largely unanswered question.

5.2.8. Epi-Aristolochene Synthase. Capsidiol is a plant phytoalexin generated in response to fungal or viral infection^{306–308} and derives from the oxidation of *S*-epi-aristolochene, also known simply as epi-aristolochene. The crystal structure of epi-aristolochene synthase from tobacco (*Nicotiana tabacum*) was the first of a plant terpenoid cyclase³⁷ and has accordingly served as a paradigm for understanding structure–function relationships in the greater family of terpenoid cyclases. The enzyme is a monomer with $\alpha\beta$ domain architecture (Figure 64),

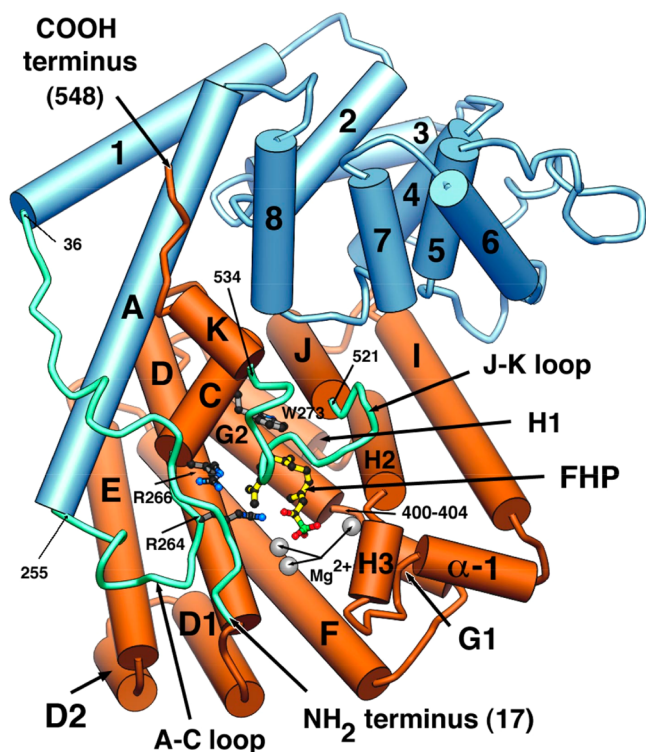


Figure 64. Crystal structure of the epi-aristolochene synthase-farnesyl hydroxyphosphonate (FHP) complex. The substrate analogue (stick figure) binds in the active site in the α domain (orange); the β domain (blue) has no known catalytic function other than to provide the N-terminal polypeptide which helps to stabilize the active site in the closed conformation. Reprinted with permission from ref 37. Copyright 1997 AAAS.

and crystal structures of complexes with FPP analogues farnesyl hydroxyphosphonate and trifluorofarnesyl diphosphate confirmed the location of the active site and illustrated how a terpenoid cyclase active site can serve as a template to chaperone the conformation of a flexible isoprenoid substrate.

Pre-steady-state kinetics indicate that the rate-determining step of catalysis occurs after the substrate binding step and after the ionization of FPP, indicating that a subsequent chemical step,

or perhaps more likely, product release, is rate-determining.³⁰⁹ Structure-based mutagenesis studies³¹⁰ as well as enzymological studies using a variety of fluorinated and deuterated substrates,^{311,312} indicate a mechanism involving metal-triggered FPP ionization, C1–C10 bond formation, and quenching of the resultant formed germacryl cation to yield intermediate germacrene A, which after reprotonation undergoes carbon–carbon bond formation to yield the eudesmane cation intermediate. Subsequently, a 1,2-hydride transfer, 1,2-methyl migration, and final proton elimination yields epi-aristolochene (Figure 65). Significantly, the chemical mechanism of epi-aristolochene formation is similar to that proposed for aristolochene synthase (section 5.2.7) but results in the formation of a different stereoisomer of aristolochene. It is remarkable that these two enzymes exert such precise conformational control over substrate and intermediates so as to generate identical carbon skeletons with alternative stereochemistries, thereby emphasizing the template function of the active site.

Even prior to the report of its three-dimensional structure, epi-aristolochene synthase served as a paradigm system for protein engineering through the construction of chimeric enzymes in which exonic domains were swapped with corresponding domains of the related sesquiterpene cyclase vetispiradiene synthase (also known as premnaspirodiene synthase) from Egyptian henbane (*Hyoscyamus muticus*).³¹³ The mechanisms of these two enzymes proceed through a common eudesmane cation intermediate; a 1,2-methyl migration leads to the formation of epi-aristolochene, whereas a 1,2-alkyl migration and ring compression leads to the formation of the quaternary carbon of the vetispiradiene product (Figure 65). Conformational control of this intermediate plays an important role in governing the rearrangement of the carbon skeleton.³¹⁴ Interestingly, a chimeric cyclase results in an enzyme capable of generating both products. Crystal structure determinations of wild-type and chimeric cyclases, including the crystal structure of an intact enzyme–substrate complex with bound FPP, revealed structural features relevant to understanding the chemical mechanisms of both cyclases.^{56,315}

Clearly, epi-aristolochene synthase is a versatile catalyst in terms of its potential for biosynthetic diversity, and this potential has been realized in recent studies. While epi-aristolochene synthase is a reasonably high-fidelity template for catalysis, generating 78.9% epi-aristolochene from substrate FPP, 24 additional minor side products are also generated, some of which require an initial ionization-recombination-reionization sequence to generate a *cis*-farnesyl cation (i.e., a “*cisoid*” pathway).³¹⁶ Strikingly, subsequent studies show that epi-aristolochene synthase can utilize (*cis,trans*)-FPP as an alternative substrate with catalytic efficiency comparable to that of the natural substrate FPP (i.e., *trans,trans*-FPP).^{56,317}

In a *tour de force* experiment that unlocked the full biosynthetic potential of epi-aristolochene synthase, 512 mutants of epi-aristolochene synthase were generated in which all possible mutations were made at nine key residues in the active site; analyzing the product arrays of the resulting 418 active enzymes, Noel and colleagues provided a definitive demonstration of how mutations influence catalysis and product specificity.³¹⁸ This study not only illuminated structural and functional aspects that drive the evolution of product specificity in terpenoid cyclases but also provided critical insight relevant to the engineering of new biosynthetic pathways through synthetic biology. Undoubtedly, such potential applications will be facilitated through

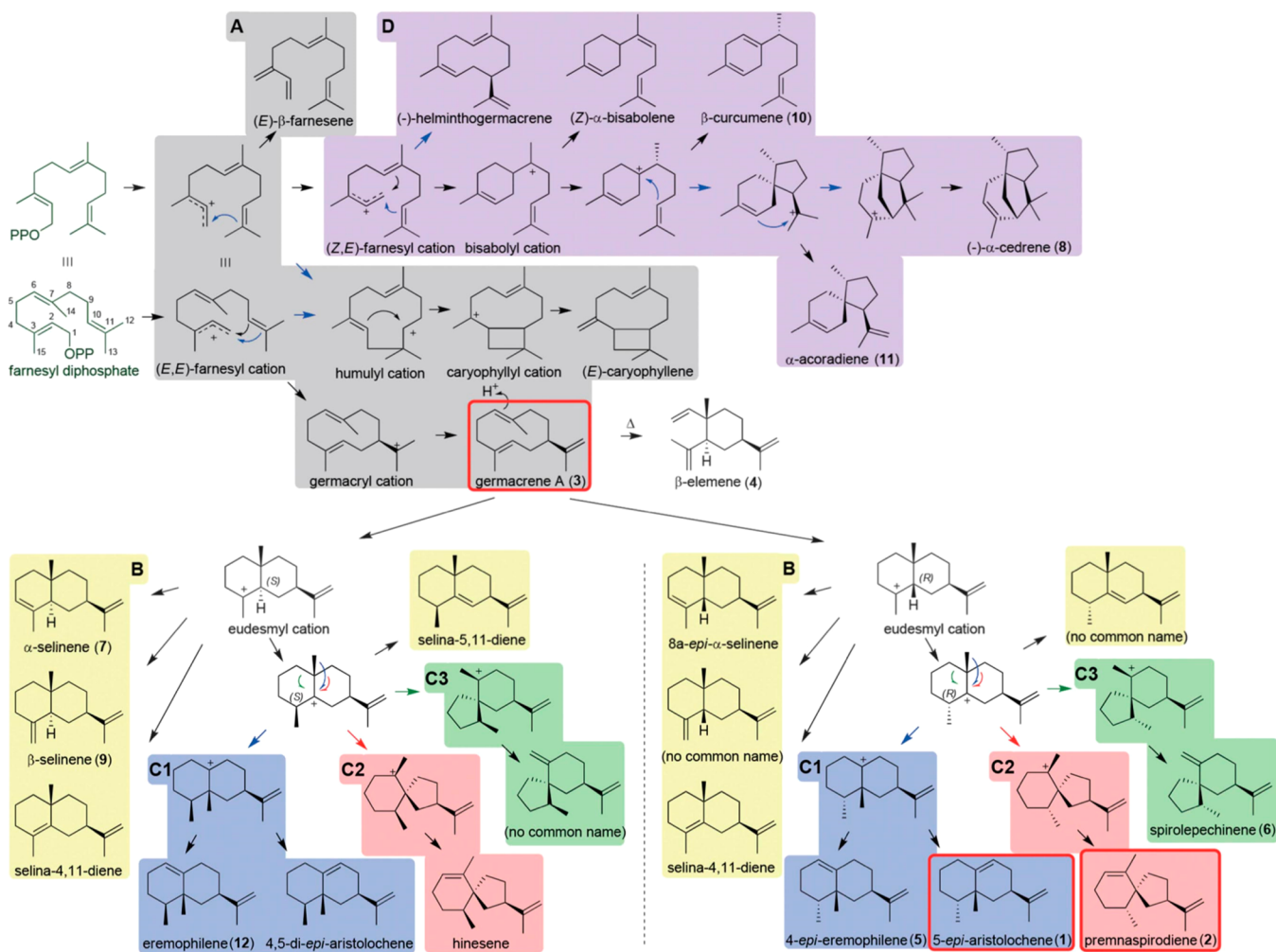


Figure 65. FPP cyclization reactions leading to the formation of major products 5-epi-aristolochene and prenaspirodiene, as well as alternative cyclization products generated by cyclase mutants classified by Noel and colleagues as follows:³⁰⁹ class A products (gray) result from quenching of early carbocation intermediates; class B products (yellow) derive from the eudesmane cation in the absence of any alkyl migrations; class C products (C1, blue; C2, red; C3, green) derive from three different alkyl migrations in the eudesmane cation; and class D products (purple) derive from the (*cis,trans*)-farnesyl cation. Reprinted with permission from ref 315. Copyright 2016 Macmillan Publishers Ltd.

the computationally guided construction of epi-aristolochene synthase mutants with substantially enhanced thermostability.³¹⁹

More recently, Noel and colleagues report studies of mutant enzymes that undergo self-alkylation through the introduction of a nucleophilic residue in the active site.³²⁰ Notably, alkylated enzymes are detected, many of which retain the ability to generate epi-aristolochene as the major product, but the site of alkylation is not the engineered residue. Instead, alkylation is detected at the aspartate residue in the DTE metal-binding motif and also a tyrosine in a loop flanking the active site. Interestingly, while alkylation is not detected in the wild-type enzyme when assayed with FPP at 25 °C, an alkylation product at the aspartate residue in the DTE motif is detected when the wild-type enzyme is assayed at 42 °C. X-ray crystallographic analysis of the W273E mutant at 2.43 Å resolution reveals alkylation of D444 in the DTE motif by a linear farnesyl group, so it is likely that the enzyme alkylation products observed in this study correspond to a farnesylation reaction that occurs immediately after FPP ionization. The active site mutation may slightly perturb the precatalytic binding conformation of FPP so that the intermolecular alkylation reaction successfully competes with the intramolecular cyclization reaction.

The catalytic versatility of epi-aristolochene synthase in the biosynthetic sequence of isoprenoid coupling and cyclization has also been explored in protein engineering experiments. Brodelius and colleagues demonstrate that epi-aristolochene synthase can be fused with either the N-terminus or the C-terminus of farnesyl diphosphate synthase from *Artemisia annua* to yield bifunctional terpenoid synthases, each of which exhibits an approximate 2-fold enhancement of epi-aristolochene generation as a function of time when incubated with GPP and IPP.³²¹ It is unlikely that a direct channel forms between the two active sites, since the same enhancement of cyclic product generation is observed regardless of the order in which the enzymes are fused. A general proximity effect³²² is more likely to account for the modest catalytic advantage observed. More recently, Chappell and colleagues show that catalytic versatility extends to the formation of terpene alkaloids, demonstrating that epi-aristolochene synthase slowly catalyzes the formation of a macrocyclic paracyclophane alkaloid from anilino geranyl diphosphate.³²³

5.2.9. Hedycaryol Synthase. Hedycaryol is a dominant sesquiterpene alcohol found in the essential oil of *Xanthocyparis vietnamensis* (Vietnamese gold cypress), a recently discovered species indigenous to Northern Vietnam.^{324,325} Also found in

flowering plants such as *Camellia brevistyla*, hedycaryol is thought to play a key role in the bouquet of terpenoids contributing to the floral scent so as to attract insects to the flowers for pollination.³²⁶

Hedycaryol synthase from *Kitasatospora setae* was recently cloned, expressed, and characterized, and the crystal structures of the unliganded enzyme and its complex with nerolidol were determined at resolutions of 2.7 and 1.5 Å, respectively.¹⁰⁸ The enzyme adopts the single α domain fold characteristic of a bacterial sesquiterpene cyclase, with nerolidol bound deep in a hydrophobic active site where it contacts the backbone carbonyl of V179 at the helix G break (Figure 66, panels A and B). As

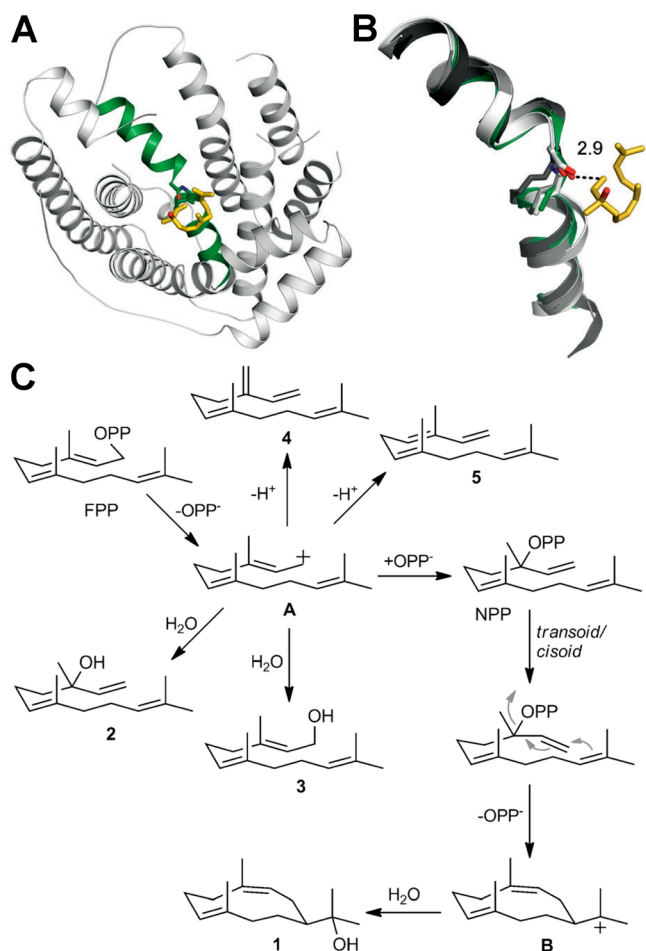


Figure 66. (A) Ribbon plot of hedycaryol synthase complexed with nerolidol (stick figure); helix G is green. (B) Close-up view of the helix G break in hedycaryol synthase, showing the 2.9 Å contact between the backbone carbonyl of V179 at the helix break and the hydroxyl group of nerolidol. (C) Mechanism of hedycaryol synthase accounting for the formation of major and minor products formed at pH 7.5: 1, hedycaryol; 2, nerolidol; 3, farnesol; 4, (*E*)- β -farnesene; 5, (3*E*,6*E*)- α -farnesene; A, farnesyl cation; B, helminthogermacradienyl cation. Reprinted with permission from ref 108. Copyright 2014 Wiley-VCH.

previously established in studies of squalene synthase, the exposed backbone carbonyl groups at the break in helix G may stabilize carbocation intermediates in catalysis.¹⁰⁷

The initial C1–C10 bond-forming reaction of hedycaryol synthase is preceded by an ionization–recombination–reionization sequence through intermediate nerolidyl diphosphate, and the cyclization reaction requires formation of the *cis*-allylic cation

prior to C1–C10 bond formation. Generation of the new C1–C10 bond results in a C11 tertiary carbocation intermediate, the helminthogermacradienyl cation,³²⁷ which is subsequently quenched by the addition of a solvent molecule to yield hedycaryol (Figure 66C).

Interestingly, pH-dependent cyclization specificity is observed. At pH 8.5, FPP is converted almost exclusively into hedycaryol, with only a trace of nerolidol detected, whereas at pH 7.5, hedycaryol remains the primary product, but significant amounts of nerolidol, farnesol, β -farnesene, and α -farnesene are detected. The generation of side products reflecting incomplete ring closure suggests that a slight pH-dependent conformational change converts the active site contour into a more permissive template for the FPP cyclization reaction. A mechanism accounting for the formation of all products generated by hedycaryol synthase is found in Figure 66C.

5.2.10. (+)- δ -Cadinene Synthase. The cyclization of FPP to form (+)- δ -cadinene is the first committed step in the biosynthesis of the phytoalexin gossypol (Figure 67),^{328–331} which is a defense metabolite in cotton that exhibits significant antimicrobial properties.³³² Interestingly, gossypol has been studied as a potential cancer chemotherapeutic agent^{333–336} as well as a male contraceptive,^{337,338} so the biosynthesis of this novel C₃₀ triterpene through the assembly and derivatization of two C₁₅ (+)- δ -cadinene precursors has served as the focus of many studies.

The catalytic mechanism of (+)- δ -cadinene synthase is similar to that of hedycaryol synthase (section 5.2.9) in that the C1–C10 cyclization reaction yielding the helminthogermacradienyl cation³²⁷ is preceded by an ionization–recombination–reionization sequence through intermediate (*R*)-nerolidyl diphosphate.^{328–331} As observed for sesquiterpene cyclases such as epi-isozizaene synthase (section 5.2.3) or trichodiene synthase (section 5.2.4), (*R*)-nerolidyl diphosphate can also lead to initial C1–C6 cyclization reaction, and Allemann and colleagues suggest this possibility under certain conditions based on mechanistic studies using fluorinated FPP analogues with (+)- δ -cadinene synthase.³³⁹ Nevertheless, presuming that the biological substrate FPP undergoes initial C1–C10 cyclization, a 1,3-hydride shift³⁴⁰ yields the 3(*Z*),7(*E*)-germacryl cation, a secondary cation which rapidly undergoes intramolecular cyclization and proton elimination to yield (+)- δ -cadinene. This is a high-fidelity reaction, since the enzyme generates >98% (+)- δ -cadinene.³⁴¹

The crystal structure of unliganded (+)- δ -cadinene synthase from *Gossypium arboreum*³⁴² reveals the characteristic $\alpha\beta$ fold of a plant terpenoid cyclase, which is monomeric in the crystal and in solution.³⁴³ The crystal structure of the complex with 3 Mg²⁺ ions and the unreactive substrate analogue 2-fluorofarnesyl diphosphate reveals a partially open active site conformation in which the flexible substrate analogue is determined to bind with a catalytically nonproductive conformation (Figure 68A). Strikingly, (+)- δ -cadinene synthase is unique among the vast majority of terpenoid cyclases in that it contains two aspartate-rich motifs DDXX(D,E) for Mg²⁺ complexation instead of one aspartate-rich motif and one NSE/DTE motif. Usually, the presence of two aspartate-rich motifs signals a coupling enzyme such as FPP synthase rather than a cyclase, so (+)- δ -cadinene synthase is an exception in this regard. Even so, superposition of metal-complexed structures of (+)- δ -cadinene synthase, aristolochene synthase, and FPP synthase reveals that the constellation of 3 Mg²⁺ ions is identical regardless of whether they are bound to a cyclase or coupling enzyme with two DDXX(D,E) motifs or

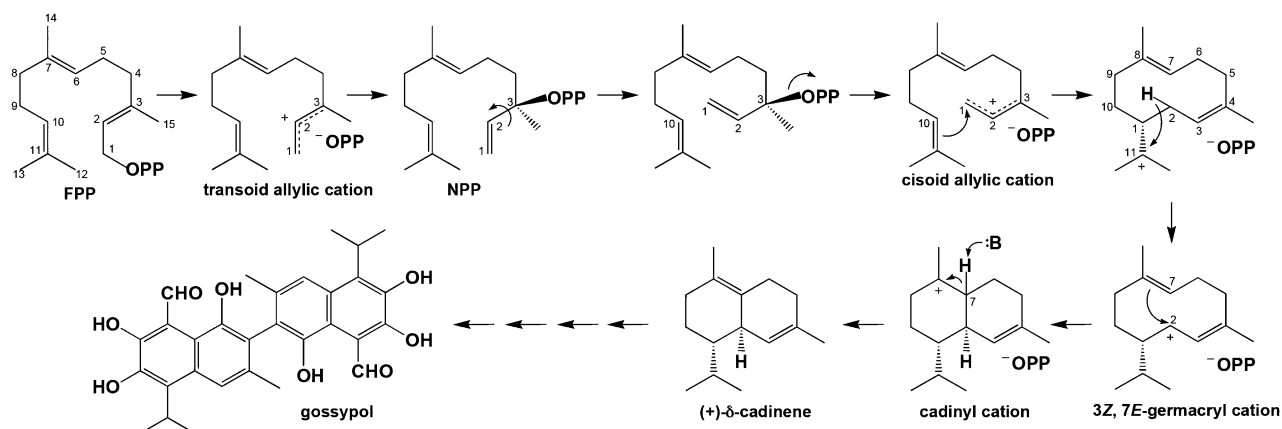


Figure 67. Proposed mechanism of (+)- δ -cadinene synthesis proceeds through an initial ionization–recombination–reionization sequence yielding a cisoid allylic cation, which then undergoes a C1–C10 cyclization reaction to yield the helminthogermacradienyl cation. A 1,3-hydride transfer and proton elimination then yield (+)- δ -cadinene. Reproduced from ref 342. Copyright 2009 American Chemical Society.

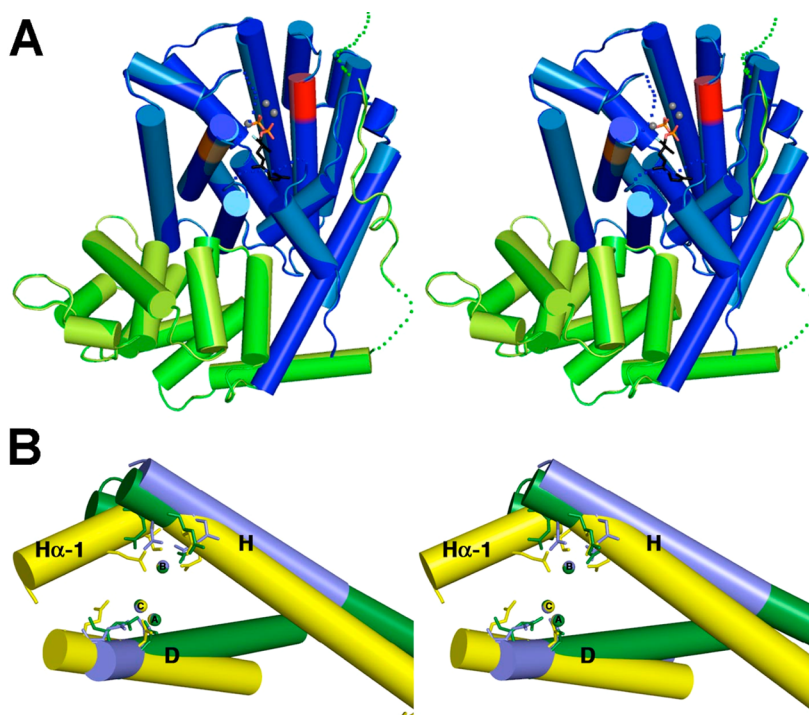


Figure 68. (A) Stereoview showing the structure of (+)- δ -cadinene synthase complexed with 3 Mg^{2+} ions (gray spheres) and 2-fluorofarnesyl diphosphate (stick figure) reveals the active site in the α domain (blue) with the N-terminus of the β domain (green) partially capping the active site. Aspartate-rich metal-binding motifs on helices D and H are red and orange, respectively. (B) Stereoview showing a superposition of helices D and H of (+)- δ -cadinene synthase (blue) with those of *A. terreus* aristolochene synthase (yellow) and *E. coli* farnesyl diphosphate synthase (green). The constellation of the 3 catalytically obligatory Mg^{2+} ions is identical regardless of whether Mg^{2+} is coordinated by an aspartate-rich or NSE/DTE motif on helix H and regardless of whether the enzyme catalyzes isoprenoid coupling or cyclization reactions. Reproduced from ref 342. Copyright 2009 American Chemical Society.

DDXX(D,E)-NSE/DTE motifs (Figure 68B). It is interesting to note that FPP synthase can generate cyclic sesquiterpene side products,³⁴⁴ so the chemical nature of metal coordination motifs in the terpenoid synthase active site do not necessarily dictate a functional difference between coupling and cyclization reactions.

Most recently, Allemann and colleagues demonstrate that the N-terminal polypeptide segment of (+)- δ -cadinene synthase is important for catalysis as it helps to cap the active site and protect carbocation intermediates from bulk solvent.³⁴⁵ Specifically, these investigators pinpoint the decapeptide segment M²¹RPKADFQPS, which is conserved in plant sesquiterpene

cyclases as XRPXXXFXPS, as critical for this activity. Although part of this segment is disordered in the crystal structure determination, it is conceivable that this segment becomes fully ordered as the active site adopts a fully closed conformation. As evident in Figure 68B, the N-terminal segment binds across the upper active site, consistent with a role in capping the active site.

5.2.11. Pentalene Synthase. The cyclization of FPP to form the tricyclic hydrocarbon pentalene represents the first committed step in the biosynthesis of the antibiotic pentalenolactone,^{346–349} which inhibits glyceraldehyde-3-phosphate dehydrogenase in Gram-negative and Gram-positive bacte-

ria.^{350–354} The reaction is catalyzed by pentalenene synthase, and the isolation and purification of the enzyme from *Streptomyces exfoliatus* UC5319 enabled the study of isotopically labeled substrates to ascertain the molecular details of the catalytic mechanism.^{347,355–357} Subsequent cloning and expression of the enzyme in *E. coli* yielded a fully functional recombinant enzyme identical in all respects to the native enzyme isolated from *S. exfoliatus*.³⁵⁸

The catalytic mechanism of pentalenene synthase as initially proposed on the basis of enzymological studies³⁵⁸ (path A in Figure 69) involved an initial C1–C11 cyclization reaction in

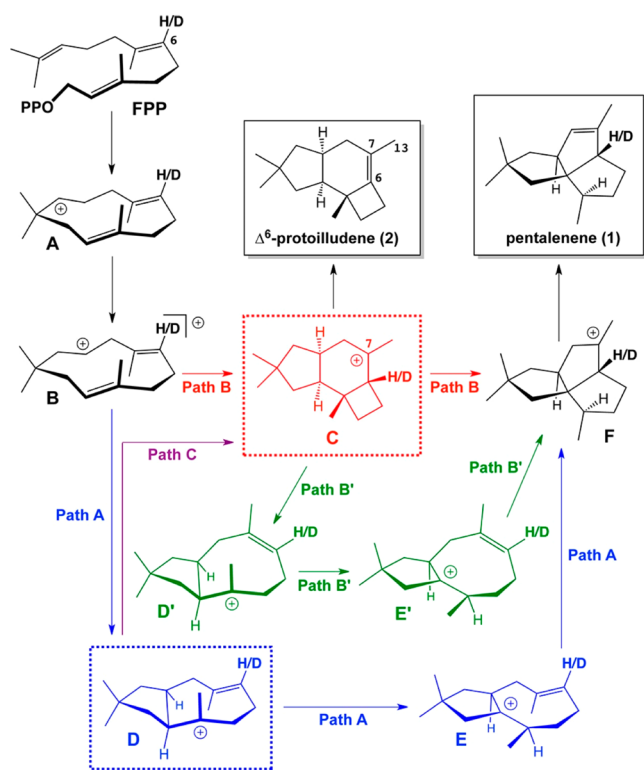


Figure 69. Possible reaction mechanisms for the cyclization of FPP to form the tricyclic sesquiterpene pentalenene. Pathway B is most consistent with all available enzymological data and chemical theory. Reproduced from ref 362. Copyright 2012 American Chemical Society.

anti-Markovnikov fashion to form humulyl cation A, which after isomerization to humulyl cation B yields secoillud-6-en-3-yl cation D; in turn, cation D undergoes a 1,2-hydride transfer and intramolecular carbon–carbon bond formation to generate pentalenyl cation F, which yields pentalenene after proton elimination. However, insightful analysis of the pentalenene synthase reaction using theoretical and computational chemistry led Gutta and Tantillo to propose an alternative cyclization pathway from humulyl cation B to pentalenyl cation F proceeding through the 7-protoilludyl cation C.³⁵⁹ This alternative pathway (path B in Figure 69) is consistent with all existing enzymological measurements using isotopically labeled substrates and also provided an easy rationalization for the generation of minor side product Δ^6 -protoilludene by certain active site mutants.^{360,361} The intermediacy of the 7-protoilludyl cation C was recently demonstrated by studying the isotopically sensitive branching ratio for the formation of pentalenene and Δ^6 -protoilludene from $[6\text{-}^2\text{H}]$ FPP as catalyzed by H309A pentalenene synthase; deprotonation of the deuterated 7-protoilludyl cation is less favorable due to the primary kinetic isotope effect and therefore yields an increased pentalenene: Δ^6 -protoilludene ratio.³⁶²

The crystal structure of unliganded pentalenene synthase was the first of a bacterial terpenoid cyclase and revealed the characteristic single α -domain structure topologically similar to that of FPP synthase, despite insignificant amino acid sequence identity between the two enzymes.³⁶ The structural homology between the enzyme that generates FPP and the enzyme that cyclizes FPP indicates that these enzymes divergently evolved from a common ancestor early in the evolution of terpenoid biosynthesis, after the gene duplication and fusion event involving the core 4-helix bundle that is the precursor to the class I terpenoid synthase fold (Figure 22). Although the active site of pentalenene synthase is predominantly hydrophobic, several polar residues are found at the mouth of the active site (e.g., the aspartate-rich motif and the NSE motif important for binding the trinuclear metal cluster required for catalysis) and other basic residues presumed to be important for binding the substrate diphosphate group (Figure 70). Also found in this region is H309, initially proposed to serve as a general base in catalysis,³⁶ but this role was ruled out on the basis of mutagenesis experiments.^{360,361} The more likely general base in the pentalenene synthase mechanism is inorganic pyrophosphate,

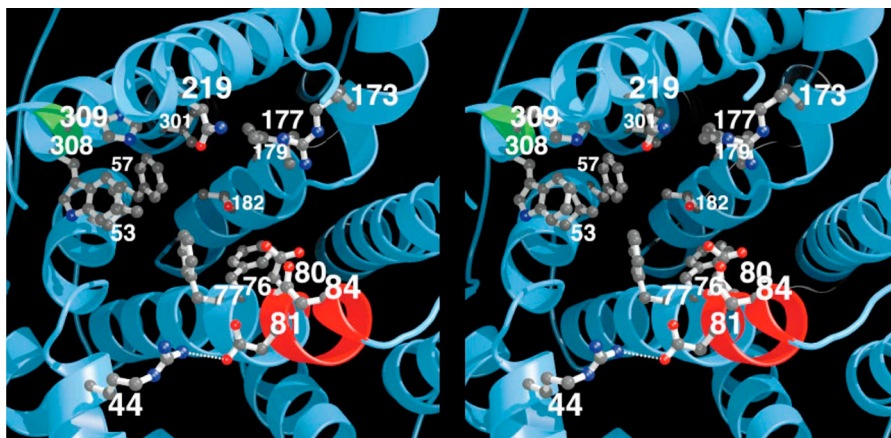


Figure 70. Stereoview of the active site of pentalenene synthase. Selected residues are indicated, and the aspartate-rich metal-binding motif is red. Reprinted with permission from ref 36. Copyright 1997 AAAS.

judged feasible in quantum chemistry calculations³⁶² and now broadly considered to serve this role.⁸⁰

5.3. Diterpene Cyclases

The possibilities for the initial cyclization of GGPP through metal-dependent ionization and departure of the diphosphate group include C1–C6, C1–C7, C1–C10, C1–C11, C1–C14, and C1–C15 bond-forming reactions, depending on which of the remaining carbon–carbon double bonds reacts with the initially formed allylic carbocation. A C3–C8 class I cyclization reaction is also possible with a bicyclic diterpene diphosphate substrate generated in a class II cyclization reaction with GGPP. As with an FPP cyclization reaction, the resulting carbocation intermediate can undergo further cyclization reactions, hydride transfers, methyl migrations, etc., before termination of the reaction by proton elimination or addition of a solvent molecule. Thus, in comparison with sesquiterpene cyclization reactions, even more diverse carbon skeletons result from diterpene cyclization reactions as a consequence of the additional carbon–carbon bond-forming trajectories available to the larger substrate.

To date, four crystal structures of monofunctional class I diterpene cyclases have been solved. Below, these cyclases are discussed in order of complexity of their initial GGPP cyclization reactions: C1–C11 (cyclooctatenol synthase), C3–C8 (*ent*-kaurene synthase), C1–C14 (taxadiene synthase), and a putative labdane-related diterpene cyclase (LrdC) for which the catalytic mechanism has not yet been established. The active site contour in the α domain of an enzyme with overall α or $\alpha\beta\gamma$ domain architecture serves as a template for catalysis by these diterpene cyclases, ensuring that substrate GGPP and subsequently formed intermediates are chaperoned through the proper sequence of reactions leading to formation of the correct product(s).

5.3.1. Cyclooctatenol Synthase (CotB2). Cyclooctatin is a tricyclic diterpene with 5–8–5 ring architecture that exhibits anti-inflammatory activity through its inhibition of lysophospholipase, which is prominent in eosinophilic inflammatory reactions and catalyzes the hydrolysis of fatty acid esters to generate free fatty acids and glycerophosphate.^{363,364} The cyclooctatin biosynthetic gene cluster in *Streptomyces melanosporofaciens* MI614–43F2 contains a GGPP synthase, cyclooctatenol synthase (CotB2), and two cytochromes P450.³⁶⁵ The structure and stereochemistry of the 5–8–5 ring system of cyclooctatin is established in the cyclization reaction catalyzed by cyclooctatenol synthase (Figure 71A).^{366,367}

The 1.64 Å resolution crystal structure of cyclooctatenol synthase was the first of a bacterial diterpene cyclase and revealed a single α -domain architecture characteristic of a class I terpenoid cyclase.³⁶⁸ The enzyme forms a dimer in solution and in the crystal, with active sites oriented in antiparallel fashion. The crystal structures of the unliganded wild-type enzyme and the F149L mutant reveal an open active site conformation, with a hydrophobic active site cleft flanked by aspartate-rich and NSE metal-binding motifs at the upper rim of the active site on helices D and H, respectively (Figure 71A). Structural comparison with taxadiene synthase reveals an active site with decreased volume, so contrasting active site contours reflect the contrasting cyclization pathways governed by these diterpene cyclases.

Mutagenesis studies reveal that the diterpene cyclization cascade can be reprogrammed by single amino acid substitutions in the active site (Figure 71B).^{368,369} Specifically, substitution of active site aromatic residues results in the formation of alternative products. For example, F149L cyclooctatenol synthase generates a tricyclic cyclooctatenol isomer, cyclooctat-7-en-3-ol, which

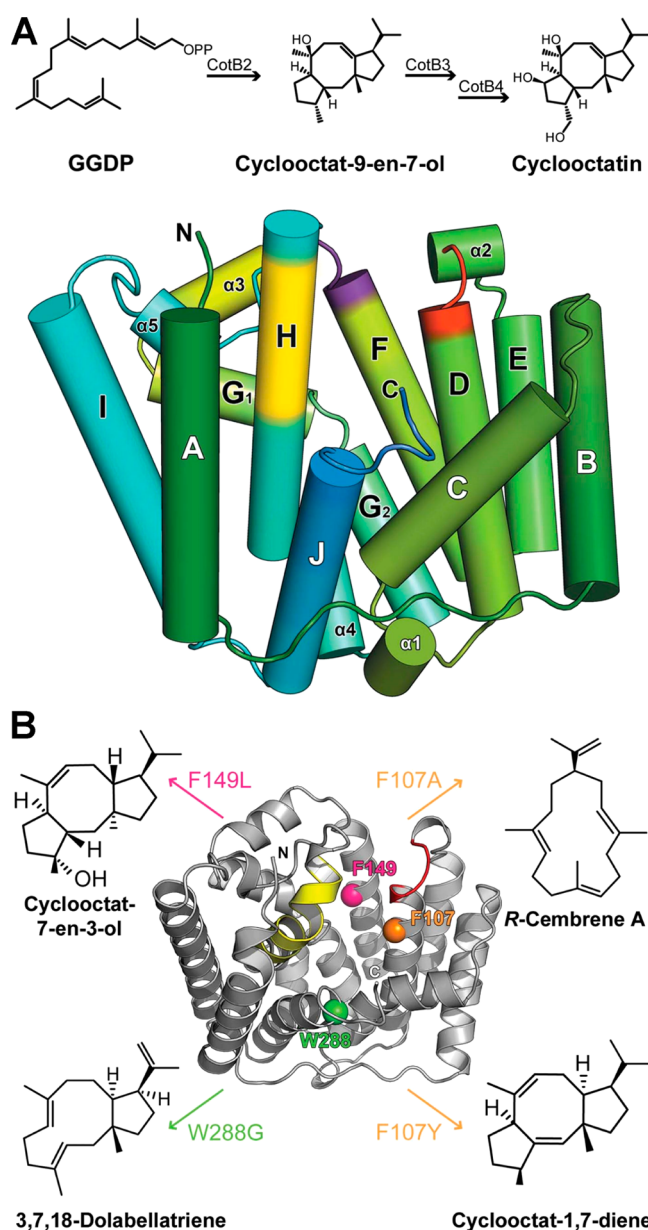


Figure 71. (A) Cyclooctatenol synthase (CotB2) catalyzes the cyclization of GGPP to form cyclooctat-9-en-7-ol, which undergoes subsequent oxidation by two separate cytochromes P450 (CotB3 and CotB4) to yield the lysophospholipase inhibitor cyclooctatin. (B) Active site mutations of cyclooctatenol synthase reprogram the cyclization cascade to generate alternative diterpene products. Reprinted with permission from ref 368. Copyright 2014 International Union of Crystallography.

reflects complete 5–8–5 ring formation with an alternative C6–C2 ring closure and quenching reaction. F107Y cyclooctatenol synthase generates the hydrocarbon cyclooctat-1,7-diene, which reflects complete 5–8–5 ring formation with an alternative proton elimination to terminate the cyclization cascade. W188H, W186L, and W288G cyclooctatenol synthases generate a bicyclic product, 3,7,18-dolabellatriene, which reflects premature derailment of the cyclization cascade by proton elimination from the first cyclic carbocation intermediate. Notably, certain dolabellatrienes exhibit antibacterial properties against multidrug resistant *Staphylococcus aureus* (MRSA),³⁷⁰ so W188H, W186L, or W288G cyclooctatenol synthases could be used for the

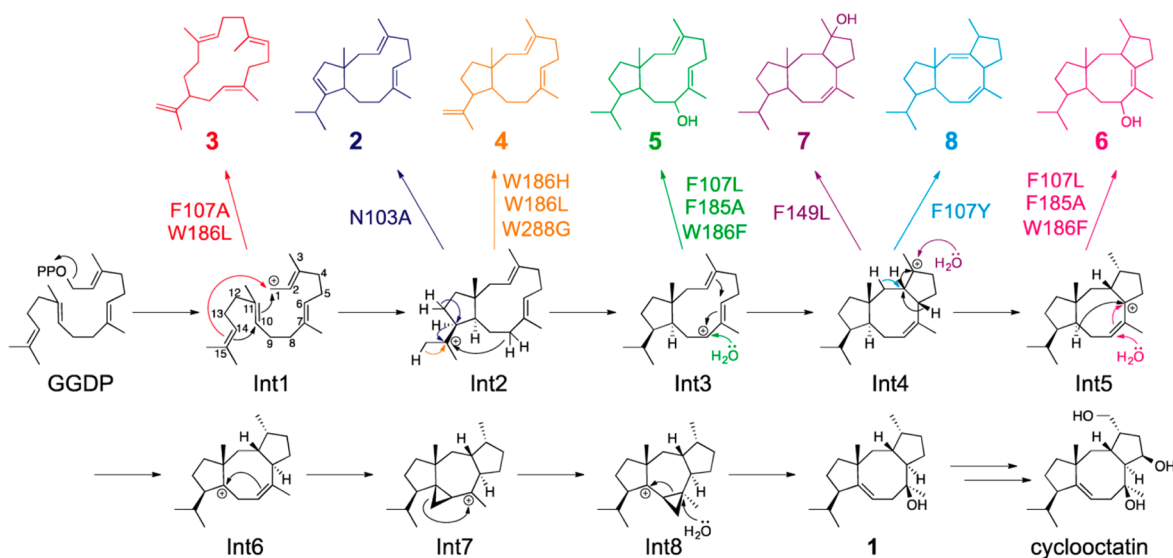


Figure 72. Cyclization mechanisms of wild-type cyclooctatenol synthase (CotB2^{wt}) and selected active site mutants that generate alternative cyclization products: cyclooctat-9-en-7-ol (1), 3,7,12-dolabellatriene (2), cembrene A (3), 3,7,18-dolabellatriene (4), 3,7-dolabellatrien-9-ol (5), cyclooctat-6-en-8-ol (6), cyclooctat-7-en-3-ol (7), and cyclooctat-1,7-diene (8). Reproduced from ref 369. Copyright 2017 American Chemical Society.

generation of a new class of antibiotics through synthetic biology approaches.^{368,369}

In contrast with the three mutants just described, for which the chemistry reflects a derailment of the natural cyclization pathway leading to product cyclooctat-9-en-7-ol, F107A and W186L cyclooctatenol synthases also generate cembrene A, which reflect an initial C1–C14 cyclization reaction instead of the initial C1–C11 cyclization reaction catalyzed by the wild-type enzyme and other mutants described above. The cyclization mechanisms of wild-type cyclooctatenol synthase and a wide array of active site mutants are summarized in Figure 72.

5.3.2. *ent*-Kaurene Synthase. Hundreds of kaurane diterpenoids have been identified to date, each of which adopts a core tetracyclic structure exemplified by that of *ent*-kaur-16-ene (Figure 75).³⁷¹ These compounds are generated mainly by plants and often serve as precursors to plant growth regulators. Kaurane diterpenoids also exhibit a variety of useful pharmacological properties, exhibiting antispasmodic, antiallergenic, and immunosuppressive effects; in contrast, others are embryotoxic, genotoxic, and insecticidal.³⁷² The complex tetracyclic kauranoid skeleton is thus a naturally occurring privileged platform in biology.

The biosynthesis of the tetracyclic kaurane skeleton requires both class I and class II cyclization reactions. For example, consider the biosynthesis of *ent*-kaur-16-ene (Figure 73). First, the class II protonation-mediated cyclization of GGPP generates *ent*-copalyl diphosphate (this reaction is discussed further in section 6.1). In the subsequent class I cyclization reaction, *ent*-copalyl diphosphate undergoes metal-dependent ionization and cyclization through several carbocation intermediates to form the tetracyclic kaurane skeleton. The class I cyclization reaction is catalyzed by *ent*-kaurene synthase, which in the soil bacterium *Bradyrhizobium japonicum* is a separate enzyme from the *ent*-copalyl diphosphate synthase.³⁷³ Interestingly, in other species such as fungi and the moss *Physcomitrella patens*, the class I and class II cyclization activities are contained in a single bifunctional enzyme.^{374–376}

The class I cyclization reaction catalyzed by *ent*-kaurene synthase from *Bradyrhizobium japonicum* is unusual in that the substrate is not the linear isoprenoid precursor GGPP but instead

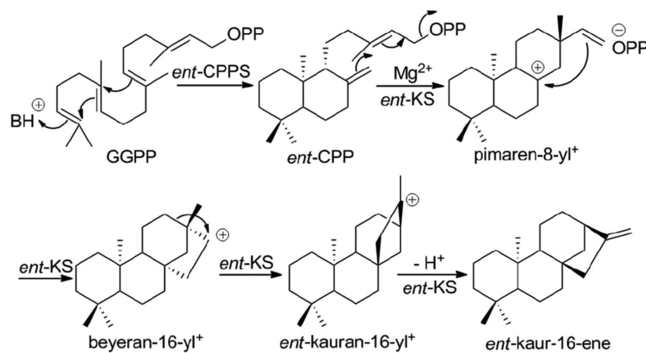


Figure 73. Biosynthesis of *ent*-kaur-16-ene, or simply *ent*-kaurene, in the soil bacterium *Bradyrhizobium japonicum* proceeds through two separate enzyme-catalyzed reactions. The first reaction is a class II protonation-initiated cyclization of GGPP to form *ent*-copalyl diphosphate (*ent*-CPP), catalyzed by *ent*-copalyl diphosphate synthase (*ent*-CPPS). The second reaction is a class I ionization-initiated cyclization of *ent*-CPP to form *ent*-kaurene, catalyzed by *ent*-kaurene synthase (*ent*-KS). Reprinted from ref 377.

the partially cyclized biosynthetic intermediate *ent*-copalyl diphosphate. Thus, the active site of *ent*-kaurene synthase does not serve as a template for the binding of GGPP but instead must specifically accommodate the bicyclic diphosphate substrate to enable the formation of the remaining two rings of the tetracyclic product through an initial C3–C8 bond-forming reaction. The recently determined 1.8–2.0 Å resolution crystal structures of the unliganded enzyme, its complex with a bisphosphonate inhibitor, and the D75C mutant complexed with *ent*-copalyl diphosphate reveal important mechanistic inferences.³⁷⁷ The enzyme adopts the characteristic single α domain fold of a class I bacterial terpenoid synthase (Figure 74A) and two monomers associate in roughly parallel fashion to form a dimer. While the electron density map of the D75C *ent*-kaurene synthase–*ent*-copalyl diphosphate complex is somewhat noisy (Figure 74B), perhaps reflecting disorder due to the lack of bound metal ions, the structure of this open-conformation enzyme–substrate complex confirms the location of the active site and provides a

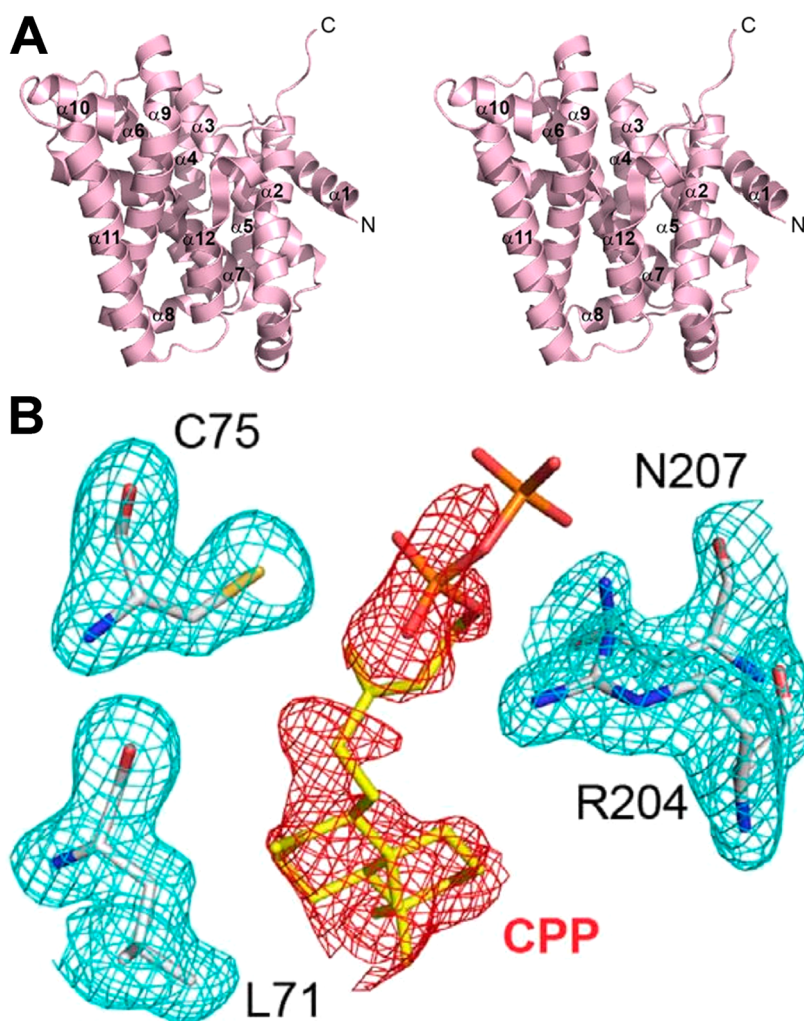


Figure 74. (A) Stereoview of *ent*-kaurene synthase from the soil bacterium *Bradyrhizobium japonicum*. (B) Omit electron density map showing the binding of the substrate *ent*-copalyl diphosphate in the active site of *ent*-kaurene synthase. Reprinted from ref 377. Copyright 2015 Nature Publishing Group.

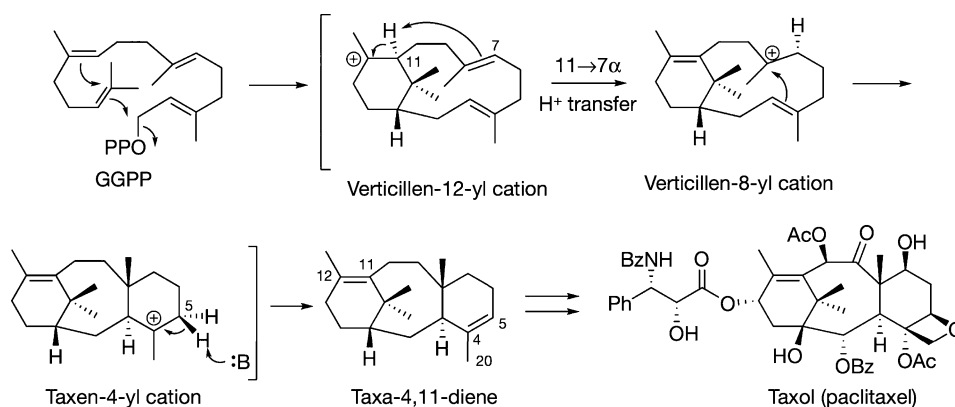


Figure 75. Catalytic mechanism of taxadiene synthase. Taxadiene undergoes subsequent biosynthetic modifications to yield the cancer chemotherapeutic drug Taxol. Reprinted with permission from ref 42. Copyright 2011 Macmillan Publishers Ltd.

view of a possible precatalytic orientation for the substrate prior to ionization and cyclization.

5.3.3. Taxadiene Synthase. The taxane diterpene paclitaxel (Taxol), isolated from the bark of the Pacific yew tree *Taxus brevifolia*,³⁷⁸ exhibits potent antitumor properties by stabilizing microtubules,^{379,380} which at higher drug concentrations leads to

cell cycle arrest and apoptosis.^{381,382} Recent data suggest an alternative mode of action at lower, clinically relevant concentrations in tumor cells, in which Taxol causes division of chromosomes on multipolar spindles, chromosomal missegregation, and cell death.^{382,383} Taxol is approved by the U.S. Food and Drug Administration for the treatment of ovarian, breast, and

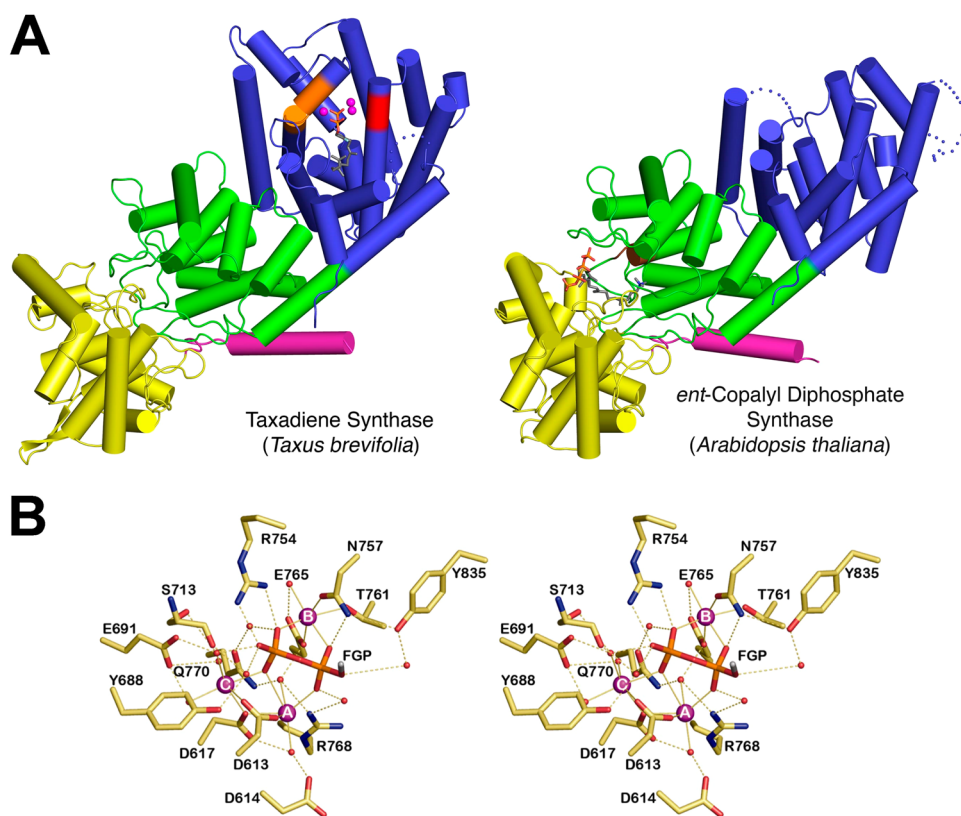


Figure 76. (A) Taxadiene synthase and *ent*-copalyl diphosphate synthase share a common $\alpha\beta\gamma$ domain architecture (α domain, blue; β domain, green; γ domain, yellow; N-terminus, magenta). The active site of taxadiene synthase is located in the α domain, where 3 Mg²⁺ ions (magenta spheres) stabilize the diphosphate group of a bound substrate analogue (stick figure). The active site of *ent*-copalyl diphosphate synthase is located at the $\beta\gamma$ domain interface, as indicated by the binding of a substrate analogue (stick figure). Reprinted with permission from ref 44. Copyright 2011 Nature Publishing Group. (B) Stereoview of the Mg²⁺₃ cluster in the active site of taxadiene synthase. The isoprenoid moiety of substrate analogue 2-fluorogeranylgeranyl diphosphate (FGP) is truncated for clarity. Reprinted from ref 44. Copyright 2011 Nature Publishing Group.

lung cancer and is used off-label in the treatment of several other cancers. By all measures, Taxol is highly regarded as a blockbuster drug for cancer chemotherapy.

Taxadiene synthase catalyzes the first committed step of Taxol biosynthesis and is responsible for the generation of the tricyclic hydrocarbon skeleton of Taxol with structural and stereochemical precision. Taxadiene synthase was first isolated from the pacific yew³⁸⁴ and cloned and expressed in *E. coli* as an 862-residue full-length protein.³⁸⁵ The amino acid sequence of the full-length protein contains a plastidial targeting sequence at the N-terminus, so the preparation of a construct lacking this sequence facilitated the overexpression of a pseudomature form of the enzyme for functional analysis.³⁸⁶ The major cyclization product of recombinant pseudomature taxadiene synthase is taxa-4(5),11(2)-diene (henceforth simply “taxadiene”), but minor side products taxa-4(20),11(12)-diene (~5%) and verticillene (~1%) are also generated.

The chemical mechanism of GGPP cyclization catalyzed by taxadiene synthase (Figure 75) has been extensively studied using isotopically labeled substrates and fluorinated substrate analogues. Metal-triggered ionization of the substrate diphosphate group enables C1–C14 bond formation with inversion of configuration at C1, quite possibly in concert with C10–C15 bond formation, to yield the verticillyl cation intermediate.^{386–388} Subsequently, an unusual intramolecular proton transfer^{387,389,390} between C11 and the *re* face of C7 followed by transannular ring closure yields the taxenyl cation, which undergoes proton elimination to yield taxadiene.

The 1.82 Å resolution crystal structure of taxadiene synthase complexed with the bicyclic diterpene analogue 13-aza-13,14-dihydrocopalyl diphosphate and the 2.25 Å resolution crystal structure of taxadiene synthase complexed with the unreactive substrate analogue 2-fluorogeranylgeranyl diphosphate were the first crystal structures reported of a diterpene synthase⁴² and revealed $\alpha\beta\gamma$ domain architecture in which the class I active site resides in the α domain; the $\beta\gamma$ domains have no known catalytic function, other than perhaps to provide the N-terminal polypeptide segment to help cap the active site upon substrate binding. This domain architecture is identical to that observed for the class II diterpene cyclase *ent*-copalyl diphosphate synthase (Figure 76A) (section 6.1). The plastidial targeting sequence plus an additional 27 residues were deleted from the N-terminus in the taxadiene synthase construct that yielded crystals, which attenuated but did not obliterate catalytic activity. It is interesting that 13-aza-13,14-dihydrocopalyl diphosphate binds in the active site of taxadiene synthase because this analogue does not mimic any intermediates in the taxadiene synthase reaction. The binding of both diterpene analogues in the active site in the α domain is accommodated by 3 Mg²⁺ ions: Mg²⁺_A and Mg²⁺_C are coordinated by D613 and D617 in the aspartate-rich motif, and Mg²⁺_B is chelated by N757, T761, and E765 in a hybrid NSE/DTE motif (Figure 76B). Given the disorder observed for the J–K loop in these structures,⁴² the active site is thought to adopt a partially closed conformation. Computational techniques have recently been employed to construct a model of the fully closed conformation of taxadiene synthase.³⁹¹

Although taxadiene synthase contains complete β and γ domains as found in class II terpenoid cyclases such as *ent*-copalyl diphosphate synthase (section 6.1), there is no corresponding catalytic function at the $\beta\gamma$ interface of taxadiene synthase since the catalytically required general acid residue is absent. Indeed, the γ domain can be spliced out of taxadiene synthase to form a smaller $\alpha\beta$ construct that retains a significant degree of cyclization specificity for taxadiene formation, although catalytic efficiency is attenuated.³⁹²

Given the high demand for Taxol in cancer chemotherapy, metabolic engineering approaches have been explored for the biosynthesis of taxadiene and other Taxol biosynthetic intermediates with the hope of providing a more economical and renewable source of the drug through synthetic biology.³⁹³ For example, taxadiene synthase has been utilized for taxadiene overproduction in *E. coli*,³⁹⁴ yeast (*Saccharomyces cerevisiae*),³⁹⁵ *Arabidopsis*,³⁹⁶ ginseng root (*Panax ginseng* C.A. Meyer),³⁹⁷ and *Artemisia annua* L.³⁹⁸ Moreover, recent studies show that the combination of mutagenesis and pathway engineering yields an alternative approach for Taxol generation through the alternative cyclization product taxa-4(20)-11(12)-diene, which is a minor product generated by the wild-type enzyme.³⁹⁹ These studies suggest a promising future for the manufacture of Taxol through synthetic biology.

5.3.4. Labdane-Related Diterpene Cyclase (LrdC).

Recently, a labdane-related biosynthetic gene cluster was identified in the soil bacterium *Streptomyces* sp. K155, isolated in Valle de Chalco, Mexico, and the putative class I diterpene cyclase LrdC encoded by this cluster was crystallized.⁴⁰⁰ The crystal structure of LrdC complexed with 3 Mg^{2+} ions and inorganic pyrophosphate has been solved and refined at 2.36 Å resolution and the coordinates deposited in the Protein Data Bank (www.rcsb.org, PDB accession code 5A0J). The structure reveals a dimer of single α domains oriented in parallel fashion (Figure 77). A full paper describing the structure and chemical

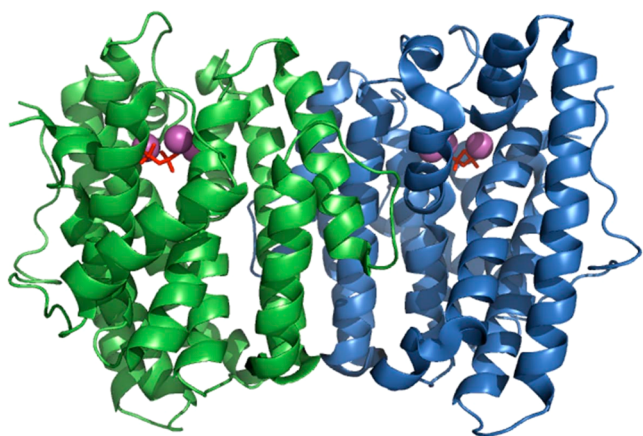


Figure 77. Crystal structure of the diterpene cyclase LrdC (PDB 5A0J).

mechanism of this diterpene cyclase has not yet appeared, so complete details regarding structure–function relationships are not yet available.

5.4. Sesterterpene Cyclases

Although sesterterpenes are comparatively rare relative to monoterpenes, sesquiterpenes, and diterpenes, examples of polycyclic C_{25} natural products are found in plants,⁴⁰¹ fungi,^{402–408} and marine organisms such as planktonic diatoms that live in open water,⁴⁰⁹ benthic diatoms that live in surface

films,⁴⁰⁹ and a variety of sponges.^{410–415} Many sesterterpenes exhibit useful pharmacological properties (e.g., as antitumor and anti-inflammatory agents);^{411,413–417} notably, an ophiobolin derivative from *Bipolaris oryzae* promotes the degradation of pathogenic α -synuclein in neural cells.⁴¹⁸ The biological and pharmaceutical importance of complex sesterterpene natural products has inspired the discovery and development of novel synthetic approaches for their generation (e.g., as recently described for the total synthesis of (–)-6-*epi*-ophiobolin N).⁴¹⁹

The first committed step of sesterterpene biosynthesis is the cyclization of geranylgeranyl diphosphate (GGPP; Figure 1) as catalyzed by a sesterterpene cyclase. At present, no crystal structures of sesterterpene cyclases have been reported, so an analysis of structure–function relationships in this enzyme family is not currently feasible. However, these enzymes catalyze metal-dependent cyclization reactions and their amino acid sequences contain conserved metal-binding motifs characteristic of the α fold of a class I terpenoid cyclase. Furthermore, fungal sesterterpene cyclases such as ophiobolin F synthase are typically coupled with a GGPP synthase to form a bifunctional $\alpha\alpha$ domain assembly.⁴⁰² Similar bifunctional assemblies function in diterpene biosynthesis and are discussed in section 7.3. Sesterterpene cyclases comprise the next frontier for terpenoid cyclase structural biology and protein engineering.

6. CLASS II TERPENOID CYCLASES

Class II terpenoid cyclases initiate catalysis by protonation of a carbon–carbon π bond or epoxide moiety in an isoprenoid substrate to yield a tertiary carbocation which can then react with one of the remaining π bonds of the substrate, typically the adjacent π bond to form a 6-membered ring in concerted or stepwise fashion. The catalytic general acid is the central aspartate in the characteristic sequence motif DXDD (this motif is unrelated to the aspartate-rich DDXXD motif of class I terpenoid cyclases). The active site of a class II terpenoid cyclase is located at the interface of the β and γ domains in a protein with overall $\beta\gamma$ or $\alpha\beta\gamma$ domain architecture. A $\beta\gamma$ enzyme is a monofunctional class II cyclase, whereas an $\alpha\beta\gamma$ enzyme can be a monofunctional class II cyclase or a bifunctional class I–class II cyclase (bifunctional terpenoid cyclases are discussed in section 7). The remainder of this section outlines structure–mechanism relationships for class II terpenoid cyclases that utilize the C_{20} substrate GGPP or the C_{30} substrates squalene or squalene oxide.

6.1. Diterpene Cyclases

Class II diterpene cyclases initiate catalysis by protonation of the terminal π bond of GGPP, likely in concert with C10–C15 bond formation and C6–C11 bond formation to yield a bicyclic tertiary carbocation intermediate. As with cyclization reactions catalyzed by class I terpenoid cyclases, the resulting carbocation intermediate can undergo further reactions, hydride transfers, methyl migrations, etc. before termination of the reaction by proton elimination or addition of a solvent molecule.

To date, two crystal structures of monofunctional class II diterpene cyclases have been solved. Both of them are *ent*-copalyl diphosphate synthases: one is a plant enzyme, the other is a bacterial enzyme. Both utilize identical chemical strategies for GGPP activation and cyclization.

6.1.1. *ent*-Copalyl Diphosphate Synthase from *Arabidopsis thaliana*. The labdane-related diterpenoids comprise a family of more than 7000 natural products that serve various functions in plants, fungi, and bacteria.^{420,421} In plants, the labdane diterpenoid *ent*-copalyl diphosphate is an intermediate

in the biosynthetic pathway leading to the formation of *ent*-kaurene and ultimately gibberellin phytohormones, which are important for plant growth and development.^{422–424} The class II diterpene cyclase that converts GGPP into *ent*-copalyl diphosphate was initially designated *ent*-kaurene synthetase A when first cloned from *Arabidopsis thaliana*,⁴²⁵ but this enzyme is now better known as *ent*-copalyl diphosphate synthase. The preparation of a pseudomature recombinant form of the enzyme lacking the N-terminal plastidial targeting sequence facilitated structural and functional analysis.⁴²⁶

The crystal structures of *ent*-copalyl diphosphate synthase complexed with substrate analogue (*S*)-15-aza-14,15-dihydrogeranylgeranyl thiolodiphosphate at 2.25 Å resolution and product analogue 13-aza-13,14-dihydrocopalyl diphosphate at 2.75 Å resolution were the first of a class II diterpenoid cyclase (analogue structures are shown in Figure 78).⁴⁴ Although the

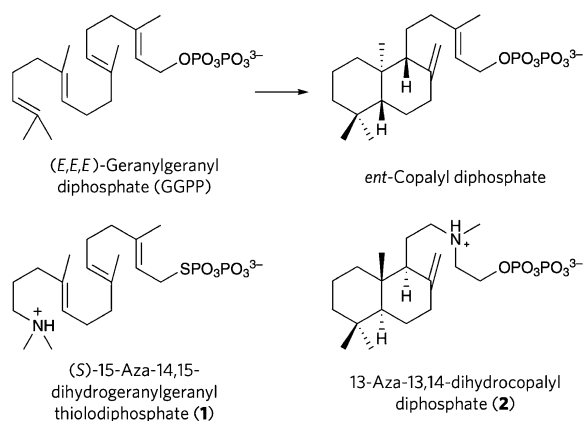


Figure 78. Cyclization of GGPP to form *ent*-copalyl diphosphate is the first committed step of gibberellin biosynthesis in *Arabidopsis thaliana* and is catalyzed by the class II diterpene cyclase *ent*-copalyl diphosphate synthase. (*S*)-15-Aza-14,15-dihydrogeranylgeranyl thiolodiphosphate (1) is an unreactive analogue of substrate GGPP, and 13-aza-13,14-dihydrocopalyl diphosphate (2) is a stereoisomer of a product analogue. Reprinted from ref 44. Copyright 2011 Nature Publishing Group.

substrate analogue binds in the enzyme active site, the product analogue does not, binding instead at an interlattice site in the crystal (a product analogue with correct stereochemistry was unavailable for this study). Since the stereochemistry of the product analogue does not match that of the actual product, its exclusion from the active site reflects the precise stereochemical control that the active site imposes on the GGPP cyclization cascade to ensure that the correct product stereoisomer is formed.

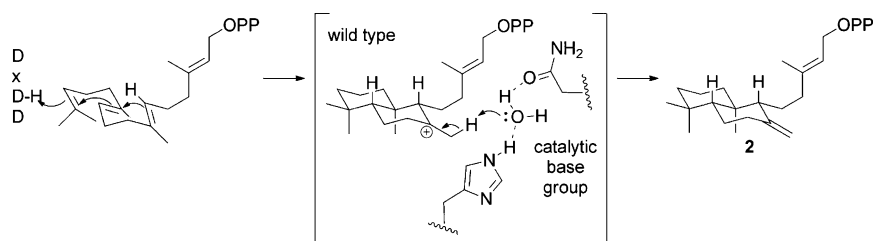


Figure 79. Cyclization of GGPP catalyzed by *ent*-copalyl diphosphate synthase is initiated by D379 in the DXDD general acid motif. Concerted carbon–carbon bond-forming reactions yield a bicyclic carbocation intermediate that is quenched by a solvent-mediated proton elimination to yield *ent*-copalyl diphosphate (2). The solvent molecule that serves as the catalytic base is oriented by hydrogen bonds with H263 and N322. Reprinted with permission from ref 429. Copyright 2014 Wiley-VCH.

The overall domain architecture of *ent*-copalyl diphosphate synthase is $\alpha\beta\gamma$, with the active site located at the $\beta\gamma$ domain interface as indicated by the binding of the substrate analogue; although the domain architecture is identical to that of taxadiene synthase, the location of the active site is not (Figure 76A). The active site cavity of *ent*-copalyl diphosphate synthase is quite hydrophobic in nature and its three-dimensional contour is defined by aromatic and aliphatic residues. The α domain lacks the characteristic aspartate-rich and NSE/DTE metal-binding motifs of a class I cyclase and has no known function, so it is presumed to be an evolutionary vestige.

The cyclization cascade is triggered by protonation of C14 of GGPP by general acid D379 in the D³⁷⁷IDD motif (Figure 79).⁴²⁷ The superacidic *anti*-oriented proton of D379, approximately 10⁴-fold more acidic than a *syn*-oriented proton,⁴²⁸ is oriented toward the substrate. Since a strong acid is required to protonate a carbon–carbon π bond (e.g., H₃O⁺ with pK_a = −1.7), the utilization of an *anti*-oriented carboxylic acid proton with a pK_a of ~0.5 is ideal for this catalytic function. The orientation of D379 is fixed by hydrogen bond interactions with N425 and a water molecule which in turn forms a hydrogen bond with T421 (Figure 80).

Following formation of the bicyclic carbocation intermediate (Figure 79), the cyclization cascade is terminated by proton elimination. Peters and colleagues show that the general base for this step is an active site water molecule bonded with H263 and N322.⁴²⁹ Interestingly, the H263F and H263Y mutants reprogram the cyclization cascade so as to allow 1,2-hydride and 1,2-methyl shifts leading to the formation of an alternative diterpene product, kolavenyl diphosphate, so both the active site contour and the position of the general base govern product outcome.⁴³⁰ Cyclases that naturally generate kolavenyl diphosphate were subsequently identified to contain phenylalanine or tyrosine residues in place of the histidine residue corresponding to H263; moreover, tyrosine-to-histidine substitution results in the generation of *ent*-copalyl diphosphate, so this residue plays a critical role in directing the termination step of a class II terpenoid cyclase.^{431–433}

The crystal structure of *ent*-copalyl diphosphate synthase complexed with substrate analogue (*S*)-15-aza-14,15-dihydrogeranylgeranyl thiolodiphosphate has been extended to 1.55 Å resolution, clarifying certain active site features that were ambiguous in the lower-resolution structures.⁴³⁴ While the tertiary ammonium cation and the thiolodiphosphate group of the substrate analogue are each disordered between two conformations in the lower resolution structure, they each adopt a single, well-ordered conformation in the higher resolution structure (Figure 80). The ordering of the thiolodiphosphate group might be attributed to the presence of

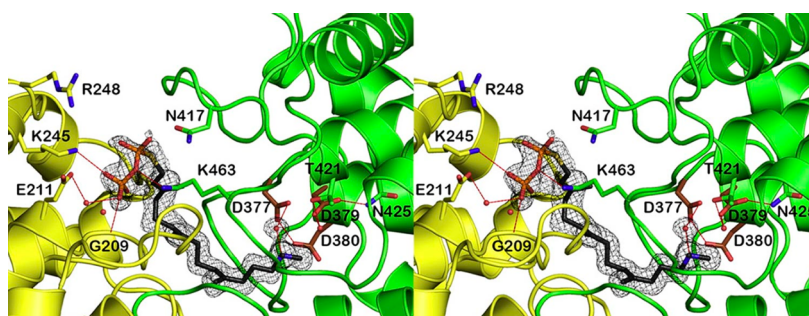


Figure 80. 1.55 Å resolution simulated annealing omit map of (*S*)-15-aza-14,15-dihydrogeranylgeranyl thiolodiphosphate (compound 1 in Figure 78) bound in the active site of *ent*-copalyl diphosphate synthase. Reprinted with permission from ref 434. Copyright 2014 Elsevier.

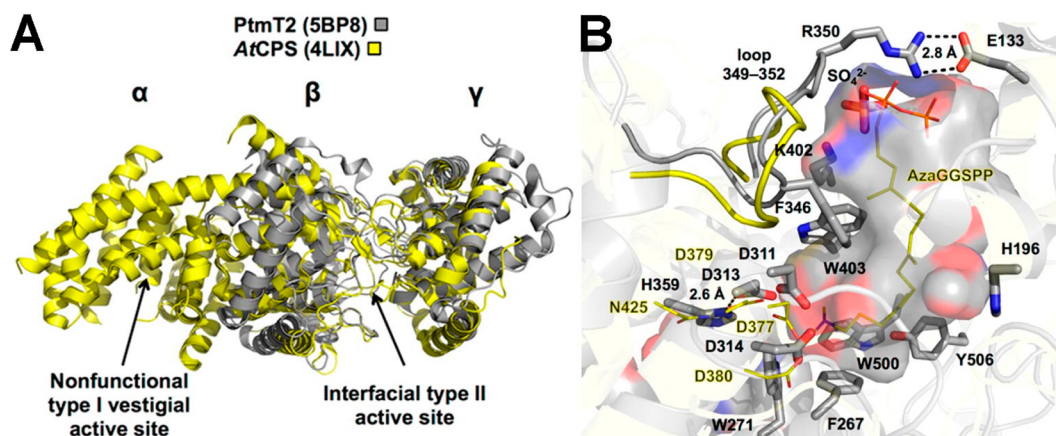


Figure 81. (A) Superposition of *ent*-copalyl diphosphate synthase from *Arabidopsis thaliana* ($\alpha\beta\gamma$ domain architecture, yellow) and *Streptomyces platensis* CB00739 ($\beta\gamma$ domain architecture, gray). (B) Superposition of *ent*-copalyl diphosphate synthase active sites. In the plant enzyme, N425 hydrogen bonds with general acid D379, whereas in the bacterial enzyme H359 hydrogen bonds with general acid D313. Reproduced from ref 435. Copyright 2016 American Chemical Society.

1.0 mM MgCl_2 in the crystallization buffer (Mg^{2+} is required for enzyme activity, presumably to accommodate substrate binding⁴²⁶); however, no well-ordered Mg^{2+} ions are observed in electron density maps, perhaps due to the acidic conditions of the crystallization drop (pH 5.4). Additionally, the higher-resolution structure reveals extensive hydrogen-bonded solvent networks between general acid D379 and bulk solvent through secondary channels distinct from the main active site cleft. Hydrogen-bonded solvent molecules may serve as “proton wires” to facilitate Grotthuss diffusion as the conjugate base of the general acid is reprotonated in catalysis.

6.1.2. *ent*-Copalyl Diphosphate Synthase from *Streptomyces platensis* CB00739. The first crystal structure of a bacterial class II diterpene cyclase, recently reported at 1.80 Å resolution, reveals $\beta\gamma$ domain architecture: the bacterial class II cyclase lacks the vestigial, nonfunctional α domain present in plant *ent*-copalyl diphosphate synthase (Figure 81A).⁴³⁵ The bacterial *ent*-copalyl diphosphate synthase is involved in the biosynthesis of kaurenoid diterpenes platensimycin and platencin, which are thought to be promising drug leads due to their inhibitory properties against fatty acid synthase.^{436,437} Catalytic residues are conserved in the active sites of plant and bacterial *ent*-copalyl diphosphate synthase, particularly with regard to the general acid function of the DXDD motif. However, a histidine residue (H359) hydrogen bonds with general acid D313 in the bacterial enzyme, whereas an asparagine residue (N425) hydrogen bonds with general acid D379 in the plant enzyme (Figure 81B). In each enzyme, the aspartic acid general acid is oriented and stabilized by hydrogen bonds for optimal

catalytic function. The catalytic mechanism proposed for the bacterial enzyme is essentially identical to that proposed for the plant enzyme in Figure 79.

6.2. Triterpene Cyclases

Class II triterpene cyclases initiate catalysis by protonation of the terminal π bond of squalene or the terminal epoxide moiety of squalene oxide, in concert with a cascade of carbon–carbon bond-forming reactions ultimately yielding a multiring product. Given the size of the substrate, a 30-carbon linear achiral isoprenoid, the role of the cyclase active site as a template to enforce a productive substrate conformation is critically important. Triterpene cyclization mechanisms have been exhaustively reviewed,¹⁰ and computational approaches for studying evolutionary relationships and cyclization specificity have been described,⁴³⁸ so structure–mechanism relationships are only briefly reviewed here for squalene-hopene cyclase and oxidosqualene cyclase.

6.2.1. Squalene-Hopene Cyclase. Hopene and related triterpene hopanoids comprise a family of pentacyclic hydrocarbons found in bacterial membranes,^{439,440} where they influence membrane fluidity^{441–443} and pH homeostasis.⁴⁴⁴ Given their exceptional chemical stability, hopanoids also serve as geological and archeological biomarkers (i.e., molecular fossils that inform the analysis of ancient rocks and sediments reflecting the evolution of life millions and even billions of years ago).^{445–448} Hopene is generated from the linear isoprenoid precursor squalene in a cyclization cascade catalyzed by squalene-hopene cyclase (Figure 82).

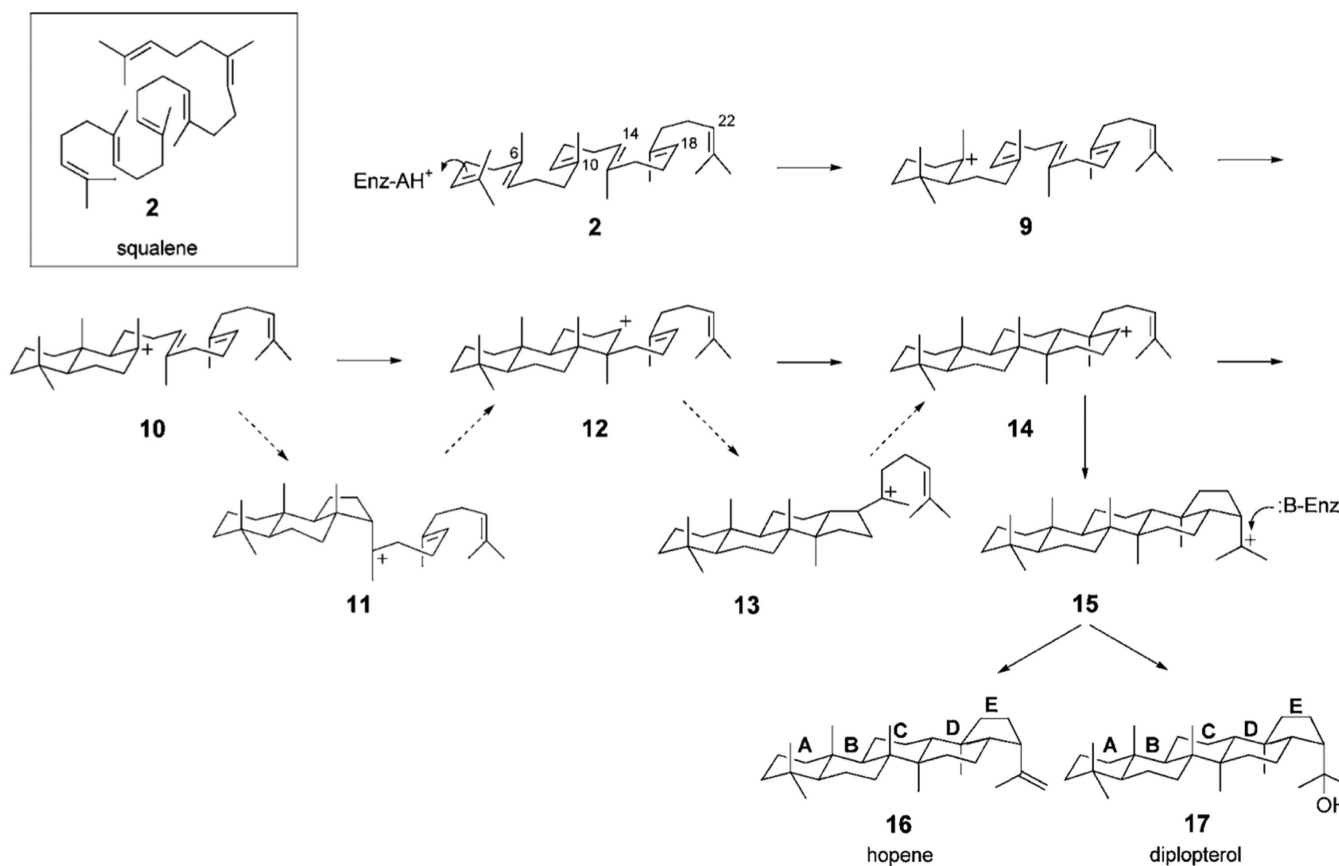


Figure 82. Class II cyclization reaction of squalene (2) is initiated by general acid D376 (AH) and proceeds through a cascade of carbon–carbon bond-forming reactions to yield the 6–6–6–5 hopenyl cation (15), which undergoes proton elimination with the assistance of a water molecule general base (B:) to yield hopene (16). Alternatively, the hopenyl cation can be quenched by addition of a water molecule to yield minor side product diplopterol (17). Reprinted with permission from ref 455. Copyright 2005 Wiley-VCH.

The 2.9 Å resolution crystal structure of squalene-hopene cyclase from *Alicyclobacillus acidocaldarius* was the first of a class II terpenoid cyclase,³⁸ and the resolution of the structure was later extended to 2.0 Å as facilitated by a new crystal form.⁴⁴⁹ This monotopic membrane protein exhibits $\beta\gamma$ domain architecture with a hydrophobic active site at the interdomain interface (Figure 5), accessible through a passageway that opens at the membrane. The surrounding protein surface is quite nonpolar, including helix 8 in the γ domain which anchors the protein in the membrane. Interestingly, comparison of the $\beta\gamma$ domain architecture of squalene-hopene cyclase with the $\alpha\beta\gamma$ domain architecture of taxadiene synthase (Figure 5) reveals that the γ domain of taxadiene synthase lacks the membrane-anchoring helix. Since taxadiene synthase functions in the lumen of the plastid, it is a soluble enzyme that does not require a membrane anchor.

The 2.13 Å resolution crystal structure determination of squalene-hopene cyclase complexed with the unreactive substrate analogue 2-azasqualene illustrates the template function of the active site: 2-azasqualene binds with the conformation that would be required for the substrate to form hopene rings A–D (Figure 83).⁴⁵⁰ The formation of rings A and B through C2–C7 and C6–C11 bond formation, respectively, could occur in concerted or stepwise fashion after protonation of C3 by the anti-oriented proton of general acid D376.^{451,452} Although C ring formation could occur in Markovnikov fashion through initial C10–C14 bond formation with subsequent ring expansion, direct anti-Markovnikov formation of the C ring

through C10–C15 bond formation with stabilization of the developing secondary carbocation by W169 and/or F601, and resultant C14–C18 bond formation to yield an initial 5-membered D ring in Markovnikov fashion, would yield a 6–6–6–5 tetracyclic carbocation with rings A–C in chair conformations. Derivatives of the 6–6–6–5 carbocation intermediate are observed as minor byproducts generated by the wild-type cyclase and major products generated by mutant cyclases,^{453,454} strongly suggesting that this tetracyclic carbocation is an intermediate in the squalene-hopene cyclization cascade. The cyclization cascade is completed by D ring expansion to form a tetracyclic 6–6–6–6 intermediate, Markovnikov formation of the E ring to generate the pentacyclic 6–6–6–6–5 hopenyl cation, and proton elimination with the assistance of a water molecule general base to yield hopene. Alternatively, direct addition of a water molecule to the hopenyl cation yields the minor side product diplopterol (Figure 82). An excellent review of the squalene-hopene cyclase mechanism has been presented by Wendt.⁴⁵⁵

Given that squalene-hopene cyclase exhibits catalytic activity with C₁₅, C₂₀, C₃₀, and C₃₅ substrates (reviewed by Hauer and colleagues^{456,457}), these enzymes have been explored as Brønsted acid catalysts for organic synthesis. For example, squalene-hopene cyclase can be engineered to serve as a general platform for the protonation and activation of alkene, epoxide, and carbonyl functional groups to enable stereoselective syntheses of various cyclohexanoids.⁴⁵⁸ The ability of squalene-hopene cyclase to perform Brønsted acid activation of various biological

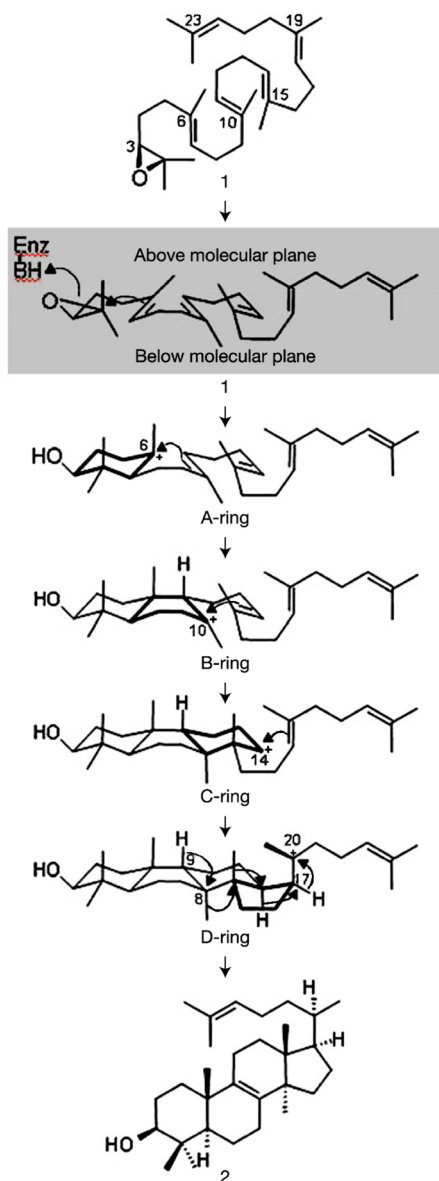


Figure 84. Oxidosqualene cyclase (lanosterol synthase) initiates the cyclization of squalene oxide through protonation by general acid D455 (BH). Chair-boat-chair substrate conformation facilitates A–C ring closure reactions; following D ring closure, rearrangement of the protosteryl cation is triggered by deprotonation at C9 and accompanied by 1,2-hydride and 1,2-methyl transfers to generate product lanosterol. Reprinted with permission from ref 462. Copyright 2004 Macmillan Publishers Ltd.

6.3. Sesquiterpene Cyclases

In comparison with other members of the greater family of terpenoid natural products, C_{35} terpenes are extremely rare: only 19 cyclic and 8 linear C_{35} terpenes have been identified to date, and both class I and class II terpenoid synthases are involved in their biosynthesis.⁴⁶⁷ Designated “sesquiterpenes” by Sato and colleagues,⁴⁶⁸ these compounds derive from the linear precursor heptaprenyl diphosphate, which in turn is generated from FPP and 4 IPP molecules in a processive head-to-tail coupling reaction catalyzed by the heterodimeric enzyme heptaprenyl diphosphate synthase in *Bacillus subtilis* (Figure 87).^{469,470} The HepT subunit of this enzyme contains signature DDXXD Mg^{2+} -binding motifs, so it most likely adopts the α fold of a class I

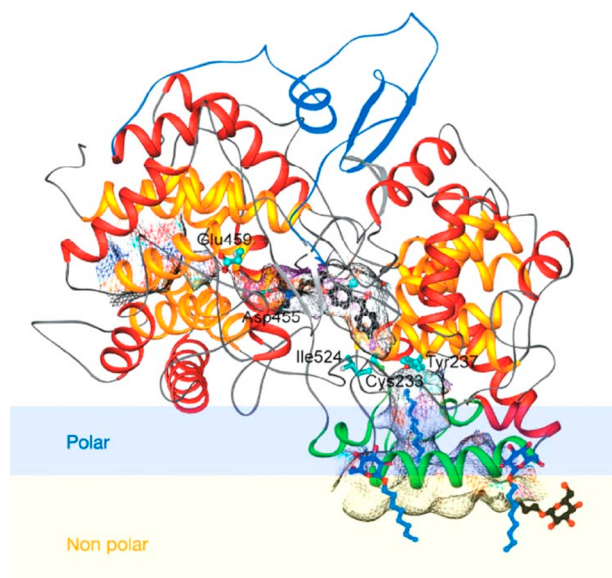


Figure 85. Human oxidosqualene cyclase is a monotopic membrane protein partially embedded in the membrane; helix 8 (green) is predominantly hydrophobic and anchors the protein in the membrane leaflet. Ordered detergent molecules and lipid fragments (blue and black stick figures) cluster around the membrane anchor, including the hydrophobic channel leading to the active site at the $\beta\gamma$ domain interface. Reprinted with permission from ref 462. Copyright 2004 Macmillan Publishers Ltd.

terpenoid synthase. The HepS subunit is required for activity, and substrate FPP is required for HepS–HepT association.⁴⁷⁰ Heptaprenyl diphosphate is the source of the prenyl side chain of menaquinone-7, which functions in electron transport. In plants, polyprenyl diphosphate synthases have been identified that generate a range of isoprenoid diphosphates, including heptaprenyl diphosphate.^{471,472}

Elegant studies by Sato and colleagues show that *Bacillus* and *Mycobacterium* species contain sesquiterpene synthases, as recently reviewed.⁴⁶⁷ Two C_{35} biosynthetic enzymes have been identified in each species, and the enzymes of *B. subtilis* are particularly well-characterized. One is the terpenoid cyclase tetraprenyl- β -curcumene synthase (YtpB), which catalyzes the ionization and cyclization of heptaprenyl diphosphate to form a C_{35} product containing a single β -curcumene ring (Figure 87).⁴⁶⁸ This reaction resembles that of a class I terpenoid synthase. Although a naturally occurring β -curcumene synthase has not yet been isolated, F95H epi-isozizaene synthase, a class I terpenoid cyclase, generates β -curcumene as its predominant product.²⁴⁴ YtpB does not contain the signature DDXXD or NSE metal-binding motifs found in epi-isozizaene synthase; however, it contains D⁸⁸NLCD and D²⁴⁹YLIDQEED segments reminiscent of metal-binding motifs in UbiA (section 3.2). Thus, YtpB might be a class I terpenoid synthase. Clearly, an X-ray crystal structure determination is required to clarify this possibility.

The second sesquiterpene cyclase identified in *B. subtilis* is tetraprenyl- β -curcumene cyclase (SqhC), which generates tetracyclic sporulene 4 shown in Figure 87.^{468,473} This C_{35} cyclase SqhC is highly similar to authentic C_{30} squalene cyclases and accordingly contains the signature general acid motif DXDD of a class II terpenoid synthase.⁴⁷³ Although no crystal structure is available for this enzyme at present, SqhC presumably adopts the $\beta\gamma$ domain architecture as observed for the squalene-hopene cyclase (Figure 5).³⁸ Assays with cell-free extracts containing

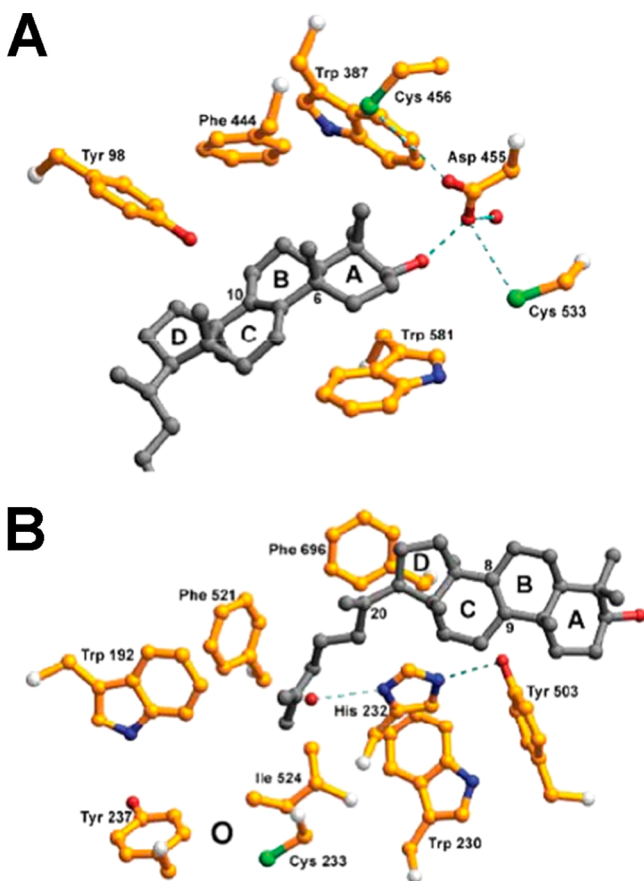


Figure 86. (A) The structure of the oxidosqualene cyclase–lanosterol complex reveals that the lanosterol hydroxyl group donates a hydrogen bond to general acid D455. The side chains of aromatic residues W387, F444, and W581 may stabilize C6 and C10 carbocation intermediates through cation– π interactions. (B) The side chains of aromatic residues F696 and H232 may stabilize the C20 carbocation of the protosterol cation through cation– π interactions. Either H232 or Y503 may deprotonate C9 to generate lanosterol. Reprinted with permission from ref 462. Copyright 2004 Macmillan Publishers Ltd.

recombinant SqhC conclusively demonstrate that this enzyme is a class II terpenoid cyclase, so the protonation of the terminal C=C bond of the isoprenoid substrate in Figure 88 is achieved by the central aspartic acid general acid in the DXDD motif.⁴⁶⁸ Interestingly, SqhC from *Bacillus megaterium* (but not SqhC from *B. subtilis*) can also utilize C₃₀ squalene as a substrate (Figure 88).⁴⁷⁴ Further sesquiterpene structural diversity emanates from nonenzymatic oxidative and thermal degradation reactions involving SqhC cyclization products (Figure 87).⁴⁷⁵

7. BIFUNCTIONAL TERPENOID CYCLASES

Terpenoid biosynthesis provides occasional examples of reaction sequences in which tandem diterpene cyclization or coupling-cyclization reactions are catalyzed in two distinct active sites on the same protein. Even in the absence of a direct channel between active sites, such systems could potentially provide a catalytic advantage through a proximity effect (“proximity channeling”)³²² but only if their active sites are appropriately oriented with regard to each other. In the case of an oligomeric protein, a catalytic advantage could result from cluster channeling: although the probability might be low that a product of one reaction will be the substrate of the second reaction in a bifunctional enzyme if the active sites are not appropriately

oriented, the probability that the second reaction will be catalyzed by one of the multiple subunits in an oligomeric assembly or aggregate can be higher (Figure 89).⁴⁷⁶

Here, three examples of bifunctional diterpene synthases are reviewed. The first, geosmin synthase, is a class I–class I sesquiterpene cyclase in which channeling does not occur. The second, abietadiene synthase, is a class I–class II diterpene cyclase with $\alpha\beta\gamma$ domain architecture in which channeling is similarly not observed. The third, fusicoccadiene synthase, is a hexameric class I–class I diterpene synthase with $(\alpha\alpha)_6$ domain architecture in which cluster channeling is implicated.

7.1. Geosmin Synthase

The characteristic odor of freshly turned earth derives from the volatile sesquiterpene geosmin,^{207,477} which is generated by various soil-dwelling *Streptomyces* species.^{478,479} With an extremely low detection threshold of less than 10 parts per trillion, geosmin is a commonly occurring contaminant of water, wine, and fish.^{480–483} While geosmin is not believed to be toxic to humans, the musty taste that it imparts to contaminated food and water makes its detection and elimination an environmental priority.

Geosmin is a noncanonical sesquiterpene in that although it derives from the universal 15-carbon precursor FPP, it only contains 12 carbons. Thus, the FPP cyclization reaction must also include a fragmentation reaction. Geosmin synthase from *S. coelicolor* is a 726-residue protein containing two class I terpenoid synthase α domains,^{484,485} both of which are required for geosmin biosynthesis.^{486,487} Thus, geosmin synthase is a bifunctional terpenoid synthase that adopts $\alpha\alpha$ domain architecture. The N-terminal domain catalyzes the Mg²⁺-dependent cyclization of FPP initially proceeding through a C1–C10 bond-forming reaction to yield two cyclic sesquiterpenes, germacadienol (85%) and germacrene D (15%).^{488,489} The C2–C3 double bond of FPP remains in the *trans* configuration for the initial C1–C10 bond-forming reaction. After fully dissociating from the N-terminal domain active site into solution, product germacadienol rebinds in the C-terminal domain active site, where it undergoes a protonation-dependent cyclization-fragmentation reaction yielding C₁₂ geosmin and C₃ acetone (Figure 90).^{490,491}

Full-length geosmin synthase proved to be refractory to crystallization, but a construct of the unliganded N-terminal domain containing residues 1–366 yielded crystals that diffracted X-rays to 3.2 Å resolution; another N-terminal domain construct consisting of residues 1–338 complexed with 3 Mg²⁺ ions and the bisphosphonate inhibitor alendronate yielded crystals that diffracted to 2.11 Å resolution.⁴⁹² Comparison of the unliganded and liganded structures reveals the structural changes and disorder–order transitions that accompany ligand binding and active site closure for catalysis (Figure 91A). The trinuclear metal cluster is coordinated by the first residue in the aspartate-rich motif, D86, the NSE motif on helix H, and the bisphosphonate moiety of alendronate. Three basic residues (R184, R236, and R325) additionally form hydrogen bonds with the bisphosphonate group (Figure 91B). Both metal coordination and hydrogen bond interactions activate the FPP diphosphate group for catalysis.

The fragmentation step in geosmin biosynthesis is unprecedented in terpenoid cyclase reactions. Intriguingly, even though the cyclization–fragmentation reaction catalyzed by the C-terminal domain does not involve FPP or inorganic pyrophosphate, this reaction is Mg²⁺-dependent.⁴⁸⁷ The chemical and/or

Enzymatic biosynthetic pathway

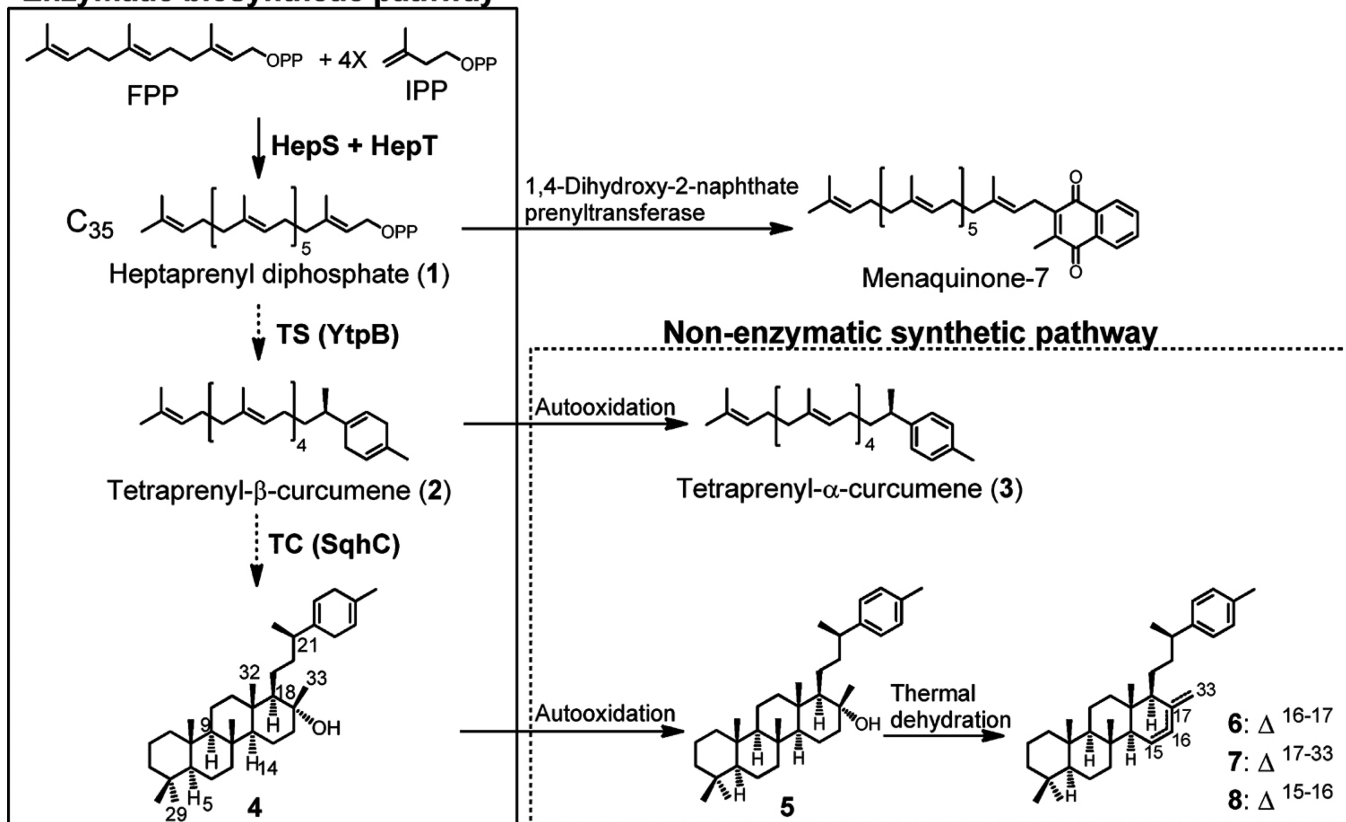


Figure 87. Sesquiterpene biosynthesis in *B. subtilis* begins with the condensation of FPP and 4 IPP molecules in a chain elongation reaction catalyzed by the heterodimeric enzyme heptaprenyl diphosphate synthase (HepS-HepT). YtpB catalyzes the cyclization of heptaprenyl diphosphate to form tetraprenyl- β -curcumene, which in turn undergoes further cyclization as catalyzed by SqhC to yield the tetracyclic sporulene 4. Nonenzymatic oxidation of 2 and 4 yields 3 and 5, respectively; thermal dehydration of 5 yields 6–8. Reproduced from ref 468. Copyright 2011 American Chemical Society.

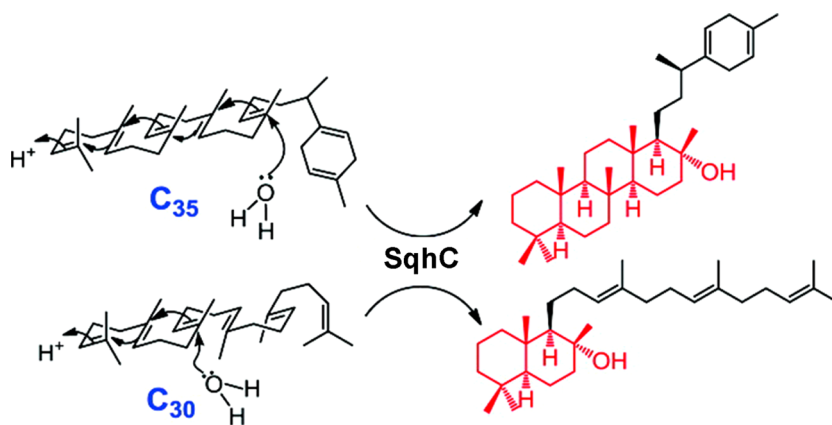


Figure 88. Tetraprenyl- β -curcumene synthase (SqhC) from *Bacillus megaterium* generates a tetracyclic C₃₅ sporulene from tetraprenyl- β -curcumene in a class II terpenoid synthase reaction (top). This enzyme also catalyzes the cyclization of C₃₀ squalene to form a bicyclic *trans*-decalin product. In both reactions, the source of the proton that initiates the cyclization cascade is the central aspartic acid in the DXDD motif. Reproduced from ref 474. Copyright 2011 American Chemical Society.

structural function of the metal ion in this domain remains unknown. Curiously, however, the amino acid sequence of the C-terminal domain reveals conservation of metal-binding motifs as well as basic residues that could interact with inorganic pyrophosphate, even though it is not required for the fragmentation reaction.⁴⁸⁷ A homology model of the C-terminal domain provides useful structural insight on domain assembly in the geosmin synthase monomer, as fit to a low-resolution molecular envelope determined by small-angle X-ray scatter-

ing.⁴⁹² However, this model does not clarify the puzzling features regarding the metal requirement for catalysis in the C-terminal domain. The answer to this question must await the crystal structure determination of a full-length α domain enzyme.

7.2. Abietadiene Synthase

(–)-Abietic acid is one of the main components of the oleoresin secreted by the grand fir (*Abies grandis*) in response to the bite of a bark beetle. Oleoresin is a complex mixture comprised mainly

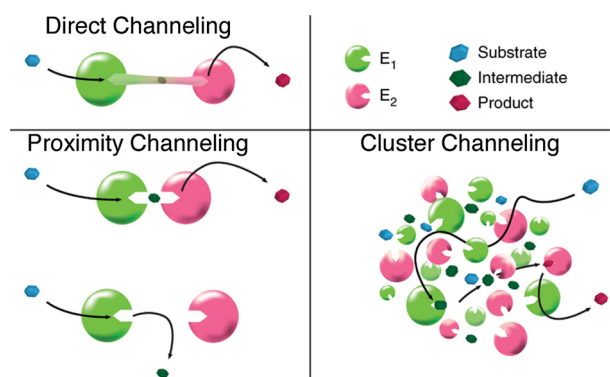


Figure 89. Hypothetical enzymes E1 and E2 catalyze successive biosynthetic reactions, such that E1 converts the substrate into an intermediate, which in turn serves as a substrate for E2 to generate the final product. The active sites of E1 and E2 can be connected by a direct channel, or they can be positioned and oriented so as to facilitate or prohibit proximity channeling. If E1 and E2 associate in a multienzyme oligomer or aggregation then cluster channeling can enhance the biosynthetic flux of product: the intermediate generated by E1 can diffuse into any number of nearby E2 active sites for the second reaction in the biosynthetic sequence. Reprinted with permission from ref 476. Copyright 2014 Macmillan Publishers Ltd.

of volatile monoterpenes (turpentine) and diterpene resin acids;⁴⁹³ bactericidal and fungicidal terpenoids are also generated.⁴⁹⁴ The monoterpenes ultimately evaporate, leaving the diterpene resin acids behind to harden into a solid resin, thereby sealing the wound. The first committed step in the biosynthesis of (–)-abietic acid is catalyzed by abietadiene synthase,^{495,496} which catalyzes the cyclization of GGPP to form (–)-abietadiene, or simply abietadiene. The overall cyclization sequence proceeds through two consecutive reactions catalyzed by class II and class I active sites in abietadiene synthase.

The mechanistic details of both reactions have been determined through enzymological studies of a pseudomature form of the enzyme lacking the N-terminal plastidial targeting sequence.¹⁹² The first reaction catalyzed is the class II cyclization reaction of GGPP, protonation of the terminal π bond of GGPP

by general acid D404 initiates a cyclization cascade forming (+)-copalyl diphosphate (a different stereoisomer from *ent*-copalyl diphosphate described in sections 6.1.1 and 6.1.2).^{497–499} This biosynthetic intermediate diffuses into bulk solvent and then rebinds in the class I active site of the enzyme; since free (+)-copalyl diphosphate is detected in solution in kinetic assays, there is no evidence for channeling in this bifunctional cyclase.⁴⁹⁷ In the class I active site, metal-triggered⁵⁰⁰ ionization of (+)-copalyl diphosphate and cyclization yields a tricyclic carbocation⁵⁰¹ that subsequently undergoes intramolecular proton transfer, 1,2-methyl migration, and deprotonation to yield abietadiene or regiomeric elimination products levopimaradiene and neoabietadiene (Figure 92).^{192,501,502} Although the class I active site in the α domain and the class II active site at the $\beta\gamma$ domain interface are independent, truncation studies demonstrate that these active sites cannot be separated into functional stand-alone α and $\beta\gamma$ domain assemblies, indicating significant interdomain contact and structural stabilization in the intact $\alpha\beta\gamma$ assembly of the full-length enzyme.⁴³

The 2.30 Å resolution X-ray crystal structure of unliganded abietadiene synthase was the first of a bifunctional terpenoid cyclase and confirmed $\alpha\beta\gamma$ domain architecture with fully functional class I and class II active sites (Figure 93).⁴⁵ The active site in the α domain contains the aspartate-rich DDXXD and NTE metal-binding motifs on helices D and H, respectively, and the active site at the $\beta\gamma$ domain interface contains the general acid motif DXDD. Interestingly, molecular dynamics simulations suggest that conformational changes of loop 482–492 in the class II active site play an important role in governing the conformation of substrate GGPP. Structural comparison of abietadiene synthase with *ent*-copalyl diphosphate synthase reveals “out” and “in” conformations for this loop, respectively (Figure 94).⁴⁵ Since the “loop-in” conformation observed in *ent*-copalyl diphosphate synthase accommodates a nonproductive binding conformation for a bound substrate analogue, the “loop-out” conformation may be required to facilitate the formation of a catalytically productive enzyme–substrate complex.

The crystal structure of abietadiene synthase provides a valuable framework for understanding protein engineering experiments that reprogram the cyclization cascade to generate

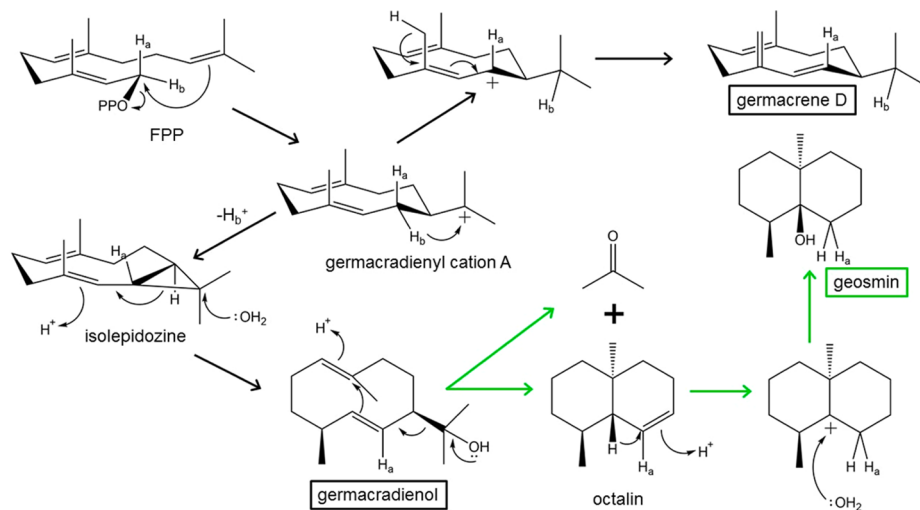


Figure 90. Cyclization of FPP to form germacrene D and germacradienol (black arrow) is catalyzed by the N-terminal α domain of geosmin synthase. The subsequent cyclization and retro-Prins fragmentation of germacradienol (green arrows) are catalyzed by the C-terminal α domain of this bifunctional cyclase. Reproduced from ref 492. Copyright 2015 American Chemical Society.

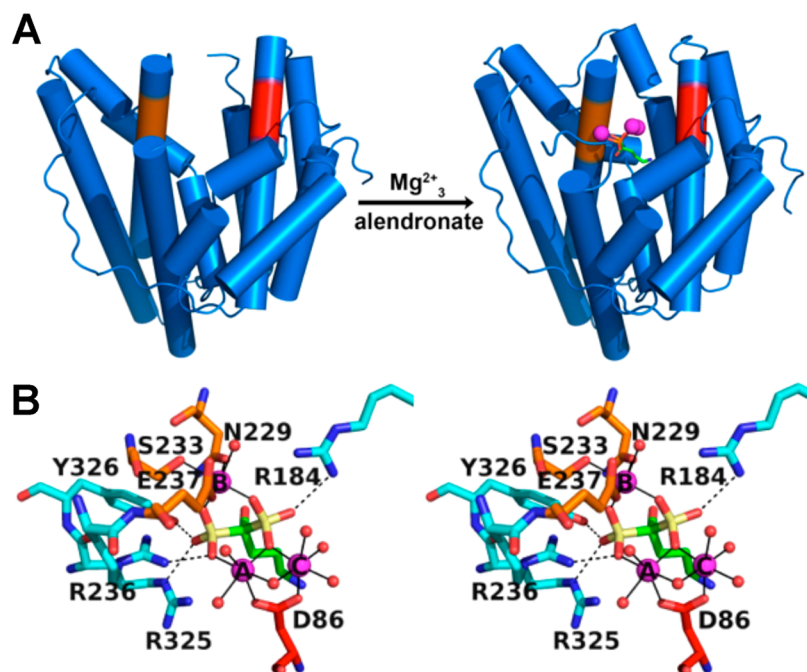


Figure 91. (A) Structural changes triggered by the binding of the bisphosphonate inhibitor alendronate (stick figure) and 3 Mg^{2+} ions (magenta) to the N-terminal domain of geosmin synthase. The aspartate-rich and NSE metal-binding motifs are red and orange, respectively. (B) Stereoview showing metal coordination and hydrogen bond interactions in the geosmin synthase-alendronate complex (thin solid and dashed lines, respectively). Reproduced from ref 492. Copyright 2015 American Chemical Society.

alternative diterpene products. For example, the H348A substitution in the class II active site allows the final carbocation intermediate to be quenched by solvent to yield 8α -hydroxycopalyl diphosphate;⁵⁰³ in the wild-type enzyme, H348 serves as the catalytic base in conjunction with a hydrogen-bonded tyrosine residue.⁵⁰⁴ In the class I active site, the A723S substitution converts abietadiene synthase into a pimaradiene synthase.⁵⁰⁵ Certain residues in each cyclase active site appear to be “hot spots” for reprogramming the respective cyclization cascades. Chemical dynamics simulations of the class I reaction suggest that the enzyme active site structure plays a vital role in steering the reaction through one particular pathway along a bifurcated potential energy surface, further demonstrating the critical role of the active site contour as a chaperone for cyclization.⁵⁰⁶

7.3. Fusicoccadiene Synthase

Fusicoccin A (Figure 95) is a diterpene glucoside^{507–509} generated by the fungus *Phomopsis amygdali*, which causes the plant disease constrictor canker as first discovered in peach orchards nearly a century ago.^{510–512} Fusicoccin A is also an emerging new lead for cancer chemotherapy due to its antitumor activity,⁵¹³ which derives from its ability to modulate protein–protein interactions involving the 14–3–3 protein^{514–516} as well as its ability to inhibit focal adhesion kinase.⁵¹⁷ The first committed step of fusicoccin A biosynthesis is the cyclization of GGPP to form fusicoccadiene, a tricyclic diterpene hydrocarbon with an unusual 5–8–5 ring system. This reaction is catalyzed by fusicoccadiene synthase, which exhibits $\alpha\alpha$ domain architecture based on analysis of its amino acid sequence: the C-terminal α domain is a coupling enzyme that catalyzes the chain elongation reaction of DMAPP and three IPP molecules to generate GGPP, and the N-terminal domain is a cyclase that converts GGPP into fusicoccadiene (Figure 95).⁵¹⁸ The overall amino acid sequence

identity between the N-terminal and C-terminal α domains is 19%.

Although full-length fusicoccadiene synthase was refractory to crystallization, the preparation of individual N-terminal and C-terminal α domain constructs enabled their crystallization and structure determination at 2.30 and 2.43 Å resolution, respectively.⁹⁵ The crystal structures of the C-terminal GGPP synthase domain in the unliganded and liganded states reveal substrate-induced conformational changes that enclose the active site, facilitated by the binding of 3 Co^{2+} ions and the bisphosphonate inhibitor pamidronate (Figure 96A). As is characteristic for a terpenoid synthase that catalyzes a coupling reaction, metal ions are coordinated by two aspartate-rich motifs on helices D and H, D⁴⁷⁴DFQD, and D⁶⁰⁵DYQN, respectively. The bisphosphonate moiety of the inhibitor is additionally stabilized by hydrogen bonds with 3 basic residues, R483, K619, and K629; an additional hydrogen bond is observed in some monomers with K561. The GGPP synthase domain adopts hexameric quaternary structure similar to that first observed for human GGPP synthase.⁸⁸

The crystal structure of the N-terminal cyclase domain complexed with 3 Mg^{2+} ions and pamidronate reveals a monomeric enzyme in which the metal ions are coordinated by an aspartate-rich motif on helix D, D⁹²DVTD, and the NSE motif on helix H, N²³²DIWSWPKE, as is characteristic for a terpenoid synthase that catalyzes a cyclization reaction (Figure 96B). The bisphosphonate moiety of the inhibitor is additionally stabilized by hydrogen bonds with 3 basic residues, R188, K239, and R325, as well as a tyrosine residue, Y326. Locked in the closed conformation by metal coordination and hydrogen bond interactions with the inhibitor bisphosphonate moiety, the active site of the N-terminal cyclase domain is fully enclosed and sequestered from bulk solvent. The three-dimensional contour of the active site is quite complementary to the three-dimensional structure of product fusicoccadiene, which enables the modeling

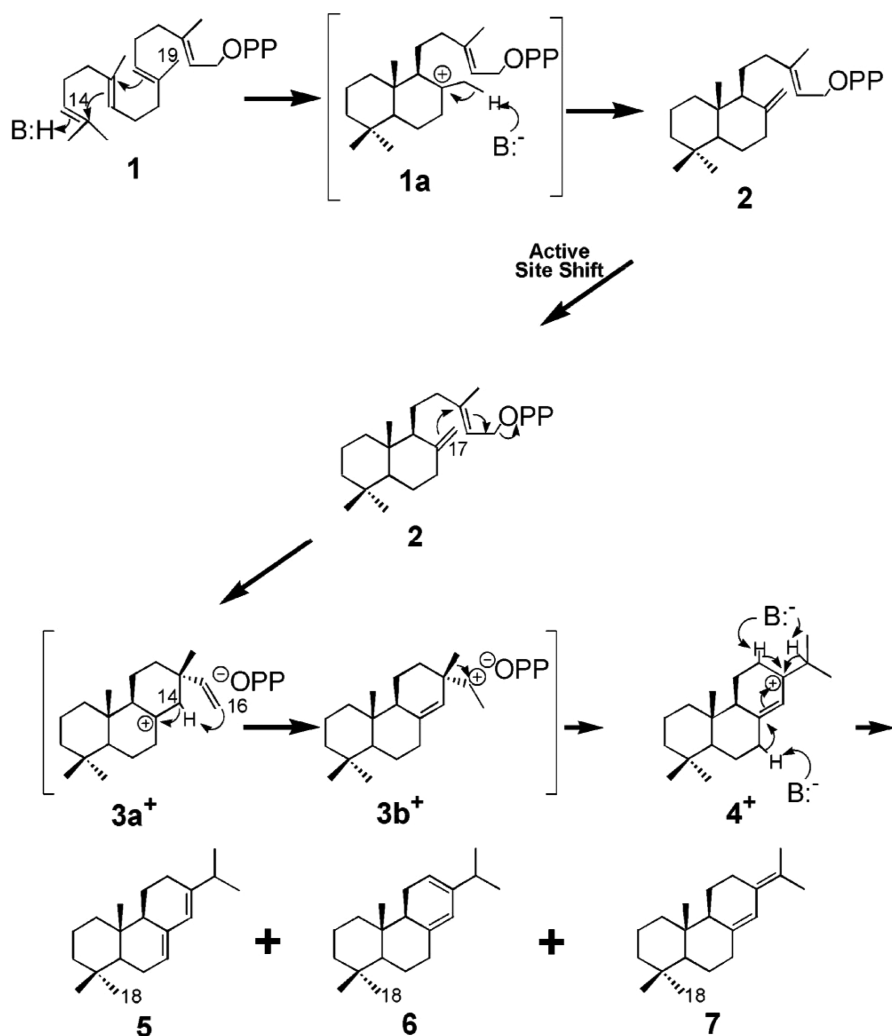


Figure 92. Cyclization of GGPP (1) is initiated in the class II active site of abietadiene synthase by general acid D404 (B:H) to yield bicyclic carbocation 1a, which undergoes proton elimination to yield (+)-copalyl diphosphate (2). This intermediate then diffuses into solution and rebinds in the class I active site, where it undergoes metal-triggered ionization to initiate the second cyclization cascade. The reaction is terminated by proton elimination (inorganic pyrophosphate may serve as the general base B:⁻) to form abietadiene (5), or side products levopimaradiene (6) or neoabietadiene (7). Reproduced from ref 43. Copyright 2003 American Chemical Society.

of the enzyme–product complex (Figure 96C). This model illustrates the critical role of the active site contour as a template for catalysis. The template also enforces an unusual transannular proton transfer in the cyclization cascade,⁵¹⁹ which generates fusicoccadiene as a major product and (+)- δ -araneosene as a minor product (Figure 97).

Given that the C-terminal GGPP synthase domain of fusicoccadiene synthase crystallizes as a hexamer, and given that full-length fusicoccadiene synthase is a hexamer in solution as determined by analytical ultracentrifugation, the crystal structure of the GGPP synthase hexamer was used as a starting point to guide the interpretation of a low-resolution molecular envelope of full-length fusicoccadiene synthase determined by small-angle X-ray scattering.⁹⁵ An optimal fit to the molecular envelope required a slight, ~ 5 Å dissociation of the hexamer into 3 dimers, which then facilitated the placement of 3 crystallographic dimers of the cyclization domain, all while maintaining the original D_3 symmetry of the GGPP synthase hexamer (Figure 98). In the model, the C-terminus of the cyclization domain and the N-terminus of the GGPP synthase domain are separated by ~ 25 Å, which would be connected by the 60-residue interdomain

linker that was excluded from both constructs. The model of hexameric fusicoccadiene synthase shown in Figure 98 provides a plausible starting point for studying the catalytic importance of quaternary structure in this system.

In particular, the close assembly of 6 GGPP synthase active sites and 6 GGPP cyclase active sites raises the possibility of cluster channeling in the hexamer: the GGPP product of one GGPP synthase domain may diffuse within the hexamer to any one of the 6 GGPP cyclase domains instead of diffusing out to bulk solvent. A competition experiment with fusicoccadiene synthase and taxadiene synthase demonstrates that when equimolar concentrations of both diterpene cyclases are incubated directly with GGPP, the fusicoccadiene/taxadiene product ratio is 4.3:1, reflecting that the catalytic efficiency of fusicoccadiene synthase is greater than that of taxadiene synthase. However, when the mixture is incubated with DMAPP and IPP, such that the only source of GGPP is that generated by the GGPP synthase domain of fusicoccadiene synthase, the fusicoccadiene/taxadiene product ratio jumps to 46:1. Hardly any taxadiene is generated when both cyclases compete for the GGPP generated by fusicoccadiene synthase, suggesting that

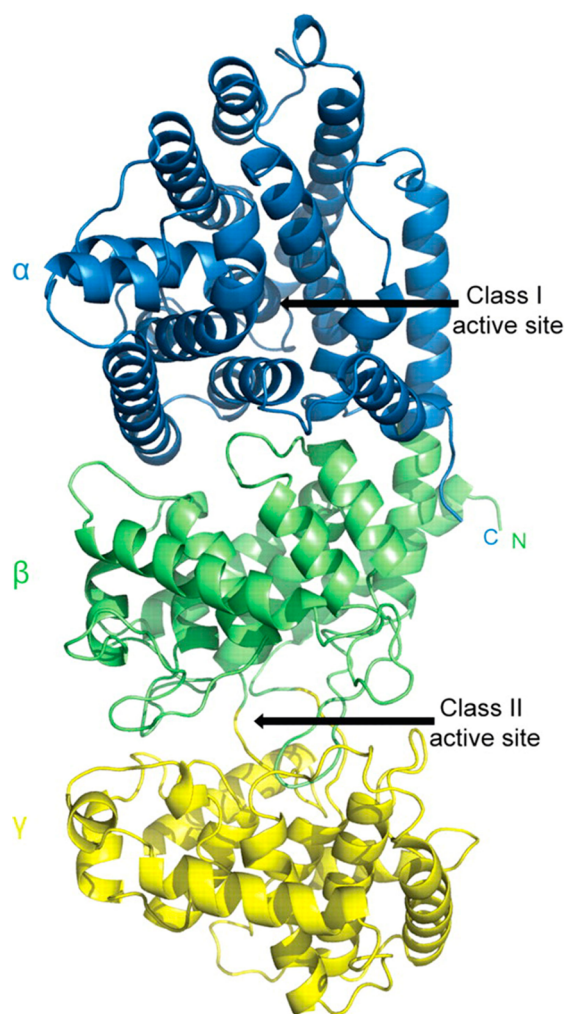


Figure 93. Crystal structure of abietadiene synthase reveals a functional class I active site in the α domain and a functional class II active site at the $\beta\gamma$ domain interface. Originally published in ref 45. Copyright 2012 American Society for Biochemistry & Molecular Biology.

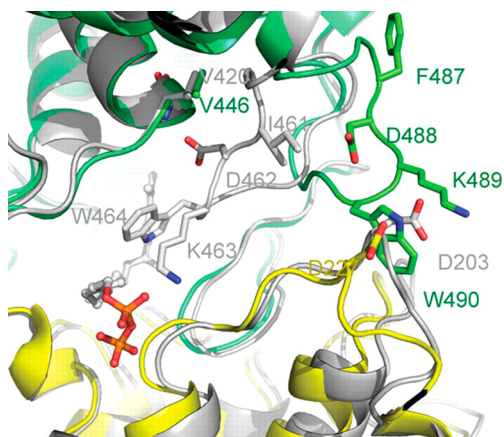


Figure 94. Loop 482–492 (green) adopts an “out” conformation in abietadiene synthase, whereas the corresponding loop of *ent*-copalyl diphosphate synthase adopts an “in” conformation. The “out” conformation of this loop may be required for productive substrate binding. Originally published in ref 45. Copyright 2012 American Society for Biochemistry & Molecular Biology.

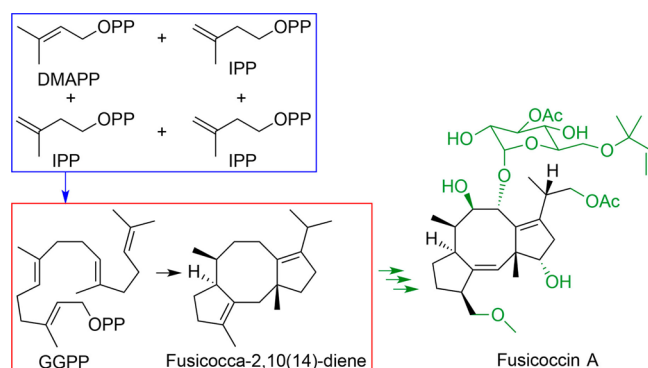


Figure 95. C-terminal α domain of fusicocadiene synthase catalyzes the coupling of DMAPP with three molecules of IPP (blue box), and the resulting molecule of GGPP is cyclized in the N-terminal α domain to yield fusicocadiene (red box). Additional biosynthetic modifications (green) yield fusicoccin A. Reproduced from ref 95. Copyright 2016 American Chemical Society.

most of the GGPP generated remains associated with the hexamer and utilized for cyclization to fusicocadiene.³⁹²

8. OXIDOREDUCTASE TERPENOID CYCLASES

While carbocations reign supreme in the terpenoid synthase and cyclization reactions discussed up until now, it is fitting to conclude this Review with two unusual examples of anionic isoprenoid cyclization reactions triggered by substrate reduction or oxidation. Notably, these reactions do not involve linear isoprenoid diphosphate precursors but instead involve GPP derivatives primed for redox chemistry.

8.1. Δ^1 -Tetrahydrocannabinolic Acid Synthase

Cannabis has been a component of the pharmacopoeia for several millennia and is mentioned in the ancient herbal medicine text, *Pên-ts'ao Ching*, attributed to Emperor Shen Nung, who is regarded as the legendary father of agriculture and herbal medicine (ca. 2700 B.C.E.):⁵²⁰ “...if taken in excess will produce hallucinations. If taken over a long-term, it makes one communicate with spirits and lightens one’s body.” More recently, cannabinoids are being used, or are being considered for use, in the treatment of glaucoma, epilepsy, multiple sclerosis, and other debilitating diseases.⁵²¹ The cannabinoid Δ^1 -tetrahydrocannabinol (THC; also known as Δ^9 -tetrahydrocannabinol using a different numbering convention) is the main psychoactive ingredient found in the *Cannabis sativa* plant.⁵²² It is not often appreciated that this plant contains more than 120 different cannabinoids that exhibit diverse and potentially beneficial physiological effects distinct from the psychoactive effects of THC.^{523,524}

The first step of cannabinoid biosynthesis is the prenylation of olivetolic acid by a Mg^{2+} -dependent prenyltransferase, geranyl-pyrophosphate:olivetolate geranyltransferase, to yield cannabigerolic acid (Figure 99).⁵²⁵ Since this enzyme is soluble and is not believed to be membrane-associated, it may be related to the ABBA prenyltransferases (section 3.1),^{119,120} although this has not been established. Cannabigerolic acid then undergoes a complex cyclization cascade to yield Δ^1 -tetrahydrocannabinolic acid (THCA) in a reaction catalyzed by THCA synthase.^{526,527} Nonenzymatic decarboxylation of THCA yields the psychoactive cannabinoid THC.

The recently determined crystal structure of THCA synthase illuminates key structure–mechanism relationships for the oxidative monoterpene cyclization reaction of cannabigerolic

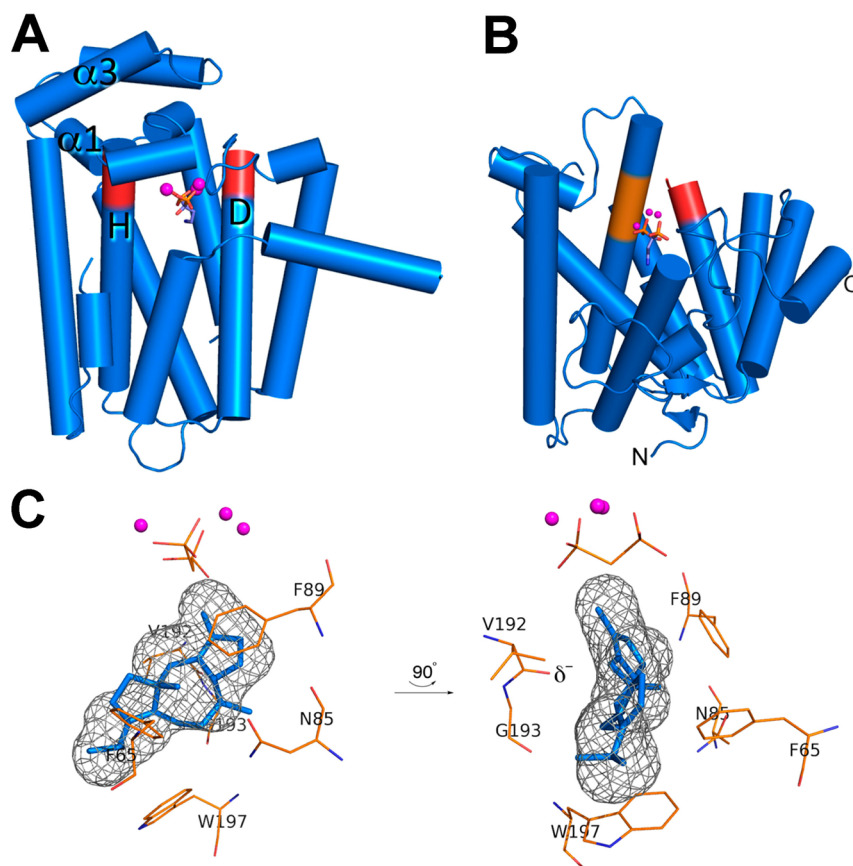


Figure 96. (A) Crystal structure of the C-terminal GGPP synthase domain of fusicoccadiene synthase. Aspartate-rich DDXXD metal-binding motifs on helices D and H (red) coordinate to 3 Co^{2+} ions (magenta spheres) along with the bisphosphonate inhibitor pamidronate (stick figure), locking the active site in the fully closed conformation. (B) Crystal structure of the N-terminal cyclase domain of fusicoccadiene synthase. Aspartate-rich DDXXD and NSE metal-binding motifs on helices D and H (red and orange, respectively) coordinate to 3 Mg^{2+} ions (magenta spheres) along with pamidronate (stick figure), locking the active site in the fully closed conformation. (C) Molecular surface of the enclosed active site in the N-terminal cyclase domain of fusicoccadiene synthase (gray meshwork), into which the product fusicoccadiene is docked. The three-dimensional contour of the active site is very productlike and reflects the role of the active site as a template for catalysis. Reproduced from ref 95. Copyright 2016 American Chemical Society.

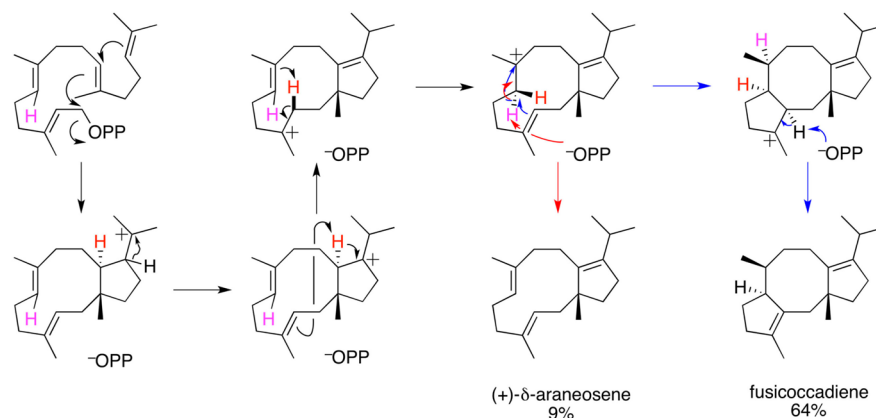


Figure 97. Cyclization of GGPP catalyzed by fusicoccadiene synthase yields fusicoccadiene as a major product and (+)- δ -araneosene as one of the minor products. Reproduced from ref 95. Copyright 2016 American Chemical Society.

acid.⁵²⁸ The FAD cofactor is covalently bound to H114 and C176 at the interface of two globular domains designated I and II, where the nucleotide moiety of FAD binds between subdomains Ia and Ib (Figure 100). Phylogenetic and structural studies indicate that THCA synthase is most closely related to another FAD-dependent enzyme, berberine bridge enzyme (39% sequence identity), which functions in benzophenanthridine biosynthesis in the California poppy, *Eschscholzia californica*.⁵²⁹

Although the crystal structure of THCA synthase was determined in the absence of bound substrate, substrate analogue, or product, analysis of the native enzyme complexed with cofactor FAD suggests that active site residue Y484 serves as a general base in catalysis, and mutagenesis data confirm that this residue is absolutely required for catalysis.⁵²⁸ This discovery is the basis of a tentative proposal for the cyclization mechanism, in which proton abstraction by the phenolate anion of Y484 triggers

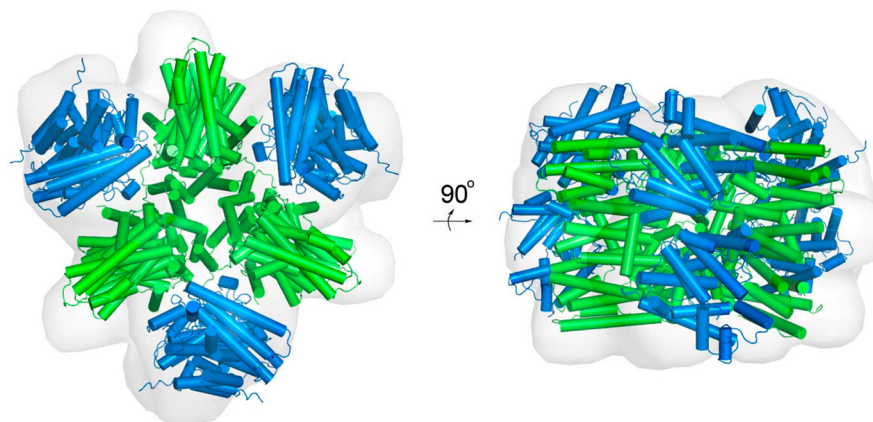


Figure 98. Model of the fusicoccadiene synthase hexamer with D_3 symmetry fit into the low-resolution ab initio molecular envelope calculated from small-angle X-ray scattering data. Dimers of the GGPP synthase domains and cyclase domains are green and blue, respectively. Reproduced from ref 95. Copyright 2016 American Chemical Society.

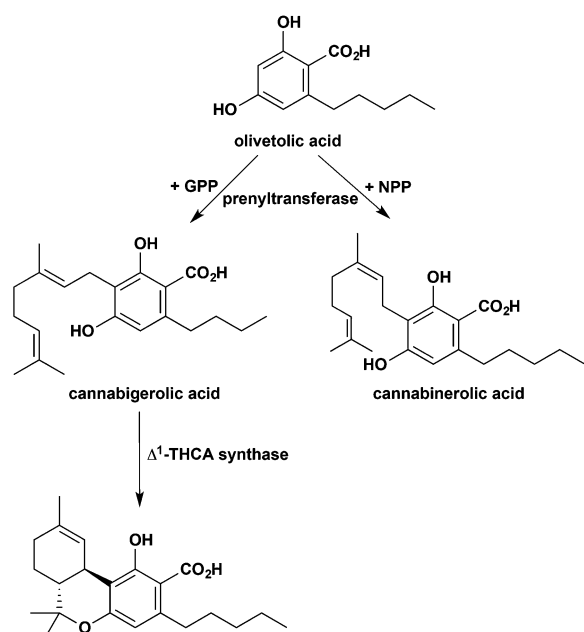


Figure 99. Biosynthesis of Δ^1 -tetrahydrocannabinolic acid (THCA).

substrate oxidation and intramolecular oxo-Diels–Alder cyclization to form the tricyclic product THCA (Figure 101). However, this mechanistic proposal remains to be fully developed, since it does not account for the *trans*–*cis* isomerization of the isoprenoid double bond in product THCA.

8.2. Iridoid Synthase

Iridoids are bicyclic monoterpenes that function in communication and defense in plants and insects.^{530,531} The core skeleton of an iridoid typically consists of a 5-membered cyclopentane ring fused with a 6-membered pyran ring, which is further derivatized and often glycosylated to yield a family of approximately 600 distinct natural products. Many iridoids exhibit useful pharmacological properties, so these compounds figure prominently in medicinal chemistry.⁵³²

The cyclization substrate for iridoid biosynthesis is not the universal monoterpene precursor GPP but instead is 8-oxogeranial, which derives from GPP through hydrolysis to geraniol and subsequent oxidation at C1 and C8 to yield the dialdehyde species (note that 8-oxogeranial is sometimes

referred to as 10-oxogeranial based on a different atomic numbering convention).^{533,534} The reductive cyclization of 8-oxogeranial with NADPH generates nepetalactol, which is in equilibrium with iridodial (Figure 102A).^{535–538}

The recently determined crystal structures^{538,539} of iridoid cyclase from *Catharanthus roseus* reveal close structural homology with the crystal structure of progesterone-5 β -reductase, an NADPH-dependent reductase that catalyzes the reduction of the double bond in the α,β -unsaturated ketone of a steroid substrate (Figure 102B).⁵⁴⁰ The structure and function of these two enzyme families are closely linked in plants.⁵⁴¹ O'Connor and colleagues elegantly demonstrate that the cyclization reaction catalyzed by iridoid synthase proceeds through an intramolecular Michael cyclization reaction; Rauhut-Currier and imine-assisted cyclization mechanisms are ruled out on the basis of the active site structure and mutagenesis studies, and a hetero Diels–Alder reaction is ruled out on the basis of reactivity differences of carefully designed substrate analogues (Figure 102C).^{536–538}

The binding of substrate and analogues in the active site of iridoid synthase along with cofactor NADP⁺ provides important mechanistic inferences.^{538,539} The crystal structure of the ternary complex with triethylene glycol carboxylic acid reveals an oxyanion hole comprised of Y178 and the backbone NH groups of I145 and K146 (Figure 103A). The structure of the ternary complex with geranic acid, which mimics the enolate intermediate resulting from hydride transfer, shows that the reactive aldehyde carbonyl of the substrate can bind in the oxyanion hole while holding the β -carbon of the substrate over the pro-S hydride of the nicotinamide ring of NADPH (Figure 103B). Interestingly, geranic acid adopts an extended conformation that is nonproductive with respect to the Michael cyclization reaction following the initial hydride transfer step in catalysis.⁵³⁸ This is consistent with the structure of the enzyme–substrate complex.⁵³⁹ The observation of “open” and “closed” active site conformations involving the G150–D162 loop (Figure 104) suggests that transition of this loop to an “open” conformation would facilitate Michael cyclization to iridodial, as confirmed by molecular modeling (Figure 103C).

9. CONCLUDING REMARKS

Given the vast chemodiversity of the terpenome, it is remarkable that only three modular protein domains, α , β , and γ , with $\gamma = \beta'$, are responsible for generating the (poly)cyclic carbon skeletons

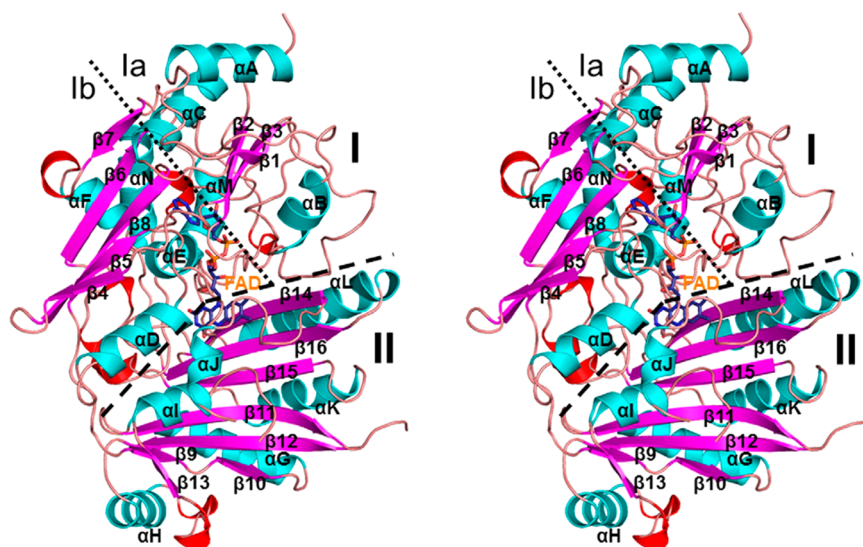


Figure 100. Stereoview of THCA synthase from *Cannabis sativa*. Cofactor FAD (orange label, blue stick figure in center) binds at the interface of domains I and II, between subdomains Ia and Ib. Reprinted with permission from ref 528. Copyright 2012 Elsevier.

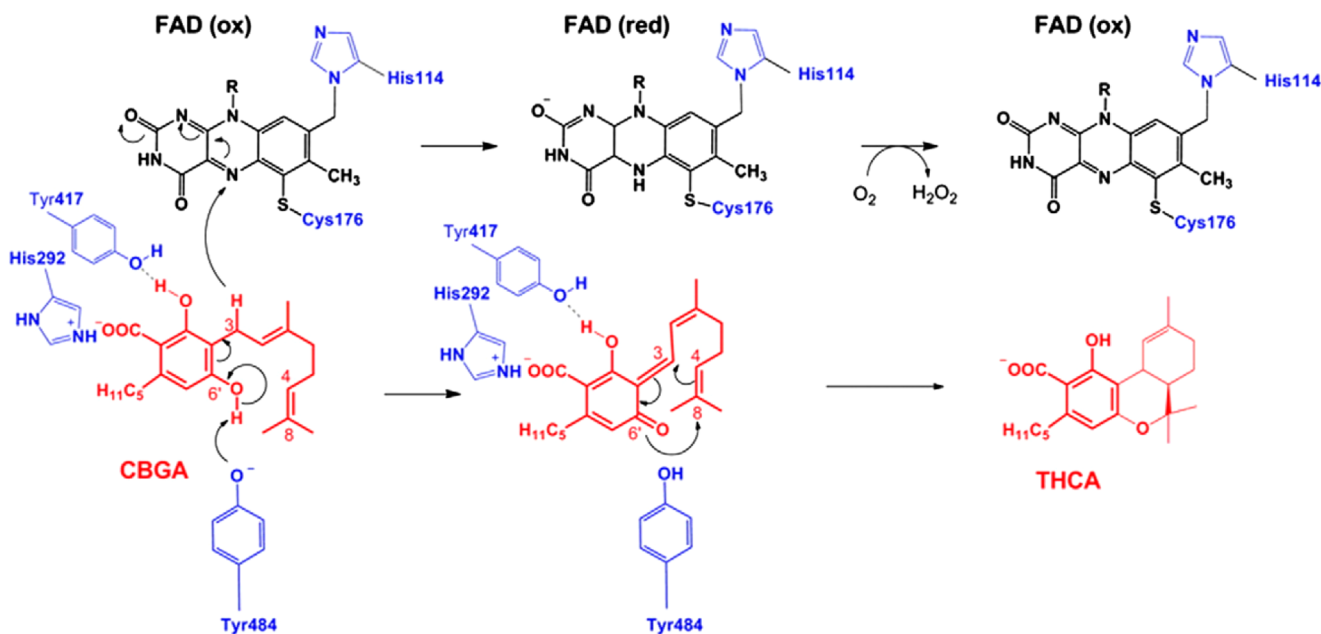


Figure 101. Proposed catalytic mechanism of THCA synthase based on crystal structure analysis. Y417 and H292 are proposed to function in substrate binding, and Y484 is the proposed general base. Cofactor flavin adenine dinucleotide (FAD), substrate cannabigerolic acid (CBGA), and product Δ^1 -tetrahydrocannabinolic acid (THCA) are indicated. It should be noted that this mechanism does not account for the *trans*-*cis* isomerization of the isoprenoid double bond in THCA. Reprinted with permission from ref 528. Copyright 2012 Elsevier.

of more than 80000 terpenoid natural products. There is no sequence identity or structural homology between the α domain fold and the β domain fold, so these folds presumably evolved independently. Evolutionarily divergent protein folds observed in the greater family of terpenoid synthases have been systematically classified.⁴⁰

The α domain fold derives from gene duplication and fusion of a primordial 4-helix bundle protein;⁴¹ characteristic metal-binding motifs are conserved at equivalent positions on topologically related helices D and H, suggesting that the original 4-helix bundle ancestor was a metal-binding protein. The crystal structure of avian FPP synthase provided the first view of the α fold,⁵⁸ which was unexpectedly observed in the first crystal structures of class I terpenoid cyclases, bacterial pentalene

synthase, and plant epi-aristolochene synthase.^{36,37} The α domain is also adapted for function as an integral membrane protein, as recently observed in the crystal structures of UbiA prenyltransferases that function in ubiquinone biosynthesis.^{41,128} The α domain fold is thus utilized for terpenoid coupling and/or cyclization reactions in all forms of life, where it is found in α , $\alpha\alpha$, $\alpha\beta$, and $\alpha\beta\gamma$ domain assemblies.

Bifunctional terpenoid synthases such as fusicoccadiene synthase contain linked cyclase and coupling domains with $\alpha\alpha$ domain architecture. The amino acid sequences of metal-binding motifs generally distinguish a terpenoid cyclase from a prenyltransferase, although there can be slight variations in metal-binding motifs in all terpenoid synthases.

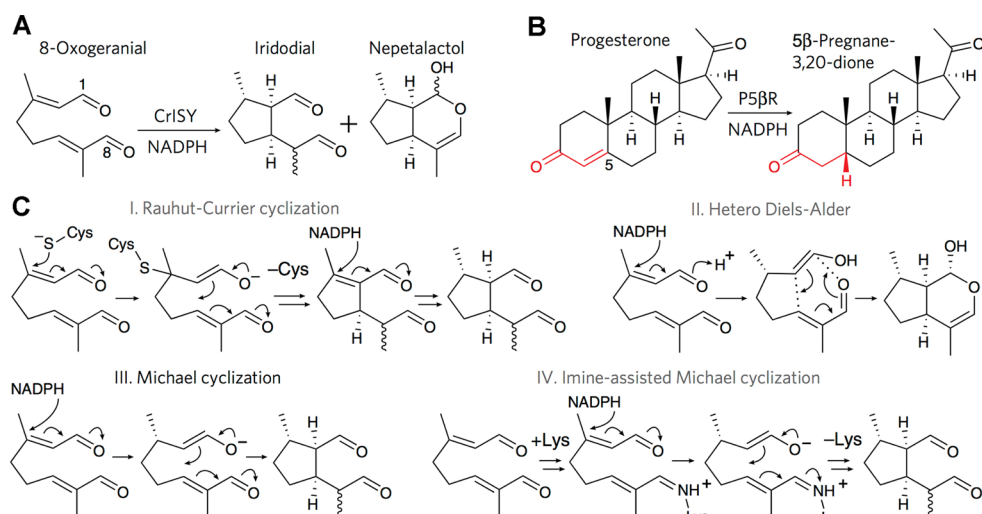


Figure 102. (A) Iridoid synthase from *Catharanthus roseus* (CrISY) catalyzes the NADPH-dependent reductive cyclization of 8-oxogeranial to form iridodial, which is in equilibrium with nepetalactol. (B) The plant enzyme progesterone 5 β -reductase (P5 β R) catalyzes the NADPH-dependent reduction of progesterone in a reaction that similarly involves the reduction of a C=C bond in an α,β -unsaturated ketone. The three-dimensional structure of P5 β R is homologous to that of CrISY. (C) Four possible mechanisms are considered for the cyclization of 8-oxogeranial; the crystal structure of CrISY as well as enzymological studies pinpoint Michael cyclization (III) as the operative mechanism. Reprinted by permission from ref 538. Copyright 2016 Macmillan Publishers Ltd.

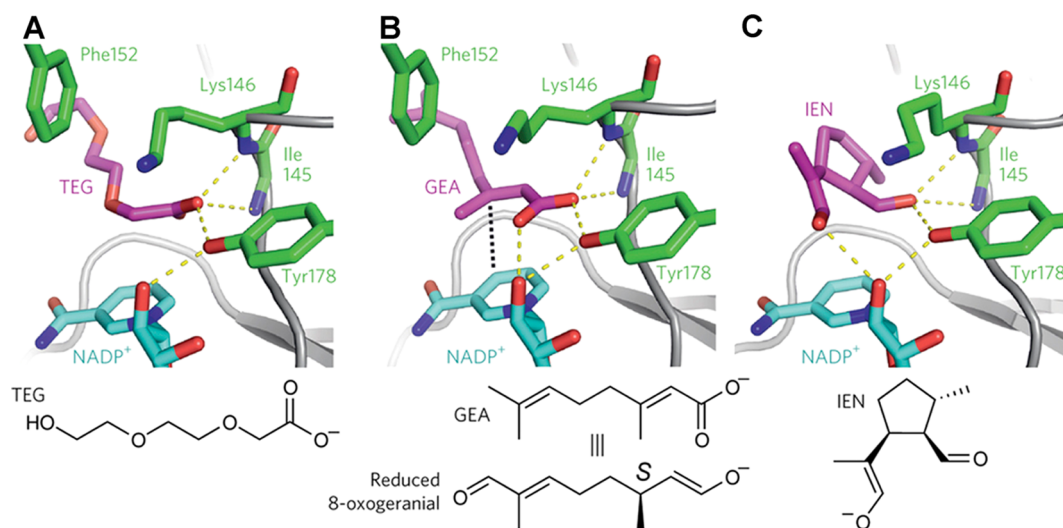


Figure 103. (A) The binding of triethylene glycol carboxylate (TEG) in the active site of the iridoid synthase–NADP⁺ complex reveals that a carboxylate oxygen receives hydrogen bonds from the backbone NH groups of I145 and K146 and the hydroxyl group of Y178. These interactions define an oxyanion hole in the active site. (B) The binding of the transition state analogue geranic acid (GEA) in the iridoid synthase–NADP⁺–GEA ternary complex reveals that its carboxylate oxygen similarly receives 3 hydrogen bonds in the oxyanion hole. These interactions likely stabilize the enolate oxyanion of reduced 8-oxogeranial formed by Michael addition of the pro-S NADPH hydride to C3 of the substrate (hydride trajectory indicated by a black dotted line). (C) Model of iridoid synthase complexed with the enolate form of iridodial (IEN) indicates that the enolate oxyanion can remain stabilized in the oxyanion hole; however, cyclization of the extended conformation represented by the binding of GEA in (B) requires a conformational change of F152, which would otherwise sterically block iridodial formation. Reprinted with permission from ref 538. Copyright 2016 Macmillan Publishers Ltd.

The β domain is found in terpenoid cyclases as an $\alpha\beta$ assembly as first observed in epi-aristolochene synthase,³⁷ as a $\beta\gamma$ assembly as first observed in squalene-hopene cyclase,³⁸ or as an $\alpha\beta\gamma$ domain assembly, as first observed in taxadiene synthase,⁴² ent-copalyl diphosphate synthase,⁴⁴ and abietadiene synthase.⁴⁵ In class I $\alpha\beta$ domain assemblies, the β domain has no direct catalytic function other than to provide an N-terminal polypeptide segment to help cap the closed conformation of the active site in the α domain. This may be an evolutionary vestige from a bifunctional copalyl diphosphate synthase-kaurene synthase that

was the ancestor to all plant terpenoid synthases,¹⁷ given that the γ domain is readily lost.⁵⁹ In class II $\beta\gamma$ or $\alpha\beta\gamma$ domain assemblies, the active site is at the $\beta\gamma$ domain interface and the catalytic general acid is contained in the β domain.^{38,44} The γ domain diverged from the β domain⁸ and is the location of a membrane-anchoring component in the monotopic membrane proteins squalene-hopene cyclase and oxidosqualene cyclase.^{38,462} Interestingly, the β domain fold is conserved in other enzymes that utilize terpenoid substrates, such as protein farnesyl transferase and linalool dehydratase isomerase.^{542,543} Nature

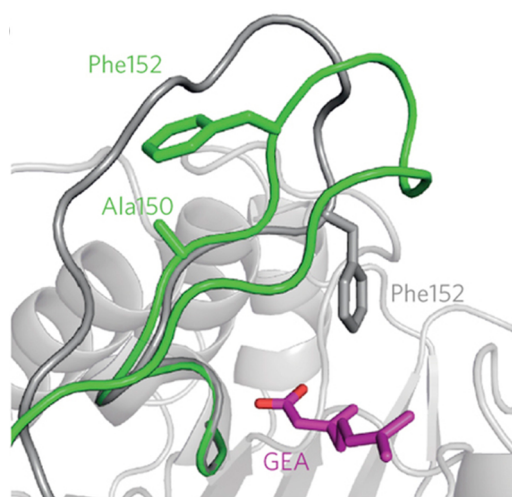


Figure 104. In the iridoid synthase-NADP⁺-GEA complex (gray), the G150-D162 loop partially encloses the active site. In order to accommodate iridodial binding, F152 and its associated loop must undergo a conformational change to an open active site conformation, represented by the structure of this loop in the G150A mutant (green). Reprinted with permission from ref 538. Copyright 2016 Macmillan Publishers Ltd.

derives impressive functionality from these basic protein folds that are readily adapted for function in the cell cytosol or the membrane. In a sense, the α , β , and γ domains comprise privileged platforms for biosynthesis.

With regard to the chemistry of catalysis, class I and class II terpenoid synthases utilize different chemical strategies to initiate carbocation formation in isoprenoid substrates: a class I cyclase or prenyltransferase utilizes 3 metal ions and 3 basic residues to trigger the departure of the substrate diphosphate group to generate an allylic cation, whereas a class II cyclase utilizes an aspartic acid general acid to protonate an isoprenoid π bond and generate a tertiary carbocation. Strikingly, both chemical strategies are in play in the bifunctional diterpene cyclase abietadiene synthase.⁴⁵

Despite differences in substrate activation, however, both class I and class II terpenoid cyclases serve critical functions as templates for catalysis. In each cyclase active site, the flexible polyisoprenoid substrate must be fixed in place prior to initial carbocation formation to ensure that the proper trajectory of carbon-carbon bond-forming reactions ensues. The correct sequence of carbon-carbon bond forming reactions in the cyclization cascade is directed by the precatalytic binding conformation of the substrate and the accessible conformation(s) of subsequently formed carbocation intermediates, so the fidelity of the cyclization pathway is encoded in the three-dimensional contour of the cyclase active site. The active site contour can be remodeled through site-directed mutagenesis to introduce new reaction pathways that generate alternative products. Accordingly, there is great promise for the use of terpenoid synthases in synthetic biology for the manufacture of commercially important chemical compounds, such as biofuels and drugs.^{167–169,394,399} The ability to do so predictably (i.e., to predict the structure of a terpenoid cyclization product based solely on analysis of the structure of the terpenoid cyclase active site) is a grand challenge for computational protein engineering, and a successful first step in this regard has been recently reported.³⁰⁵

The active sites of both class I and class II terpenoid cyclases contain at least 2–3 aromatic residues capable of stabilizing high-energy carbocation intermediates and their flanking transition states through cation- π interactions. Additional stabilization of carbocation intermediates in class I cyclases may derive from the helix dipole at the break in helix G, as first suggested for the coupling enzyme squalene synthase¹⁰⁷ and subsequently noted for hedycaryol synthase¹⁰⁸ and selinadiene synthase.²⁷¹ Additionally, the negative electrostatic potential of the inorganic pyrophosphate coproduct provides electrostatic stabilization of carbocation intermediates. Inorganic pyrophosphate may also serve widely as a general base to terminate the reaction sequence in class I terpenoid cyclization and coupling reactions,^{3,75,80} and a water molecule may serve this function in class II terpenoid cyclases.⁴²⁹ For class I or class II cyclases in which a water molecule adds to the final carbocation intermediate to terminate the reaction, the water molecule must be highly controlled so that it does not prematurely quench the sequence of carbocation intermediates in the cyclization cascade.

In closing, it is interesting to consider the glimpse of assembly line biosynthesis in more complex terpenoid synthase structures containing multidomain bifunctional assemblies such as abietadiene synthase ($\alpha\beta\gamma$ domain architecture),⁴⁵ or oligomeric multidomain bifunctional assemblies such as fusicoccadiene synthase [$(\alpha\alpha)_6$ domain architecture and oligomeric assembly].⁹⁵ Reaction flux in such systems can be enhanced through cluster channeling, as recently demonstrated for fusicoccadiene synthase.³⁹² Moreover, combinations of class I and class II cyclases lead to the generation of cyclic diterpenes that are “new to nature”,^{544,545} and computational analyses of monoterpene carbocation structures indicate that known cyclic terpenoids represent just a small subset of the theoretically maximum number of possible carbon skeletons that can be formed from the linear achiral precursor GPP.⁵⁴⁶ Thus, there is tremendous untapped potential in terpenoid chemodiversity that can be explored through protein engineering. Future studies will undoubtedly continue to illuminate the versatility and utility of terpenoid synthase structure and function, which promises to play an increasingly prominent role in synthetic biology approaches for the manufacture of carbon-based materials.

AUTHOR INFORMATION

Corresponding Author

*E-mail: chris@sas.upenn.edu. Tel: +1 215 898 5714.

ORCID

David W. Christianson: 0000-0002-0194-5212

Notes

The author declares no competing financial interest.

Biography

David W. Christianson received the A.B. (1983), A.M. (1985), and Ph.D. (1987) degrees in chemistry from Harvard University and joined the faculty of the University of Pennsylvania in 1988. Currently the Roy and Diana Vagelos Professor in Chemistry and Chemical Biology, Christianson has been studying enzymes of terpenoid biosynthesis ever since he reported the first bacterial terpenoid cyclase structure 20 years ago.³⁶ Christianson's research has been recognized by several awards, including a Searle Scholar Award (1989), an Alfred P. Sloan Fellowship (1992), a Camille and Henry Dreyfus Teacher-Scholar Award (1993), the Pfizer Award in Enzyme Chemistry (1999), a Guggenheim Fellowship (2006), and the Repligen Award in Chemistry of Biological

Processes (2013). Christianson was also Visiting Professor and Fellow in the Natural Sciences at Sidney Sussex College, University of Cambridge (2006), the Elizabeth S. and Richard M. Cashin Fellow at the Radcliffe Institute for Advanced Study at Harvard University (2015), and Visiting Professor of Chemistry and Chemical Biology at Harvard University (2016). An avid sailor, Christianson can often be found on the Chesapeake Bay and beyond as captain of the sloop *Sea Symphony*, berthed at home port Annapolis, Maryland.

ACKNOWLEDGMENTS

I am grateful to Drs. David Cane, Golda Harris, Sarah O'Connor, Travis Pemberton, Reuben Peters, Brittany Petros, and Dale Poulter for their careful reading and thoughtful comments on this review prior to publication. I thank Timothy S. Oey for his assistance with the figures. Additionally, I thank the NIH for Grant GM56838 in support of my research on terpenoid cyclase structure and function.

REFERENCES

- (1) *Dictionary of Natural Products*; Buckingham, J., Ed.; Chapman & Hall, London, 1994; Vol. 7.
- (2) Buckingham, J.; Cooper, C. M.; Purchase, R. *Natural Products Desk Reference*; CRC Press, Taylor & Francis Group: Boca Raton, 2016; p 235.
- (3) Poulter, C. D.; Rilling, H. C. The Prenyl Transfer Reaction. Enzymatic and Mechanistic Studies of the 1'-4 Coupling Reaction in the Terpene Biosynthetic Pathway. *Acc. Chem. Res.* **1978**, *11*, 307–313.
- (4) Kellogg, B. A.; Poulter, C. D. Chain Elongation in the Isoprenoid Biosynthetic Pathway. *Curr. Opin. Chem. Biol.* **1997**, *1*, 570–578.
- (5) Croteau, R. Biosynthesis and Catabolism of Monoterpenoids. *Chem. Rev.* **1987**, *87*, 929–954.
- (6) Cane, D. E. Enzymatic Formation of Sesquiterpenes. *Chem. Rev.* **1990**, *90*, 1089–1103.
- (7) Lesburg, C. A.; Caruthers, J. M.; Paschall, C. M.; Christianson, D. W. Managing and Manipulating Carbocations in Biology: Terpenoid Cyclase Structure and Mechanism. *Curr. Opin. Struct. Biol.* **1998**, *8*, 695–703.
- (8) Wendt, K. U.; Schulz, G. E. Isoprenoid Biosynthesis: Manifold Chemistry Catalyzed by Similar Enzymes. *Structure* **1998**, *6*, 127–133.
- (9) Davis, E. M.; Croteau, R. Cyclization Enzymes in the Biosynthesis of Monoterpenes, Sesquiterpenes, and Diterpenes. *Top. Curr. Chem.* **2000**, *209*, 53–95.
- (10) Wendt, K. U.; Schulz, G. E.; Corey, E. J.; Liu, D. R. Enzyme Mechanisms for Polycyclic Triterpene Formation. *Angew. Chem., Int. Ed.* **2000**, *39*, 2812–2833.
- (11) Pichersky, E.; Noel, J. P.; Dudareva, N. Biosynthesis of Plant Volatiles: Nature's Diversity and Ingenuity. *Science* **2006**, *311*, 808–811.
- (12) Tholl, D. Terpene Synthases and the Regulation, Diversity and Biological Roles of Terpene Metabolism. *Curr. Opin. Plant Biol.* **2006**, *9*, 297–304.
- (13) Christianson, D. W. Structural Biology and Chemistry of the Terpenoid Cyclases. *Chem. Rev.* **2006**, *106*, 3412–3442.
- (14) Christianson, D. W. Unearthing the Roots of the Terpenome. *Curr. Opin. Chem. Biol.* **2008**, *12*, 141–150.
- (15) Degenhardt, J.; Köllner, T. G.; Gershenzon, J. Monoterpene and Sesquiterpene Synthases and the Origin of Terpene Skeletal Diversity in Plants. *Phytochemistry* **2009**, *70*, 1621–1637.
- (16) Miller, D. J.; Allemann, R. K. Sesquiterpene Synthases: Passive Catalysts or Active Players? *Nat. Prod. Rep.* **2012**, *29*, 60–71.
- (17) Gao, Y.; Honzatko, R. B.; Peters, R. J. Terpenoid Synthase Structures: A So Far Yet Incomplete View of Complex Catalysis. *Nat. Prod. Rep.* **2012**, *29*, 1153–1175.
- (18) Cane, D. E.; Ikeda, H. Exploration and Mining of the Bacterial Terpenome. *Acc. Chem. Res.* **2012**, *45*, 463–472.
- (19) Quin, M. B.; Flynn, C. M.; Schmidt-Dannert, C. Traversing the Fungal Terpenome. *Nat. Prod. Rep.* **2014**, *31*, 1449–1473.
- (20) Poulter, C. D. Biosynthesis of Non-Head-to-Tail Terpenes. Formation of 1'-1 and 1'-3 Linkages. *Acc. Chem. Res.* **1990**, *23*, 70–77.
- (21) Sacchettini, J. C.; Poulter, C. D. Creating Isoprenoid Diversity. *Science* **1997**, *277*, 1788–1789.
- (22) Christianson, D. W. Roots of Biosynthetic Diversity. *Science* **2007**, *316*, 60–61.
- (23) Whittington, D. A.; Wise, M. L.; Urbansky, M.; Coates, R. M.; Croteau, R. B.; Christianson, D. W. Bornyl Diphosphate Synthase: Structure and Strategy for Carbocation Manipulation by a Terpenoid Cyclase. *Proc. Natl. Acad. Sci. U. S. A.* **2002**, *99*, 15375–15380.
- (24) Chen, M.; Al-lami, N.; Janvier, M.; D'Antonio, E. L.; Faraldos, J. A.; Cane, D. E.; Allemann, R. K.; Christianson, D. W. (2013) Mechanistic Insights from the Binding of Substrate and Intermediate Analogues to Aristolochene Synthase. *Biochemistry* **2013**, *52*, 5441–5453.
- (25) Chen, M.; Chou, W. K. W.; Al-Lami, N.; Faraldos, J. A.; Allemann, R. K.; Cane, D. E.; Christianson, D. W. Probing the Role of Active Site Water in the Sesquiterpene Cyclization Reaction Catalyzed by Aristolochene Synthase. *Biochemistry* **2016**, *55*, 2864–2874.
- (26) Tantillo, D. J. The Carbocation Continuum in Terpene Biosynthesis—Where are the Secondary Cations? *Chem. Soc. Rev.* **2010**, *39*, 2847–2854.
- (27) Tantillo, D. J. Biosynthesis Via Carbocations: Theoretical Studies on Terpene Formation. *Nat. Prod. Rep.* **2011**, *28*, 1035–1053.
- (28) Hare, S. R.; Tantillo, D. J. Dynamic Behavior of Rearranging Carbocations—Implications for Terpene Biosynthesis. *Beilstein J. Org. Chem.* **2016**, *12*, 377–390.
- (29) Dougherty, D. A. Cation- π Interactions in Chemistry and Biology: A New View of Benzene, Phe, Tyr, and Trp. *Science* **1996**, *271*, 163–168.
- (30) Ma, J. C.; Dougherty, D. A. The Cation- π Interaction. *Chem. Rev.* **1997**, *97*, 1303–1324.
- (31) Jenson, C.; Jorgensen, W. L. Computational Investigations of Carbenium Ion Reactions Relevant to Sterol Biosynthesis. *J. Am. Chem. Soc.* **1997**, *119*, 10846–10854.
- (32) Baunach, M.; Franke, J.; Hertweck, C. Terpenoid Biosynthesis Off the Beaten Track: Unconventional Cyclases and Their Impact on Biomimetic Synthesis. *Angew. Chem., Int. Ed.* **2015**, *54*, 2604–2626.
- (33) Hasserodt, J.; Janda, K. D.; Lerner, R. A. Formation of Bridge-Methylated Decalins by Antibody-Catalyzed Tandem Cationic Cyclization. *J. Am. Chem. Soc.* **1997**, *119*, 5993–5998.
- (34) Hasserodt, J.; Janda, K. D.; Lerner, R. A. Antibodies Mimic Natural Oxidosqualene-Cyclase Action in Steroid Ring A Formation. *J. Am. Chem. Soc.* **2000**, *122*, 40–45.
- (35) Paschall, C. M.; Hasserodt, J.; Jones, T.; Lerner, R. A.; Janda, K. D.; Christianson, D. W. Convergence of Catalytic Antibody and Terpene Cyclase Mechanisms: Polyene Cyclization Directed by Carbocation- π Interactions. *Angew. Chem., Int. Ed.* **1999**, *38*, 1743–1747.
- (36) Lesburg, C. A.; Zhai, G.; Cane, D. E.; Christianson, D. W. (1997) Crystal Structure of Pentalene Synthase: Mechanistic Insights on Terpenoid Cyclization Reactions in Biology. *Science* **1997**, *277*, 1820–1824.
- (37) Starks, C. M.; Back, K.; Chappell, J.; Noel, J. P. Structural Basis for Cyclic Terpene Biosynthesis by Tobacco 5-epi-Aristolochene Synthase. *Science* **1997**, *277*, 1815–1820.
- (38) Wendt, K. U.; Poralla, K.; Schulz, G. E. Structure and Function of a Squalene Cyclase. *Science* **1997**, *277*, 1811–1815.
- (39) Cao, R.; Zhang, Y.; Mann, F. M.; Huang, C.; Mukkamala, D.; Hudock, M. P.; Mead, M. E.; Priscic, S.; Wang, K.; Lin, F.-Y.; Chang, T.-K.; Peters, R. J.; Oldfield, E. Diterpene Cyclases and the Nature of the Isoprene Fold. *Proteins: Struct., Funct., Genet.* **2010**, *78*, 2417–2432.
- (40) Oldfield, E.; Lin, F.-Y. Terpene Biosynthesis: Modularity Rules. *Angew. Chem., Int. Ed.* **2012**, *51*, 1124–1137.
- (41) Huang, H.; Levin, E. J.; Liu, S.; Bai, Y.; Lockless, S. W.; Zhou, M. Structure of a Membrane-Embedded Prenyltransferase Homologous to UBIAD1. *PLoS Biol.* **2014**, *12* (7), e1001911.

- (42) Köksal, M.; Jin, Y.; Coates, R. M.; Croteau, R.; Christianson, D. W. Taxadiene Synthase Structure and Evolution of Modular Architecture in Terpene Biosynthesis. *Nature* **2011**, *469*, 116–120.
- (43) Peters, R. J.; Carter, O. A.; Zhang, Y.; Matthews, B. W.; Croteau, R. B. Bifunctional Abietadiene Synthase: Mutual Structural Dependence of the Active Sites for Protonation-Initiated and Ionization-Initiated Cyclizations. *Biochemistry* **2003**, *42*, 2700–2707.
- (44) Köksal, M.; Hu, H.; Coates, R. M.; Peters, R. J.; Christianson, D. W. Structure and Mechanism of the Diterpene Cyclase *ent*-Copalyl Diphosphate Synthase. *Nat. Chem. Biol.* **2011**, *7*, 431–433.
- (45) Zhou, K.; Gao, Y.; Hoy, J. A.; Mann, F. M.; Honzatko, R. B.; Peters, R. J. Insights into Diterpene Cyclization from Structure of Bifunctional Abietadiene Synthase from *Abies grandis*. *J. Biol. Chem.* **2012**, *287*, 6840–6850.
- (46) McAndrew, R. P.; Peralta-Yahya, P. P.; DeGiovanni, A.; Pereira, J. H.; Hadi, M. Z.; Keasling, J. D.; Adams, P. D. Structure of a Three-Domain Sesquiterpene Synthase: A Prospective Target for Advanced Biofuels Production. *Structure* **2011**, *19*, 1876–1884.
- (47) Kharel, Y.; Koyama, T. Molecular Analysis of *cis*-Prenyl Chain Elongating Enzymes. *Nat. Prod. Rep.* **2003**, *20*, 111–118.
- (48) Surmacz, L.; Swiezewska, E. Polyisoprenoids—Secondary Metabolites or Physiologically Important Superlipids? *Biochem. Biophys. Res. Commun.* **2011**, *407*, 627–632.
- (49) Schilmiller, A. L.; Schauvinhold, I.; Larson, M.; Xu, R.; Charbonneau, A. L.; Schmidt, A.; Wilkerson, C.; Last, R. L.; Pichersky, E. Monoterpenes in the Glandular Trichomes of Tomato Are Synthesized from a Neryl Diphosphate Precursor Rather Than Geranyl Diphosphate. *Proc. Natl. Acad. Sci. U. S. A.* **2009**, *106*, 10865–10870.
- (50) Sallaud, C.; Rontein, D.; Onillon, S.; Jabès, F.; Duffé, P.; Giacalone, C.; Thoraval, S.; Escoffier, C.; Herbette, G.; Leonhardt, N.; Causse, M.; Tissier, A. A Novel Pathway for Sesquiterpene Biosynthesis from *Z,Z*-Farnesyl Pyrophosphate in the Wild Tomato *Solanum habrochaites*. *Plant Cell* **2009**, *21*, 301–317.
- (51) Zi, J.; Matsuba, Y.; Hong, Y. J.; Jackson, A. J.; Tantillo, D. J.; Pichersky, E.; Peters, R. J. Biosynthesis of Lycosantalanol, a *cis*-Prenyl Derived Diterpenoid. *J. Am. Chem. Soc.* **2014**, *136*, 16951–16953.
- (52) Teng, K.-H.; Liang, P.-H. Structures, Mechanisms and Inhibitors of Undecaprenyl Diphosphate Synthase: A *cis*-Prenyltransferase for Bacterial Peptidoglycan Biosynthesis. *Bioorg. Chem.* **2012**, *43*, 51–57.
- (53) Fujihashi, M.; Zhang, Y.-W.; Higuchi, Y.; Li, X.-Y.; Koyama, T.; Miki, K. Crystal Structure of *cis*-Prenyl Chain Elongating Enzyme, Undecaprenyl Diphosphate Synthase. *Proc. Natl. Acad. Sci. U. S. A.* **2001**, *98*, 4337–4342.
- (54) Thulasiram, H. V.; Poulter, C. D. Farnesyl Diphosphate Synthase: The Art of Compromise between Substrate Selectivity and Stereoselectivity. *J. Am. Chem. Soc.* **2006**, *128*, 15819–15823.
- (55) Schulbach, M. C.; Brennan, P. J.; Crick, D. C. Identification of a Short (C₁₅) Chain *Z*-Isoprenyl Diphosphate Synthase and a Homologous Long (C₅₀) Chain Isoprenyl Diphosphate Synthase in *Mycobacterium tuberculosis*. *J. Biol. Chem.* **2000**, *275*, 22876–22881.
- (56) Noel, J. P.; Dellas, N.; Faraldos, J. A.; Zhao, M.; Hess, B. A., Jr.; Smentek, L.; Coates, R. M.; O'Maille, P. E. Structural Elucidation of Cisoid and Transoid Cyclization Pathways of a Sesquiterpene Synthase Using 2-Fluorofarnesyl Diphosphates. *ACS Chem. Biol.* **2010**, *5*, 377–392.
- (57) Jia, M.; Peters, R. J. *Cis* or *Trans* with Class II Diterpene Cyclases. *Org. Biomol. Chem.* **2017**, *15*, 3158–3160.
- (58) Tarshis, L. C.; Yan, M.; Poulter, C. D.; Sacchettini, J. C. Crystal Structure of Recombinant Farnesyl Diphosphate Synthase at 2.6-Å Resolution. *Biochemistry* **1994**, *33*, 10871–10877.
- (59) Hillwig, M. L.; Xu, M.; Toyomasu, T.; Tiernan, M. S.; Wei, G.; Cui, G.; Huang, L.; Peters, R. J. Domain Loss has Independently Occurred Multiple Times in Plant Terpene Synthase Evolution. *Plant J.* **2011**, *68*, 1051–1060.
- (60) Ashby, M. N.; Edwards, P. A. Elucidation of the Deficiency in Two Yeast Coenzyme Q Mutants: Characterization of the Structural Gene Encoding Hexaprenyl Pyrophosphate Synthetase. *J. Biol. Chem.* **1990**, *265*, 13157–13164.
- (61) Ashby, M. N.; Kutsunai, S. Y.; Ackerman, S.; Tzagoloff, A.; Edwards, P. A. *COQ2* is a Candidate for the Structural Gene Encoding *para*-Hydroxybenzoate:Polyprenyltransferase. *J. Biol. Chem.* **1992**, *267*, 4128–4136.
- (62) Joly, A.; Edwards, P. A. Effect of Site-Directed Mutagenesis of Conserved Aspartate and Arginine Residues upon Farnesyl Diphosphate Synthase Activity. *J. Biol. Chem.* **1993**, *268*, 26983–26989.
- (63) Song, L.; Poulter, C. D. Yeast Farnesyl-Diphosphate Synthase: Site-Directed Mutagenesis of Residues in Highly Conserved Prenyltransferase Domains I and II. *Proc. Natl. Acad. Sci. U. S. A.* **1994**, *91*, 3044–3048.
- (64) Tarshis, L. C.; Proteau, P. J.; Kellogg, B. A.; Sacchettini, J. C.; Poulter, C. D. Regulation of Product Chain Length by Isoprenyl Diphosphate Synthases. *Proc. Natl. Acad. Sci. U. S. A.* **1996**, *93*, 15018–15023.
- (65) Hosfield, D. J.; Zhang, Y.; Dougan, D. R.; Broun, A.; Tari, L. W.; Swanson, R. V.; Finn, J. Structural Basis for Bisphosphonate-Mediated Inhibition of Isoprenoid Biosynthesis. *J. Biol. Chem.* **2004**, *279*, 8526–8529.
- (66) Aaron, J. A.; Christianson, D. W. Trinuclear Metal Clusters in Catalysis by Terpenoid Synthases. *Pure Appl. Chem.* **2010**, *82*, 1585–1597.
- (67) Poulter, C. D.; Wiggins, P. L.; Le, A. T. Farnesylpyrophosphate Synthetase. A Stepwise Mechanism for the 1'–4 Condensation Reaction. *J. Am. Chem. Soc.* **1981**, *103*, 3926–3927.
- (68) Poulter, C. D.; Satterwhite, D. M. Mechanism of the Prenyl-Transfer Reaction. Studies with (E)- and (Z)-3-Trifluoromethyl-2-buten-1-yl Pyrophosphate. *Biochemistry* **1977**, *16*, 5470–5478.
- (69) Poulter, C. D.; Argyle, J. C.; Mash, E. A. Farnesyl Pyrophosphate Synthetase: Mechanistic Studies of the 1'–4 Coupling Reaction with 2-Fluorogeranyl Pyrophosphate. *J. Biol. Chem.* **1978**, *253*, 7227–7233.
- (70) Lynen, F.; Eggerer, U.; Henning, V.; Kessel, I. Farnesyl-Pyrophosphat und 3-Methyl- Δ^3 -Butenyl-1-Pyrophosphat, die Biologischen Vorstufen des Squalens. *Angew. Chem.* **1958**, *70*, 738–742.
- (71) Rilling, H. C.; Bloch, K. On the Mechanism of Squalene Biogenesis from Mevalonic Acid. *J. Biol. Chem.* **1959**, *234*, 1424–1432.
- (72) Cornforth, J. W.; Popják, G. Mechanism of Biosynthesis of Squalene from Sesquiterpenoids. *Tetrahedron Lett.* **1959**, *1*, 29–35.
- (73) Davisson, V. J.; Neal, T. R.; Poulter, C. D. Farnesyl-Diphosphate Synthase. Catalysis of an Intramolecular Prenyl Transfer with Bisubstrate Analogs. *J. Am. Chem. Soc.* **1993**, *115*, 1235–1245.
- (74) Cornforth, J. W. Olefin Alkylolation in Biosynthesis. *Angew. Chem., Int. Ed. Engl.* **1968**, *7*, 903–964.
- (75) Popják, G. Specificity of Enzymes of Sterol Biosynthesis. *Harvey Lect.* **1971**, *65*, 127–156.
- (76) Poulter, C. D.; Rilling, H. C. Prenyltransferase: The Mechanism of the Reaction. *Biochemistry* **1976**, *15*, 1079–1083.
- (77) King, H. L., Jr.; Rilling, H. C. Avian Liver Prenyltransferase. The Role of Metal in Substrate Binding and the Orientation of Substrates during Catalysis. *Biochemistry* **1977**, *16*, 3815–3819.
- (78) Rilling, H. C. Prenyltransferase. *Pure Appl. Chem.* **1979**, *51*, 597–608.
- (79) Caruthers, J. M.; Kang, I.; Rynkiewicz, M. J.; Cane, D. E.; Christianson, D. W. Crystal Structure Determination of Aristolochene Synthase from the Blue Cheese Mold, *Penicillium roqueforti*. *J. Biol. Chem.* **2000**, *275*, 25533–25539.
- (80) Pemberton, T. A.; Christianson, D. W. General Base-General Acid Catalysis by Terpenoid Cyclases. *J. Antibiot.* **2016**, *69*, 486–493.
- (81) Stanley Fernandez, S. M.; Kellogg, B. A.; Poulter, C. D. Farnesyl Diphosphate Synthase. Altering the Catalytic Site to Select for Geranyl Diphosphate Activity. *Biochemistry* **2000**, *39*, 15316–15321.
- (82) Ohnuma, S.-i.; Nakazawa, T.; Hemmi, H.; Hallberg, A.-M.; Koyama, T.; Ogura, K.; Nishino, T. Conversion from Farnesyl Diphosphate Synthase to Geranylgeranyl Diphosphate Synthase by Random Chemical Mutagenesis. *J. Biol. Chem.* **1996**, *271*, 10087–10095.
- (83) Guo, R.-T.; Kuo, C.-J.; Chou, C.-C.; Ko, T.-P.; Shr, H.-L.; Liang, P.-H.; Wang, A. H.-J. Crystal Structure of Octaprenyl Pyrophosphate Synthase from Hyperthermophilic *Thermotoga maritima* and Mecha-

nism of Product Chain Length Determination. *J. Biol. Chem.* **2004**, *279*, 4903–4912.

(84) Guo, R.-T.; Kuo, C.-J.; Ko, T.-P.; Chou, C.-C.; Liang, P.-H.; Wang, A. H.-J. A Molecular Ruler for Chain Elongation Catalyzed by Octaprenyl Pyrophosphate Synthase and Its Structure-Based Engineering to Produce Unprecedented Long Chain *trans*-Prenyl Products. *Biochemistry* **2004**, *43*, 7678–7686.

(85) Sun, H.-Y.; Ko, T.-P.; Kuo, C.-J.; Guo, R.-T.; Chou, C.-C.; Liang, P.-H.; Wang, A. H.-J. Homodimeric Hexaprenyl Pyrophosphate Synthase from the Thermoacidophilic Crenarchaeon *Sulfolobus solfataricus* Displays Asymmetric Subunit Structures. *J. Bacteriol.* **2005**, *187*, 8137–8148.

(86) Kloer, D. P.; Welsch, R.; Beyer, P.; Schulz, G. E. Structure and Reaction Geometry of Geranylgeranyl Diphosphate Synthase from *Sinapis alba*. *Biochemistry* **2006**, *45*, 15197–15204.

(87) Chang, T. H.; Guo, R. T.; Ko, T. P.; Wang, A. H.-J.; Liang, P. H. Crystal Structure of Type-III Geranylgeranyl Pyrophosphate Synthase from *Saccharomyces cerevisiae* and the Mechanism of Product Chain Length Determination. *J. Biol. Chem.* **2006**, *281*, 14991–15000.

(88) Kavanagh, K. L.; Dunford, J. E.; Bunkoczi, G.; Russell, R. G. G.; Oppermann, U. The Crystal Structure of Human Geranylgeranyl Pyrophosphate Synthase Reveals a Novel Hexameric Arrangement and Inhibitory Product Binding. *J. Biol. Chem.* **2006**, *281*, 22004–22012.

(89) Chang, T. H.; Hsieh, F. L.; Ko, T. P.; Teng, K. H.; Liang, P. H.; Wang, A. H.-J. Structure of a Heterotetrameric Geranyl Pyrophosphate Synthase from Mint (*Mentha piperita*) Reveals Intersubunit Regulation. *Plant Cell* **2010**, *22*, 454–467.

(90) Sasaki, D.; Fujihashi, M.; Okuyama, N.; Kobayashi, Y.; Noike, M.; Koyama, T.; Miki, K. Crystal Structure of Heterodimeric Hexaprenyl Diphosphate Synthase from *Micrococcus luteus* B-P 26 Reveals that the Small Subunit is Directly Involved in the Product Chain Length Regulation. *J. Biol. Chem.* **2011**, *286*, 3729–3740.

(91) No, J. H.; de Macedo Dossin, F.; Zhang, Y.; Liu, Y.-L.; Zhu, W.; Feng, X.; Yoo, J. A.; Lee, E.; Wang, K.; Hui, R.; et al. Lipophilic Analogs of Zoledronate and Risedronate Inhibit *Plasmodium* Geranylgeranyl Diphosphate Synthase (GGPPS) and Exhibit Potent Antimalarial Activity. *Proc. Natl. Acad. Sci. U. S. A.* **2012**, *109*, 4058–4063.

(92) Wallrapp, F. H.; Pan, J.-J.; Ramamoorthy, G.; Almonacid, D. E.; Hillerich, B. S.; Seidel, R.; Patskovsky, Y.; Babbitt, P. C.; Almo, S. C.; Jacobson, M. P.; Poulter, C. D. Prediction of Function for the Polyprenyl Transferase Subgroup in the Isoprenoid Synthase Superfamily. *Proc. Natl. Acad. Sci. U. S. A.* **2013**, *110*, E1196–E1202.

(93) Han, X.; Chen, C.-C.; Kuo, C.-J.; Huang, C.-H.; Zheng, Y.; Ko, T.-P.; Zhu, Z.; Feng, X.; Wang, K.; Oldfield, E.; et al. Crystal Structures of Ligand-Bound Octaprenyl Pyrophosphate Synthase from *Escherichia coli* Reveal the Catalytic and Chain-Length Determining Mechanisms. *Proteins: Struct., Funct., Genet.* **2015**, *83*, 37–45.

(94) Ricci, C. G.; Liu, Y.-L.; Zhang, Y.; Wang, Y.; Zhu, W.; Oldfield, E.; McCammon, J. A. Dynamic Structure and Inhibition of a Malaria Drug Target: Geranylgeranyl Diphosphate Synthase. *Biochemistry* **2016**, *55*, 5180–5190.

(95) Chen, M.; Chou, W. K. W.; Toyomasu, T.; Cane, D. E.; Christianson, D. W. Structure and Function of Fusicocadiene Synthase, a Hexameric Bifunctional Diterpene Synthase. *ACS Chem. Biol.* **2016**, *11*, 889–899.

(96) Kamtekar, S.; Schiffer, J. M.; Xiong, H.; Babik, J. M.; Hecht, M. H. Protein Design by Binary Patterning of Polar and Nonpolar Amino Acids. *Science* **1993**, *262*, 1680–1685.

(97) Choma, C. T.; Lear, J. D.; Nelson, M. J.; Dutton, P. L.; Robertson, D. E.; DeGrado, W. F. Design of a Heme-Binding Four-Helix Bundle. *J. Am. Chem. Soc.* **1994**, *116*, 856–865.

(98) Lu, Y.; Yeung, N.; Sieracki, N.; Marshall, N. M. Design of Functional Metalloproteins. *Nature* **2009**, *460*, 855–862.

(99) Smith, B. A.; Hecht, M. H. Novel Proteins: From Fold to Function. *Curr. Opin. Chem. Biol.* **2011**, *15*, 421–426.

(100) Zastrow, M. L.; Peacock, A. F. A.; Stuckey, J. A.; Pecoraro, V. L. Hydrolytic Catalysis and Structural Stabilization in a Designed Metalloprotein. *Nat. Chem.* **2011**, *4*, 118–123.

(101) Fletcher, J. M.; Boyle, A. L.; Bruning, M.; Bartlett, G. J.; Vincent, T. L.; Zaccai, N. R.; Armstrong, C. T.; Bromley, E. H.; Booth, P. J.; Brady, R. L.; et al. A Basis Set of *de Novo* Coiled-Coil Peptide Oligomers for Rational Protein Design and Synthetic Biology. *ACS Synth. Biol.* **2012**, *1*, 240–250.

(102) Yu, F.; Cangelosi, V. M.; Zastrow, M. L.; Tegoni, M.; Plegaria, J. S.; Tebo, A. G.; Mocny, C. S.; Ruckthong, L.; Qayyum, H.; Pecoraro, V. L. Protein Design: Toward Functional Metalloenzymes. *Chem. Rev.* **2014**, *114*, 3495–3578.

(103) Atkinson, H. J.; Morris, J. H.; Ferrin, T. E.; Babbitt, P. C. Using Sequence Similarity Networks for Visualization of Relationships across Diverse Protein Superfamilies. *PLoS One* **2009**, *4*, e4345.

(104) Barber, A. E., II; Babbitt, P. C. Pythoscape: A Framework for Generation of Large Protein Similarity Networks. *Bioinformatics* **2012**, *28*, 2845–2846.

(105) Thulasiram, H. V.; Erickson, H. K.; Poulter, C. D. Chimeras of Two Isoprenoid Synthases Catalyze All Four Coupling Reactions in Isoprenoid Biosynthesis. *Science* **2007**, *316*, 73–76.

(106) Liu, M.; Chen, C.-C.; Chen, L.; Xiao, X.; Zheng, Y.; Huang, J.-W.; Liu, W.; Ko, T.-P.; Cheng, Y.-S.; Feng, X.; et al. Structure and Function of a "Head-to-Middle" Prenyltransferase: Lavandulyl Diphosphate Synthase. *Angew. Chem., Int. Ed.* **2016**, *55*, 4721–4724.

(107) Pandit, J.; Danley, D. E.; Schulte, G. K.; Mazzalupo, S.; Pauly, T. A.; Hayward, C. M.; Hamanaka, E. S.; Thompson, J. F.; Harwood, H. J. Crystal Structure of Human Squalene Synthase. *J. Biol. Chem.* **2000**, *275*, 30610–30617.

(108) Baer, P.; Rabe, P.; Citron, C. A.; de Oliveira Mann, C. C.; Kaufmann, N.; Groll, M.; Dickschat, J. S. Hedycaryl Synthase in Complex with Nerolidol Reveals Terpene Cyclase Mechanism. *ChemBioChem* **2014**, *15*, 213–216.

(109) Liu, C.-I.; Liu, G. Y.; Song, Y.; Yin, F.; Hensler, M. E.; Jeng, W.-Y.; Nizet, V.; Wang, A. H.-J.; Oldfield, E. A Cholesterol Biosynthetic Inhibitor Blocks *Staphylococcus aureus* Virulence. *Science* **2008**, *319*, 1391–1394.

(110) Liu, G. Y.; Essex, A.; Buchanan, J. T.; Datta, V.; Hoffman, H. M.; Bastian, J. F.; Fierer, J.; Nizet, V. *Staphylococcus aureus* Golden Pigment Impairs Neutrophil Killing and Promotes Virulence Through Its Antioxidant Activity. *J. Exp. Med.* **2005**, *202*, 209–215.

(111) Clauditz, A.; Resch, A.; Wieland, K.-P.; Peschel, A.; Götz, F. Staphyloxanthin Plays a Role in the Fitness of *Staphylococcus aureus* and Its Ability to Cope with Oxidative Stress. *Infect. Immun.* **2006**, *74*, 4950–4953.

(112) Song, Y.; Lin, F.-Y.; Yin, F.; Hensler, M.; Rodrigues Poveda, C. A.; Mukkamala, D.; Cao, R.; Wang, H.; Morita, C. T.; González Pacanowska, D.; et al. Phosphonosulfonates are Potent, Selective Inhibitors of Dehydroqualene Synthase and Staphyloxanthin Biosynthesis in *Staphylococcus aureus*. *J. Med. Chem.* **2009**, *52*, 976–988.

(113) Song, Y.; Liu, C.-I.; Lin, F.-Y.; No, J. H.; Hensler, M.; Liu, Y.-L.; Jeng, W.-Y.; Low, J.; Liu, G. Y.; Nizet, V.; et al. Inhibition of Staphyloxanthin Virulence Factor Biosynthesis in *Staphylococcus aureus*: In Vitro, in Vivo, and Crystallographic Results. *J. Med. Chem.* **2009**, *52*, 3869–3880.

(114) Lin, F.-Y.; Liu, C.-I.; Liu, Y.-L.; Zhang, Y.; Wang, K.; Jeng, W.-Y.; Ko, T.-P.; Cao, R.; Wang, A. H.-J.; Oldfield, E. Mechanism of Action and Inhibition of Dehydroqualene Synthase. *Proc. Natl. Acad. Sci. U. S. A.* **2010**, *107*, 21337–21342.

(115) Oldfield, E. Targeting Isoprenoid Biosynthesis for Drug Discovery: Bench to Bedside. *Acc. Chem. Res.* **2010**, *43*, 1216–1226.

(116) Lin, F.-Y.; Zhang, Y.; Hensler, M.; Liu, Y.-L.; Chow, O. A.; Zhu, W.; Wang, K.; Pang, R.; Thienphrapa, W.; Nizet, V.; Oldfield, E. Dual Dehydroqualene/Squalene Synthase Inhibitors: Leads for Innate Immune System Based Therapeutics. *ChemMedChem* **2012**, *7*, 561–564.

(117) Lin, F.-Y.; Liu, Y.-L.; Li, K.; Cao, R.; Zhu, W.; Axelson, J.; Pang, R.; Oldfield, E. Head-to-Head Prenyl Transferases: Anti-Infective Drug Targets. *J. Med. Chem.* **2012**, *55*, 4367–4372.

(118) Pan, J.-J.; Solbiati, J. O.; Ramamoorthy, G.; Hillerich, B. S.; Seidel, R. D.; Cronan, J. E.; Almo, S. C.; Poulter, C. D. Biosynthesis of

Squalene from Farnesyl Diphosphate in Bacteria: Three Steps Catalyzed by Three Enzymes. *ACS Cent. Sci.* **2015**, *1*, 77–82.

(119) Kuzuyama, T.; Noel, J. P.; Richard, S. B. Structural Basis for the Promiscuous Biosynthetic Prenylation of Aromatic Natural Products. *Nature* **2005**, *435*, 983–987.

(120) Tello, M.; Kuzuyama, T.; Heide, L.; Noel, J. P.; Richard, S. B. The ABBA Family of Aromatic Prenyltransferases: Broadening Natural Product Diversity. *Cell. Mol. Life Sci.* **2008**, *65*, 1459–1463.

(121) Metzger, U.; Schall, C.; Zocher, G.; Unsöld, I.; Stec, E.; Li, S.-M.; Heide, L.; Stehle, T. The Structure of Dimethylallyl Tryptophan Synthase Reveals a Common Architecture of Aromatic Prenyltransferases in Fungi and Bacteria. *Proc. Natl. Acad. Sci. U. S. A.* **2009**, *106*, 14309–14314.

(122) Li, W. Bringing Bioactive Compounds into Membranes: The UbiA Superfamily of Intramembrane Aromatic Prenyltransferases. *Trends Biochem. Sci.* **2016**, *41*, 356–370.

(123) Young, I. G.; Leppik, R. A.; Hamilton, J. A.; Gibson, F. Biochemical and Genetic Studies on Ubiquinone Biosynthesis in *Escherichia coli* K-12:4-Hydroxybenzoate Octaprenyltransferase. *J. Bacteriol.* **1972**, *110*, 18–25.

(124) Melzer, M.; Heide, L. Characterization of Polyprenyldiphosphate: 4-Hydroxybenzoate Polyprenyltransferase from *Escherichia coli*. *Biochim. Biophys. Acta, Lipids Lipid Metab.* **1994**, *1212*, 93–102.

(125) Nakagawa, K.; Hirota, Y.; Sawada, N.; Yuge, N.; Watanabe, M.; Uchino, Y.; Okuda, N.; Shimomura, Y.; Suhara, Y.; Okano, T. Identification of UBIAD1 as a Novel Human Menaquinone-4 Biosynthetic Enzyme. *Nature* **2010**, *468*, 117–121.

(126) Suvarna, K.; Stevenson, D.; Meganathan, R.; Hudspeth, M. E. Menaquinone from *Escherichia coli*. *J. Bacteriol.* **1998**, *180*, 2782–2787.

(127) Forsgren, M.; Attersand, A.; Lake, S.; Grünler, J.; Swiezewska, E.; Dallner, G.; Climent, I. Isolation and Functional Expression of Human COQ2, a Gene Encoding a Polyprenyl Transferase Involved in the Synthesis of CoQ. *Biochem. J.* **2004**, *382*, 519–526.

(128) Cheng, W.; Li, W. Structural Insights into Ubiquinone Biosynthesis in Membranes. *Science* **2014**, *343*, 878–881.

(129) Sanadze, G. A. The Nature of Gaseous Substances Emitted by Leaves of *Robinia pseudoacacia*. *Soobshch. Akad. Nauk Gruz. SSR* **1957**, *19*, 83–86.

(130) Guenther, A.; Hewitt, C. N.; Erickson, D.; Fall, R.; Geron, C.; Graedel, T.; Harley, P.; Klinger, L.; Lerdau, M.; McKay, W. A.; et al. A Global Model of Natural Volatile Organic Compound Emissions. *J. Geophys. Res.* **1995**, *100*, 8873–8892.

(131) Wang, K. Y.; Shallcross, D. E. Modelling Terrestrial Biogenic Isoprene Fluxes and Their Potential Impact on Global Chemical Species Using a Coupled LSM-CTM Mode. *Atmos. Environ.* **2000**, *34*, 2909–2925.

(132) Monson, R. K.; Holland, E. A. Biospheric Trace Gas Fluxes and Their Control Over Tropospheric Chemistry. *Annu. Rev. Ecol. Syst.* **2001**, *32*, 547–576.

(133) Purves, D. W.; Caspersen, J. P.; Moorcroft, P. R.; Hurtt, G. C.; Pacala, S. W. Human-Induced Changes in US Biogenic Volatile Organic Compound Emissions: Evidence from Long-Term Forest Inventory Data. *Global Change Biol.* **2004**, *10*, 1737–1755.

(134) Went, G. Blue Hazes in the Atmosphere. *Nature* **1960**, *187*, 641–643.

(135) Kuzma, J.; Nemecek-Marshall, M.; Pollock, W. H.; Fall, R. Bacteria Produce the Volatile Hydrocarbon Isoprene. *Curr. Microbiol.* **1995**, *30*, 97–103.

(136) Gelmont, D.; Stein, R. A.; Mead, J. F. Isoprene – The Main Hydrocarbon in Human Breath. *Biochem. Biophys. Res. Commun.* **1981**, *99*, 1456–1460.

(137) Stöner, C.; Williams, J. Goals Change Crowd Chemistry. *Nature* **2016**, *535*, 355.

(138) Deneris, E. S.; Stein, R. A.; Mead, J. F. *In Vitro* Biosynthesis of Isoprene from Mevalonate Utilizing a Rat Liver Cytosolic Fraction. *Biochem. Biophys. Res. Commun.* **1984**, *123*, 691–696.

(139) Stone, B. G.; Besse, T. J.; Duane, W. C.; Dean Evans, C.; DeMaster, E. G. Effect of Regulating Cholesterol Biosynthesis on Breath Isoprene Excretion in Men. *Lipids* **1993**, *28*, 705–708.

(140) Karl, T.; Prazeller, P.; Mayr, D.; Jordan, A.; Rieder, J.; Fall, R.; Lindinger, W. Human Breath Isoprene and Its Relation to Blood Cholesterol Levels: New Measurements and Modeling. *J. Appl. Physiol.* **2001**, *91*, 762–770.

(141) King, J.; Mochalski, P.; Unterkofler, K.; Teschl, G.; Klieber, M.; Stein, M.; Amann, A.; Baumann, M. Breath Isoprene: Muscle Dystrophy Patients Support the Concept of a Pool of Isoprene in the Periphery of the Human Body. *Biochem. Biophys. Res. Commun.* **2012**, *423*, 526–530.

(142) Alkhouri, N.; Singh, T.; Alsabbagh, E.; Guirguis, J.; Chami, T.; Hanouneh, I.; Grove, D.; Lopez, R.; Dweik, R. Isoprene in the Exhaled Breath is a Novel Biomarker for Advanced Fibrosis in Patients with Chronic Liver Disease: A Pilot Study. *Clin. Transl. Gastroenterol.* **2015**, *6*, e112.

(143) Das, S.; Pal, S.; Mitra, M. Significance of Exhaled Breath Test in Clinical Diagnosis: A Special Focus on the Detection of Diabetes Mellitus. *J. Med. Biol. Eng.* **2016**, *36*, 605–624.

(144) Bajtarevic, A.; Ager, C.; Pienz, M.; Klieber, M.; Schwarz, K.; Ligor, M.; Ligor, T.; Filipiak, W.; Denz, H.; Fiegl, M.; et al. Noninvasive Detection of Lung Cancer by Analysis of Exhaled Breath. *BMC Cancer* **2009**, *9*, 348.

(145) Sharkey, T. D. Isoprene Synthesis by Plants and Animals. *Endeavour* **1996**, *20*, 74–78.

(146) Sharkey, T. D.; Wiberley, A. E.; Donohue, A. R. Isoprene Emission from Plants: Why and How. *Ann. Bot.* **2007**, *101*, 5–18.

(147) Sharkey, T. D.; Monson, R. K. Isoprene Research – 60 Years Later, the Biology Is Still Enigmatic. *Plant, Cell Environ.* **2017**, *40*, 1671–1678.

(148) Silver, G. M.; Fall, R. Enzymatic Synthesis of Isoprene from Dimethylallyl Diphosphate in Aspen Leaf Extracts. *Plant Physiol.* **1991**, *97*, 1588–1591.

(149) Silver, G. M.; Fall, R. Characterization of Aspen Isoprene Synthase, an Enzyme Responsible for Leaf Isoprene Emission to the Atmosphere. *J. Biol. Chem.* **1995**, *270*, 13010–13016.

(150) Miller, B.; Oschinski, C.; Zimmer, W. First Isolation of an Isoprene Synthase Gene from Poplar and Successful Expression of the Gene in *Escherichia coli*. *Planta* **2001**, *213*, 483–487.

(151) Schnitzler, J. P.; Zimmer, I.; Bachl, A.; Arend, M.; Fromm, J.; Fischbach, R. J. Biochemical Properties of Isoprene Synthase in Poplar (*Populus x canescens*). *Planta* **2005**, *222*, 777–786.

(152) Köksal, M.; Zimmer, I.; Schnitzler, J.-P.; Christianson, D. W. Structure of Isoprene Synthase Illuminates the Chemical Mechanism of Teragram Atmospheric Carbon Emission. *J. Mol. Biol.* **2010**, *402*, 363–373.

(153) Thulasiram, H. V.; Phan, R. M.; Rivera, S. B.; Poulter, C. D. Synthesis of Deuterium-Labeled Derivatives of Dimethylallyl Diphosphate. *J. Org. Chem.* **2006**, *71*, 1739–1741.

(154) Faraldos, J. A.; Gonzalez, V.; Li, A.; Yu, F.; Köksal, M.; Christianson, D. W.; Allemann, R. K. Probing the Mechanism of 1,4-Conjugate Elimination Reactions Catalyzed by Terpene Synthases. *J. Am. Chem. Soc.* **2012**, *134*, 20844–20848.

(155) Kim, J.-H.; Wang, C.; Jang, H.-J.; Cha, M.-S.; Park, J.-E.; Jo, S.-Y.; Choi, E.-S.; Kim, S.-W. Isoprene Production by *Escherichia coli* through the Exogenous Mevalonate Pathway with Reduced Formation of Fermentation Byproducts. *Microb. Cell Fact.* **2016**, *15*, 214.

(156) Ye, L.; Lv, X.; Yu, H. Engineering Microbes for Isoprene Production. *Metab. Eng.* **2016**, *38*, 125–138.

(157) Lindberg, P.; Park, S.; Melis, A. Engineering a Platform for Photosynthetic Isoprene Production in Cyanobacteria, using *Synechocystis* as the Model Organism. *Metab. Eng.* **2010**, *12*, 70–79.

(158) Xue, J.; Ahring, B. K. Enhancing Isoprene Production by Genetic Modification of the 1-Deoxy-D-Xylulose-5-Phosphate Pathway in *Bacillus subtilis*. *Appl. Environ. Microbiol.* **2011**, *77*, 2399–2405.

(159) Zhao, Y.; Yang, J.; Qin, B.; Li, Y.; Sun, Y.; Su, S.; Xian, M. Biosynthesis of Isoprene in *Escherichia coli* via Methylerythritol Phosphate (MEP) Pathway. *Appl. Microbiol. Biotechnol.* **2011**, *90*, 1915–1922.

(160) Erickson, B.; Singh, R.; Winters, P. Synthetic Biology: Regulating Industry Uses of New Biotechnologies. *Science* **2011**, *333*, 1254–1256.

- (161) Bohlmann, J.; Steele, C. L.; Croteau, R. Monoterpene Synthases from Grand Fir (*Abies grandis*): cDNA Isolation, Characterization, and Functional Expression of Myrcene Synthase, (-)-(4S)-Limonene Synthase, and (-)-(1S,5S)-Pinene Synthase. *J. Biol. Chem.* **1997**, *272*, 21784–21792.
- (162) Crock, J.; Wildung, M.; Croteau, R. Isolation and Bacterial Expression of a Sesquiterpene Synthase cDNA Clone from Peppermint (*Mentha x piperita*, L.) that Produces the Aphid Alarm Pheromone (E)- β -Farnesene. *Proc. Natl. Acad. Sci. U. S. A.* **1997**, *94*, 12833–12838.
- (163) Maruyama, T.; Ito, M.; Honda, G. Molecular Cloning, Functional Expression and Characterization of (E)- β -Farnesene Synthase from *Citrus junos*. *Biol. Pharm. Bull.* **2001**, *24*, 1171–1175.
- (164) Picaud, S.; Brodelius, M.; Brodelius, P. E. Expression, Purification and Characterization of Recombinant (E)- β -Farnesene Synthase from *Artemisia annua*. *Phytochemistry* **2005**, *66*, 961–967.
- (165) Ruan, J.-X.; Li, J.-X.; Fang, X.; Wang, L.-J.; Hu, W.-L.; Chen, X.-Y.; Yang, C.-Q. Isolation and Characterization of Three New Monoterpene Synthases from *Artemisia annua*. *Front. Plant Sci.* **2016**, *7*, 638.
- (166) Zhao, B.; Lei, L.; Vassilyev, D. G.; Lin, X.; Cane, D. E.; Kelly, S. L.; Yuan, H.; Lamb, D. C.; Waterman, M. R. Crystal Structure of Albaflavonone Monooxygenase Containing a Moonlighting Terpene Synthase Active Site. *J. Biol. Chem.* **2009**, *284*, 36711–36719.
- (167) Kung, Y.; Runguphan, W.; Keasling, J. D. From Fields to Fuels: Recent Advances in the Microbial Production of Biofuels. *ACS Synth. Biol.* **2012**, *1*, 498–513.
- (168) d'Espaux, L.; Mendez-Perez, D.; Li, R.; Keasling, J. D. Synthetic Biology for Microbial Production of Lipid-Based Biofuels. *Curr. Opin. Chem. Biol.* **2015**, *29*, 58–65.
- (169) George, K. W.; Alonso-Gutierrez, J.; Keasling, J. D.; Lee, T. S. Isoprenoid Drugs, Biofuels, and Chemicals—Artemisinin, Farnesene, and Beyond. *Adv. Biochem. Eng./Biotechnol.* **2015**, *148*, 355–389.
- (170) Rynkiewicz, M. J.; Cane, D. E.; Christianson, D. W. Structure of Trichodiene Synthase from *Fusarium sporotrichioides* Provides Mechanistic Inferences on the Terpene Cyclization Cascade. *Proc. Natl. Acad. Sci. U. S. A.* **2001**, *98*, 13543–13548.
- (171) Wise, M. L.; Savage, T. J.; Katahira, E.; Croteau, R. Monoterpene Synthases from Common Sage (*Salvia officinalis*): cDNA Isolation, Characterization, and Functional Expression of (+)-Sabinene Synthase, 1,8-Cineole Synthase, and (+)-Bornyl Diphosphate Synthase. *J. Biol. Chem.* **1998**, *273*, 14891–14899.
- (172) Croteau, R.; Felton, M. Conversion of [1-³H₂,G-¹⁴C]Geranyl Pyrophosphate to Cyclic Monoterpenes without Loss of Tritium. *Arch. Biochem. Biophys.* **1981**, *207*, 460–464.
- (173) Croteau, R.; Felton, N. M.; Wheeler, C. J. Stereochemistry at C-1 of Geranyl Pyrophosphate and Neryl Pyrophosphate in the Cyclization to (+)- and (-)-Bornyl Pyrophosphate. *J. Biol. Chem.* **1985**, *260*, 5956–5962.
- (174) Croteau, R.; Satterwhite, D. M.; Wheeler, C. J.; Felton, N. M. Biosynthesis of Monoterpenes. Stereochemistry of the Enzymatic Cyclizations of Geranyl Pyrophosphate to (+)- α -Pinene and (-)- β -Pinene. *J. Biol. Chem.* **1989**, *264*, 2075–2080.
- (175) Wise, M. L.; Pyun, H.-J.; Helms, G.; Assink, B.; Coates, R. M.; Croteau, R. B. Stereochemical Disposition of the Geminal Dimethyl Groups in the Enzymatic Cyclization of Geranyl Diphosphate to (+)-Bornyl Diphosphate by Recombinant (+)-Bornyl Diphosphate Synthase from *Salvia officinalis*. *Tetrahedron* **2001**, *57*, 5327–5334.
- (176) Cane, D. E.; Saito, A.; Croteau, R.; Shaskus, J.; Felton, M. Enzymatic Cyclization of Geranyl Pyrophosphate to Bornyl Pyrophosphate. Role of the Pyrophosphate Moiety. *J. Am. Chem. Soc.* **1982**, *104*, 5831–5833.
- (177) Croteau, R. B.; Shaskus, J. J.; Renström, B.; Felton, N. M.; Cane, D. E.; Saito, A.; Chang, C. Mechanism of the Pyrophosphate Migration in the Enzymatic Cyclization of Geranyl and Linalyl Pyrophosphates to (+)- and (-)-Bornyl Pyrophosphates. *Biochemistry* **1985**, *24*, 7077–7085.
- (178) Vedula, L. S.; Rynkiewicz, M. J.; Pyun, H. J.; Coates, R. M.; Cane, D. E.; Christianson, D. W. Molecular Recognition of the Substrate Diphosphate Group Governs Product Diversity in Trichodiene Synthase Mutants. *Biochemistry* **2005**, *44*, 6153–6163.
- (179) Weitman, M.; Major, D. T. Challenges Posed to Bornyl Diphosphate Synthase: Diverging Reaction Mechanisms in Monoterpenes. *J. Am. Chem. Soc.* **2010**, *132*, 6349–6360.
- (180) Hong, Y. J.; Tantillo, D. J. Quantum Chemical Dissection of the Classic Terpinyl/Pinyl/Bornyl/Camphyl Cation Conundrum—The Role of Pyrophosphate in Manipulating Pathways to Monoterpenes. *Org. Biomol. Chem.* **2010**, *8*, 4589–4600.
- (181) Major, D. T.; Weitman, M. Electrostatically Guided Dynamics—The Root of Fidelity in a Promiscuous Terpene Synthase? *J. Am. Chem. Soc.* **2012**, *134*, 19454–19462.
- (182) Major, D. T.; Freud, Y.; Weitman, M. Catalytic Control in Terpenoid Cyclases: Multiscale Modeling of Thermodynamic, Kinetic, and Dynamic Effects. *Curr. Opin. Chem. Biol.* **2014**, *21*, 25–33.
- (183) Hong, Y. J.; Tantillo, D. J. Biosynthetic Consequences of Multiple Sequential Post-Transition-State Bifurcations. *Nat. Chem.* **2014**, *6*, 104–111.
- (184) Kjonaas, R.; Croteau, R. Demonstration that Limonene is the First Cyclic Intermediate in the Biosynthesis of Oxygenated p-Menthane Monoterpenes in *Mentha piperita* and Other *Mentha* Species. *Arch. Biochem. Biophys.* **1983**, *220*, 79–89.
- (185) Gershenzon, J.; Maffei, M.; Croteau, R. Biochemical and Histochemical Localization of Monoterpene Biosynthesis in the Glandular Trichomes of Spearmint (*Mentha spicata*). *Plant Physiol.* **1989**, *89*, 1351–1357.
- (186) McCaskill, D.; Gershenzon, J.; Croteau, R. Morphology and Monoterpene Biosynthetic Capabilities of Secretory Cell Clusters Isolated from Glandular Trichomes of Peppermint (*Mentha piperita* L.). *Planta* **1992**, *187*, 445–454.
- (187) Alonso, W. R.; Rajaonarivony, J. I. M.; Gershenzon, J.; Croteau, R. Purification of 4S-Limonene Synthase, a Monoterpene Cyclase from the Glandular Trichomes of Peppermint (*Mentha x piperita*) and Spearmint (*Mentha spicata*). *J. Biol. Chem.* **1992**, *267*, 7582–7587.
- (188) Rajaonarivony, J. I. M.; Gershenzon, J.; Miyazaki, J.; Croteau, R. Evidence for an Essential Histidine Residue in 4S-Limonene Synthase and Other Terpene Cyclases. *Arch. Biochem. Biophys.* **1992**, *299*, 77–82.
- (189) Williams, D. C.; McGarvey, D. J.; Katahira, E. J.; Croteau, R. Truncation of Limonene Synthase Preprotein Provides a Fully Active 'Pseudomature' Form of this Monoterpene Cyclase and Reveals the Function of the Amino-Terminal Arginine Pair. *Biochemistry* **1998**, *37*, 12213–12220.
- (190) Hyatt, D. C.; Youn, B.; Zhao, Y.; Santhamma, B.; Coates, R. M.; Croteau, R. B.; Kang, C. Structure of Limonene Synthase, a Simple Model for Terpenoid Cyclase Catalysis. *Proc. Natl. Acad. Sci. U. S. A.* **2007**, *104*, 5360–5365.
- (191) Trapp, S. C.; Croteau, R. B. Genomic Organization of Plant Terpene Synthases and Molecular Evolutionary Implications. *Genetics* **2001**, *158*, 811–832.
- (192) Peters, R. J.; Flory, J. E.; Jetter, R.; Ravn, M. M.; Lee, H. J.; Coates, R. M.; Croteau, R. B. Abietadiene Synthase from Grand Fir (*Abies grandis*): Characterization and Mechanism of Action of the "Pseudomature" Recombinant Enzyme. *Biochemistry* **2000**, *39*, 15592–15602.
- (193) Li, Z.; Gao, R.; Hao, Q.; Zhao, H.; Cheng, L.; He, F.; Liu, L.; Liu, X.; Chou, W. K. W.; Zhu, H.; Cane, D. E. The T296V Mutant of Amorpha-4,11-Diene Synthase is Defective in Allylic Diphosphate Isomerization but Retains the Ability to Cyclize the Intermediate (3R)-Nerolidyl Diphosphate to Amorpha-4,11-Diene. *Biochemistry* **2016**, *55*, 6599–6604.
- (194) Morehouse, B. R.; Kumar, R. P.; Matos, J. O.; Olsen, S. N.; Entova, S.; Oprian, D. D. Functional and Structural Characterization of a (+)-Limonene Synthase from *Citrus sinensis*. *Biochemistry* **2017**, *56*, 1706–1715.
- (195) Kumar, R. P.; Morehouse, B. R.; Matos, J. O.; Malik, K.; Lin, H.; Krauss, I. J.; Oprian, D. D. Structural Characterization of Early Michaelis Complexes in the Reaction Catalyzed by (+)-Limonene Synthase from *Citrus sinensis* Using Fluorinated Substrate Analogues. *Biochemistry* **2017**, *56*, 1716–1725.

- (196) Ultee, A.; Slump, R. A.; Steging, G.; Smid, E. J. Antimicrobial Activity of Carvacrol toward *Bacillus cereus* on Rice. *J. Food Prot.* **2000**, *63*, 620–624.
- (197) Palaniappan, K.; Holley, R. A. Use of Natural Antimicrobials to Increase Antibiotic Susceptibility of Drug Resistant Bacteria. *Int. J. Food Microbiol.* **2010**, *140*, 164–168.
- (198) Lima, A. S.; Schimmel, J.; Lukas, B.; Novak, J.; Barroso, J. G.; Figueiredo, A. C.; Pedro, L. G.; Degenhardt, J.; Trindade, H. Genomic Characterization, Molecular Cloning and Expression Analysis of Two Terpene Synthases from *Thymus caespititius* (Lamiaceae). *Planta* **2013**, *238*, 191–204.
- (199) Rudolph, K.; Parthier, C.; Egerer-Sieber, C.; Geiger, D.; Muller, Y. A.; Kreis, W.; Müller-Urri, F. Expression, Crystallization and Structure Elucidation of γ -Terpinene Synthase from *Thymus vulgaris*. *Acta Crystallogr., Sect. F: Struct. Biol. Commun.* **2016**, *72*, 16–23.
- (200) Seol, G. H.; Kim, K. Y. Eucalyptol and Its Role in Chronic Diseases. *Adv. Exp. Med. Biol.* **2016**, *929*, 389–398.
- (201) Juergens, U. R. Anti-Inflammatory Properties of the Monoterpene 1,8-Cineole: Current Evidence for Co-Medication in Inflammatory Airway Diseases. *Drug Res.* **2014**, *64*, 638–646.
- (202) Kampranis, S. C.; Ioannidis, D.; Purvis, A.; Mahrez, W.; Ninga, E.; Katerelos, N. A.; Anssour, S.; Dunwell, J. M.; Degenhardt, J.; Makris, A. M.; et al. Rational Conversion of Substrate and Product Specificity in a *Salvia* Monoterpene Synthase: Structural Insights into the Evolution of Terpene Synthase Function. *Plant Cell* **2007**, *19*, 1994–2005.
- (203) Martin, J. F.; Bennett, L. W.; Graham, W. H. Off-Flavor in the Channel Catfish (*Ictalurus punctatus*) Due to 2-Methylisoborneol and its Dehydration Products. *Water Sci. Technol.* **1988**, *20*, 99–105.
- (204) McCallum, R.; Pendleton, P.; Schumann, R.; Trinh, M. U. Determination of Geosmin and 2-Methylisoborneol in Water Using Solid-Phase Microextraction and Gas Chromatography-Chemical Ionisation/Electron Impact Ionisation-Ion-Trap Mass Spectrometry. *Analyst* **1998**, *123*, 2155–2160.
- (205) Jüttner, F.; Watson, S. B. Biochemical and Ecological Control of Geosmin and 2-Methylisoborneol in Source Waters. *Appl. Environ. Microbiol.* **2007**, *73*, 4395–4406.
- (206) Karahadian, C.; Josephson, D. B.; Lindsay, R. C. Volatile Compounds from *Penicillium* sp. Contributing Musty-Earthy Notes to Brie and Camembert Cheese Flavors. *J. Agric. Food Chem.* **1985**, *33*, 339–343.
- (207) Bentley, R.; Meganathan, R. Geosmin and Methylisoborneol Biosynthesis in *Streptomyces*. Evidence for an Isoprenoid Pathway and Its Absence in Non-Differentiating Isolates. *FEBS Lett.* **1981**, *125*, 220–222.
- (208) Dickschat, J. S.; Nawrath, T.; Thiel, V.; Kunze, B.; Müller, R.; Schulz, S. Biosynthesis of the Off-Flavor 2-Methylisoborneol by the Myxobacterium *Nannocystis exedens*. *Angew. Chem., Int. Ed.* **2007**, *46*, 8287–8290.
- (209) Komatsu, M.; Tsuda, M.; Omura, S.; Oikawa, H.; Ikeda, H. Identification and Functional Analysis of Genes Controlling Biosynthesis of 2-Methylisoborneol. *Proc. Natl. Acad. Sci. U. S. A.* **2008**, *105*, 7422–7427.
- (210) Wang, C.-M.; Cane, D. E. Biochemistry and Molecular Genetics of the Biosynthesis of the Earthy Odorant Methylisoborneol in *Streptomyces coelicolor*. *J. Am. Chem. Soc.* **2008**, *130*, 8908–8909.
- (211) Köksal, M.; Chou, W. K. W.; Cane, D. E.; Christianson, D. W. Structure of Geranyl Diphosphate C-Methyltransferase from *Streptomyces coelicolor* and Implications for the Mechanism of Isoprenoid Modification. *Biochemistry* **2012**, *51*, 3003–3010.
- (212) Köksal, M.; Chou, W. K. W.; Cane, D. E.; Christianson, D. W. Structure of 2-Methylisoborneol Synthase from *Streptomyces coelicolor* and Implications for the Cyclization of a Noncanonical C-Methylated Monoterpenoid Substrate. *Biochemistry* **2012**, *51*, 3011–3020.
- (213) Köksal, M.; Chou, W. K. W.; Cane, D. E.; Christianson, D. W. Unexpected Reactivity of 2-Fluorolinalyl Diphosphate in the Active Site of 2-Methylisoborneol Synthase. *Biochemistry* **2013**, *52*, S247–S255.
- (214) Cane, D. E.; Yang, G.; Xue, Q.; Shim, J. H. Trichodiene Synthase. Substrate Specificity and Inhibition. *Biochemistry* **1995**, *34*, 2471–2479.
- (215) Srivastava, J. K.; Shankar, E.; Gupta, S. Chamomile: A Herbal Medicine of the Past with Bright Future. *Mol. Med. Rep.* **2010**, *3*, 895–901.
- (216) Singh, O.; Khanam, Z.; Misra, N.; Srivastava, M. K. Chamomile (*Matricaria chamomilla* L.): An Overview. *Pharmacogn. Rev.* **2011**, *5*, 82–95.
- (217) Brehm-Stecher, B. F.; Johnson, E. A. Sensitization of *Staphylococcus aureus* and *Escherichia coli* to Antibiotics by the Sesquiterpenoids Nerolidol, Farnesol, Bisabolol, and Apritone. *Antimicrob. Agents Chemother.* **2003**, *47*, 3357–3360.
- (218) Russell, K.; Jacob, S. E. Bisabolol. *Dermatitis* **2010**, *21*, 57–58.
- (219) Forrer, M.; Kulik, E. M.; Filippi, A.; Waltimo, T. The Antimicrobial Activity of α -Bisabolol and Tea Tree Oil against *Solobacterium moorei*, a Gram-Positive Bacterium Associated with Halitosis. *Arch. Oral Biol.* **2013**, *58*, 10–16.
- (220) Seki, T.; Kokuryo, T.; Yokoyama, Y.; Suzuki, H.; Itatsu, K.; Nakagawa, A.; Mizutani, T.; Miyake, T.; Uno, M.; Yamauchi, K.; Nagino, M. Antitumor Effects of α -Bisabolol against Pancreatic Cancer. *Cancer Sci.* **2011**, *102*, 2199–2205.
- (221) Uno, M.; Kokuryo, T.; Yokoyama, Y.; Senga, T.; Nagino, M. α -Bisabolol Inhibits Invasiveness and Motility in Pancreatic Cancer through KISS1R Activation. *Anticancer Res.* **2016**, *36*, 583–589.
- (222) Murata, Y.; Kokuryo, T.; Yokoyama, Y.; Yamaguchi, J.; Miwa, T.; Shibuya, M.; Yamamoto, Y.; Nagino, M. The Anticancer Effects of Novel α -Bisabolol Derivatives Against Pancreatic Cancer. *Anticancer Res.* **2017**, *37*, 589–598.
- (223) Attia, M.; Kim, S.-U.; Ro, D.-K. Molecular Cloning and Characterization of (+)-*epi*- α -Bisabolol Synthase, Catalyzing the First Step in the Biosynthesis of the Natural Sweetener, Hernandulcin, in *Lippia dulcis*. *Arch. Biochem. Biophys.* **2012**, *527*, 37–44.
- (224) Cane, D. E. The Stereochemistry of Allylic Pyrophosphate Metabolism. *Tetrahedron* **1980**, *36*, 1109–1159.
- (225) Li, J.-X.; Fang, X.; Zhao, Q.; Ruan, J.-X.; Yang, C.-Q.; Wang, L.-J.; Miller, D. J.; Faraldos, J. A.; Allemann, R. K.; Chen, X.-Y.; Zhang, P. Rational Engineering of Plasticity Residues of Sesquiterpene Synthases from *Artemisia annua*: Product Specificity and Catalytic Efficiency. *Biochem. J.* **2013**, *451*, 417–426.
- (226) Zhou, K.; Peters, R. J. Investigating the Conservation Pattern of a Putative Second Terpene Synthase Divalent Metal Binding Motif in Plants. *Phytochemistry* **2009**, *70*, 366–369.
- (227) Langenheim, J. H. Amber: A Botanical Inquiry. *Science* **1969**, *163*, 1157–1169.
- (228) Lewinsohn, E.; Savage, T. J.; Gijzen, M.; Croteau, R. Simultaneous Analysis of Monoterpenes and Diterpenoids of Conifer Oleoresin. *Phytochem. Anal.* **1993**, *4*, 220–225.
- (229) Steele, C. L.; Crock, J.; Bohlmann, J.; Croteau, R. Sesquiterpene Synthases from Grand Fir (*Abies grandis*): Comparison of Constitutive and Wound-Induced Activities, and cDNA Isolation, Characterization, and Bacterial Expression of δ -Selinene Synthase and γ -Humulene Synthase. *J. Biol. Chem.* **1998**, *273*, 2078–2089.
- (230) Johnson, M. A.; Croteau, R. Biochemistry of Conifer Resistance to Bark Beetles and Their Fungal Symbionts. *Am. Chem. Soc. Symp. Ser.* **1987**, *325*, 76–92.
- (231) Sláma, K.; Williams, C. M. Juvenile Hormone Activity for the Bug *Pyrrhocoris apterus*. *Proc. Natl. Acad. Sci. U. S. A.* **1965**, *54*, 411–414.
- (232) Sláma, K.; Williams, C. M. 'Paper Factor' as an Inhibitor of the Embryonic Development of the European Bug *Pyrrhocoris apterus*. *Nature* **1966**, *210*, 329–330.
- (233) Bowers, W. S.; Fales, H. M.; Thompson, M. J.; Uebel, E. C. Juvenile Hormone: Identification of an Active Compound from Balsam Fir. *Science* **1966**, *154*, 1020–1021.
- (234) Manville, J. F. Juvabione and Its Analogues. II. Isolation, Identification, and Occurrence of Juvabiol and Its Epimer Isojuvabiol from the Whole Wood of *Abies balsamea*. *Can. J. Chem.* **1976**, *54*, 2365–2371.
- (235) Rogers, I. H.; Manville, J. F. Juvenile Hormone Mimics in Conifers. I. Isolation of (–)-*cis*-4-[1'(R)-5'-Dimethyl-3'-Oxohexyl]-Cyclohexane-1-Carboxylic Acid from Douglas-Fir Wood. *Can. J. Chem.* **1972**, *50*, 2380–2382.

- (236) Bohlmann, J.; Crock, J.; Jetter, R.; Croteau, R. Terpenoid-Based Defenses in Conifers: cDNA Cloning, Characterization, and Functional Expression of Wound-Inducible (*E*)- α -Bisabolene Synthase from Grand Fir (*Abies grandis*). *Proc. Natl. Acad. Sci. U. S. A.* **1998**, *95*, 6756–6761.
- (237) Peralta-Yahya, P. P.; Ouellet, M.; Chan, R.; Mukhopadhyay, A.; Keasling, J. D.; Lee, T. S. Identification and Microbial Production of a Terpene-Based Advanced Biofuel. *Nat. Commun.* **2011**, *2*, 483.
- (238) Davies, F. K.; Work, V. H.; Beliaev, A. S.; Posewitz, M. C. Engineering Limonene and Bisabolene Production in Wild Type and a Glycogen-Deficient Mutant of *Synechococcus* sp. PCC 7002. *Front. Bioeng. Biotechnol.* **2014**, *2*, 21.
- (239) Gürtler, H.; Pedersen, R.; Anthoni, U.; Christophersen, C.; Nielsen, P. H.; Wellington, E. M.; Pedersen, C.; Bock, K. Albaflavone, a Sesquiterpene Ketone with a Zizaene Skeleton Produced by a Streptomycete with a New Rope Morphology. *J. Antibiot.* **1994**, *47*, 434–437.
- (240) Zhao, B.; Lin, X.; Lei, L.; Lamb, D. C.; Kelly, S. L.; Waterman, M. R.; Cane, D. E. Biosynthesis of the Sesquiterpene Antibiotic Albaflavone in *Streptomyces coelicolor* A3(2). *J. Biol. Chem.* **2008**, *283*, 8183–8189.
- (241) Lin, X.; Hopson, R.; Cane, D. E. Genome Mining in *Streptomyces coelicolor*. Molecular Cloning and Characterization of a New Sesquiterpene Synthase. *J. Am. Chem. Soc.* **2006**, *128*, 6022–6023.
- (242) Lin, X.; Cane, D. E. Biosynthesis of the Sesquiterpene Antibiotic Albaflavone in *Streptomyces coelicolor*. Mechanism and Stereochemistry of the Enzymatic Formation of Epi-Isozizaene. *J. Am. Chem. Soc.* **2009**, *131*, 6332–6333.
- (243) Aaron, J. A.; Lin, X.; Cane, D. E.; Christianson, D. W. Structure of Epi-Isozizaene Synthase from *Streptomyces coelicolor* A3(2), a Platform for New Terpenoid Cyclization Templates. *Biochemistry* **2010**, *49*, 1787–1797.
- (244) Li, R.; Chou, W. K. W.; Himmelberger, J. A.; Litwin, K. M.; Harris, G. G.; Cane, D. E.; Christianson, D. W. Reprogramming the Chemodiversity of Terpenoid Cyclization by Remolding the Active Site Contour of epi-Isozizaene Synthase. *Biochemistry* **2014**, *53*, 1155–1168.
- (245) Vesonder, R. F.; Ciegler, A.; Jensen, A. H.; Rohwedder, W. K.; Weisleder, D. Co-Identity of the Refusal and Emetic Principle from *Fusarium*-Infected Corn. *Appl. Environ. Microbiol.* **1976**, *31*, 280–285.
- (246) Tanaka, T.; Hasegawa, A.; Yamamoto, S.; Lee, U.-S.; Sugiura, Y.; Ueno, Y. Worldwide Contamination of Cereals by the *Fusarium* Mycotoxins Nivalenol, Deoxynivalenol, and Zearalenone. 1. Survey of 19 Countries. *J. Agric. Food Chem.* **1988**, *36*, 979–983.
- (247) Amarasinghe, C. C.; Dilantha Fernando, W. G. Comparative Analysis of Deoxynivalenol Biosynthesis Related Gene Expression among Different Chemotypes of *Fusarium graminearum* in Spring Wheat. *Front. Microbiol.* **2016**, *7*, 1229.
- (248) Henghold, W. B. Other Biological Toxin Bioweapons: Ricin, Staphylococcal Enterotoxin B, and Trichothecene Mycotoxins. *Dermatol. Clin.* **2004**, *22*, 257–262.
- (249) Dembek, Z. F.; Anderson, E. L. Food, Waterborne, and Agricultural Diseases. In *Medical Aspects of Biological Warfare*; Office of the Surgeon General, 2007; pp 21–38.
- (250) Hohn, T. M.; Beremand, P. D. Isolation and Nucleotide Sequence of a Sesquiterpene Cyclase Gene from the Trichothecene-Producing Fungus *Fusarium sporotrichioides*. *Gene* **1989**, *79*, 131–138.
- (251) Cane, D. E.; Swanson, S.; Murthy, P. P. N. Trichodiene Biosynthesis and the Enzymic Cyclization of Farnesyl Pyrophosphate. *J. Am. Chem. Soc.* **1981**, *103*, 2136–2138.
- (252) Hohn, T. M.; Van Middlesworth, F. Purification and Characterization of the Sesquiterpene Cyclase Trichodiene Synthetase from *Fusarium sporotrichioides*. *Arch. Biochem. Biophys.* **1986**, *251*, 756–761.
- (253) Hohn, T. M.; Plattner, R. D. Expression of the Trichodiene Synthase Gene of *Fusarium sporotrichioides* in *Escherichia coli* Results in Sesquiterpene Production. *Arch. Biochem. Biophys.* **1989**, *275*, 92–97.
- (254) Cane, D. E.; Zhen, W.; Oliver, J. S.; Hohn, T. M. Overproduction of Soluble Trichodiene Synthase from *Fusarium sporotrichioides* in *Escherichia coli*. *Arch. Biochem. Biophys.* **1993**, *300*, 416–422.
- (255) Cane, D. E.; Ha, H.-J. Trichodiene Biosynthesis and the Enzymatic Cyclization of Nerolidyl Pyrophosphate. *J. Am. Chem. Soc.* **1986**, *108*, 3097–3099.
- (256) Cane, D. E.; Ha, H.-J. Trichodiene Biosynthesis and the Role of Nerolidyl Pyrophosphate in the Enzymic Cyclization of Farnesyl Pyrophosphate. *J. Am. Chem. Soc.* **1988**, *110*, 6865–6870.
- (257) Cane, D. E.; Chiu, H.-T.; Liang, P.-H.; Anderson, K. S. Pre-Steady-State Kinetic Analysis of the Trichodiene Synthase Reaction Pathway. *Biochemistry* **1997**, *36*, 8332–8339.
- (258) Cane, D. E.; Pawlak, J. L.; Horak, R. M.; Hohn, T. M. Studies of the Cryptic Allylic Pyrophosphate Isomerase Activity of Trichodiene Synthase Using the Anomalous Substrate 6,7-Dihydrofarnesyl Pyrophosphate. *Biochemistry* **1990**, *29*, 5476–5490.
- (259) Cane, D. E.; Yang, G.; Coates, R. M.; Pyun, H.-J.; Hohn, T. M. Trichodiene Synthase. Synergistic Inhibition by Inorganic Pyrophosphate and Aza Analogs of the Bisabolylyl Cation. *J. Org. Chem.* **1992**, *57*, 3454–3462.
- (260) Vedula, L. S.; Cane, D. E.; Christianson, D. W. Role of Arginine-304 in the Diphosphate-Triggered Active Site Closure Mechanism of Trichodiene Synthase. *Biochemistry* **2005**, *44*, 12719–12727.
- (261) Rynkiewicz, M. J.; Cane, D. E.; Christianson, D. W. X-ray Crystal Structures of D100E Trichodiene Synthase and Its Pyrophosphate Complex Reveal the Basis for Terpene Product Diversity. *Biochemistry* **2002**, *41*, 1732–1741.
- (262) Cane, D. E.; Shim, J.-H.; Xue, Q.; Fitzsimons, B. C.; Hohn, T. M. Trichodiene Synthase. Identification of Active Site Residues by Site-Directed Mutagenesis. *Biochemistry* **1995**, *34*, 2480–2488.
- (263) Cane, D. E.; Xue, Q.; Fitzsimons, B. C. Trichodiene Synthase. Probing the Role of the Highly Conserved Aspartate-Rich Region by Site-Directed Mutagenesis. *Biochemistry* **1996**, *35*, 12369–12376.
- (264) Cane, D. E.; Xue, Q. Trichodiene Synthase. Enzymatic Formation of Multiple Sesquiterpenes by Alteration of the Cyclase Active Site. *J. Am. Chem. Soc.* **1996**, *118*, 1563–1564.
- (265) Cane, D. E.; Xue, Q.; Van Epp, J. E.; Tsantrizos, Y. S. Enzymatic Formation of Isochamigrene, a Novel Sesquiterpene, by Alteration of the Aspartate-Rich Region of Trichodiene Synthase. *J. Am. Chem. Soc.* **1996**, *118*, 8499–8500.
- (266) Vedula, L. S.; Zhao, Y.; Coates, R. M.; Koyama, T.; Cane, D. E.; Christianson, D. W. Exploring Biosynthetic Diversity with Trichodiene Synthase. *Arch. Biochem. Biophys.* **2007**, *466*, 260–266.
- (267) Hong, Y. J.; Tantillo, D. J. Branching Out from the Bisabolylyl Cation. Unifying Mechanistic Pathways to Barbatene, Bazzanene, Chamigrene, Chamipinene, Cumacrene, Cuprenene, Dunningene, Iso-bazzanene, Iso- γ -Bisabolene, Isochamigrene, Laurene, Microbiotene, Sesquithujene, Sesquisabinene, Thujopsene, Trichodiene, and Widdradene Sesquiterpenes. *J. Am. Chem. Soc.* **2014**, *136*, 2450–2463.
- (268) Tressl, R.; Engel, K.-H.; Kossa, M.; Köppler, H. Characterization of Tricyclic Sesquiterpenes in Hop (*Humulus lupulus*, var. *Hersbrucker Spät*). *J. Agric. Food Chem.* **1983**, *31*, 892–897.
- (269) Rega, B.; Fournier, N.; Nicklaus, S.; Guichard, E. Role of Pulp in Flavor Release and Sensory Perception in Orange Juice. *J. Agric. Food Chem.* **2004**, *52*, 4204–4212.
- (270) Pino, J. A.; Mesa, J.; Muñoz, Y.; Martí, M. P.; Marbot, R. Volatile Components from Mango (*Mangifera indica* L.) Cultivars. *J. Agric. Food Chem.* **2005**, *53*, 2213–2223.
- (271) Baer, P.; Rabe, P.; Fischer, K.; Citron, C. A.; Klapschinski, T. A.; Groll, M.; Dickschat, J. S. Induced-Fit Mechanism in Class I Terpene Cyclases. *Angew. Chem., Int. Ed.* **2014**, *53*, 7652–7656.
- (272) Das, S.; Dixit, M.; Major, D. T. First Principles Model Calculations of the Biosynthetic Pathway in Selinadiene Synthase. *Bioorg. Med. Chem.* **2016**, *24*, 4867–4870.
- (273) Haack, R. A.; Mattson, W. J. Life History Patterns of North American Tree-Feeding Sawflies. In *Sawfly Life History Adaptations to Woody Plants*; Wagner, M. R., Raffa, K. F., Eds.; Academic Press, Inc., 1993; pp 503–545.
- (274) Bohlmann, F.; Knoll, K.-H.; Zdero, C.; Mahanta, P. K.; Grenz, M.; Suwita, A.; Ehlers, D.; Van, N. L.; Abraham, W.-R.; Natsu, A. A. Terpen-Derivate aus *Senecio*-Arten. *Phytochemistry* **1977**, *16*, 965–985.

- (275) Bergström, G.; Wassgren, A.-B.; Birgersson, G.; Springborg, J.; Wang, D.-N.; Paulsen, G. B.; Nielsen, R. I.; Olsen, C. E.; Pedersen, C.; Stidsen, C. E. 1,6-Germacradien-5-ol Identified in the Larval Discharge of the Pine Sawfly *Neodiprion sertifer*. *Acta Chem. Scand.* **1994**, *48*, 187–188.
- (276) Nordin, O.; Hedenström, E.; Högborg, H.-E. Stereochemistry of 1,6-Germacradien-5-ol, a Constituent of the Needles of Scots Pine (*Pinus sylvestris*) and of the Defence Secretion from Larvae of the Pine Sawfly *Neodiprion sertifer*. *Acta Chem. Scand.* **1999**, *53*, 124–132.
- (277) Smitt, O.; Högborg, H.-E. First Total Synthesis of (–)-1(10),5-Germacradien-4-ol. *Synlett* **2002**, *8*, 1273–1276.
- (278) Nakano, C.; Kudo, F.; Eguchi, T.; Ohnishi, Y. Genome Mining Reveals Two Novel Bacterial Sesquiterpene Cyclases: (–)-Germacradien-4-ol and (–)-*epi-α*-Bisabolol Synthases from *Streptomyces citricolor*. *ChemBioChem* **2011**, *12*, 2271–2275.
- (279) Grundy, D. J.; Chen, M.; González, V.; Leoni, S.; Miller, D. J.; Christianson, D. W.; Allemann, R. K. Mechanism of Germacradien-4-ol Synthase-Controlled Water Capture. *Biochemistry* **2016**, *55*, 2112–2121.
- (280) Goldschmidt, L.; Cooper, D. R.; Derewenda, Z. S.; Eisenberg, D. Toward Rational Protein Crystallization: A Web Server for the Design of Crystallizable Protein Variants. *Protein Sci.* **2007**, *16*, 1569–1576.
- (281) Cane, D. E.; Rawlings, B. J.; Yang, C.-C. Isolation of (–)- γ -Cadinene and Aristolochene from *Aspergillus terreus*. *J. Antibiot.* **1987**, *40*, 1331–1334.
- (282) Proctor, R. H.; Hohn, T. M. Aristolochene Synthase: Isolation, Characterization, and Bacterial Expression of a Sesquiterpenoid Biosynthetic Gene (*Ari1*) from *Penicillium roqueforti*. *J. Biol. Chem.* **1993**, *268*, 4543–4548.
- (283) Hohn, T. M.; Plattner, R. D. Purification and Characterization of the Sesquiterpene Cyclase Aristolochene Synthase from *Penicillium roqueforti*. *Arch. Biochem. Biophys.* **1989**, *272*, 137–143.
- (284) Cane, D. E.; Wu, Z.; Proctor, R. H.; Hohn, T. M. Overexpression in *Escherichia coli* of Soluble Aristolochene Synthase from *Penicillium roqueforti*. *Arch. Biochem. Biophys.* **1993**, *304*, 415–419.
- (285) Cane, D. E.; Kang, I. Aristolochene Synthase: Purification, Molecular Cloning, High-Level Expression in *Escherichia coli*, and Characterization of the *Aspergillus terreus* Cyclase. *Arch. Biochem. Biophys.* **2000**, *376*, 354–364.
- (286) Shishova, E. Y.; Di Costanzo, L.; Cane, D. E.; Christianson, D. W. X-ray Crystal Structure of Aristolochene Synthase from *Aspergillus terreus* and Evolution of Templates for the Cyclization of Farnesyl Diphosphate. *Biochemistry* **2007**, *46*, 1941–1951.
- (287) Shishova, E. Y.; Yu, F.; Miller, D. J.; Faraldos, J. A.; Zhao, Y.; Coates, R. M.; Allemann, R. K.; Cane, D. E.; Christianson, D. W. X-ray Crystallographic Studies of Substrate Binding to Aristolochene Synthase Suggest a Metal Ion Binding Sequence for Catalysis. *J. Biol. Chem.* **2008**, *283*, 15431–15439.
- (288) Cane, D. E.; Prabhakaran, P. C.; Salaski, E. J.; Harrison, P. H. M.; Noguchi, H.; Rawlings, B. J. Aristolochene Biosynthesis and Enzymatic Cyclization of Farnesyl Pyrophosphate. *J. Am. Chem. Soc.* **1989**, *111*, 8914–8916.
- (289) Cane, D. E.; Prabhakaran, P. C.; Oliver, J. S.; McIlwaine, D. B. Aristolochene Biosynthesis. Stereochemistry of the Deprotonation Steps in the Enzymatic Cyclization of Farnesyl Pyrophosphate. *J. Am. Chem. Soc.* **1990**, *112*, 3209–3210.
- (290) Cane, D. E.; Bryant, C. Aristolochene Synthase. Mechanism-Based Inhibition of a Terpenoid Cyclase. *J. Am. Chem. Soc.* **1994**, *116*, 12063–12064.
- (291) Cane, D. E.; Tsantrizos, Y. S. Aristolochene Synthase. Elucidation of the Cryptic Germacrene A Synthase Activity Using the Anomalous Substrate Dihydrofarnesyl Diphosphate. *J. Am. Chem. Soc.* **1996**, *118*, 10037–10040.
- (292) Calvert, M. J.; Ashton, P. R.; Allemann, R. K. Germacrene A is a Product of the Aristolochene Synthase-Mediated Conversion of Farnesylpyrophosphate to Aristolochene. *J. Am. Chem. Soc.* **2002**, *124*, 11636–11641.
- (293) Calvert, M. J.; Taylor, S. E.; Allemann, R. K. Tyrosine 92 of Aristolochene Synthase Directs Cyclisation of Farnesyl Pyrophosphate. *Chem. Commun.* **2002**, 2384–2385.
- (294) Deligeorgopoulou, A.; Allemann, R. K. Evidence for Differential Folding of Farnesyl Pyrophosphate in the Active Site of Aristolochene Synthase: A Single-Point Mutation Converts Aristolochene Synthase into an (*E*)- β -Farnesene Synthase. *Biochemistry* **2003**, *42*, 7741–7747.
- (295) Deligeorgopoulou, A.; Taylor, S. E.; Forcat, S.; Allemann, R. K. Stabilisation of Eudesmane Cation by Tryptophan 334 During Aristolochene Synthase Catalysis. *Chem. Commun.* **2003**, 2162–2163.
- (296) Forcat, S.; Allemann, R. K. Dual Role for Phenylalanine 178 During Catalysis by Aristolochene Synthase. *Chem. Commun.* **2004**, 2094–2095.
- (297) Forcat, S.; Allemann, R. K. Stabilisation of Transition States Prior to and Following Eudesmane Cation in Aristolochene Synthase. *Org. Biomol. Chem.* **2006**, *4*, 2563–2567.
- (298) Faraldos, J. A.; Antonczak, A. K.; González, V.; Fullerton, R.; Tippmann, E. M.; Allemann, R. K. Probing Eudesmane Cation- π Interactions in Catalysis by Aristolochene Synthase with Non-Canonical Amino Acids. *J. Am. Chem. Soc.* **2011**, *133*, 13906–13909.
- (299) Faraldos, J. A.; Kariuki, B.; Allemann, R. K. Intermediacy of Eudesmane Cation During Catalysis by Aristolochene Synthase. *J. Org. Chem.* **2010**, *75*, 1119–1125.
- (300) Faraldos, J. A.; Allemann, R. K. Inhibition of (+)-Aristolochene Synthase with Iminium Salts Resembling Eudesmane Cation. *Org. Lett.* **2011**, *13*, 1202–1205.
- (301) Miller, D. J.; Yu, F.; Allemann, R. K. Aristolochene Synthase-Catalyzed Cyclization of 2-Fluorofarnesyl-Diphosphate to 2-Fluorogermacrene A. *ChemBioChem* **2007**, *8*, 1819–1825.
- (302) Miller, D. J.; Yu, F.; Knight, D. W.; Allemann, R. K. 6- and 14-Fluoro Farnesyl Diphosphate: Mechanistic Probes for the Reaction Catalysed by Aristolochene Synthase. *Org. Biomol. Chem.* **2009**, *7*, 962–975.
- (303) Yu, F.; Miller, D. J.; Allemann, R. K. Probing the Reaction Mechanism of Aristolochene Synthase with 12,13-Difluorofarnesyl Diphosphate. *Chem. Commun.* **2007**, 4155–4157.
- (304) Felicetti, B.; Cane, D. E. Aristolochene Synthase: Mechanistic Analysis of Active Site Residues by Site-Directed Mutagenesis. *J. Am. Chem. Soc.* **2004**, *126*, 7212–7221.
- (305) Chow, J.-Y.; Tian, B.-X.; Ramamoorthy, G.; Hillerich, B. S.; Seidel, R. D.; Almo, S. C.; Jacobson, M. P.; Poulter, C. D. Computational-Guided Discovery and Characterization of a Sesquiterpene Synthase from *Streptomyces clavuligerus*. *Proc. Natl. Acad. Sci. U. S. A.* **2015**, *112*, 5661–5666.
- (306) Threlfall, D. R.; Whitehead, I. M. Co-ordinated Inhibition of Squalene Synthetase and Induction of Enzymes of Sesquiterpenoid Phytoalexin Biosynthesis in Cultures of *Nicotiana tabacum*. *Phytochemistry* **1988**, *27*, 2567–2580.
- (307) Whitehead, I. M.; Threlfall, D. R.; Ewing, D. F. 5-Epi-Aristolochene is a Common Precursor of the Sesquiterpenoid Phytoalexins Capsidiol and Debneyol. *Phytochemistry* **1989**, *28*, 775–779.
- (308) Li, R.; Tee, C. S.; Jiang, Y. L.; Jiang, X. Y.; Venkatesh, P. N.; Sarojam, R.; Ye, J. A Terpenoid Phytoalexin Plays a Role in Basal Defense of *Nicotiana bethamiana* against Potato Virus X. *Sci. Rep.* **2015**, *5*, 9682.
- (309) Mathis, J. R.; Back, K.; Starks, C.; Noel, J.; Poulter, C. D.; Chappell, J. Pre-Steady-State Study of Recombinant Sesquiterpene Cyclases. *Biochemistry* **1997**, *36*, 8340–8348.
- (310) Rising, K. A.; Starks, C. M.; Noel, J. P.; Chappell, J. Demonstration of Germacrene A as an Intermediate in 5-Epi-Aristolochene Synthase Catalysis. *J. Am. Chem. Soc.* **2000**, *122*, 1861–1866.
- (311) Faraldos, J. A.; Zhao, Y.; O'Maille, P. E.; Noel, J. P.; Coates, R. M. Interception of the Enzymatic Conversion of Farnesyl Diphosphate to 5-Epi-Aristolochene by Using a Fluoro Substrate Analogue: 1-Fluorogermacrene A from (2*E*,6*Z*)-6-Fluorofarnesyl Diphosphate. *ChemBioChem* **2007**, *8*, 1826–1833.

- (312) Schenk, D. J.; Starks, C. M.; Manna, K. R.; Chappell, J.; Noel, J. P.; Coates, R. M. Stereochemistry and Deuterium Isotope Effects Associated with the Cyclization-Rearrangements Catalyzed by Tobacco Epiaristolochene and Hyoscyamus Premnaspirodiene Synthases, and the Chimeric CH₄ Hybrid Cyclase. *Arch. Biochem. Biophys.* **2006**, *448*, 31–44.
- (313) Back, K.; Chappell, J. Identifying Functional Domains within Terpene Cyclases using a Domain-Swapping Strategy. *Proc. Natl. Acad. Sci. U. S. A.* **1996**, *93*, 6841–6845.
- (314) Hess, B. A., Jr.; Smentek, L.; Noel, J. P.; O'Maille, P. E. Physical Constraints on Sesquiterpene Diversity Arising from Cyclization of the Eudesm-5-yl Carbocation. *J. Am. Chem. Soc.* **2011**, *133*, 12632–12641.
- (315) Koo, H. J.; Vickery, C. R.; Xu, Y.; Louie, G. V.; O'Maille, P. E.; Bowman, M.; Nartey, C. M.; Burkart, M. D.; Noel, J. P. Biosynthetic Potential of Sesquiterpene Synthases: Product Profiles of Egyptian Henbane Premnasporadiene Synthase and Related Mutants. *J. Antibiot.* **2016**, *69*, 524–533.
- (316) O'Maille, P. E.; Chappell, J.; Noel, J. P. Biosynthetic Potential of Sesquiterpene Synthases: Alternative Products of Tobacco 5-*epi*-Aristolochene Synthase. *Arch. Biochem. Biophys.* **2006**, *448*, 73–82.
- (317) Faraldos, J. A.; O'Maille, P. E.; Dellas, N.; Noel, J. P.; Coates, R. M. Bisabolyl-Derived Sesquiterpenes from Tobacco 5-*Epi*-Aristolochene Synthase-Catalyzed Cyclization of (2Z,6E)-Farnesyl Diphosphate. *J. Am. Chem. Soc.* **2010**, *132*, 4281–4289.
- (318) O'Maille, P. E.; Malone, A.; Dellas, N.; Andes Hess, B., Jr.; Smentek, L.; Sheehan, I.; Greenhagen, B. T.; Chappell, J.; Manning, G.; Noel, J. P. Quantitative Exploration of the Catalytic Landscape Separating Divergent Plant Sesquiterpene Synthases. *Nat. Chem. Biol.* **2008**, *4*, 617–623.
- (319) Diaz, J. E.; Lin, C.-S.; Kunishiro, K.; Feld, B. K.; Avrantinis, S. K.; Bronson, J.; Greaves, J.; Saven, J. G.; Weiss, G. A. Computational Design and Selections for an Engineered, Thermostable Terpene Synthase. *Protein Sci.* **2011**, *20*, 1597–1606.
- (320) Kersten, R. D.; Diedrich, J. K.; Yates, J. R., III; Noel, J. P. Mechanism-Based Post-Translational Modification and Inactivation in Terpene Synthases. *ACS Chem. Biol.* **2015**, *10*, 2501–2511.
- (321) Brodelius, M.; Lundgren, A.; Mercke, P.; Brodelius, P. E. Fusion of Farnesyl diphosphate Synthase and *epi*-Aristolochene Synthase, a Sesquiterpene Cyclase Involved in Capsidiol Biosynthesis. *Eur. J. Biochem.* **2002**, *269*, 3570–3577.
- (322) Bauler, P.; Huber, G.; Leyh, T.; McCammon, J. A. Channeling by Proximity: The Catalytic Advantages of Active Site Colocalization using Brownian Dynamics. *J. Phys. Chem. Lett.* **2010**, *1*, 1332–1335.
- (323) Rising, K. A.; Crenshaw, C. M.; Koo, H. J.; Subramanian, T.; Chehade, K. A. H.; Starks, C.; Allen, K. D.; Andres, D. A.; Spielmann, H. P.; Noel, J. P.; Chappell, J. Formation of a Novel Macrocyclic Alkaloid from the Unnatural Farnesyl Diphosphate Analogue Anilino geranyl Diphosphate by 5-*Epi*-Aristolochene Synthase. *ACS Chem. Biol.* **2015**, *10*, 1729–1736.
- (324) Farjon, A. The Discovery of a New Genus of Conifer in Northern Vietnam. *Dendrology* **2002**, 142–144.
- (325) Bazzali, O.; Thai, T. H.; Hoi, T. M.; Khang, N. S.; Hien, N. T.; Casanova, J.; Bighelli, A.; Tomi, F. Integrated Analysis of the Wood Oil from *Xanthocyparis vietnamensis* Farjon & Hiep. by Chromatographic and Spectroscopic Techniques. *Molecules* **2016**, *21*, 840.
- (326) Hattan, J.-i.; Shindo, K.; Ito, T.; Shibuya, Y.; Watanabe, A.; Tagaki, C.; Ohno, F.; Sasaki, T.; Ishii, J.; Kondo, A.; Misawa, N. Identification of a Novel Hedycaryol Synthase Gene Isolated from *Camellia brevistyla* Flowers and Floral Scent of *Camellia* Cultivars. *Planta* **2016**, *243*, 959–972.
- (327) Arigoni, D. Stereochemical Aspects of Sesquiterpene Biosynthesis. *Pure Appl. Chem.* **1975**, *41*, 219–245.
- (328) Benedict, C. R.; Alchanati, I.; Harvey, P. J.; Liu, J.; Stipanovic, R. D.; Bell, A. A. The Enzymatic Formation of δ -Cadinene from Farnesyl Diphosphate in Extracts of Cotton. *Phytochemistry* **1995**, *39*, 327–331.
- (329) Chen, X. Y.; Chen, Y.; Heinstein, P.; Davisson, V. J. Cloning, Expression, and Characterization of (+)- δ -Cadinene Synthase: A Catalyst for Cotton Phytoalexin Biosynthesis. *Arch. Biochem. Biophys.* **1995**, *324*, 255–266.
- (330) Davis, G. D.; Essenberg, M. (+)- δ -Cadinene is a Product of Sesquiterpene Cyclase Activity in Cotton. *Phytochemistry* **1995**, *39*, 553–567.
- (331) Hu, Y.; Chou, W. K. W.; Hopson, R.; Cane, D. E. Genome Mining in *Streptomyces clavuligerus*: Expression and Biochemical Characterization of Two New Cryptic Sesquiterpene Synthases. *Chem. Biol.* **2011**, *18*, 32–37.
- (332) Bell, A. A.; Stipanovic, R. D.; Howell, C. R.; Fryxell, P. A. Antimicrobial Terpenoids of *Gossypium*: Hemigossypol, 6-Methoxyhemigossypol and 6-Deoxyhemigossypol. *Phytochemistry* **1975**, *14*, 225–231.
- (333) Band, V.; Hoffer, A. P.; Band, H.; Rhinehardt, A. E.; Knapp, R. C.; Matlin, S. A.; Anderson, D. J. Antiproliferative Effect of Gossypol and Its Optical Isomers on Human Reproductive Cancer Cell Lines. *Gynecol. Oncol.* **1989**, *32*, 273–277.
- (334) Balci, A.; Sahin, F. I.; Ekmekci, A. Gossypol Induced Apoptosis in the Human Promyelocytic Leukemia Cell Line HL 60. *Tohoku J. Exp. Med.* **1999**, *189*, 51–57.
- (335) Wang, X.; Wang, J.; Wong, S. C.; Chow, L. S.; Nicholls, J. M.; Wong, Y. C.; Liu, Y.; Kwong, D. L.; Sham, J. S.; Tsao, S. W. Cytotoxic Effect of Gossypol on Colon Carcinoma Cells. *Life Sci.* **2000**, *67*, 2663–2671.
- (336) Zhang, M.; Liu, H.; Guo, R.; Ling, Y.; Wu, X.; Li, B.; Roller, P. P.; Wang, S.; Yang, D. Molecular Mechanism of Gossypol-Induced Cell Growth Inhibition and Cell Death of HT-29 Human Colon Carcinoma Cells. *Biochem. Pharmacol.* **2003**, *66*, 93–103.
- (337) Coutinho, E. M. Gossypol: A Contraceptive for Men. *Contraception* **2002**, *65*, 259–263.
- (338) Cui, G. H.; Xu, Z. L.; Yang, Z. J.; Xu, Y. Y.; Xue, S. P. A Combined Regimen of Gossypol plus Methyltestosterone and Ethinylestradiol as a Contraceptive Induces Germ Cell Apoptosis and Expression of Its Related Genes in Rats. *Contraception* **2004**, *70*, 335–342.
- (339) Faraldos, J. A.; Miller, D. J.; González, V.; Yoosuf-Aly, Z.; Cascón, O.; Li, A.; Allemann, R. K. A 1,6-Ring Closure Mechanism for (+)- δ -Cadinene Synthase? *J. Am. Chem. Soc.* **2012**, *134*, 5900–5908.
- (340) Benedict, C. R.; Lu, J.-L.; Pettigrew, D. W.; Liu, J.; Stipanovic, R. D.; Williams, H. J. The Cyclization of Farnesyl Diphosphate and Nerolidyl Diphosphate by a Purified Recombinant δ -Cadinene Synthase. *Plant Physiol.* **2001**, *125*, 1754–1765.
- (341) Yoshikuni, Y.; Martin, V. J. J.; Ferrin, T. E.; Keasling, J. D. Engineering Cotton (+)- δ -Cadinene Synthase to an Altered Function: Germacrene D-4-ol Synthase. *Chem. Biol.* **2006**, *13*, 91–98.
- (342) Gennadios, H. A.; Gonzalez, V.; Di Costanzo, L.; Li, A.; Yu, F.; Miller, D. J.; Allemann, R. K.; Christianson, D. W. Crystal Structure of (+)- δ -Cadinene Synthase from *Gossypium arboreum* and Evolutionary Divergence of Metal Binding Motifs for Catalysis. *Biochemistry* **2009**, *48*, 6175–6183.
- (343) Davis, E. M.; Tsuji, J.; Davis, G. D.; Pierce, M. L.; Essenberg, M. Purification of (+)- δ -Cadinene Synthase, a Sesquiterpene Cyclase from Bacteria-Inoculated Cotton Foliar Tissue. *Phytochemistry* **1996**, *41*, 1047–1055.
- (344) Saito, A.; Rilling, H. C. The Formation of Cyclic Sesquiterpenes from Farnesyl Pyrophosphate by Prenyltransferase. *Arch. Biochem. Biophys.* **1981**, *208*, 508–511.
- (345) González, V.; Grundy, D. J.; Faraldos, J. A.; Allemann, R. K. The Amino-Terminal Segment in the β -Domain of δ -Cadinene Synthase is Essential for Catalysis. *Org. Biomol. Chem.* **2016**, *14*, 7451–7454.
- (346) Cane, D. E.; Rossi, T.; Tillman, M. A.; Pachlatko, J. P. Stereochemical Studies of Isoprenoid Biosynthesis. Biosynthesis of Pentalenolactone from [U-¹³C₆]Glucose and [6-²H₂]Glucose. *J. Am. Chem. Soc.* **1981**, *103*, 1838–1843.
- (347) Cane, D. E.; Oliver, J. S.; Harrison, P. H. M.; Abell, C.; Hubbard, B. R.; Kane, C. T.; Lattman, R. Biosynthesis of Pentalenene and Pentalenolactone. *J. Am. Chem. Soc.* **1990**, *112*, 4513–4524.
- (348) Seo, M. J.; Zhu, D.; Endo, S.; Ikeda, H.; Cane, D. E. Genome Mining in *Streptomyces*. Elucidation of the Role of Baeyer-Villiger Monooxygenases and Non-Heme Iron-Dependent Dehydrogenase/

Oxygenases in the Final Steps of the Biosynthesis of Pentalenolactone and Neopentalenolactone. *Biochemistry* **2011**, *50*, 1739–1754.

(349) Zhu, D.; Wang, Y.; Zhang, M.; Ikeda, H.; Deng, Z.; Cane, D. E. Product-Mediated Regulation of Pentalenolactone Biosynthesis in *Streptomyces* Species by the MarR/SlyA Family Activators PenR and PntR. *J. Bacteriol.* **2013**, *195*, 1255–1266.

(350) Koe, B. K.; Sobin, B. A.; Celmer, W. D. PA 132, a New Antibiotic. I. Isolation and Chemical Properties. *Antibiot. Annu.* **1957**, 672–675.

(351) Hartmann, S.; Neeff, J.; Heer, U.; Mecke, D. Arenaemycin (Pentalenolactone): A Specific Inhibitor of Glycolysis. *FEBS Lett.* **1978**, *93*, 339–342.

(352) Mann, K.; Mecke, D. Inhibition of Spinach Glyceraldehyde-3-Phosphate Dehydrogenases by Pentalenolactone. *Nature* **1979**, *282*, 535–536.

(353) Cane, D. E.; Sohng, J. K. Inhibition of Glyceraldehyde-3-Phosphate Dehydrogenase by Pentalenolactone: Kinetic and Mechanistic Studies. *Arch. Biochem. Biophys.* **1989**, *270*, 50–61.

(354) Cane, D. E.; Sohng, J. K. Inhibition of Glyceraldehyde-3-Phosphate Dehydrogenase by Pentalenolactone. 2. Identification of the Site of Alkylation by Tetrahydropentalenolactone. *Biochemistry* **1994**, *33*, 6524–6530.

(355) Cane, D. E.; Tillman, A. M. Pentalenene Biosynthesis and the Enzymatic Cyclization of Farnesyl Pyrophosphate. *J. Am. Chem. Soc.* **1983**, *105*, 122–124.

(356) Cane, D. E.; Abell, C.; Tillman, A. M. Pentalenene Biosynthesis and the Enzymatic Cyclization of Farnesyl Pyrophosphate: Proof that the Cyclization is Catalyzed by a Single Enzyme. *Bioorg. Chem.* **1984**, *12*, 312–328.

(357) Cane, D. E.; Weiner, S. W. Cyclization of Farnesyl Diphosphate to Pentalenene. Orthogonal Stereochemistry in an Enzyme-Catalyzed S_E Reaction. *Can. J. Chem.* **1994**, *72*, 118–127.

(358) Cane, D. E.; Sohng, J.-K.; Lamberson, C. R.; Rudnicki, S. M.; Wu, Z.; Lloyd, M. D.; Oliver, J. S.; Hubbard, B. R. Pentalenene Synthase. Purification, Molecular Cloning, Sequencing, and High-Level Expression in *Escherichia coli* of a Terpenoid Cyclase from *Streptomyces* UC5319. *Biochemistry* **1994**, *33*, 5846–5857.

(359) Gutta, P.; Tantillo, D. J. Theoretical Studies on Farnesyl Cation Cyclization: Pathways to Pentalenene. *J. Am. Chem. Soc.* **2006**, *128*, 6172–6179.

(360) Seemann, M.; Zhai, Z.; Umezawa, K.; Cane, D. E. Pentalenene Synthase. Histidine-309 Is Not Required for Catalytic Activity. *J. Am. Chem. Soc.* **1999**, *121*, 591–592.

(361) Seemann, M.; Zhai, G.; de Kraker, J.-W.; Paschall, C. M.; Christianson, D. W.; Cane, D. E. Pentalenene Synthase. Analysis of Active Site Residues by Site-Directed Mutagenesis. *J. Am. Chem. Soc.* **2002**, *124*, 7681–7689.

(362) Zu, L.; Xu, M.; Lodewyk, M. W.; Cane, D. E.; Peters, R. J.; Tantillo, D. J. Effect of Isotopically Sensitive Branching on Product Distribution for Pentalenene Synthase: Support for a Mechanism Predicted by Quantum Chemistry. *J. Am. Chem. Soc.* **2012**, *134*, 11369–11371.

(363) Aoyagi, T.; Aoyama, T.; Kojima, F.; Hattori, S.; Honma, Y.; Hamada, M.; Takeuchi, T. Cyclooctatin, a New Inhibitor of Lysophospholipase, Produced by *Streptomyces melanosporofaciens* MI614–43F2: Taxonomy, Production, Isolation, Physico-Chemical Properties and Biological Activities. *J. Antibiot.* **1992**, *45*, 1587–1591.

(364) Aoyama, T.; Naganawa, H.; Muraoka, Y.; Aoyagi, T.; Takeuchi, T. The Structure of Cyclooctatin, a New Inhibitor of Lysophospholipase. *J. Antibiot.* **1992**, *45*, 1703–1704.

(365) Kim, S. Y.; Zhao, P.; Igarashi, M.; Sawa, R.; Tomita, T.; Nishiyama, M.; Kuzuyama, T. Cloning and Heterologous Expression of the Cyclooctatin Biosynthetic Gene Cluster Afford a Diterpene Cyclase and Two P450 Hydroxylases. *Chem. Biol.* **2009**, *16*, 736–743.

(366) Meguro, A.; Motoyoshi, Y.; Teramoto, K.; Ueda, S.; Totsuka, Y.; Ando, Y.; Tomita, T.; Kim, S.-Y.; Kimura, T.; Igarashi, M.; et al. An Unusual Terpene Cyclization Mechanism Involving a Carbon-Carbon Bond Rearrangement. *Angew. Chem., Int. Ed.* **2015**, *54*, 4353–4356.

(367) Sato, H.; Teramoto, K.; Masumoto, Y.; Tezuka, N.; Sakai, K.; Ueda, S.; Totsuka, Y.; Shinada, T.; Nishiyama, M.; Wang, C.; et al.

“Cation-Stitching Cascade”: Exquisite Control of Terpene Cyclization in Cyclooctatin Biosynthesis. *Sci. Rep.* **2016**, *5*, 18471.

(368) Janke, R.; Görner, C.; Hirte, M.; Brück, T.; Loll, B. The First Structure of a Bacterial Diterpene Cyclase: CotB2. *Acta Crystallogr., Sect. D: Biol. Crystallogr.* **2014**, *70*, 1528–1537.

(369) Tomita, T.; Kim, S.-Y.; Teramoto, K.; Meguro, A.; Ozaki, T.; Yoshida, A.; Motoyoshi, Y.; Mori, N.; Ishigami, K.; Watanabe, H.; et al. Structural Insights into the CotB2-Catalyzed Cyclization of Geranylgeranyl Diphosphate to the Diterpene Cyclooctat-9-en-7-ol. *ACS Chem. Biol.* **2017**, *12*, 1621–1628.

(370) Ioannou, E.; Quesada, A.; Rahman, M. M.; Gibbons, S.; Vagias, C.; Roussis, V. Dolabellanes with Antibacterial Activity from the Brown Alga *Dilophus spiralis*. *J. Nat. Prod.* **2011**, *74*, 213–222.

(371) Sun, H.-D.; Huang, S.-X.; Han, Q.-B. Diterpenoids from *Isodon* Species and their Biological Activities. *Nat. Prod. Rep.* **2006**, *23*, 673–698.

(372) García, P. A.; de Oliveira, A. B.; Batista, R. Occurrence, Biological Activities and Synthesis of Kaurane Diterpenes and their Glycosides. *Molecules* **2007**, *12*, 455–483.

(373) Morrone, D.; Chambers, J.; Lowry, L.; Kim, G.; Anterola, A.; Bender, K.; Peters, R. J. Gibberellin Biosynthesis in Bacteria: Separate *ent*-Copalyl Diphosphate and *ent*-Kaurene Synthases in *Bradyrhizobium japonicum*. *FEBS Lett.* **2009**, *583*, 475–480.

(374) von Schwartzberg, K.; Schultze, W.; Kassner, H. The Moss *Physcomitrella patens* Releases a Tetracyclic Diterpene. *Plant Cell Rep.* **2004**, *22*, 780–786.

(375) Hayashi, K.; Kawaide, H.; Notomi, M.; Sakigi, Y.; Matsuo, A.; Nozaki, H. Identification and Functional Analysis of Bifunctional *ent*-Kaurene Synthase from the Moss *Physcomitrella patens*. *FEBS Lett.* **2006**, *580*, 6175–6181.

(376) Bömke, C.; Tudzynski, B. Diversity, Regulation, and Evolution of the Gibberellin Biosynthetic Pathway in Fungi Compared to Plants and Bacteria. *Phytochemistry* **2009**, *70*, 1876–1893.

(377) Liu, W.; Feng, X.; Zheng, Y.; Huang, C.-H.; Nakano, C.; Hoshino, T.; Bogue, S.; Ko, T.-P.; Chen, C.-C.; Cui, Y.; et al. Structure, Function and Inhibition of *ent*-Kaurene Synthase from *Bradyrhizobium japonicum*. *Sci. Rep.* **2014**, *4*, 6214.

(378) Wani, M. C.; Taylor, H. L.; Wall, M. E.; Coggon, P.; McPhail, A. T. Plant Antitumor Agents. IV. Isolation and Structure of Taxol, a Novel Antileukemic and Antitumor Agent from *Taxus brevifolia*. *J. Am. Chem. Soc.* **1971**, *93*, 2325–2327.

(379) Schiff, P. B.; Fant, J.; Horwitz, S. B. Promotion of Microtubule Assembly *in vitro* by Taxol. *Nature* **1979**, *277*, 665–667.

(380) Schiff, P. B.; Horwitz, S. B. Taxol Stabilizes Microtubules in Mouse Fibroblast Cells. *Proc. Natl. Acad. Sci. U. S. A.* **1980**, *77*, 1561–1565.

(381) Band Horwitz, S. Mechanism of Action of Taxol. *Trends Pharmacol. Sci.* **1992**, *13*, 134–136.

(382) Weaver, B. A. How Taxol/Paclitaxel Kills Cancer Cells. *Mol. Biol. Cell* **2014**, *25*, 2677–2681.

(383) Zasadil, L. M.; Andersen, K. A.; Yeum, D.; Rocque, G. B.; Wilke, L. G.; Tevaarwerk, A. J.; Raines, R. T.; Burkard, M. E.; Weaver, B. A. Cytotoxicity of Paclitaxel in Breast Cancer is Due to Chromosome Missegregation on Multipolar Spindles. *Sci. Transl. Med.* **2014**, *6*, 229ra43.

(384) Hezari, M.; Lewis, N. G.; Croteau, R. Purification and Characterization of Taxa-4(5),11(12)-diene Synthase from Pacific Yew (*Taxus brevifolia*) that Catalyzes the First Committed Step of Taxol Biosynthesis. *Arch. Biochem. Biophys.* **1995**, *322*, 437–444.

(385) Wildung, M. R.; Croteau, R. A cDNA Clone for Taxadiene Synthase, the Diterpene Cyclase that Catalyzes the Committed Step of Taxol Biosynthesis. *J. Biol. Chem.* **1996**, *271*, 9201–9204.

(386) Williams, D. C.; Wildung, M. R.; Jin, A. Q.; Dalal, D.; Oliver, J. S.; Coates, R. M.; Croteau, R. Heterologous Expression and Characterization of a “Pseudomature” Form of Taxadiene Synthase Involved in Paclitaxel (Taxol) Biosynthesis and Evaluation of a Potential Intermediate and Inhibitors of the Multistep Diterpene Cyclization Reaction. *Arch. Biochem. Biophys.* **2000**, *379*, 137–146.

- (387) Lin, X.; Hezari, M.; Koeppe, A. E.; Floss, H. G.; Croteau, R. Mechanism of Taxadiene Synthase, a Diterpene Cyclase that Catalyzes the First Step of Taxol Biosynthesis in Pacific Yew. *Biochemistry* **1996**, *35*, 2968–2977.
- (388) Jin, Q.; Williams, D. C.; Hezari, M.; Croteau, R.; Coates, R. M. Stereochemistry of the Macrocyclization and Elimination Steps in Taxadiene Biosynthesis through Deuterium Labeling. *J. Org. Chem.* **2005**, *70*, 4667–4675.
- (389) Williams, D. C.; Carroll, B. J.; Jin, Q.; Rithner, C. D.; Lenger, S. R.; Floss, H. G.; Coates, R. M.; Williams, R. M.; Croteau, R. Intramolecular Proton Transfer in the Cyclization of Geranylgeranyl Diphosphate to the Taxadiene Precursor of Taxol Catalyzed by Recombinant Taxadiene Synthase. *Chem. Biol.* **2000**, *7*, 969–977.
- (390) Jin, Y.; Williams, D. C.; Croteau, R.; Coates, R. M. Taxadiene Synthase-Catalyzed Cyclization of 6-Fluorogeranylgeranyl Diphosphate to 7-Fluorovercillenes. *J. Am. Chem. Soc.* **2005**, *127*, 7834–7842.
- (391) Schrepfer, P.; Buettner, A.; Goerner, C.; Hertel, M.; van Rijn, J.; Wallrapp, F.; Eisenreich, W.; Sieber, V.; Kourist, R.; Brück, T. Identification of Amino Acid Networks Governing Catalysis in the Closed Complex of Class I Terpene Synthases. *Proc. Natl. Acad. Sci. U. S. A.* **2016**, *113*, E958–E967.
- (392) Pemberton, T. A.; Chen, M.; Harris, G. G.; Chou, W. K. W.; Duan, L.; Köksal, M.; Genshaft, A. S.; Cane, D. E.; Christianson, D. W. Exploring the Influence of Domain Architecture on the Catalytic Function of Diterpene Synthases. *Biochemistry* **2017**, *56*, 2010–2023.
- (393) Soliman, S.; Tang, Y. Natural and Engineered Production of Taxadiene with Taxadiene Synthase. *Biotechnol. Bioeng.* **2015**, *112*, 229–235.
- (394) Ajikumar, P. K.; Xiao, W.-H.; Tyo, K. E. J.; Wang, Y.; Simeon, F.; Leonard, E.; Mucha, O.; Phon, T. H.; Pfeifer, B.; Stephanopoulos, G. Isoprenoid Pathway Optimization for Taxol Precursor Overproduction in *Escherichia coli*. *Science* **2010**, *330*, 70–74.
- (395) Engels, B.; Dahm, P.; Jennewein, S. Metabolic Engineering of Taxadiene Biosynthesis in Yeast as a First Step toward Taxol (Paclitaxel) Production. *Metab. Eng.* **2008**, *10*, 201–206.
- (396) Besumbes, Ó.; Sauret-Güeto, S.; Phillips, M. A.; Imperial, S.; Rodríguez-Concepción, M.; Boronat, A. Metabolic Engineering of Isoprenoid Biosynthesis in *Arabidopsis* for the Production of Taxadiene, the First Committed Precursor of Taxol. *Biotechnol. Bioeng.* **2004**, *88*, 168–175.
- (397) Cha, M.; Shim, S. H.; Kim, S. H.; Kim, O. T.; Lee, S.-W.; Kwon, S.-Y.; Baek, K.-H. Production of Taxadiene from Cultured Ginseng Roots Transformed with Taxadiene Synthase Gene. *BMB Reports* **2012**, *45*, 589–594.
- (398) Li, M.; Jiang, F.; Yu, X.; Miao, Z. Engineering Isoprenoid Biosynthesis in *Artemisia annua* L. for the Production of Taxadiene: a Key Intermediate of Taxol. *BioMed Res. Int.* **2015**, *2015*, 1.
- (399) Edgar, S.; Li, F. S.; Qiao, K.; Weng, J. K.; Stephanopoulos, G. Engineering of Taxadiene Synthase for Improved Selectivity and Yield of a Key Taxol Biosynthetic Intermediate. *ACS Synth. Biol.* **2017**, *6*, 201–205.
- (400) Serrano-Posada, H.; Centeno-Leija, S.; Rojas-Trejo, S.; Stojanoff, V.; Rodríguez-Sanoja, R.; Rudiño-Piñera, E.; Sánchez, S. Crystallization and X-ray Diffraction Analysis of a Putative Bacterial Class I Labdane-Related Diterpene Synthase. *Acta Crystallogr., Sect. F: Struct. Biol. Commun.* **2015**, *71*, 1194–1199.
- (401) Shao, J.; Chen, Q.-W.; Lv, H.-J.; He, J.; Liu, Z.-F.; Lu, Y.-N.; Liu, H.-L.; Wang, G.-D.; Wang, Y. +)-Thalianatriene and (–)-Retigeranin B Catalyzed by Sesterterpene Synthases from *Arabidopsis thaliana*. *Org. Lett.* **2017**, *19*, 1816–1819.
- (402) Chiba, R.; Minami, A.; Gomi, K.; Oikawa, H. Identification of Ophiobolin F Synthase by a Genome Mining Approach: A Sesterterpene Synthase from *Aspergillus clavatus*. *Org. Lett.* **2013**, *15*, 594–597.
- (403) Matsuda, Y.; Mitsuhashi, T.; Quan, Z.; Abe, I. Molecular Basis for Stellatic Acid Biosynthesis: A Genome Mining Approach for Discovery of Sesterterpene Synthases. *Org. Lett.* **2015**, *17*, 4644–4647.
- (404) Ye, Y.; Minami, A.; Mandi, A.; Liu, C.; Taniguchi, T.; Kuzuyama, T.; Monde, K.; Gomi, K.; Oikawa, H. Genome Mining for Sesterterpenes Using Bifunctional Terpene Synthases Reveals a Unified Intermediate of Di/Sesterterpenes. *J. Am. Chem. Soc.* **2015**, *137*, 11846–11853.
- (405) Okada, M.; Matsuda, Y.; Mitsuhashi, T.; Hoshino, S.; Mori, T.; Nakagawa, K.; Quan, Z.; Qin, B.; Zhang, H.; Hayashi, F.; et al. Genome-Based Discovery of an Unprecedented Cyclization Mode in Fungal Sesterterpenoid Biosynthesis. *J. Am. Chem. Soc.* **2016**, *138*, 10011–10018.
- (406) Matsuda, Y.; Mitsuhashi, T.; Lee, S.; Hoshino, M.; Mori, T.; Okada, M.; Zhang, H.; Hayashi, F.; Fujita, M.; Abe, I. Astellifadiene: Structure Determination by NMR Spectroscopy and Crystalline Sponge Method, and Elucidation of its Biosynthesis. *Angew. Chem., Int. Ed.* **2016**, *55*, 5785–5788.
- (407) Qin, B.; Matsuda, Y.; Mori, T.; Okada, M.; Quan, Z.; Mitsuhashi, T.; Wakimoto, T.; Abe, I. An Unusual Chimeric Diterpene Synthase from *Emericella varicolor* and its Functional Conversion into a Sesterterpene Synthase by Domain Swapping. *Angew. Chem., Int. Ed.* **2016**, *55*, 1658–1661.
- (408) Chai, H.; Yin, R.; Liu, Y.; Meng, H.; Zhou, X.; Zhou, G.; Bi, X.; Yang, X.; Zhu, T.; Zhu, W.; et al. Sesterterpene Ophiobolin Biosynthesis Involving Multiple Gene Clusters in *Aspergillus ustus*. *Sci. Rep.* **2016**, *6*, 27181.
- (409) Massé, G.; Belt, S. T.; Rowland, S. J.; Rohmer, M. Isoprenoid Biosynthesis in the Diatoms *Rhizosolenia setigera* (Brightwell) and *Haslea ostrearia* (Simonsen). *Proc. Natl. Acad. Sci. U. S. A.* **2004**, *101*, 4413–4418.
- (410) Tsoukatou, M.; Siapi, H.; Vagias, C.; Roussis, V. New Sesterterpene Metabolites from the Mediterranean Sponge *Cacospongia scalaris*. *J. Nat. Prod.* **2003**, *66*, 444–446.
- (411) Wonganuchitmeta, S.-n.; Yuenyongsawad, S.; Keawpradub, N.; Plubrukarn, A. Antitubercular Sesterterpenes from the Thai Sponge *Brachiaster* sp. *J. Nat. Prod.* **2004**, *67*, 1767–1770.
- (412) Song, J.; Jeong, W.; Wang, N.; Lee, H.-S.; Sim, C. J.; Oh, K.-B.; Shin, J. Scalarene Sesterterpenes from the Sponge *Smenospongia* sp. *J. Nat. Prod.* **2008**, *71*, 1866–1871.
- (413) Margarucci, L.; Monti, M. C.; Tosco, A.; Riccio, R.; Casapullo, A. Chemical Proteomics Discloses Petrosapongiolide M, an Antiinflammatory Marine Sesterterpene, as a Proteasome Inhibitor. *Angew. Chem., Int. Ed.* **2010**, *49*, 3960–3963.
- (414) Li, J.; Du, L.; Kelly, M.; Zhou, Y.-D.; Nagle, D. G. Structures and Potential Antitumor Activity of Sesterterpenes from the Marine Sponge *Hyrtios communis*. *J. Nat. Prod.* **2013**, *76*, 1492–1497.
- (415) Abdjul, D. B.; Yamazaki, H.; Takahashi, O.; Kirikoshi, R.; Mangindaan, R. E. P.; Namikoshi, M. Two New Protein Tyrosine Phosphatase 1B Inhibitors, Hyattellactones A and B, from the Indonesian Marine Sponge *Hyattella* sp. *Bioorg. Med. Chem. Lett.* **2015**, *25*, 904–907.
- (416) Rodolfo, C.; Rocco, M.; Cattaneo, L.; Tartaglia, M.; Sassi, M.; Aducci, P.; Scaloni, A.; Camoni, L.; Marra, M. Ophiobolin A Induces Autophagy and Activates the Mitochondrial Pathway of Apoptosis in Human Melanoma Cells. *PLoS One* **2016**, *11*, e0167672.
- (417) Bury, M.; Novo-Uzal, E.; Andolfi, A.; Cimini, S.; Wauthoz, N.; Heffeter, P.; Lallemand, B.; Avolio, F.; Delporte, C.; Cimmino, A.; et al. Ophiobolin A, a Sesterterpenoid Fungal Phytotoxin, Displays Higher *in vitro* Growth-Inhibitory Effects in Mammalian than in Plant Cells and Displays *in vivo* Antitumor Activity. *Int. J. Oncol.* **2013**, *43*, 575–585.
- (418) Xue, D.; Wang, Q.; Chen, Z.; Cai, L.; Bao, L.; Qi, Q.; Liu, L.; Wang, X.; Jin, H.; Wang, J.; et al. 3-Anhydro-6-Hydroxy-Ophiobolin A, a Fungal Sesterterpene from *Bipolaris oryzae* Induced Autophagy and Promoted the Degradation of α -Synuclein in PC12 Cells. *Bioorg. Med. Chem. Lett.* **2015**, *25*, 1464–1470.
- (419) Brill, Z. G.; Grover, H. K.; Maimone, T. J. Enantioselective Synthesis of an Ophiobolin Sesterterpene via a Programmed Radical Cascade. *Science* **2016**, *352*, 1078–1082.
- (420) Peters, R. J. Two Rings in Them All: The Labdane-Related Diterpenoids. *Nat. Prod. Rep.* **2010**, *27*, 1521–1530.
- (421) Xu, M.; Hillwig, M. L.; Tiernan, M. S.; Peters, R. J. Probing Labdane-Related Diterpenoid Biosynthesis in the Fungal Genus *Aspergillus*. *J. Nat. Prod.* **2017**, *80*, 328–333.

- (422) Fleet, C. M.; Sun, T.-P. A DELLAcate Balance: The Role of Gibberellin in Plant Morphogenesis. *Curr. Opin. Plant Biol.* **2005**, *8*, 77–85.
- (423) Yamaguchi, S. Gibberellin Metabolism and Its Regulation. *Annu. Rev. Plant Biol.* **2008**, *59*, 225–251.
- (424) Hedden, P.; Thomas, S. G. Gibberellin Biosynthesis and Its Regulation. *Biochem. J.* **2012**, *444*, 11–25.
- (425) Sun, T. P.; Kamiya, Y. The Arabidopsis *GA1* Locus Encodes the Cyclase *ent*-Kaurene Synthetase A of Gibberellin Biosynthesis. *Plant Cell* **1994**, *6*, 1509–1518.
- (426) Prisic, S.; Peters, R. J. Synergistic Substrate Inhibition of *ent*-Copalyl Diphosphate Synthase: A Potential Feed-Forward Inhibition Mechanism Limiting Gibberellin Metabolism. *Plant Physiol.* **2007**, *144*, 445–454.
- (427) Prisic, S.; Xu, J.; Coates, R. M.; Peters, R. J. Probing the Role of the DXDD Motif in Class II Diterpene Cyclases. *ChemBioChem* **2007**, *8*, 869–874.
- (428) Gandour, R. D. On the Importance of Orientation in General Base Catalysis by Carboxylate. *Bioorg. Chem.* **1981**, *10*, 169–176.
- (429) Potter, K.; Criswell, J.; Zi, J.; Stubbs, A.; Peters, R. J. Novel Product Chemistry from Mechanistic Analysis of *ent*-Copalyl Diphosphate Synthases from Plant Hormone Biosynthesis. *Angew. Chem., Int. Ed.* **2014**, *53*, 7198–7202.
- (430) Potter, K. C.; Zi, J.; Hong, Y. J.; Schulte, S.; Malchow, B.; Tantillo, D. J.; Peters, R. J. Blocking Deprotonation with Retention of Aromaticity in a Plant *ent*-Copalyl Diphosphate Synthase Leads to Product Rearrangement. *Angew. Chem., Int. Ed.* **2016**, *55*, 634–638.
- (431) Chen, X.; Berim, A.; Dayan, F. E.; Gang, D. R. A (–)-Kolavenyl Diphosphate Synthase Catalyzes the First Step of Salvinorin A Biosynthesis in *Salvia divinorum*. *J. Exp. Bot.* **2017**, *68*, 1109–1122.
- (432) Pelot, K. A.; Mitchell, R.; Kwon, M.; Hagelthorn, D. M.; Wardman, J. F.; Chiang, A.; Bohlmann, J.; Ro, D.-K.; Zerbe, P. Biosynthesis of the Psychotropic Plant Diterpene Salvinorin A: Discovery and Characterization of the *Salvia divinorum* Clerodienyl Diphosphate Synthase. *Plant J.* **2017**, *89*, 885–897.
- (433) Hansen, N. L.; Nissen, J. N.; Hamberger, B. Two Residues Determine the Product Profile of the Class II Diterpene Synthases TPS14 and TPS21 of *Tripterygium wilfordii*. *Phytochemistry* **2017**, *138*, 52–56.
- (434) Köksal, M.; Potter, K.; Peters, R. J.; Christianson, D. W. 1.55 Å-Resolution Structure of *ent*-Copalyl Diphosphate Synthase and Exploration of General Acid Function by Site-Directed Mutagenesis. *Biochim. Biophys. Acta, Gen. Subj.* **2014**, *1840*, 184–190.
- (435) Rudolf, J. D.; Dong, L.-B.; Cao, H.; Hatzos-Skintges, C.; Osipiuk, J.; Endres, M.; Chang, C.-Y.; Ma, M.; Babnigg, G.; Joachimiak, A.; et al. Structure of the *ent*-Copalyl Diphosphate Synthase PtmT2 from *Streptomyces platensis* CB00739, a Bacterial Type II Diterpene Synthase. *J. Am. Chem. Soc.* **2016**, *138*, 10905–10915.
- (436) Smanski, M. J.; Yu, Z.; Casper, J.; Lin, S.; Peterson, R. M.; Chen, Y.; Wendt-Pienkowski, E.; Rajski, S. R.; Shen, B. Dedicated *ent*-Kaurene and *ent*-Atiserene Synthases for Platensimycin and Platencin Biosynthesis. *Proc. Natl. Acad. Sci. U. S. A.* **2011**, *108*, 13498–13503.
- (437) Rudolf, J. D.; Dong, L.-B.; Huang, T.; Shen, B. A Genetically Amenable Platensimycin- and Platencin-Overproducer as a Platform for Biosynthetic Explorations: A Showcase of PtmO4, a Long-Chain Acyl-CoA Dehydrogenase. *Mol. Biosyst.* **2015**, *11*, 2717–2726.
- (438) Tian, B.-X.; Wallrapp, F. H.; Holiday, G. L.; Chow, J.-Y.; Babbitt, P. C.; Poulter, C. D.; Jacobson, M. P. Predicting the Functions and Specificity of Triterpenoid Synthases: A Mechanism-Based Multi-Intermediate Docking Approach. *PLoS Comput. Biol.* **2014**, *10*, e1003874.
- (439) De Rosa, M.; Gambacorta, A.; Minala, L.; Bu'Lock, J. D. Bacterial Triterpenes. *J. Chem. Soc. D* **1971**, 619–620.
- (440) De Rosa, M.; Gambacorta, A.; Minala, L.; Bu'Lock, J. D. Isoprenoids of *Bacillus acidocaldarius*. *Phytochemistry* **1973**, *12*, 1117–1123.
- (441) Kannenberg, E. L.; Poralla, K. Hopanoid Biosynthesis and Function in Bacteria. *Naturwissenschaften* **1999**, *86*, 168–176.
- (442) Siedenburg, G.; Jendrossek, D. Squalene-Hopene Cyclases. *Appl. Environ. Microbiol.* **2011**, *77*, 3905–3915.
- (443) Sáenz, J. P.; Grosser, D.; Bradley, A. S.; Lagny, T. J.; Lavrynenko, O.; Broda, M.; Simons, K. Hopanoids as Functional Analogues of Cholesterol in Bacterial Membranes. *Proc. Natl. Acad. Sci. U. S. A.* **2015**, *112*, 11971–11976.
- (444) Welander, P. V.; Hunter, R. C.; Zhang, L.; Sessions, A. L.; Summons, R. E.; Newman, D. K. Hopanoids Play a Role in Membrane Integrity and pH Homeostasis in *Rhodospseudomonas palustris* TIE-1. *J. Bacteriol.* **2009**, *191*, 6145–6156.
- (445) Summons, R. E.; Jahnke, L. L.; Hope, J. M.; Logan, G. A. 2-Methylhopanoids as Biomarkers for Cyanobacterial Oxygenic Photosynthesis. *Nature* **1999**, *400*, 554–557.
- (446) van Dongen, B. E.; Talbot, H. M.; Schouten, S.; Pearson, P. N.; Pancost, R. D. Well Preserved Palaeogene and Cretaceous Biomarkers from the Kilwa Area, Tanzania. *Org. Geochem.* **2006**, *37*, 539–557.
- (447) Banta, A. B.; Wei, J. H.; Gill, C. C. C.; Giner, J.-L.; Welander, P. V. Synthesis of Arborane Triterpenols by a Bacterial Oxidosqualene Cyclase. *Proc. Natl. Acad. Sci. U. S. A.* **2017**, *114*, 245–250.
- (448) Newman, D. K.; Neubauer, C.; Ricci, J. N.; Wu, C.-H.; Pearson, A. Cellular and Molecular Biological Approaches to Interpreting Ancient Biomarkers. *Annu. Rev. Earth Planet. Sci.* **2016**, *44*, 493–522.
- (449) Wendt, K. U.; Lenhart, A.; Schulz, G. E. The Structure of the Membrane Protein Squalene-Hopene Cyclase at 2.0 Å Resolution. *J. Mol. Biol.* **1999**, *286*, 175–187.
- (450) Reinert, D. J.; Balliano, G.; Schulz, G. E. Conversion of Squalene to the Pentacarbocyclic Hopene. *Chem. Biol.* **2004**, *11*, 121–126.
- (451) Abe, I.; Prestwich, G. D. Identification of the Active Site of Vertebrate Oxidosqualene Cyclase. *Lipids* **1995**, *30*, 231–234.
- (452) Feil, C.; Süssmuth, R.; Jung, G.; Poralla, K. Site-Directed Mutagenesis of Putative Active-Site Residues in Squalene-Hopene Cyclase. *Eur. J. Biochem.* **1996**, *242*, 51–55.
- (453) Pale-Grosdemange, C.; Feil, C.; Rohmer, M.; Poralla, K. Occurrence of Cationic Intermediates and Deficient Control during the Enzymatic Cyclization of Squalene to Hopanoids. *Angew. Chem., Int. Ed.* **1998**, *37*, 2237–2240.
- (454) Hoshino, T.; Sato, T. Squalene-Hopene Cyclase: Catalytic Mechanism and Substrate Recognition. *Chem. Commun.* **2002**, *4*, 291–301.
- (455) Wendt, K. U. Enzyme Mechanisms for Triterpene Cyclization: New Pieces of the Puzzle. *Angew. Chem., Int. Ed.* **2005**, *44*, 3966–3971.
- (456) Hammer, S. C.; Syrén, P.-O.; Seitz, M.; Nestl, B. M.; Hauer, B. Squalene Hopene Cyclases: Highly Promiscuous and Evolvable Catalysts for Stereoselective C–C and C–X Bond Formation. *Curr. Opin. Chem. Biol.* **2013**, *17*, 293–300.
- (457) Syrén, P.-O.; Henche, S.; Eichler, A.; Nestl, B. M.; Hauer, B. Squalene-Hopene Cyclases – Evolution, Dynamics and Catalytic Scope. *Curr. Opin. Struct. Biol.* **2016**, *41*, 73–82.
- (458) Hammer, S. C.; Marjanovic, A.; Dominicus, J. M.; Nestl, B. M.; Hauer, B. Squalene Hopene Cyclases are Protonases for Stereoselective Brønsted Acid Catalysis. *Nat. Chem. Biol.* **2014**, *11*, 121–126.
- (459) Ruf, A.; Müller, F.; D'Arcy, B.; Stihle, M.; Kuszniir, E.; Handschin, C.; Morand, O. H.; Thoma, R. The Monotopic Membrane Protein Human Oxidosqualene Cyclase is Active as a Monomer. *Biochem. Biophys. Res. Commun.* **2004**, *315*, 247–254.
- (460) Corey, E. J.; Cheng, H.; Baker, C. H.; Matsuda, S. P. T.; Li, D.; Song, X. Methodology for the Preparation of Pure Recombinant *S. cerevisiae* Lanosterol Synthase Using a Baculovirus Expression System. Evidence That Oxirane Cleavage and A-Ring Formation are Concerted in the Biosynthesis of Lanosterol from 2,3-Oxidosqualene. *J. Am. Chem. Soc.* **1997**, *119*, 1277–1288.
- (461) Corey, E. J.; Cheng, H.; Baker, C. H.; Matsuda, S. P. T.; Li, D.; Song, X. Studies on the Substrate Binding Segments and Catalytic Action of Lanosterol Synthase. Affinity Labeling with Carbocations Derived from Mechanism-Based Analogs of 2,3-Oxidosqualene and Site-Directed Mutagenesis Probes. *J. Am. Chem. Soc.* **1997**, *119*, 1289–1296.
- (462) Thoma, R.; Schulz-Gasch, T.; D'Arcy, B.; Benz, J.; Aebi, J.; Dehmlow, H.; Hennig, M.; Stihle, M.; Ruf, A. Insight into Steroid

Scaffold Formation from the Structure of Human Oxidosqualene Cyclase. *Nature* **2004**, *432*, 118–122.

(463) Chen, N.; Wang, S.; Smentek, L.; Hess, B. A., Jr.; Wu, R. Biosynthetic Mechanism of Lanosterol: Cyclization. *Angew. Chem., Int. Ed.* **2015**, *54*, 8693–8696.

(464) Staedler, D.; Chapuis-Bernasconi, C.; Dehmlow, H.; Fischer, H.; Juillerat-Jeanneret, L.; Aebi, J. D. Cytotoxic Effects of Combination of Oxidosqualene Cyclase Inhibitors with Atorvastatin in Human Cancer Cells. *J. Med. Chem.* **2012**, *55*, 4990–5002.

(465) Maione, F.; Oliaro-Bosso, S.; Meda, C.; Di Nicolantonio, F.; Bussolino, F.; Balliano, G.; Viola, F.; Giraud, E. The Cholesterol Biosynthesis Enzyme Oxidosqualene Cyclase is a New Target to Impair Tumor Angiogenesis and Metastasis Dissemination. *Sci. Rep.* **2015**, *5*, 9054.

(466) Thimmappa, R.; Geisler, K.; Louveau, T.; O'Maille, P.; Osbourn, A. Triterpene Biosynthesis in Plants. *Annu. Rev. Plant Biol.* **2014**, *65*, 225–257.

(467) Sato, T. Unique Biosynthesis of Sesquiterpenes (C₃₅ Terpenes). *Biosci., Biotechnol., Biochem.* **2013**, *77*, 1155–1159.

(468) Sato, T.; Yoshida, S.; Hoshino, H.; Tanno, M.; Nakajima, M.; Hoshino, T. Sesquiterpenes (C₃₅ Terpenes) Biosynthesized via the Cyclization of a Linear C₃₅ Isoprenoid by a Tetraprenyl- β -Curcumenyl Synthase and a Tetraprenyl- β -Curcumenyl Cyclase: Identification of a New Terpene Cyclase. *J. Am. Chem. Soc.* **2011**, *133*, 9734–9737.

(469) Takahashi, I.; Ogura, K.; Seto, S. Heptaprenyl Pyrophosphate Synthetase from *Bacillus subtilis*. *J. Biol. Chem.* **1980**, *255*, 4539–4543.

(470) Zhang, Y.-W.; Koyama, T.; Marecak, D. M.; Prestwich, G. D.; Maki, Y.; Ogura, K. Two Subunits of Heptaprenyl Diphosphate Synthase of *Bacillus subtilis* Form a Catalytically Active Complex. *Biochemistry* **1998**, *37*, 13411–13420.

(471) Nagel, R.; Bernholz, C.; Vranová, E.; Košuth, J.; Bergau, N.; Ludwig, S.; Wessjohann, L.; Gershenzon, J.; Tissier, A.; Schmidt, A. *Arabidopsis thaliana* Isoprenyl Diphosphate Synthases Produce the C₂₅ Intermediate Geranylgeranyl Diphosphate. *Plant J.* **2015**, *84*, 847–859.

(472) Wang, C.; Chen, Q.; Fan, D.; Li, J.; Wang, G.; Zhang, P. Structural Analyses of Short-Chain Prenyltransferases Identify an Evolutionarily Conserved GFPPS Clade in Brassicaceae Plants. *Mol. Plant* **2016**, *9*, 195–204.

(473) Bosak, T.; Losick, R. M.; Pearson, A. A Polycyclic Terpenoid that Alleviates Oxidative Stress. *Proc. Natl. Acad. Sci. U. S. A.* **2008**, *105*, 6725–6729.

(474) Sato, T.; Hoshino, H.; Yoshida, S.; Nakajima, M.; Hoshino, T. Bifunctional Triterpene/Sesquiterpene Cyclase: Tetraprenyl- β -Curcumenyl Synthase is also Squalene Cyclase in *Bacillus megaterium*. *J. Am. Chem. Soc.* **2011**, *133*, 17540–17543.

(475) Takigawa, H.; Sugiyama, M.; Shibuya, Y. C₃₅-Terpenes from *Bacillus subtilis* KSM 6–10. *J. Nat. Prod.* **2010**, *73*, 204–207.

(476) Castellana, M.; Wilson, M. Z.; Xu, Y.; Joshi, P.; Cristea, I. M.; Rabinowitz, J. D.; Gitai, Z.; Wingreen, N. S. Enzyme Clustering Accelerates Processing of Intermediates through Metabolic Channeling. *Nat. Biotechnol.* **2014**, *32*, 1011–1018.

(477) Gerber, N. N. Geosmin, from Microorganisms, is *trans*-1,10-Dimethyl-*trans*-9-Decalol. *Tetrahedron Lett.* **1968**, *9*, 2971–2974.

(478) Gerber, N. N.; Lechevalier, H. A. Geosmin, an Earthy-Smelling Substance Isolated from Actinomycetes. *Appl. Microbiol.* **1965**, *13*, 935–938.

(479) Gerber, N. N. Volatile Substances from Actinomycetes: Their Role in the Odor Pollution of Water. *CRC Crit. Rev. Microbiol.* **1979**, *7*, 191–214.

(480) Heil, T. P.; Lindsay, R. C. Volatile Compounds in Flavor-Tainted Fish from the Upper Wisconsin River. *J. Environ. Sci. Health, Part B* **1988**, *23*, 489–512.

(481) Jardine, C. G.; Gibson, N.; Hrudey, S. E. Detection of Odour and Health Risk Perception of Drinking Water. *Water Sci. Technol.* **1999**, *40*, 91–98.

(482) Schrader, K. K.; Dennis, M. E. Cyanobacteria and Earthy/Musty Compounds Found in Commercial Catfish (*Ictalurus punctatus*) Ponds in the Mississippi Delta and Mississippi-Alabama Blackland Prairie. *Water Res.* **2005**, *39*, 2807–2814.

(483) Darriet, P.; Pons, M.; Lamy, S.; Dubourdieu, D. Identification and Quantification of Geosmin, an Earthy Odorant Contaminating Wines. *J. Agric. Food Chem.* **2000**, *48*, 4835–4838.

(484) Gust, B.; Challis, G. L.; Fowler, K.; Kieser, T.; Chater, K. F. PCR-Targeted *Streptomyces* Gene Replacement Identifies a Protein Domain Needed for Biosynthesis of the Sesquiterpene Soil Odor Geosmin. *Proc. Natl. Acad. Sci. U. S. A.* **2003**, *100*, 1541–1546.

(485) Cane, D. E.; Watt, R. M. Expression and Mechanistic Analysis of a Germacradienol Synthase from *Streptomyces coelicolor* Implicated in Geosmin Biosynthesis. *Proc. Natl. Acad. Sci. U. S. A.* **2003**, *100*, 1547–1551.

(486) Jiang, J.; He, X.; Cane, D. E. Geosmin Biosynthesis. *Streptomyces coelicolor* Germacradienol/Germacrene D Synthase Converts Farnesyl Diphosphate to Geosmin. *J. Am. Chem. Soc.* **2006**, *128*, 8128–8129.

(487) Jiang, J.; He, X.; Cane, D. E. Biosynthesis of the Earthy Odorant Geosmin by a Bifunctional *Streptomyces coelicolor* Enzyme. *Nat. Chem. Biol.* **2007**, *3*, 711–715.

(488) He, X.; Cane, D. E. Mechanism and Stereochemistry of the Germacradienol/Germacrene D Synthase of *Streptomyces coelicolor* A3(2). *J. Am. Chem. Soc.* **2004**, *126*, 2678–2679.

(489) Cane, D. E.; He, X.; Kobayashi, S.; Omura, S.; Ikeda, H. Geosmin Biosynthesis in *Streptomyces avermitilis*. Molecular Cloning, Expression, and Mechanistic Study of the Germacradienol/Geosmin Synthase. *J. Antibiot.* **2006**, *59*, 471–479.

(490) Jiang, J.; Cane, D. E. Geosmin Biosynthesis. Mechanism of the Fragmentation-Rearrangement in the Conversion of Germacradienol to Geosmin. *J. Am. Chem. Soc.* **2008**, *130*, 428–429.

(491) Nawrath, T.; Dickschat, J. S.; Müller, R.; Jiang, J.; Cane, D. E.; Schulz, S. Identification of (8S,9S,10S)-8,10-Dimethyl-1-Octalin, a Key Intermediate in the Biosynthesis of Geosmin in Bacteria. *J. Am. Chem. Soc.* **2008**, *130*, 430–431.

(492) Harris, G. G.; Lombardi, P. M.; Pemberton, T. A.; Matsui, T.; Weiss, T. M.; Cole, K. E.; Köksal, M.; Murphy, F. V., IV; Vedula, L. S.; Chou, W. K. W.; et al. Structural Studies of Geosmin Synthase, a Bifunctional Sesquiterpene Synthase with $\alpha\alpha$ Domain Architecture that Catalyzes a Unique Cyclization-Fragmentation Reaction Sequence. *Biochemistry* **2015**, *54*, 7142–7155.

(493) Phillips, M. A.; Croteau, R. B. Resin-Based Defenses in Conifers. *Trends Plant Sci.* **1999**, *4*, 184–190.

(494) Raffa, K. F.; Berryman, A. A.; Simasko, J.; Teal, W.; Wong, B. L. Effects of Grand Fir Monoterpenes on the Fir Engraver, *Scolytus ventralis* (Coleoptera: Scolytidae), and its Symbiotic Fungus. *Environ. Entomol.* **1985**, *14*, 552–556.

(495) LaFever, R. E.; Vogel, B. S.; Croteau, R. Diterpenoid Resin Acid Biosynthesis in Conifers: Enzymatic Cyclization of Geranylgeranyl Pyrophosphate to Abietadiene, the Precursor of Abietic Acid. *Arch. Biochem. Biophys.* **1994**, *313*, 139–149.

(496) Stofer Vogel, B.; Wildung, M. R.; Vogel, G.; Croteau, R. Abietadiene Synthase from Grand Fir (*Abies grandis*). cDNA Isolation, Characterization, and Bacterial Expression of a Bifunctional Diterpene Cyclase Involved in Resin Acid Biosynthesis. *J. Biol. Chem.* **1996**, *271*, 23262–23268.

(497) Peters, R. J.; Ravn, M. M.; Coates, R. M.; Croteau, R. B. Bifunctional Abietadiene Synthase: Free Diffusive Transfer of the (+)-Copalyl Diphosphate Intermediate between Two Distinct Active Sites. *J. Am. Chem. Soc.* **2001**, *123*, 8974–8978.

(498) Peters, R. J.; Croteau, R. B. Abietadiene Synthase Catalysis: Conserved Residues Involved in Protonation-Initiated Cyclization of Geranylgeranyl Diphosphate to (+)-Copalyl Diphosphate. *Biochemistry* **2002**, *41*, 1836–1842.

(499) Ravn, M. M.; Coates, R. M.; Jetter, R.; Croteau, R. B.; Ravn, M. M. Stereospecific Intramolecular Proton Transfer in the Cyclization of Geranylgeranyl Diphosphate to (–)-Abietadiene Catalyzed by Recombinant Cyclase from Grand Fir (*Abies grandis*). *Chem. Commun.* **1998**, 21–22.

(500) Peters, R. J.; Croteau, R. B. Abietadiene Synthase Catalysis: Mutational Analysis of a Prenyl Diphosphate Ionization-Initiated Cyclization and Rearrangement. *Proc. Natl. Acad. Sci. U. S. A.* **2002**, *99*, 580–584.

- (501) Ravn, M. M.; Coates, R. M.; Flory, J. E.; Peters, R. J.; Croteau, R. Stereochemistry of the Cyclization-Rearrangement of (+)-Copalyl Diphosphate to (–)-Abietadiene Catalyzed by Recombinant Abietadiene Synthase from *Abies grandis*. *Org. Lett.* **2000**, *2*, 573–576.
- (502) Ravn, M. M.; Peters, R. J.; Coates, R. M.; Croteau, R. Mechanism of Abietadiene Synthase Catalysis: Stereochemistry and Stabilization of the Cryptic Pimaranyl Carbocation Intermediates. *J. Am. Chem. Soc.* **2002**, *124*, 6998–7006.
- (503) Criswell, J.; Potter, K.; Shephard, F.; Beale, M. H.; Peters, R. J. A Single Residue Change Leads to a Hydroxylated Product from the Class II Diterpene Cyclization Catalyzed by Abietadiene Synthase. *Org. Lett.* **2012**, *14*, 5828–5831.
- (504) Mafu, S.; Potter, K. C.; Hillwig, M. L.; Schulte, S.; Criswell, J.; Peters, R. J. Efficient Heterocyclisation by (Di)Terpene Synthases. *Chem. Commun.* **2015**, *51*, 13485–13487.
- (505) Wilderman, P. R.; Peters, R. J. A Single Residue Switch Converts Abietadiene Synthase into a Pimaradiene Specific Cyclase. *J. Am. Chem. Soc.* **2007**, *129*, 15736–15737.
- (506) Siebert, M. R.; Zhang, J.; Addepalli, S. V.; Tantillo, D. J.; Hase, W. L. The Need for Enzymatic Steering in Abietic Acid Biosynthesis: Gas-Phase Chemical Dynamics Simulations of Carbocation Rearrangements on a Bifurcating Potential Energy Surface. *J. Am. Chem. Soc.* **2011**, *133*, 8335–8343.
- (507) Ballio, A.; Chain, E. B.; de Leo, P.; Erlanger, B. F.; Mauri, M.; Tonolo, A. Fusicoccin: A New Wilting Toxin Produced by *Fusicoccum amygdali* Del. *Nature* **1964**, *203*, 297.
- (508) Ballio, A.; Brufani, M.; Casinovi, C. G.; Cerrini, S.; Fedeli, W.; Pellicciari, R.; Santurbano, B.; Vaciego, A. The Structure of Fusicoccin A. *Experientia* **1968**, *24*, 631–635.
- (509) Barrow, K. D.; Barton, D. H. R.; Chain, E. B.; Ohnsorge, U. F. W.; Thomas, R. The Constitution of Fusicoccin. *Chem. Commun.* **1968**, 1198–1200.
- (510) Daines, R. H.; Cohoon, D. F.; Leone, I.; Brennan, E. Control of *Fusicoccum* Canker of Peach by Nutrition, Defoliation, and Protective Fungicides. *Phytopathology* **1958**, *48*, 400–407.
- (511) Weaver, L. O. The Constriction Disease of Peach in Maryland. *Plant Dis. Rep.* **1951**, *35*, 144.
- (512) Lalancette, N.; Polk, D. F. Estimating Yield and Economic Loss from Constriction Canker of Peach. *Plant Dis.* **2000**, *84*, 941–946.
- (513) de Vries-van Leeuwen, I. J.; Kortekaas-Thijssen, C.; Nzigou Mandouckou, J. A.; Kas, S.; Evidente, A.; de Boer, A. H. Fusicoccin-A Selectively Induces Apoptosis in Tumor Cells after Interferon- α Priming. *Cancer Lett.* **2010**, *293*, 198–206.
- (514) Bunney, T. D.; De Boer, A. H.; Levin, M. Fusicoccin Signaling Reveals 14–3-3 Protein Function as a Novel Step in Left-Right Patterning During Amphibian Embryogenesis. *Development* **2003**, *130*, 4847–4858.
- (515) de Boer, A. H.; de Vries-van Leeuwen, I. J. Fusicoccanes: Diterpenes with Surprising Biological Functions. *Trends Plant Sci.* **2012**, *17*, 360–368.
- (516) Milroy, L.-G.; Brunsveld, L.; Ottmann, C. Stabilization and Inhibition of Protein-Protein Interactions: the 14–3-3 Case Study. *ACS Chem. Biol.* **2013**, *8*, 27–35.
- (517) Bury, M.; Andolfi, A.; Rogister, B.; Cimmino, A.; Mègalizzi, V.; Mathieu, V.; Feron, O.; Evidente, A.; Kiss, R. Fusicoccin A, a Phytotoxic Carbocyclic Diterpene Glucoside of Fungal Origin, Reduces Proliferation and Invasion of Glioblastoma Cells by Targeting Multiple Tyrosine Kinases. *Transl. Oncol.* **2013**, *6*, 112–123.
- (518) Toyomasu, T.; Tsukahara, M.; Kaneko, A.; Niida, R.; Mitsushashi, W.; Dairi, T.; Kato, N.; Sassa, T. Fusicocins are Biosynthesized by an Unusual Chimera Diterpene Synthase in Fungi. *Proc. Natl. Acad. Sci. U. S. A.* **2007**, *104*, 3084–3088.
- (519) Toyomasu, T.; Tsukahara, M.; Kenmoku, H.; Anada, M.; Nitta, H.; Ohkanda, J.; Mitsushashi, W.; Sassa, T.; Kato, N. Transannular Proton Transfer in the Cyclization of Geranylgeranyl Diphosphate to Fusicocadiene, a Biosynthetic Intermediate of Fusicocins. *Org. Lett.* **2009**, *11*, 3044–3047.
- (520) Li, H.-L. An Archaeological and Historical Account of Cannabis in China. *Econ. Bot.* **1973**, *28*, 437–448.
- (521) Ben Amar, M. Cannabinoids in Medicine: A Review of their Therapeutic Potential. *J. Ethnopharmacol.* **2006**, *105*, 1–25.
- (522) Gaoni, Y.; Mechoulam, R. Isolation, Structure, and Partial Synthesis of an Active Constituent of Hashish. *J. Am. Chem. Soc.* **1964**, *86*, 1646–1647.
- (523) Hill, A. J.; Williams, C. M.; Whalley, B. J.; Stephens, G. J. Phytocannabinoids as Novel Therapeutic Agents in CNS Disorders. *Pharmacol. Ther.* **2012**, *133*, 79–97.
- (524) Turner, S. E.; Williams, C. M.; Iversen, L.; Whalley, B. J. *Molecular Pharmacology of Phytocannabinoids*; Progress in the Chemistry of Organic Natural Products; 2017; Vol. 103, pp 61–101.
- (525) Fellermeier, M.; Zenk, M. H. Prenylation of Olivetolate by a Hemp Transferase Yields Cannabigerolic Acid, the Precursor of Tetrahydrocannabinol. *FEBS Lett.* **1998**, *427*, 283–285.
- (526) Taura, F.; Morimoto, S.; Shoyama, Y.; Mechoulam, R. First Direct Evidence for the Mechanism of Δ^1 -Tetrahydrocannabinolic Acid Biosynthesis. *J. Am. Chem. Soc.* **1995**, *117*, 9766–9767.
- (527) Sirikantaramas, S.; Morimoto, S.; Shoyama, Y.; Ishikawa, Y.; Wada, Y.; Shoyama, Y.; Taura, F. The Gene Controlling Marijuana Psychoactivity: Molecular Cloning and Heterologous Expression of Δ^1 -Tetrahydrocannabinolic Acid Synthase from *Cannabis sativa* L. *J. Biol. Chem.* **2004**, *279*, 39767–39774.
- (528) Shoyama, Y.; Tamada, T.; Kurihara, K.; Takeuchi, A.; Taura, F.; Arai, S.; Blaber, M.; Shoyama, Y.; Morimoto, S.; Kuroki, R. Structure and Function of Δ^1 -Tetrahydrocannabinolic Acid (THCA) Synthase, the Enzyme Controlling the Psychoactivity of *Cannabis sativa*. *J. Mol. Biol.* **2012**, *423*, 96–105.
- (529) Winkler, A.; Lyskowski, A.; Riedl, S.; Puhl, M.; Kutchan, T. M.; Macheroux, P.; Gruber, K. A Concerted Mechanism for Berberine Bridge Enzyme. *Nat. Chem. Biol.* **2008**, *4*, 739–741.
- (530) Ilc, T.; Parage, C.; Boachon, B.; Navrot, N.; Werck-Reichhart, D. Monoterpenol Oxidative Metabolism: Adaptation and Potential Applications. *Front. Plant Sci.* **2016**, *7*, Article 509. doi: [10.3389/fpls.2016.00509](https://doi.org/10.3389/fpls.2016.00509).
- (531) Dinda, B.; Debnath, S.; Banik, R. Naturally-Occurring Iridoids and Secoiridoids. An Updated Review, Part 4. *Chem. Pharm. Bull.* **2011**, *59*, 803–833.
- (532) Tundis, R.; Loizzo, M. R.; Menichini, F.; Statti, G. A.; Menichini, F. Biological and Pharmacological Activities of Iridoids: Recent Developments. *Mini-Rev. Med. Chem.* **2008**, *8*, 399–420.
- (533) Uesato, S.; Ueda, S.; Kobayashi, K.; Inouye, H. Mechanism of Iridane Skeleton Formation in the Biosynthesis of Iridoid Glucosides in *Gardenia jasminoides* Cell Cultures. *Chem. Pharm. Bull.* **1983**, *31*, 4185–4188.
- (534) Uesato, S.; Matsuda, S.; Inouye, H. Mechanism for Iridane Skeleton Formation from Acyclic Monoterpenes in the Biosynthesis of Secologanin and Vindoline in *Catharanthus roseus* and *Lonicera morrowii*. *Chem. Pharm. Bull.* **1984**, *32*, 1671–1674.
- (535) Uesato, S.; Ikeda, H.; Fujita, T.; Inouye, H.; Zenk, M. H. Elucidation of Iridodial Formation Mechanism – Partial Purification and Characterization of the Novel Monoterpene Cyclase from *Rauwolfia serpentina* Cell Suspension Cultures. *Tetrahedron Lett.* **1987**, *28*, 4431–4434.
- (536) Geu-Flores, F.; Sherden, N. H.; Courdavault, V.; Burlat, V.; Glenn, W. S.; Wu, C.; Nims, E.; Cui, Y.; O'Connor, S. E. An Alternative Route to Cyclic Terpenes by Reductive Cyclization in Iridoid Biosynthesis. *Nature* **2012**, *492*, 138–142.
- (537) Lindner, S.; Geu-Flores, F.; Bråse, S.; Sherden, N. H.; O'Connor, S. E. Conversion of Substrate Analogs Suggests a Michael Cyclization in Iridoid Biosynthesis. *Chem. Biol.* **2014**, *21*, 1452–1456.
- (538) Kries, H.; Caputi, L.; Stevenson, C. E. M.; Kamileen, M. O.; Sherden, N. H.; Geu-Flores, F.; Lawson, D. M.; O'Connor, S. E. Structural Determinants of Reductive Terpene Cyclization in Iridoid Biosynthesis. *Nat. Chem. Biol.* **2015**, *12*, 6–8.
- (539) Hu, Y.; Liu, W.; Malwal, S. R.; Zheng, Y.; Feng, X.; Ko, T.-P.; Chen, C.-C.; Xu, Z.; Liu, M.; Han, X.; et al. Structures of Iridoid Synthase from *Cantharanthus roseus* with Bound NAD⁺, NADPH, or NAD⁺/10-Oxogeranial: Reaction Mechanisms. *Angew. Chem., Int. Ed.* **2015**, *54*, 15478–15482.

(540) Thorn, A.; Egerer-Sieber, C.; Jäger, C. M.; Herl, V.; Müller-Uri, F.; Kreis, W.; Muller, Y. A. The Crystal Structure of Progesterone 5β -Reductase from *Digitalis lanata* Defines a Novel Class of Short Chain Dehydrogenases/Reductases. *J. Biol. Chem.* **2008**, *283*, 17260–17269.

(541) Munkert, J.; Pollier, J.; Miettinen, M.; Van Moerkercke, A.; Payne, R.; Müller-Uri, F.; Burlat, V.; O'Connor, S. E.; Memelink, J.; Kreis, W.; Goossens, A. Iridoid Synthase Activity is Common among the Plant Progesterone 5β -Reductase Family. *Mol. Plant* **2015**, *8*, 136–152.

(542) Park, H. W.; Boduluri, S. R.; Moomaw, J. F.; Casey, P. J.; Beese, L. S. Crystal Structure of Protein Farnesyltransferase at 2.25 Å Resolution. *Science* **1997**, *275*, 1800–1805.

(543) Nestl, B. M.; Geinitz, C.; Popa, S.; Rizek, S.; Haselbeck, R. J.; Stephen, R.; Noble, M. A.; Fischer, M.-P.; Ralph, E. C.; Hau, H. T.; et al. Structural and Functional Insights into Asymmetric Enzymatic Dehydration of Alkenols. *Nat. Chem. Biol.* **2017**, *13*, 275–281.

(544) Andersen-Ranberg, J.; Kongstad, K. T.; Nielsen, M. T.; Jensen, N. B.; Pateraki, I.; Bach, S. S.; Hamberger, B.; Zerbe, P.; Staerk, D.; Bohlmann, J.; et al. Expanding the Landscape of Diterpene Structural Diversity through Stereochemically Controlled Combinatorial Biosynthesis. *Angew. Chem., Int. Ed.* **2016**, *55*, 2142–2146.

(545) Jia, M.; Potter, K. C.; Peters, R. J. Extreme Promiscuity of a Bacterial and a Plant Diterpene Synthase Enables Combinatorial Biosynthesis. *Metab. Eng.* **2016**, *37*, 24–34.

(546) Tian, B.; Poulter, C. D.; Jacobson, M. P. Defining the Product Chemical Space of Monoterpenoid Synthases. *PLoS Comput. Biol.* **2016**, *12*, e1005053.

(547) Liaci, E.; Fischer, A.; Heinrichs, M.; van Elst, L. T.; Kornmeier, J. Mona Lisa is Always Happy: And Only Sometimes Sad. *Sci. Rep.* **2017**, *7*, 43511.